Galileo AltBOC receivers - Analysis of receiver architectures, acquisition strategies and multipath mitigation techniques for the E5 AltBOC signal

POLITECNICO DI TORINO

III Facoltà di Ingegneria dell'Informazione

Corso di Laurea Specialistica in Ingegneria delle Telecomunicazioni

Tesi di Laurea

Galileo AltBOC Receivers

Analysis of Receiver Architectures, Acquisition Strategies
and Multipath Mitigation Techniques for the E5 AltBOC Signal

Relatori:
prof. Letizia Lo Presti
prof. Fabio Dovis
ing. Paolo Mulassano

Candidato:
Davide Margaria

Gennaio 2007

A mio padre

Nobile semplicità,
serena grandezza.

[J. J. Winckelmann]

Sommario

Il sistema di radionavigazione satellitare **Galileo** é un'iniziativa dell'*Unione Europea*, in collaborazione con l'*Agenzia Spaziale Europea* (ESA) ed alcune industrie europee, che prevede lo sviluppo ed il lancio di un nuovo *Sistema Globale di Navigazione Satellitare* (GNSS), simile al sistema Americano GPS, ma completamente finanziato dall'Europa e sotto controllo civile. La *Commissione Europea* ha infatti riconosciuto l'importanza economica e politica delle attuali tecnologie di radionavigazione satellitare ed ha deciso di finanziare lo sviluppo di un sistema compatibile con gli attuali sistemi di navigazione satellitare (GPS e GLONASS), ma indipendente da essi. Il sistema Galileo sarà operativo già a partire dal 2008 ed entrerà in funzione a pieno regime nel 2011, quando verrà completata la sua costellazione con il lancio dei 30 satelliti previsti. Galileo sarà quindi un sistema innovativo e basato su tecnologie che sono l'attuale stato dell'arte per le trasmissioni satellitari: in tal modo verranno forniti nuovi servizi, garantendo una copertura globale, una maggiore sicurezza e continuità (*integrità*) dei segnali trasmessi e soprattutto permettendo ai futuri ricevitori Galileo di raggiungere migliori prestazioni (migliore accuratezza nella stima della posizione) rispetto agli attuali ricevitori GPS.

In particolare, il segnale più promettente previsto per il sistema Galileo è la nuova modulazione a banda larga **AltBOC** (*Alternative Binary Offset Carrier*), che verrà utilizzata dai satelliti per trasmettere i segnali nella banda di frequenza **E5** (1164-1215 MHz). La modulazione AltBOC rappresenta dal punto di vista scientifico una delle innovazioni più importanti: alcuni recenti articoli nella letteratura scientifica affermano che i futuri ricevitori Galileo, sfruttando i segnali trasmessi con questa nuova modulazione, saranno in grado di raggiungere eccezionali prestazioni in presenza di rumore e cammini multipli, che rappresentano le principali fonti di errore nelle misure di posizionamento eseguite dagli attuali ricevitori GPS.

In questo ambito, lo studio della modulazione AltBOC è dunque di primaria importanza per lo sviluppo dei nuovi ricevitori per i segnali Galileo. Va però notato che sino ad ora sono stati pubblicati solo pochi articoli, che trattano i segnali AltBOC e le possibili tecniche di ricezione adatte a tali segnali in modo sintetico e generico. L'obiettivo di questa tesi è quindi uno studio approfondito delle caratteristiche dei segnali AltBOC: in tal modo sarà possibile definire le possibili architetture per i futuri ricevitori AltBOC e confrontarne sia la

complessità e i problemi di implementazione, sia le prestazioni. In particolare, dopo aver definito l'architettura e il funzionamento dei vari possibili ricevitori nella fase di inseguimento (*tracking*) del segnale AltBOC, verranno studiate le procedure di acquisizione della sincronia adatte ai segnali AltBOC e verranno valutate le prestazioni dei ricevitori AltBOC in presenza di cammini multipli (il cosiddetto effetto *multipath*), adattando le tecniche di acquisizione e di mitigazione dei cammini multipli attualmente usate nei ricevitori GPS alle nuove architetture ed ai nuovi segnali. Verranno inoltre proposte e studiate anche alcune soluzioni innovative, adatte ai segnali AltBOC.

I segnali AltBOC nella banda E5 di Galileo

L'acronimo AltBOC può essere tradotto in italiano come "modulazione alternativa con spostamenti binari della portante". Questo tipo di modulazione deriva dalle modulazioni BOC (*Binary Offset Carrier*), conosciute da alcuni anni per le loro proprietà spettrali: esse sono dette modulazioni *split spectrum*, in quanto lo spettro di frequenza del segnale modulato risulta diviso in due o più lobi attorno alla frequenza della portante.

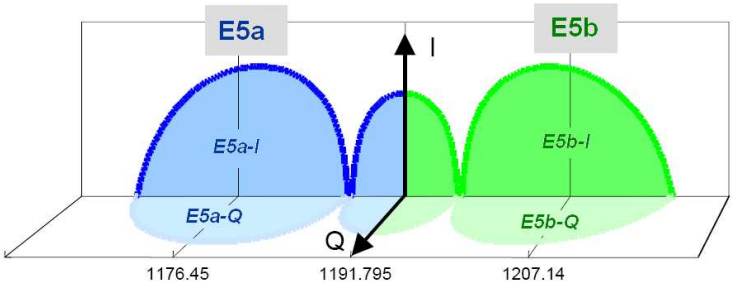

Figura 1: Schema spettrale dei segnali trasmessi nella banda di frequenza E5 del sistema di radionavigazione satellitare Galileo

La modulazione AltBOC che verrà usata nel sistema Galileo é un'estensione delle modulazioni BOC, con analoghe proprietà spettrali e che permette di trametterе quattro segnali diversi in due semi-bande adiacenti. Infatti, come è schematizzato in Figura 1, ogni satellite Galileo trasmetterà quattro segnali (*E5a-I*, *E5a-Q*, *E5b-I* ed *E5b-Q*) nella banda E5, usando la modulazione AltBOC. Il segnale modulato verrà trasmesso su una banda di 92.07 MHz, con polarizzazione circolare destrorsa (RHCP), attorno ad una frequenza centrale di portante (f_{E5}) pari a 1191.795 MHz (vedi [4]). Grazie alla modulazione AltBOC, il segnale trasmesso risulterà diviso in due bande laterali:

- la banda **E5a**, con frequenza centrale (f_{E5a}) pari a 1176.45 MHz;
- la banda **E5b**, con frequenza centrale (f_{E5b}) pari a 1207.14 MHz.

In particolare, quattro segnali verranno trasmessi usando la modulazione AltBOC in queste due bande laterali: due di essi (*E5a-I* e *E5b-I*) saranno componenti in fase (I) del segnale modulato e conterranno dati di navigazione, rispettivamente per il cosiddetto *Open Service* (F/NAV) di Galileo e per il *Safety-of-Life Service* (I/NAV), mentre gli altri due segnali (*E5a-Q* e *E5b-Q*) saranno trasmessi in quadratura (Q) e non conterranno dati. Questi ultimi due segnali, i cosiddetti canali *pilota*, risulteranno particolarmente utili per semplificare le procedure di acquisizione e di *tracking* e per migliorare le prestazioni del ricevitore. Nella Tabella 1 sono riassunte le principali caratteristiche di questi quattro segnali.

Banda	**Canale**	**Frequenza dei codici [Mchip/s]**	**Frequenza di simbolo [simboli/s]**	**Servizio offerto**
E5a	I	10.23	50	F/NAV
	Q	10.23	Nessun dato	Pilota
E5b	I	10.23	250	I/NAV
	Q	10.23	Nessun dato	Pilota

Tabella 1: Caratteristiche delle componenti di segnale usate nella modulazione AltBOC per la banda E5

Per potere modulare i quattro canali con la modulazione AltBOC è necessario l'uso di particolari sotto-portanti, di codici pseudo-causali (PRN) e la generazione dei dati per i segnali di navigazione, come spiegato di seguito. Solo dopo aver discusso nel dettaglio la generazione di queste componenti del segnale AltBOC, l'espressione della modulazione AltBOC verrà illustrata, in modo da favorire la comprensione.

• Sotto-portanti ad onda quadra

Due diverse sotto-portanti sono necessarie per la modulazione AltBOC: esse sono le due funzioni $sc_{E5\text{-}S}(t)$ e $sc_{E5\text{-}P}(t)$, rappresentate in Figura 2.

Va notato che queste due funzioni sono delle onde quadre su 4 livelli e un loro periodo $T_{S,E5}$ è suddiviso in 8 sotto-periodi. La prima funzione $sc_{E5\text{-}S}(t)$ ha una forma che assomiglia ad un coseno campionato e il pedice S serve per indicare che verrà utilizzata per le cosiddette **componenti di segnale** nell'espressione della modulazione AltBOC (come spiegato più avanti). Invece, l'altra funzione $sc_{E5\text{-}P}(t)$ presenta un'ampiezza minore e una forma irregolare, e verrà utilizzata per i cosiddetti **segnali prodotto** (pedice P). Va notato che la potenza relativa di $sc_{E5\text{-}P}(t)$ rispetto a $sc_{E5\text{-}S}(t)$ è pari a $P_{rel} \cong 15\%$.

Queste due forme d'onda devono essere generate con una frequenza pari a $R_{S,E5} = 1/T_{S,E5} = 15.345\,\text{MHz}$, che corrisponde a 15 volte la frequenza di riferimento $f_0 = 1.023\,\text{MHz}$ (è la frequenza del codice C/A del GPS).

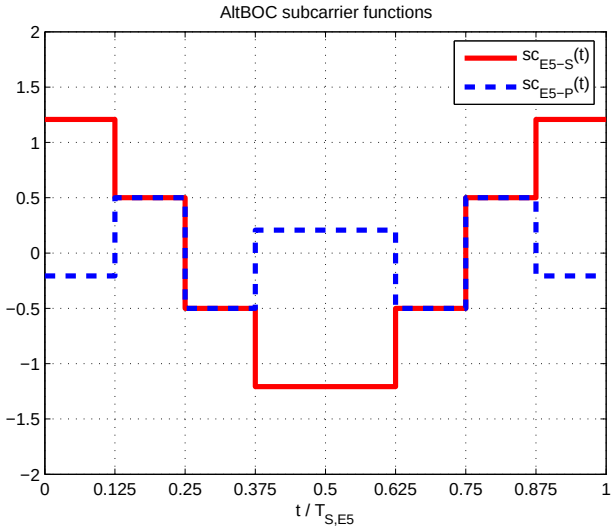

Figura 2: Rappresentazione di un periodo delle due sotto-portanti $sc_{E5\text{-}S}(t)$ e $sc_{E5\text{-}P}(t)$, utilizzate nella modulazione AltBOC

• Codici pseudo-casuali (PRN)

Per ognuno dei quattro canali (*E5a-I*, *E5a-Q*, *E5b-I* ed *E5b-Q*) trasmessi da ogni satellite Galileo nella banda E5 verrà utilizzato un diverso codice pseudo-casuale (PRN). Questi codici sono anche detti sequenze di *spreading*, in quanto permettono una multiplazione di codice per l'accesso al sistema (CDMA): in effetti questi codici verranno assegnati in modo univoco ai satelliti Galileo[1] in modo che un ricevitore possa distinguere ogni canale trasmesso da ogni satellite del sistema. Questo è possibile in quanto le sequenze pseudo-casuali scelte per il sistema Galileo sono delle sequenze di Gold troncate, che presentano una *quasi-ortogonalità* per quanto riguarda le proprietà di mutua correlazione.

I codici PRN in un sistema di navigazione satellitare sono anche tipicamente chiamati *ranging codes* perché, sfruttando le loro proprietà di autocorrelazione, permettono ad un ricevitore di stimare la sua distanza dal satellite che ha trasmesso il segnale, allineando una replica locale del codice con il segnale ricevuto.

Per la banda E5 del sistema Galileo sono previsti dei codici PRN con una struttura particolare, ottenuta come sovrapposizione tra un **codice primario** e un **codice secondario** (*tiered code structure*), diversi per ogni canale da trasmettere. Questa struttura di codici è basata sull'idea di utilizzare successive ripetizioni di un codice primario, tipicamente con un periodo di durata pari a 1 ms, su cui viene sovrapposto un codice secondario, in cui ogni simbolo binario del codice (chiamato in gergo *chip*) corrisponde ad un intero

[1] L'attuale struttura dei codici può ancora subire variazioni e non è ancora stata definita l'assegnazione dei vari codici ai vari satelliti (per maggiori dettagli vedi [4]).

periodo del codice primario. In questo modo si possono ottenere dei codici compositi molto lunghi, con ottime proprietà di correlazione.

Quattro diversi codici verranno quindi usati da ogni satellite Galileo per trasmettere i quattro canali (*E5a-I*, *E5a-Q*, *E5b-I* ed *E5b-Q*) nella banda E5: per convenzione questi codici vengono indicati come $c_{E5a\text{-}I}$, $c_{E5a\text{-}Q}$, $c_{E5b\text{-}I}$ e $c_{E5b\text{-}Q}$. Questi codici verranno generati con una frequenza di chip pari a $R_C = 1/T_C = 10.23\,\text{Mchip/s}$. Le lunghezze di questi codici sono illustrate nella Tabella 2, considerando sia i codici primari, sia i codici secondari.

Canale	**Lunghezza complessiva del codice [ms]**	**Lunghezza del codice [chips]**	
		Primario	**Secondario**
E5a-I	20	10230	20
E5a-Q	100	10230	100
E5b-I	4	10230	4
E5b-Q	100	10230	100

Tabella 2: Lunghezze dei codici PRN per la banda E5

Va notato che i codici primari avranno tutti una lunghezza pari ad 1 ms: questo servirà per facilitare e velocizzare l'acquisizione dei segnali, che potrà essere effettuata sfruttando questa periodicità su breve periodo (1 ms). Invece, per effetto dei codici secondari, i codici completi avranno lunghezze comprese tra 4 ms e 100 ms.

In particolare, i due canali pilota (*E5a-Q* ed *E5b-Q*) avranno i codici più lunghi (100 ms), in modo da permettere ai futuri ricevitori Galileo di ottenere eccellenti prestazioni nella fase di *tracking*. Invece i due canali dati (*E5a-I* ed *E5b-I*) useranno codici più corti e con lunghezze diverse, in quanto sui due canali verranno trasmessi dati con frequenze di simbolo diverse (come spiegato nella prossima sezione): va notato che un periodo del codice usato corrisponderà esattamente alla durata di un simbolo trasmesso (per maggiori dettagli a proposito dei codici, vedi [4]).

• Dati di navigazione

Come accennato in precedenza, i due segnali in fase (I) nella banda E5 conterranno due distinti messaggi di navigazione:

- il canale *E5a-I* è destinato all'*Open Service* (F/NAV) e conterrà i dati di navigazione (d_{E5a-I}), trasmessi a 50 simboli/s (effemeridi dei satelliti, informazioni di temporizzazione, correzioni, stato della costellazione di satelliti, ecc.);
- il canale *E5b-I* invece conterrà i dati di integrità (d_{E5b-I}), trasmessi a 250 simboli/s, per il *Safety-of-Life Service* (I/NAV).

Va notato che una codifica convoluzionale di Viterbi con rapporto 1/2 verrà usata per tutti i canali dati del sistema Galileo: questo significa che la vera frequenza di trasmissione dei dati (in bits/s) è la metà della frequenza di simbolo indicata (in simboli/s). Per maggiori dettagli sul formato dei dati trasmessi, si veda il SIS-ICD [4].

La modulazione AltBOC

Tutte le componenti di segnale illustrate nelle precedenti sezioni (cioè sotto-portanti, codici PRN e dati di navigazione) sono utilizzate per ottenere il segnale a banda larga AltBOC, che verrà trasmesso nella banda E5 del sistema Galileo. Lo schema di modulazione AltBOC (*Alternative BOC*) è un'estensione delle modulazioni BOC (ampiamente descritte in letteratura), come precedentemente accennato. Essa presenta analoghe caratteristiche spettrali rispetto alle modulazioni BOC (spettro di frequenza diviso in due bande laterali), ma si differenzia da esse principalmente perché vengono trasmessi ben quattro distinti canali ed il segnale modulato presenta un inviluppo costante (simile a quello di una modulazione 8-PSK).

Nel testo della tesi è riportata una derivazione completa della modulazione AltBOC, partendo da un approccio generale *BOC*, discutendo poi la modulazione *Complex-BOC* e la cosiddetta *Standard AltBOC*, per arrivare poi infine allo schema che verrà effettivamente utilizzato per la banda E5: la cosiddetta **E5 AltBOC**, detta anche modulazione *AltBOC ad inviluppo costante*. Ma questo esula i limiti di spazio di questo sommario, dunque solo l'espressione finale del segnale E5 AltBOC è qui riportata, usando le notazioni del SIS-ICD [4].

Questa modulazione è convenzionalmente chiamata anche $AltBOC(m,n)$ e quella che verrà usata nella banda E5 del sistema Galileo sarà la modulazione **E5 AltBOC(15,10)**, dove:

- $m = 15$ indica la frequenza delle sotto-portanti ($R_{S,E5} = 15.345\,\text{MHz}$), normalizzata con la frequenza di riferimento $f_0 = 1.023\,\text{MHz}$;
- $n = 10$ indica la frequenza di chip dei codici PRN ($R_C = 10.23\,\text{Mchip/s}$), anch'essa normalizzata con $f_0 = 1.023\,\text{MHz}$.

Come accennato in precedenza, la modulazione AltBOC permette di trametter quattro canali (*E5a-I*, *E5a-Q*, *E5b-I* ed *E5b-Q*), che contengono quattro codici PRN diversi e quasi-ortogonali tra di loro. Inoltre, due canali contengono anche dei dati di navigazione mentre gli altri due, senza dati, sono i cosiddetti *canali pilota*. Di seguito sono riportate le espressioni analitiche dei segnali trasmessi nei quattro canali, ottenute componendo in modo opportuno i codici e i dati di navigazione presentati in precedenza: queste espressioni sono dette **componenti di segnale** della modulazione.

$$e_{E5a\text{-}I}(t) = \sum_{i=-\infty}^{+\infty} \left[c_{E5a\text{-}I,|i|_{L_{E5a\text{-}I}}} \cdot d_{E5a\text{-}I,[i]_{DC_{E5a\text{-}I}}} \cdot \mathrm{rect}_{T_{c,E5a\text{-}I}}(t - i \cdot T_{c,E5a\text{-}I}) \right] \quad (1)$$

$$e_{E5a\text{-}Q}(t) = \sum_{i=-\infty}^{+\infty} \left[c_{E5a\text{-}Q,|i|_{L_{E5a\text{-}Q}}} \cdot \mathrm{rect}_{T_{c,E5a\text{-}Q}}(t - i \cdot T_{c,E5a\text{-}Q}) \right] \quad (2)$$

$$e_{E5b\text{-}I}(t) = \sum_{i=-\infty}^{+\infty} \left[c_{E5b\text{-}I,|i|_{L_{E5b\text{-}I}}} \cdot d_{E5b\text{-}I,[i]_{DC_{E5b\text{-}I}}} \cdot \mathrm{rect}_{T_{c,E5b\text{-}I}}(t - i \cdot T_{c,E5b\text{-}I}) \right] \quad (3)$$

$$e_{E5b\text{-}Q}(t) = \sum_{i=-\infty}^{+\infty} \left[c_{E5b\text{-}Q,|i|_{L_{E5b\text{-}Q}}} \cdot \mathrm{rect}_{T_{c,E5b\text{-}Q}}(t - i \cdot T_{c,E5b\text{-}Q}) \right] \quad (4)$$

$$\text{dove } \mathrm{rect}_T(t) = \begin{array}{ll} 1 & \text{per } 0 < t < T \\ 0 & \text{altrimenti} \end{array}$$

Usando queste quattro componenti, il segnale a banda larga ottenuto con la modulazione **E5 AltBOC(15,10)** è definito dalla seguente espressione:

$$\begin{aligned} s_{E5}(t) = & \frac{1}{2 \cdot \sqrt{2}} \cdot [e_{E5a\text{-}I}(t) + \mathrm{j} \cdot e_{E5a\text{-}Q}(t)] \cdot [sc_{E5\text{-}S}(t) - \mathrm{j} \cdot sc_{E5\text{-}S}(t - T_{s,E5}/4)] + \\ & + \frac{1}{2 \cdot \sqrt{2}} \cdot [e_{E5b\text{-}I}(t) + \mathrm{j} \cdot e_{E5b\text{-}Q}(t)] \cdot [sc_{E5\text{-}S}(t) + \mathrm{j} \cdot sc_{E5\text{-}S}(t - T_{s,E5}/4)] + \\ & + \frac{1}{2 \cdot \sqrt{2}} \cdot [\overline{e}_{E5a\text{-}I}(t) + \mathrm{j} \cdot \overline{e}_{E5a\text{-}Q}(t)] \cdot [sc_{E5\text{-}P}(t) - \mathrm{j} \cdot sc_{E5\text{-}P}(t - T_{s,E5}/4)] + \\ & + \frac{1}{2 \cdot \sqrt{2}} \cdot [\overline{e}_{E5b\text{-}I}(t) + \mathrm{j} \cdot \overline{e}_{E5b\text{-}Q}(t)] \cdot [sc_{E5\text{-}P}(t) + \mathrm{j} \cdot sc_{E5\text{-}P}(t - T_{s,E5}/4)] \end{aligned} \quad (5)$$

dove le due funzioni $sc_{E5\text{-}S}(t)$ e $sc_{E5\text{-}P}(t)$ sono le sotto-portanti ad onda quadra illustrate in precedenza ed il segnale $s_{E5}(t)$ è rappresentato come inviluppo complesso:

I primi due termini dell'Equazione (5) contengono le componenti di segnale $e_{E5a\text{-}I}(t)$, $e_{E5a\text{-}Q}(t)$, $e_{E5b\text{-}I}(t)$ ed $e_{E5b\text{-}Q}(t)$. Ognuna di queste componenti, presenta uno spettro di frequenza con la tipica forma di *sinc*, con la larghezza del lobo principale pari a due volte la frequenza di chip dei codici ($R_C = 10.23\,\mathrm{Mchip/s}$). Questi termini sono moltiplicati per dei termini complessi, ottenuti con la sotto-portante $sc_{E5\text{-}S}(t)$, che sono equivalenti a degli esponenziali complessi. In particolare, i due canali $e_{E5b\text{-}I}(t)$ ed $e_{E5b\text{-}Q}(t)$, nel secondo termine, sono moltiplicati per:

$$sc_{E5\text{-}S}(t) + \mathrm{j} \cdot sc_{E5\text{-}S}\left(t - T_{s,E5}/4\right)$$

Questa espressione può essere interpretata come un "esponenziale complesso", in quanto $sc_{E5\text{-}S}(t)$ assomiglia ad un coseno e $sc_{E5\text{-}S}\left(t - T_{s,E5}/4\right)$ ad un seno: in tal modo si ottiene uno spostamento di frequenza dei due canali $e_{E5b\text{-}I}(t)$ ed $e_{E5b\text{-}Q}(t)$, pari alla frequenza della sotto-portante (15.345 MHz), che vanno a finite proprio nella banda laterale E5b.

Analogamente, nel primo termine dell'Equazione (5), l'esponenziale:

$$sc_{E5\text{-}S}(t) - \mathrm{j} \cdot sc_{E5\text{-}S}\left(t - T_{s,E5}/4\right)$$

opera uno spostamento di frequenza di segno opposto (-15.345 MHz) per i due canali $e_{E5a\text{-}I}(t)$ ed $e_{E5a\text{-}Q}(t)$, che in tal modo vengono trasmessi nella banda laterale E5a.

Lo spettro del segnale modulato $s_{E5}(t)$ è quindi rappresentato in Figura 3, dove è evidente il tipico spettro AltBOC(15,10) con due lobi principali spostati rispettivamente di -15.345 e $+15.345$ MHz rispetto alla frequenza della portante.

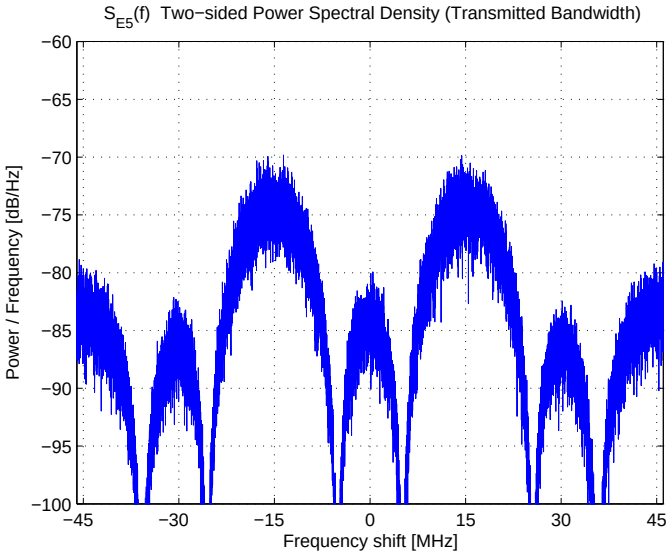

Figura 3: Spettro di frequenza del segnale E5 AltBOC(15,10)

Gli ultimi due termini dell'Equazione (5) contengono i cosiddetti **segnali prodotto**, che sono definiti dalle seguenti espressioni:

$$\overline{e}_{E5a\text{-}I}(t) = e_{E5a\text{-}Q}(t) \cdot e_{E5b\text{-}I}(t) \cdot e_{E5b\text{-}Q}(t) \quad (6)$$

$$\overline{e}_{E5a\text{-}Q}(t) = e_{E5a\text{-}I}(t) \cdot e_{E5b\text{-}I}(t) \cdot e_{E5b\text{-}Q}(t) \quad (7)$$

$$\overline{e}_{E5b\text{-}I}(t) = e_{E5a\text{-}I}(t) \cdot e_{E5a\text{-}Q}(t) \cdot e_{E5b\text{-}Q}(t) \quad (8)$$

$$\overline{e}_{E5b\text{-}Q}(t) = e_{E5a\text{-}I}(t) \cdot e_{E5a\text{-}Q}(t) \cdot e_{E5b\text{-}I}(t) \quad (9)$$

Questi termini sono ottenuti come prodotti tra le quattro componenti di segnale e nell'Equazione (5) vengono moltiplicati per degli esponenziali complessi ottenuti con la sotto-portante $sc_{E5\text{-}P}(t)$, che ha ampiezza minore rispetto alla sotto-portante $sc_{E5\text{-}S}(t)$. La presenza di questi termini nell'espressione della modulazione AltBOC è necessaria per garantire l'inviluppo costante del segnale modulato, come verrà discusso più avanti, a proposito delle caratteristiche del segnale AltBOC.

Va infine notato lo schema di modulazione ad inviluppo costante AltBOC appena presentato risulta abbastanza complicato e richiede la generazione separata di tutte le *componenti di segnale* e dei *segnali prodotto*. Tuttavia,

come notato in alcuni articoli, esiste anche una tecnica semplificata per implementare un generatore di segnali digitali AltBOC, sfruttando una **Look-Up Table** (LUT), ossia una tabella in cui dati in ingresso i quattro canali da trasmettere nella banda E5 viene fornito in uscita il segnale modulato, rappresentato in fase e in quadratura (per maggiori dettagli vedi [4] e [9]). Questa tecnica verrà usata per i generatori di segnali a bordo dei satelliti Galileo e costituisce anche un buon approccio per simulare in modo veloce ed efficiente i segnali AltBOC[2].

Caratteristiche del segnale AltBOC

Le modulazioni e gli schemi di multiplazione che verranno utilizzati nel sistema Galileo sono il risultato di un'attenta scelta, volta ad ottenere ottime prestazioni per quanto riguarda i satelliti ed i futuri ricevitori, garantendo allo stesso tempo una interoperabilità tra il sistema Galileo e il GPS e riducendo al minimo le interferenze tra i due sistemi.

Per quanto riguarda la modulazione AltBOC, che verrà utilizzata nella banda E5, si può dire che essa è il risultato di un processo di ottimizzazione ed un compromesso tra diverse esigenze. In particolare, essa presenta i seguenti vantaggi:

- una semplificazione del generatore di segnale a bordo dei satelliti, dato che un singolo modulatore AltBOC genererà l'intero segnale a banda larga E5, senza dover usare due distinti modulatori QPSK per le due bande laterali E5a ed E5b;
- gli amplificatori a bordo dei satelliti, che tipicamente lavorano in saturazione, potranno essere sfruttati in modo efficiente, dato che il segnale AltBOC presenta inviluppo costante;
- un'ottimizzazione dell'architettura dei ricevitori, che con il segnale AltBOC potranno demodulare contemporaneamente i dati di navigazione trasmessi nelle due bande laterali E5a ed E5b;
- un miglioramento delle prestazioni dei ricevitori in presenza di rumore e cammini multipli, grazie alle caratteristiche del segnale AltBOC (banda larga e funzione di correlazione ripida).

Le caratteristiche più interessanti del segnale AltBOC sono quindi elencate e discusse nelle seguenti sezioni.

[2]Le simulazioni necessarie per questa tesi sono state svolte implementando in linguaggio C e MATLAB® sia un generatore di segnali AltBOC basato su una LUT, sia un generatore meno efficiente, basato sulle equazioni presentate in precedenza, che ha però il vantaggio di essere più flessibile e permette di generare anche solo singole componenti del segnale.

• Inviluppo costante e transizioni alternative

Il segnale AltBOC per la banda E5 presenta un **inviluppo costante**. Infatti l'inviluppo del segnale modulato $s_{E5}(t)$ è simile ad una costellazione 8-PSK, con qualche piccola differenza, come rappresentato in Figura 4. Va notato che i punti della costellazione di segnale giacciono su un cerchio, come nel caso di un segnale 8-PSK, ed hanno tutti energia unitaria, ma questo è valido solo se si considera una banda infinita sia per il trasmettitore a bordo del satellite, sia per il ricevitore[3].

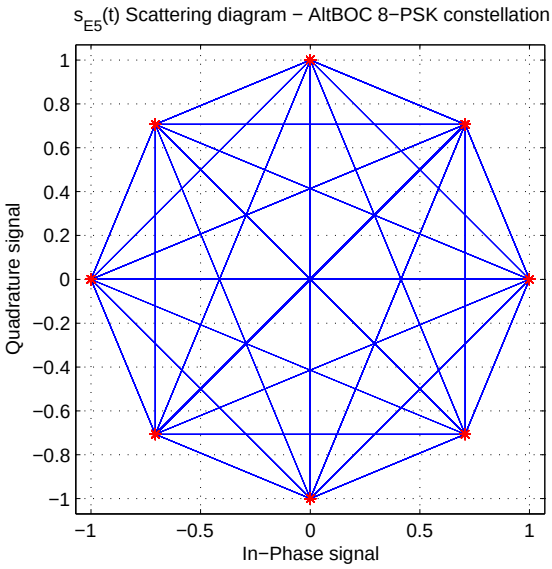

Figura 4: Diagramma scattering del segnale E5 AltBOC(15,10)

La principale differenza rispetto ad un segnale 8-PSK sono le **transizioni alternative**, evidenti nel diagramma *scattering* (linee tra gli 8 punti della costellazione). Studiando con opportune simulazioni l'evoluzione nel tempo del segnale AltBOC, si è visto che le transizioni da un punto all'altro della costellazione avvengono non lungo il cerchio unitario, ma con oscillazioni alternative tra i vari punti, che sono dovute alle sotto-portanti e alle transizioni dei chip dei codici usati nella modulazione AltBOC. In particolare, va notato che per il segnale AltBOC(15,10), date le frequenze delle sotto-portanti e dei codici, nella durata di un chip di codice è presente un periodo e mezzo di sotto-portante ($T_{C,E5} = 1.5 \cdot T_{S,E5}$). Quindi, durante un tempo di un chip (fissati i quattro chip di codice trasmessi ad un certo istante di tempo dai quattro canali) le sotto-portanti presenti nell'espressione del segnale AltBOC

[3]Considerando una banda realistica (ad esempio 51.150 MHz), il segnale AltBOC risulta leggermente distorto e l'inviluppo diventa *quasi costante*. Questo effetto però è trascurabile, considerando una banda sufficientemente ampia, dunque di seguito si assume un inviluppo costante per il segnale AltBOC.

causano dei cambi alternativi di posizione nel diagramma scattering, spostando il segnale da un punto della costellazione al suo opposto. Alla fine del tempo di chip si verifica un'altra transizione: i nuovi chip di codice trasmessi nei quattro canali implicano una nuova posizione nella costellazione, scegliendo fra una delle otto possibili. Dopo questo, nel successivo tempo di chip le sotto-portanti producono di nuovo un movimento alternato, partendo dalla nuova posizione.

In conclusione si può affermare che nel diagramma scattering le transizioni alternative che attraversano lo zero (orizzontali, verticali e diagonali) sono dovute alle sotto-portanti, mentre tutte le altre transizioni sono causate dai cambiamenti nei chip di codice trasmessi.

• Segnali prodotto nell'espressione del segnale AltBOC

Un'altra caratteristica che distingue la modulazione E5 AltBOC(15,10) da altri schemi di modulazione sono i **segnali prodotto**. La presenza di queste componenti nell'espressione della modulazione AltBOC, presentata prima nell'Equazione (5), distingue la modulazione che verrà usata nella banda E5 di Galileo dalla cosiddetta *Standard AltBOC* (vedi [10]). Quest'ultima modulazione è caratterizzata un inviluppo non costante e rappresenta lo schema di partenza da cui è stato derivata la modulazione E5 AltBOC: nella *Standard AltBOC* non sono presenti i segnali prodotto (ci sono solo le quattro *componenti di segnale*) e le sotto-portanti sono delle semplici onde quadre. Quindi i segnali prodotto nell'espressione dell'E5 AltBOC sono indispensabili per ottenere una costellazione ad inviluppo costante.

I segnali prodotto possono anche essere spiegati come **prodotti di intermodulazione** (vedi [12]). Come accennato in precedenza, la modulazione AltBOC è una tecnica di multiplazione che permette di trasmettere quattro canali nelle due bande laterali E5a ed E5b, senza il bisogno di usare due separati modulatori QPSK (uno per ogni banda). Quindi i segnali prodotto possono essere interpretati come prodotti di intermodulazione, che devono essere aggiunti all'espressione della *Standard AltBOC* per ottenere un segnale ad inviluppo costante, analogo a quello che si otterrebbe con due modulatori QPSK separati per le due bande laterali E5a ed E5b.

• Sotto-portanti ad onda quadra multi-livello

Come descritto in precedenza, per la modulazione E5 AltBOC sono necessarie le due funzioni $sc_{E5\text{-}S}(t)$ e $sc_{E5\text{-}P}(t)$, che sono delle sotto-portanti ad onda quadra su 4 livelli. Questa caratteristica può essere spiegata considerando che in letteratura (vedi [10]) sono proposte diverse varianti della modulazione AltBOC, che usano sotto-portanti multi-livello per ridurre l'energia trasmessa nei lobi secondari dello spettro di frequenza del segnale. Questa tecnica è

basata sull'idea di arrotondare la forma d'onda delle sotto-portanti, rimpiazzando una semplice onda quadra con delle forme d'onda a 3 o più livelli: in questo modo si riduce il livello delle armoniche indesiderate, lasciando intatti i lobi principali (E5a ed E5b) dello spettro del segnale.

La modulazione E5 AltBOC può quindi essere spiegata come il risultato di un processo di **ottimizzazione**, che ha avuto come punto di partenza lo schema di modulazione *Standard AltBOC*. Le semplici sotto-portanti ad onda quadra di questa modulazione sono state sostituite con la funzione $sc_{E5\text{-}S}(t)$, che equivale ad un coseno campionato su 4 livelli, ottenendo una riduzione dei lobi secondari dello spettro. Successivamente è stato necessario aggiungere i segnali prodotto, con la sotto-portante $sc_{E5\text{-}P}(t)$, per ottenere una costellazione ad inviluppo costante (come spiegato nella precedente sezione). Ma l'introduzione di queste componenti aggiuntive causa un peggioramento dei lobi secondari. Tuttavia, il risultato finale non è peggiore rispetto ai lobi secondari che si avevano con la modulazione *Standard AltBOC*.

In conclusione, la modulazione per la banda E5 di Galileo è stata ottimizzata, partendo dalla *Standard AltBOC*, in modo da ottenere un segnale ad inviluppo costante, senza degradare le proprietà spettrali della *Standard AltBOC*.

• Proprietà di correlazione

Le ultime caratteristiche della modulazione E5 AltBOC che verranno discusse sono le proprietà di correlazione, che possono essere sfruttate dai ricevitori per il *tracking* del segnale ricevuto.

Come discusso in precedenza, il segnale modulato $s_{E5}(t)$ contiene i quattro canali $e_{E5a\text{-}I}(t)$, $e_{E5a\text{-}Q}(t)$, $e_{E5b\text{-}I}(t)$ ed $e_{E5b\text{-}Q}(t)$. Nell'articolo [11] è proposta una tecnica che permette di eseguire un tracking coerente dei due canali pilota $e_{E5a\text{-}Q}(t)$ ed $e_{E5b\text{-}Q}(t)$, sfruttando le caratteristiche di correlazione del segnale AltBOC e la quasi-ortogonalità dei codici, e quindi di demodulare i dati di navigazione contenuti negli altri due canali $e_{E5a\text{-}I}(t)$ ed $e_{E5b\text{-}I}(t)$. Infatti, il sincronismo recuperato dal ricevitore inseguendo i due canali pilota può essere usato per demodulare anche i canali dati, visto che i quattro canali sono trasmessi sincroni tra loro. Inoltre il tracking basato sui canali pilota risulta più semplice e robusto, perché nel processo di correlazione non è richiesta la rimozione dei bit con i dati di navigazione.

In generale ogni canale del segnale nella banda E5 può essere demodulato correlando il segnale complesso $s_{E5}(t)$ con un segnale complesso generato localmente, che contiene la sequenza di codice PRN del canale desiderato moltiplicata per un esponenziale complesso, costruito usando la sotto-portante $sc_{E5\text{-}S}$. In questo modo è possibile definire una **funzione di correlazione complessa per una banda laterale**, ad esempio sfruttando il canale *E5a-Q*:

$$\mathcal{C}_{E5a\text{-}Q}(\tau) = \int_0^{T_{int}} s_{E5}(t) \cdot g_{E5a\text{-}Q}(t-\tau)\, dt \tag{10}$$

dove:

- $s_{E5}(t)$ è il segnale ricevuto, espresso come inviluppo complesso in banda base:
$$s_{E5}(t) = s_{E5\mathbf{I}}(t) + \mathrm{j} \cdot s_{E5\mathbf{Q}}(t)$$
- $g_{E5a\text{-}Q}(t)$ è il segnale complesso generato localmente. In particolare, esso corrisponde al complesso coniugato del termine per la componente $e_{E5a\text{-}Q}(t)$ per il segnale AltBOC, nella Equazione (5) illustrata in precedenza:
$$g_{E5a\text{-}Q}(t) = e_{E5a\text{-}Q}(t) \cdot \left[sc_{E5\text{-}S}\left(t - \frac{T_{s,E5}}{4}\right) - \mathrm{j} \cdot sc_{E5\text{-}S}(t) \right]$$
- τ è il ritardo relativo tra il segnale ricevuto $s_{E5}(t)$ e il segnale locale $g_{E5a\text{-}Q}(t)$;
- T_{int} è il cosiddetto *tempo di integrazione* (tipicamente 1 ms).

In modo analogo, considerando l'altro canale pilota (*E5b-Q*), si può definire la seguente **funzione di correlazione complessa per la banda laterale E5b**:

$$\mathcal{C}_{E5b\text{-}Q}(\tau) = \int_0^{T_{int}} s_{E5}(t) \cdot g_{E5b\text{-}Q}(t-\tau)\, dt \tag{11}$$

$$\text{dove} \qquad g_{E5b\text{-}Q}(t) = e_{E5b\text{-}Q}(t) \cdot \left[-sc_{E5\text{-}S}\left(t - \frac{T_{s,E5}}{4}\right) - \mathrm{j} \cdot sc_{E5\text{-}S}(t) \right]$$

Va notato che le due funzioni di correlazione $\mathcal{C}_{E5a\text{-}Q}(\tau)$ e $\mathcal{C}_{E5b\text{-}Q}(\tau)$ sono delle funzioni complesse, con una parte reale e una parte immaginaria. Risulta quindi difficile sfruttare separatamente queste due funzioni per il tracking. Esse diventano però utili se vengono sommate tra loro, definendo la **funzione di correlazione complessa combinata**:

$$\mathcal{C}_{\mathbf{E5Q}}(\tau) = \mathcal{C}_{E5a\text{-}Q}(\tau) + \mathcal{C}_{E5b\text{-}Q}(\tau) \tag{12}$$

Questa funzione di correlazione è stata simulata[4] ed il risultato ottenuto è disegnato in Figura 5.

L'importanza di questa funzione di correlazione è legata al fatto che in questo modo le due parti immaginarie delle funzioni $\mathcal{C}_{E5a\text{-}Q}(\tau)$ e $\mathcal{C}_{E5b\text{-}Q}(\tau)$ si annullano, mentre le parti reali si combinano in modo coerente. Si ottiene così

[4] La simulazione è stata condotta generando il segnale *E5 AltBOC(15,10)*, sovracampionato con 16 campioni per periodo di sotto-portante, ovvero 24 campioni per chip di codice, e considerando una banda infinita (senza applicare un filtraggio). Il segnale è stato correlato con un segnale locale, usando un tempo di integrazione $T_{int} = 1$ ms (pari a 1 periodo del codice primario) e normalizzando in risultato in modo che il picco di correlazione fosse pari a 1.

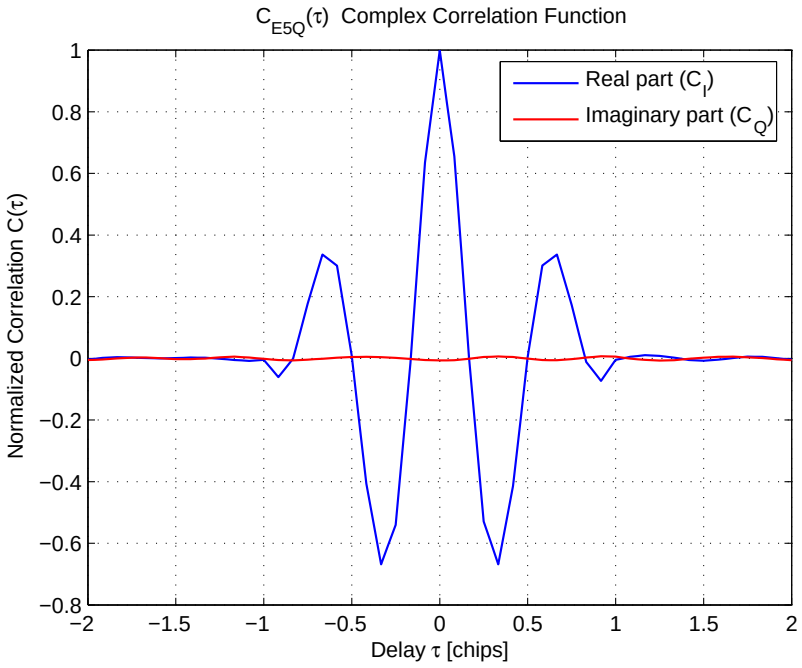

Figura 5: Funzione di correlazione complessa combinata $\mathcal{C}_{\mathbf{E5Q}}(\tau)$

la funzione $\mathcal{C}_{\mathbf{E5Q}}(\tau)$, che è una funzione reale con un picco ripido ed alcune oscillazioni decrescenti. Questa funzione di correlazione è simile a quella che sarebbe possibile ottenere con una modulazione BOC(15,10) trasmessa sull'intera banda E5, però il picco principale è più ripido con l'AltBOC: questo implica delle migliori prestazioni per il ricevitore, giustificando quindi l'impiego della modulazione AltBOC per la banda E5.

Inoltre, come evidenziato in Figura 5, la parte immaginaria di $\mathcal{C}_{\mathbf{E5Q}}(\tau)$ è praticamente nulla, ma questo è valido solo che il ricevitore è correttamente sincronizzato (PLL e DLL correttamente agganciati al segnale ricevuto). Quindi la parte immaginaria di $\mathcal{C}_{\mathbf{E5Q}}(\tau)$ può essere usata per individuare eventuali errori nella fase di tracking: se non è nulla, significa che il segnale locale non è sincrono con quello ricevuto.

Va infine notato che le Equazioni (10), (11) e (12) sono soltanto delle espressioni analitiche, con segnali a tempo continuo. Per studiare e simulare l'architettura di un ricevitore AltBOC è stato necessario implementare tali formule con segnali a tempo discreto, sfruttando degli accorgimenti per ridurre la complessità di calcolo. In particolare va considerato che per implementare ogni operazione di correlazione complessa, eseguita tra due segnali complessi (il segnale ricevuto e il segnale locale), sono necessari 4 correlatori reali, per calcolare la parte reale e la parte immaginaria della funzione di correlazione (per maggiori dettagli si veda il testo completo della tesi). Le diverse possibili architetture per i ricevitori AltBOC sono quindi discusse di seguito, analizzando le loro prestazioni e la complessità implementativa.

Architetture per ricevitori AltBOC

La ricezione del segnale a banda larga AltBOC implica considerevoli difficoltà per i futuri ricevitori, principalmente per due ragioni:

- per elaborare correttamente il segnale AltBOC(15,10), l'intera banda E5 deve essere ricevuta, spostando il segnale in banda base con un'unica catena a radiofrequenza e a frequenza intermedia (RF/IF). La banda minima necessaria per il ricevitore è circa 50 MHz (considerando solo i due lobi principali E5a ed E5b). Questo implica una frequenza di campionamento ed una frequenza di clock più alte di quelle attualmente usate nei ricevitori GPS;
- l'elaborazione digitale dei segnali risulta alquanto complicata, per la natura complessa del segnale AltBOC in banda base.

Alcune differenti architetture sono quindi ipotizzabili per i ricevitori AltBOC, a seconda del tipo di correlatori usati e della capacità del ricevitore di elaborare una singola banda laterale (E5a oppure E5b) o di lavorare in una modalità a doppia banda in modo coerente. In particolare, le future architetture per ricevitori AltBOC possono essere classificate nelle seguenti tre categorie:

1. **ricevitore a banda singola**,
2. **ricevitore non coerente a due bande**,
3. **ricevitore coerente a due bande**.

Di seguito queste tre architetture sono presentate e discusse in dettaglio, analizzando le loro prestazioni e la complessità implementativa. Per facilitare la comprensione, il funzionamento di questi tre ricevitori è discusso solo per la fase di *tracking* del segnale, mentre la fase di acquisizione è considerata più avanti. Inoltre, nella tesi sono presentati e discussi anche altri tre schemi di ricevitore:

- un ricevitore AltBOC coperto da una brevetto (vedi [13]);
- un ricevitore basato sull'*Offset-Carrier Single Side Band Tracking* [8];
- un'architettura innovativa, basata su un *correlatore-discriminatore*.

In pratica questi tre ricevitori appaiono simili al *ricevitore coerente a due bande*: i primi due presentano solo piccole differenze implementative rispetto al ricevitore coerente a due bande, ma hanno prestazioni leggermente inferiori, quindi non vengono riportati in questo sommario.

Invece, il ricevitore con il *correlatore-discriminatore* presenta un'architettura innovativa, proposta per la prima volta in questa tesi per il segnale AltBOC. Infatti esso può essere considerato come una variante del ricevitore coerente a due bande, ma con sostanziali differenze per quanto riguarda il suo funzionamento e l'*hardware* necessario.

• Ricevitore a banda singola

Questa architettura, conosciuta anche come *Central-Carrier Single Side Band Tracking* (CC SSB [8]), è il più semplice schema che si può usare per ricevere i segnali della banda E5 del sistema Galileo. Lo schema a blocchi di questo ricevitore è presentato in Figura 6.

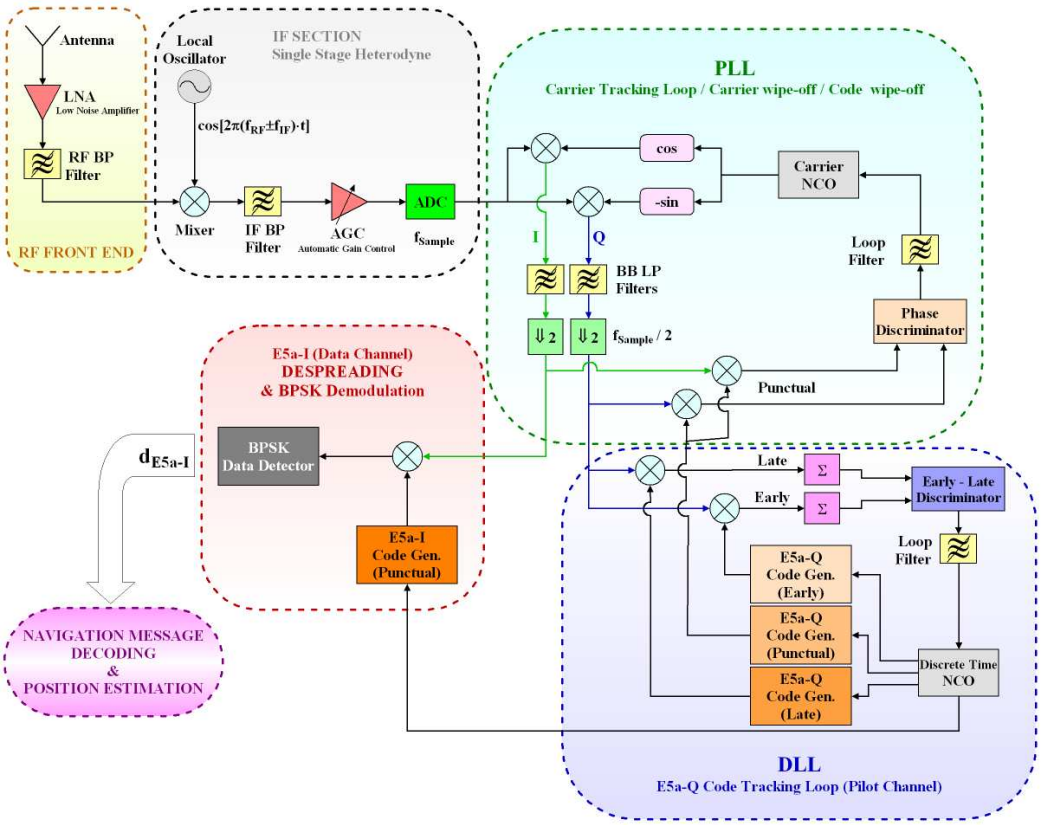

Figura 6: Schema a blocchi dell'architettura di un ricevitore a banda singola

Il suo funzionamento è basato sulla ricezione di una singola banda laterale (ad esempio E5a) del segnale nella banda E5 del sistema Galileo, che viene elaborata come una semplice modulazione QPSK. Infatti, ogni lobo dello spettro del segnale AltBOC contiene un canale dati (che è un segnale BPSK) ed un canale pilota (un altro segnale BPSK), trasmessi in quadratura. Complessivamente il ricevitore a banda singola non ha una architettura molto diversa da quella di un comune ricevitore GPS, in quanto il segnale ricevuto viene trattato considerandolo come due modulazioni BPSK disposte in quadratura: la prima corrisponde al canale pilota (*E5a-Q*), che viene sfruttato per sincronizzare i codici locali, mentre la seconda (*E5a-I*) viene demodulata per estrarre i dati di navigazione.

In particolare, se si sceglie di ricevere solo la banda E5a, il ricevitore deve eseguire il tracking del segnale inseguendo con il PLL (*Phase Locked Loop*) la frequenza centrale della banda laterale (1176.45 MHz) e selezionando solo

il segnale di questa banda, con un filtraggio a banda stretta (circa 20 MHz, per ricevere solo il lobo principale nella banda E5a). Il DLL (*Delay Locked Loop*) del ricevitore funziona inseguendo il canale pilota (*E5a-Q*) presente nel segnale ricevuto, sfruttando le ben note tecniche di correlazione utilizzate negli attuali ricevitori GPS. Il sincronismo di chip recuperato dal DLL viene quindi usato per demodulare i dati di navigazione dal canale dati (*E5a-I*).

Va notato che, siccome viene sfruttato un canale pilota in cui il codice PRN non è modulato con dei dati (non ci sono salti di fase di 180°) per eseguire il tracking dei segnali ricevuti, nel PLL si può usare un discriminatore ad *arcotangente su quattro quadranti* (questa configurazione è detta a 360°) invece del discriminatore *Costas* che viene tipicamente usato nei ricevitori GPS (come affermato in [14]). Questo implica un netto miglioramento delle prestazioni del ricevitore.

Considerando la ricezione del segnale AltBOC, il ricevitore a banda singola rappresenta l'architettura più semplice che può essere usata, in quanto richiede tecniche di elaborazione dei segnali e componenti hardware non molto diverse da quelle usate nei comuni ricevitori GPS (segnali BPSK). L'hardware e la capacità di calcolo richiesta è vantaggiosa rispetto alle altre architetture illustrate di seguito, dato che è necessario ricevere ed elaborare solo una banda laterale del segnale AltBOC, non l'intera banda E5: la frequenza di campionamento e la larghezza di banda per le sezioni analogiche e digitali del ricevitore sono più basse. Tuttavia questa architettura presenta prestazioni inferiori rispetto agli altri ricevitori in presenza di rumore, cammini multipli ed altre tipiche cause di errore.

In conclusione questa architettura a banda singola è adatta solo per ricevitori semplici ed a basso costo, che non raggiungono elevate precisioni nella stima di posizione.

• Ricevitore non coerente a due bande

L'architettura del *ricevitore non coerente a due bande* è un'estensione dell'architettura a banda singola, ottenuta duplicando i blocchi funzionali dopo il front-end a radiofrequenza. In questo modo è possibile ricevere separatamente (in modo non coerente) le due bande laterali E5a ed E5b, ricuperando i dati trasmessi in entrambi i canali dati della banda E5. Lo schema a blocchi di questo ricevitore è presentato in Figura 7.

I singoli blocchi funzionali nello schema di questo ricevitore sono praticamente uguali a quelli usati nella precedente architettura e svolgono funzioni analoghe. L'unica differenza riguarda il front-end a RF, perché in questo caso le componenti di questo blocco devono essere in grado di ricevere l'intera banda E5, non solo una banda laterale.

Elaborando entrambe le bande laterali E5a ed E5b, questo ricevitore è in grado di raggiungere migliori prestazioni nella stima di posizione rispetto al

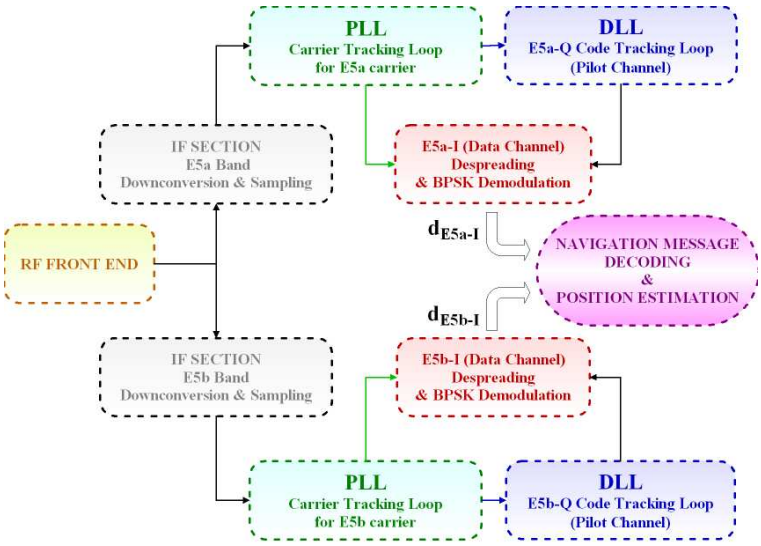

Figura 7: Schema a blocchi del ricevitore non coerente a due bande

ricevitore a banda singola. Infatti è possibile calcolare una stima di posizione combinata, ottenuta mediando le *pseudo-distanze* misurate con le due bande. Inoltre, dato che il ricevitore elabora due segnali a frequenze diverse, è anche possibile stimare e correggere l'errore ionosferico (che causa ritardi diversi per segnali a frequenza diversa).

In conclusione, questa architettura permette un miglioramento di prestazioni rispetto al ricevitore a banda singola, però è la più costosa perché usa il doppio di componenti hardware (in particolare si usano due PLL e due DLL).

• Ricevitore coerente a due bande

Il ricevitore coerente a due bande è un'architettura in grado di sfruttare appieno i vantaggi del segnale a banda larga AltBOC, ottenendo prestazioni decisamente migliori rispetto ai precedenti ricevitori. Per la sua implementazione è però necessario usare un hardware diverso, come si vede nel suo schema a blocchi in Figura 8.

Le principali differenze di questa architettura rispetto a quelle precedenti sono evidenti nel DLL (*Delay Locked Loop*) e nel blocco di *despreading* e demodulazione del ricevitore.

Il DLL funziona in modo simile rispetto agli schemi precedenti: in questo caso il classico schema con discriminatore *Early-Late* viene sfruttato per il tracking dei due canali pilota (*E5a-Q* and *E5b-Q*). La principale differenza è legata al fatto che le tre operazioni di correlazione necessarie per i canali *Early*, *Punctual* e *Late* in questo caso sono svolte da tre **correlatori complessi**, mentre nelle precedenti architetture le operazioni di correlazione erano eseguite sfruttando dei semplici moltiplicatori, seguiti da degli accumulatori.

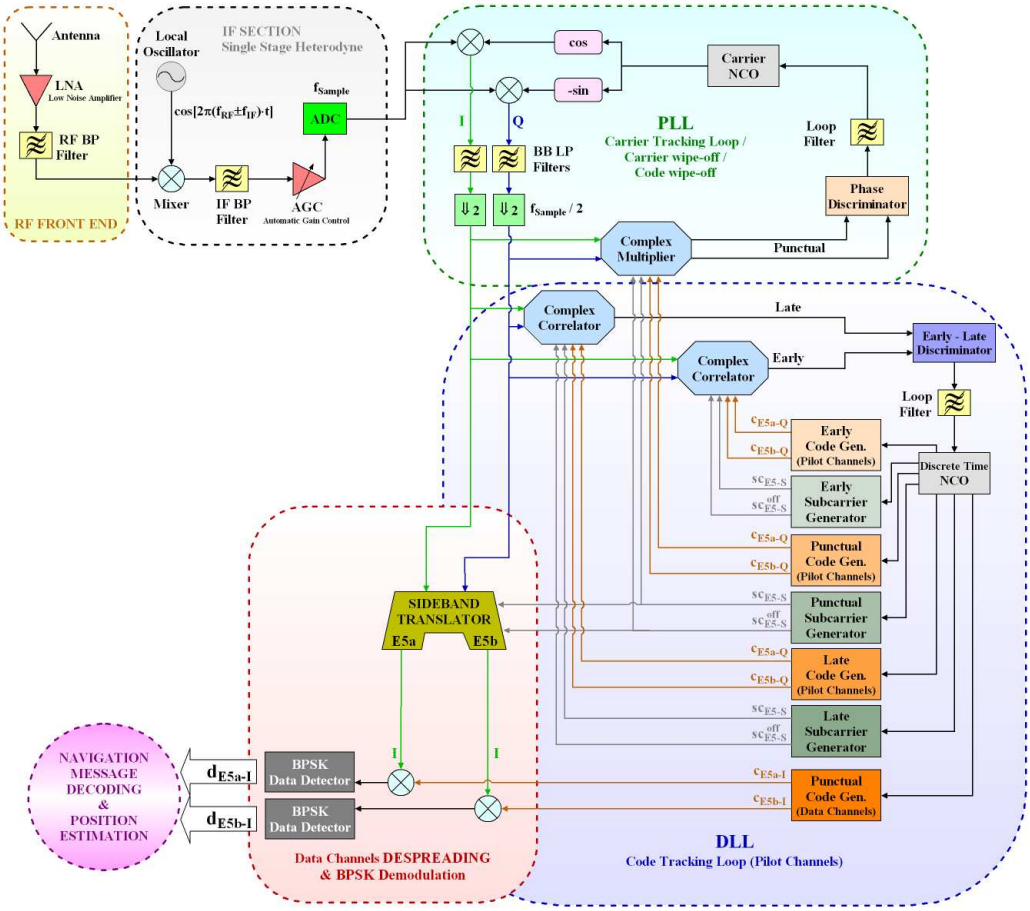

Figura 8: Schema a blocchi del ricevitore coerente a due bande

Ogni correlatore complesso è un blocco che è stato studiato nel dettaglio nel corso di questa tesi, implementando in modo efficiente (con un significativo risparmio computazionale) le operazioni necessarie per calcolare la *funzione di correlazione complessa combinata* (presentata in precedenza) nel dominio a tempo discreto, ossia con segnali campionati.

In particolare va notato che ogni correlatore complesso ha in ingresso due segnali complessi. Il primo è il segnale ricevuto, scomposto nel ramo in fase ($s_{E5\mathbf{I}}$) e in quadratura ($s_{E5\mathbf{Q}}$), mentre il secondo è un segnale locale con la giusta temporizzazione, formato da quattro componenti: i due codici pilota ($c_{E5a\text{-}Q}$ e $c_{E5b\text{-}Q}$), i campioni della sotto-portante $sc_{E5\text{-}S}(t)$ e la sua versione ritardata $sc_{E5\text{-}S}\left(t - T_{s,E5}/4\right)$, indicate rispettivamente come $sc_{E5\text{-}S}$ e $sc^{off}_{E5\text{-}S}$ nello schema in Figura 8. Per il DLL sono quindi necessari tre generatori di codice e tre generatori per le sotto-portanti, controllati dall'NCO per generare i segnali locali con le corrette temporizzazioni (*Early*, *Punctual* e *Late*). Va notato che i **generatori delle sotto-portanti** non sono presenti nelle precedenti architetture e sono dei componenti addizionali richiesti per questo ricevitore.

Il blocco di despreading e demodulazione del ricevitore coerente a due bande invece si distingue da quello dei precedenti ricevitori per la presenza del cosiddetto **sideband translator** (che può essere tradotto in italiano come *traslatore delle bande laterali*). Questo blocco è un componente innovativo, introdotto e descritto per la prima volta in questa tesi, per cui si sta valutando la possibilità di un brevetto. Esso si basa sull'idea di estrarre i dati di navigazione contenuti nel segnale a banda larga AltBOC eseguendo una traslazione in frequenza delle due bande laterali, in modo da recuperare separatamente i due canali dati (*E5a-I* e *E5b-I*). Sui segnali all'uscita del sideband translator è poi necessario eseguire il despreading con i codici per i canali dati ($c_{E5a\text{-}I}$ e $c_{E5b\text{-}I}$), generati localmente da un generatore di codice addizionale (quindi complessivamente l'NCO del DLL deve controllare quattro generatori di codice). A questo punto, i dati di navigazione possono essere facilmente demodulati come semplici segnali BPSK.

Il principale vantaggio del ricevitore coerente a due bande è costituito dalla sue migliori prestazioni in presenza di rumore, cammini multipli e altre tipiche cause di errore, rispetto alle precedenti architetture. Questo è motivato dal fatto che con questa architettura si sfruttano al meglio le proprietà di correlazione del segnale AltBOC, calcolando la *funzione di correlazione complessa combinata*, mentre con i precedenti ricevitori, che lavorano con semplici segnali BPSK, la funzione di correlazione ha la tipica forma triangolare: il picco centrale della funzione di correlazione ottenuta con il ricevitore coerente a due bande è più stretto e ripido e comporta quindi migliori prestazioni.

L'architettura coerente a due bande ha però lo svantaggio di una maggiore complessità implementativa, dato che sono richiesti nuovi blocchi funzionali (correlatori complessi, generatori delle sotto-portanti e sideband translator) che non sono presenti negli attuali ricevitori GPS. Inoltre esso richiede una frequenza di campionamento più elevata ed una banda più larga per tutti i suoi componenti, dato che l'intera banda E5 del sistema Galileo deve essere ricevuta.

• Ricevitore innovativo (con correlatore-discriminatore)

Il ricevitore con il correlatore-discriminatore è un'architettura innovativa, che può anche essere considerata come una variante del precedente ricevitore coerente a due bande. Attualmente questo ricevitore, schematizzato in Figura 9, non è trattato in nessun articolo presente in letteratura per il segnale AltBOC ed è proposto e discusso in questa tesi per la prima volta.

La principale differenza tra questa architettura e le precedenti è la presenza di un **correlatore modificato**, a cui si è dato il nome di *correlatore-discriminatore*. Esso è in grado di calcolare direttamente una funzione di discriminazione, senza bisogno di usare due o più correlatori (*Early* e *Late*) e un blocco di discriminazione, come nelle precedenti architetture. In questo

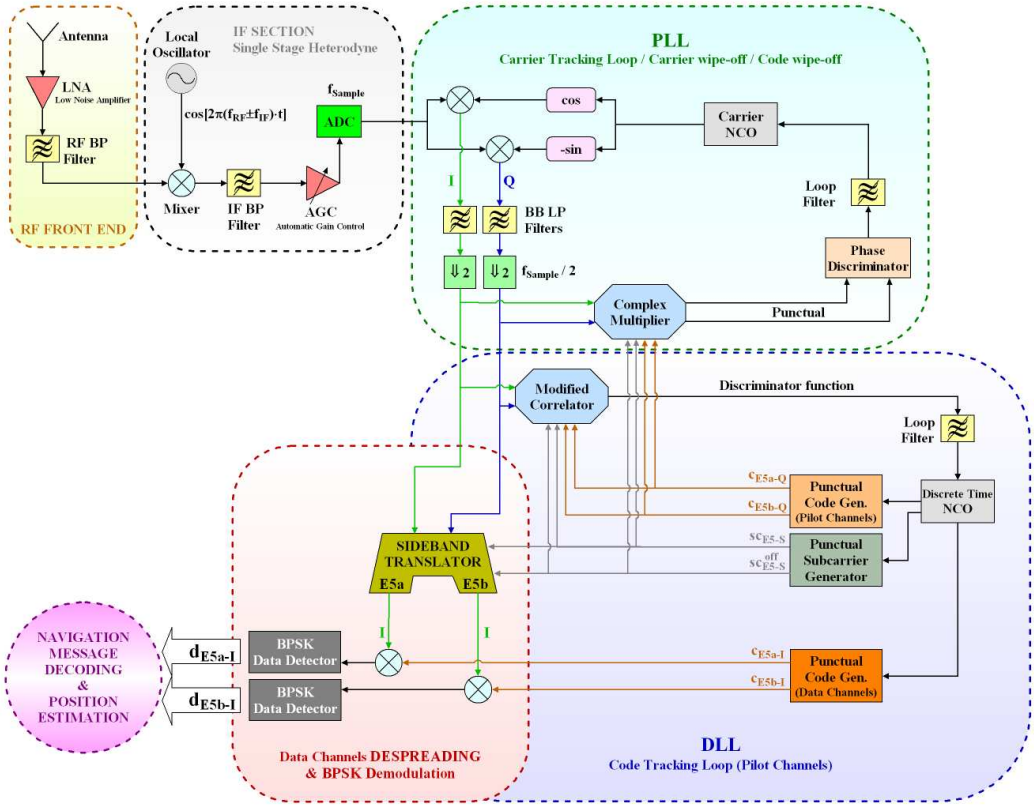

Figura 9: Schema a blocchi del ricevitore innovativo con il correlatore-discriminatore

modo si ottiene un considerevole risparmio di risorse hardware e software: infatti si usa solo un correlatore modificato, invece di due correlatori e un discriminatore, ed anche la generazione dei segnali locali è più semplice, dato che solo i codici e le sotto-portanti puntuali (*Punctual*) sono necessarie.

L'idea di usare un correlatore modificato, proposta inizialmente nell'articolo [15] per i segnali BOC(n,n) del sistema Galileo, è stata adattata in questa tesi anche per la ricezione di segnali AltBOC, tenendo conto ovviamente delle difficoltà di implementazione legate alla complessità del segnale AltBOC. Una trattazione dettagliata, con la derivazione analitica della funzione di discriminazione all'uscita del correlatore modificato, è riportata solo nel testo della tesi in quando esula i limiti di spazio di questo sommario. Va comunque notato che la funzione di discriminazione ottenuta con questa architettura ha una forma particolarmente ripida nel punto usato dal DLL per il tracking e questo permette di prevedere delle buone prestazioni.

Il ricevitore innovativo con il correlatore-discriminatore è quindi un'architettura interessante, dato che presenta considerevoli vantaggi per quanto riguarda l'hardware necessario. Nel seguito di questa tesi le prestazioni di questo ricevitore sono state valuate e confrontate con quelle degli altri ricevitori, in particolare in presenza di errori dovuti ai cammini multipli.

Strategie di acquisizione per il segnale AltBOC

Nelle precedenti sezioni gli schemi delle architetture per i ricevitori AltBOC sono stati proposti e discussi considerando solo il funzionamento nella fase di *tracking* del segnale. Ma prima di ricevere e demodulare il segnale, stimando la distanza da quattro o più satelliti, il ricevitore deve eseguire le operazioni necessarie per l'**acquisizione** dei segnali dei vari satelliti, in modo analogo a quanto viene fatto dai comuni ricevitori GPS.

Il processo di acquisizione ha lo scopo di stimare il ritardo del codice e lo spostamento di frequenza *Doppler* del segnale ricevuto da ogni satellite: una ricerca bi-dimensionale nel dominio del tempo (ritardo del codice Θ) e nel dominio della frequenza (spostamento Doppler $f_{Doppler}$) deve essere eseguita per acquisire il segnale proveniente da un satellite, usando una soglia di decisione per stimare i due parametri incogniti (Θ e $f_{Doppler}$). Appena il ricevitore ottiene una stima di questi due parametri con una sufficiente precisione, il processo di tracking può iniziare.

Sebbene le tecniche di acquisizione siano discusse in dettaglio in molti articoli per i segnali del sistema GPS e per le modulazioni BOC, per quanto riguarda i segnali nella banda E5 di Galileo sono stati pubblicati solo pochi articoli, dove solo alcune architetture del ricevitore sono considerate (tipicamente si considerano solo schemi a banda singola). Perciò in questa tesi è presente uno studio completo delle strategie di acquisizione adatte al segnale AltBOC e sono evidenziate le differenze tra le tecniche convenzionali usate nei ricevitori GPS e quelle che possono essere usate per i ricevitori AltBOC illustrati in precedenza.

Considerando le condizioni operative di un ricevitore di un sistema di navigazione satellitare, due tipiche situazioni si possono verificare per le procedure di acquisizione:

- la condizione di **cold start**, che si verifica quando il ricevitore non è in possesso di nessuna informazione riguardo alla sua posizione e a quella dei satelliti. In questo caso una ricerca completa di tutti i satelliti della costellazione Galileo deve essere eseguita, provando per ogni satellite tutti le possibili frequenze Doppler e tutti i possibili ritardi di codice;
- la condizione di **warm start**, che si presenta invece quando il ricevitore possiede alcune conoscenze a priori, sulla sua posizione, su quella dei satelliti o sull'ora esatta. In questo caso la ricerca necessaria per l'acquisizione è più veloce, dato che solo un limitato numero di satelliti deve essere cercato.

Per semplicità, nella seguente discussione si assume una situazione di *cold start*, in cui un ricevitore AltBOC debba acquisire un singolo satellite del sistema Galileo. Lo spazio di ricerca è quindi bi-dimensionale (tempo-frequenza)

e le due incognite (Θ e $f_{Doppler}$) possono essere stimate con tecniche di acquisizione simili a quelle usate nei ricevitori GPS: lo spazio di ricerca è suddiviso secondo una griglia con una certa risoluzione ($\Delta\Theta$ e Δf) ed ogni cella della griglia viene analizzata, calcolando la correlazione tra il segnale ricevuto e un segnale locale, generato con la fase del codice e lo spostamento Doppler corrispondenti alla cella. Quando si verifica un picco di correlazione, il cui valore supera una certa soglia, la cella analizzata è quella corretta e il ricevitore ha in questo modo acquisito il segnale del satellite.

• Tecniche di acquisizione adatte al segnale AltBOC

Per quanto riguarda l'acquisizione del segnale AltBOC, è necessario prestare particolare attenzione al modo con cui viene calcolata la funzione di correlazione dal ricevitore. Come accennato in precedenza infatti le architetture per i ricevitori AltBOC possono sfruttare due tipi di funzione di correlazione per il tracking dei codici:

- una semplice **funzione di correlazione triangolare**, per i ricevitori che si basano sull'elaborazione di semplici segnali BPSK, ossia il *ricevitore a banda singola* ed il *ricevitore non coerente a due bande*;
- la **funzione di correlazione complessa combinata** del segnale AltBOC, che viene sfruttata dal *ricevitore coerente a due bande* ed dal *ricevitore con il correlatore-discriminatore* (però con alcune modifiche).

Nel primo caso le tecniche convenzionalmente usate nei ricevitori GPS possono essere usate per acquisire la funzione di correlazione triangolare: essa è una funzione semplice ed il suo picco può essere facilmente stimato, ottenendo un risultato non ambiguo.

Invece, nel secondo caso, la funzione di correlazione del segnale AltBOC presenta una forma oscillante, con molteplici picchi: in presenza di rumore o di cammini multipli può risultare difficile distinguere il picco corretto e si possono verificare errori di acquisizione. Questo problema può essere risolto usando le stesse tecniche di acquisizione che sono proposte in diversi articoli per i segnali BOC, che hanno proprietà di correlazione (molteplici picchi) e caratteristiche spettrali (spettro diviso) simili a quelle dell'AltBOC. Considerando il *ricevitore coerente a due bande*, le procedure di acquisizione possono quindi essere svolte in tre modi diversi:

1. con un'**acquisizione diretta** della funzione di correlazione AltBOC;
2. con un'**acquisizione di una singola banda laterale** (SSB);
3. con un'**acquisizione di entrambe le bande laterali** (DSB).

Nel primo caso la procedura di acquisizione deve tenere conto del problema di ambiguità, dovuto ai molteplici picchi della funzione di correlazione. Per acquisire il picco corretto è necessario usare un frequenza di campionamento (f_{Sample}) elevata, incrementando eccessivamente la complessità di calcolo ed il tempo di acquisizione. Inoltre è anche necessario applicare un algoritmo aggiuntivo in grado di risolvere il problema di ambiguità del picco di correlazione (ad esempio la tecnica del *bump-jumping*, presentata in [32] per i segnali BOC). Quindi l'approccio dell'acquisizione diretta risulta eccessivamente dispendioso e quindi è sconsigliato.

Invece le altre due tecniche di acquisizione (SSB e DSB) sono delle soluzioni interessanti che possono essere facilmente applicate anche ai ricevitori AltBOC, dato che permettono di acquisire in modo semplice, veloce e robusto (senza ambiguità) una funzione di correlazione con molteplici picchi. Queste due tecniche si basano sull'idea di elaborare solo una banda laterale del segnale AltBOC (SSB) o entrambe le bande laterali in modo separato (DSB): in questo modo il segnale ricevuto può essere elaborato come un semplice segnale BPSK, ottenendo il classico picco di correlazione triangolare che può essere facilmente acquisito.

Va inoltre notato che con l'acquisizione SSB (ad esempio della banda laterale *E5a*) è possibile scegliere di acquisire solo uno dei due codici (tipicamente il codice pilota *E5a-Q*) o entrambi i codici (*E5a-I* ed *E5a-Q*) trasmessi nella banda laterale. Invece con l'acquisizione DSB è possibile calcolare la correlazione anche con tutti i quattro codici trasmessi dal satellite (*E5a-I*, *E5a-Q*, *E5b-I* ed *E5b-Q*). Va però notato che usando più di un codice per l'acquisizione è necessario combinare tra i loro i risultati di correlazione di ogni codice in modo non coerente: una somma coerente sarebbe più vantaggiosa, ma non è possibile a causa della presenza dei dati di navigazione e dei codici secondari, che sono diversi per ogni canale trasmesso. Inoltre, l'acquisizione di più codici richiede l'uso di generatori di codici locali e di canali di correlazione separati per ogni codice, complicando notevolmente l'implementazione della procedura di acquisizione.

La tecnica che risulta preferibile è quindi l'acquisizione SSB sfruttando un solo codice pilota (ad esempio *E5a-Q*): questo approccio semplifica notevolmente l'implementazione della sezione di acquisizione e può raggiungere le stesse prestazioni in presenza di rumore delle altre tecniche (con la stessa ampiezza del picco di correlazione), incrementando il numero di accumulazioni non coerenti (come spiegato più avanti). L'unico vantaggio che si ha nel caso di acquisizione DSB è che questa tecnica risulta più robusta in presenza di interferenze, dato che un segnale di disturbo su una delle due bande laterali non influenza la corretta acquisizione del segnale sull'altra banda, ma richiede un hardware più costoso.

Per effettuare l'acquisizione è necessario ripetere il calcolo della correlazione tra il segnale ricevuto ed i segnali locali per tutte le celle dello spazio di

ricerca (Θ, $f_{Doppler}$). Le tecniche usate per esplorare lo spazio di ricerca sono tipicamente classificate in due categorie:

- **ricerca lineare** (anche chiamata ricerca *sequenziale*), quando ogni cella dello spazio di ricerca è analizzata separatamente;
- **ricerca parallela**, quando più celle sono analizzate simultaneamente.

La ricerca lineare di solito non è usata negli attuali ricevitori GPS, dove invece sono sfruttate delle tecniche parallele per velocizzare i tempi di acquisizione. In particolare vengono di solito utilizzati i **matched filters** per implementare con un hardware semplice e veloce le operazioni di correlazione, mentre per ricevitori in cui le operazioni di acquisizione sono eseguite a livello software (ad esempio su un DSP) viene sovente sfruttata la **trasformata di Fourier veloce** (FFT), che permette un notevole risparmio in termini di complessità di calcolo. Inoltre la ricerca parallela basata sulla FFT è utile anche nel caso si debba simulare un sistema di acquisizione, dato che permette di ridurre considerevolmente i tempi di simulazione.

Le tecniche di ricerca parallela possono essere facilmente sfruttate anche per implementare un sistema di acquisizione efficiente e veloce per la banda E5, ma nella seguente discussione si è scelto di considerare la tecnica di ricerca lineare, per rendere più semplice la comprensione della operazioni svolte dal ricevitore. Inoltre l'acquisizione con una ricerca lineare permette di usare le stesse componenti hardware del ricevitore che sono necessarie per la successiva fase di tracking: in questo modo le procedure di acquisizione possono essere spiegate riutilizzando gli stessi schemi delle architetture dei ricevitori AltBOC precedentemente illustrati. In pratica, come si vede in Figura 10, la sezione a radiofrequenza (RF) e quella a frequenza intermedia (IF) rimangono inalterate, eseguendo le stesse operazioni nel dominio analogico sul segnale ricevuto. Invece dopo la digitalizzazione (eseguita dall'ADC), i campioni del segnale ricevuto vengono elaborati in modo diverso dalla *sezione di acquisizione*, usando in modo diverso le componenti del PLL e del DLL.

In particolare, il PLL e il DLL vengono usati in una configurazione ad *anello aperto* e vengono pilotati da una logica di controllo, che in questo modo esegue la ricerca del picco di correlazione nel dominio tempo-frequenza (ritardo del codice locale nel DLL e frequenza del segnale generato nel PLL). I risultati all'uscita dei due correlatori per i rami in fase (I) ed in quadratura (Q) possono essere accumulati in modo **coerente** (vedi Figura 10), scegliendo un opportuno tempo di integrazione, per migliorare l'ampiezza del picco di correlazione. Dopo il rivelatore d'inviluppo, si può inoltre effettuare una ulteriore accumulazione **non coerente**. Questi due tipi di accumulazione hanno lo scopo di migliorare le prestazioni della sezione di acquisizione in presenza di rumore: rendendo più evidente il picco di correlazione all'interno dello spazio di ricerca, si riduce la *probabilità di falso allarme* e si aumenta la *probabilità di rilevamento*. Ma queste operazioni di integrazione implicano

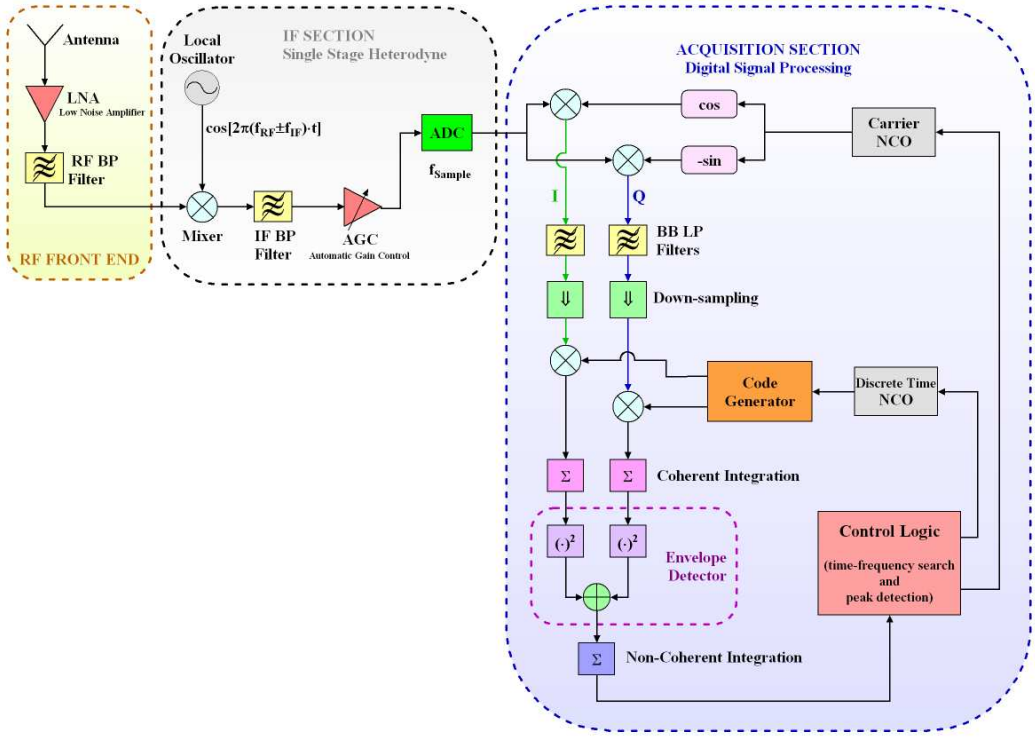

Figura 10: Schema di funzionamento della sezione di acquisizione per un ricevitore AltBOC (a banda singola)

anche una maggiore complessità di calcolo ed un maggior tempo necessario per l'acquisizione.

Per quanto riguarda i codici che verranno usati nella banda E5 del sistema Galileo, va notato che tipicamente si può usare un tempo di integrazione coerente al massimo di 1 ms (cioè pari ad un periodo del codice primario): infatti questi codici hanno una struttura sovrapposta, con un codice secondario sovrapposto ad un codice primario più corto, ed usando tempi di integrazione più lunghi il codice secondario può creare problemi, annullando il risultato all'uscita dei correlatori. In pratica è necessario calcolare la correlazione usando la ben nota tecnica della *correlazione a finestra*, in cui i campioni locali corrispondenti ad un periodo di codice primario (1 ms) vengono correlati con il segnale ricevuto, facendo scorrere la finestra di correlazione. Se poi si usa la tecnica basata sulla FFT per velocizzare l'acquisizione, la correlazione a finestra può essere implementata usando una finestra di 2 ms, con 1 ms di codice locale ed uno *zero padding* per i restanti campioni locali. In questo modo le transizioni dovute al codice secondario non creano problemi ed i valori di correlazione ottenuti sono corretti.

Per migliorare le prestazioni della sezione di acquisizione si può usare un numero elevato di accumulazioni non coerenti, che sono meno vantaggiose delle accumulazioni coerenti in termini di *rapporto segnale-rumore* (SNR) ma non risentono degli effetti del codice secondario. Un'altro modo per migliorare le

prestazioni consiste nell'utilizzare degli **algoritmi di miglioramento statistico**, esattamente come viene fatto negli attuali ricevitori GPS: ad esempio l'algoritmo M su N o l'algoritmo di *Tong* possono essere fruttati senza grosse modifiche anche per i ricevitori AltBOC.

Al termine delle procedure di acquisizione, se un picco di correlazione è stato individuato, la sezione di acquisizione dichiara di aver acquisito un satellite e fornisce al ricevitore i parametri stimati (ritardo del codice $\widetilde{\Theta}$ e spostamento Doppler $\widetilde{f}_{Doppler}$), che verranno utilizzati per iniziare la successiva fase di tracking. Va però notato che una **fase di transizione** tra l'acquisizione ed il tracking può essere necessaria, dato che i due parametri $\widetilde{\Theta}$ e $\widetilde{f}_{Doppler}$ vengono di solito stimati con una risoluzione grossolana (ad esempio $\Delta\Theta = 0.5\,\text{chip}$ e $\Delta f = 500\,\text{Hz}$), per ridurre il numero di celle dello spazio di ricerca e velocizzare l'acquisizione. Tipicamente nei ricevitori GPS la fase di transizione viene svolta usando temporaneamente il PLL in configurazione di *Frequency Lock Loop* (FLL) ed il DLL con una configurazione con discriminatore ampio, in grado di accettare le incertezze iniziali nella stima dei parametri e di convergere verso delle stime più precise. Questa tecnica può essere facilmente sfruttata anche per il *ricevitore a banda singola* ed il *ricevitore non coerente a due bande*, che lavorano in pratica con dei semplici segnali BPSK.

Invece, con il *ricevitore coerente a due bande* (e le altre architetture da esso derivate) è richiesta una risoluzione più elevata nella stima dei parametri $\widetilde{\Theta}$ e $\widetilde{f}_{Doppler}$, altrimenti la fase di tracking non può iniziare correttamente, dato che può avvenire l'aggancio di un picco laterale della funzione di correlazione complessa del segnale AltBOC. Una possibile soluzione, proposta in questa tesi, è la tecnica dell'**acquisizione progressiva**, schematizzata nella Figura 11. Essa consiste in un'acquisizione iniziale con una bassa risoluzione (ad esempio $\Delta\Theta = 0.5$ chip e $\Delta f = 500$ Hz) di un singolo codice del segnale AltBOC su una banda laterale (SSB), seguita poi da un'ulteriore ricerca con una risoluzione più fine (ad esempio $\Delta\Theta = 1/12$ chip e $\Delta f = 100$ Hz) solo in prossimità della cella individuata con l'acquisizione iniziale. In questo modo è possibile ottenere una sufficiente precisione nella stima dei parametri $\widetilde{\Theta}$ e $\widetilde{f}_{Doppler}$, senza incrementare troppo la complessità di calcolo ed il tempo di acquisizione, dato che è necessario analizzare con un'elevata risoluzione solo una piccola porzione dello spazio di ricerca.

Nella fase di transizione vanno anche considerati i **codici secondari** usati nella banda E5. Come accennato in precedenza, può essere conveniente sfruttare un periodo di codice primario (1 ms) per effettuare l'acquisizione in modo rapido e semplice. Tuttavia, per potere iniziare correttamente la fase di tracking, generando localmente l'intera struttura dei codici, anche i codici secondari devono essere acquisiti. Un semplice approccio che si può usare è quello di demodulare i chip del codice secondario, dopo aver acquisito il codice primario, e memorizzare questi chip in un vettore temporaneo. La sincronizzazione del codice secondario può quindi essere ottenuta eseguendo un'ulteriore *correlazione circolare* tra i chip memorizzati nel vettore ed una

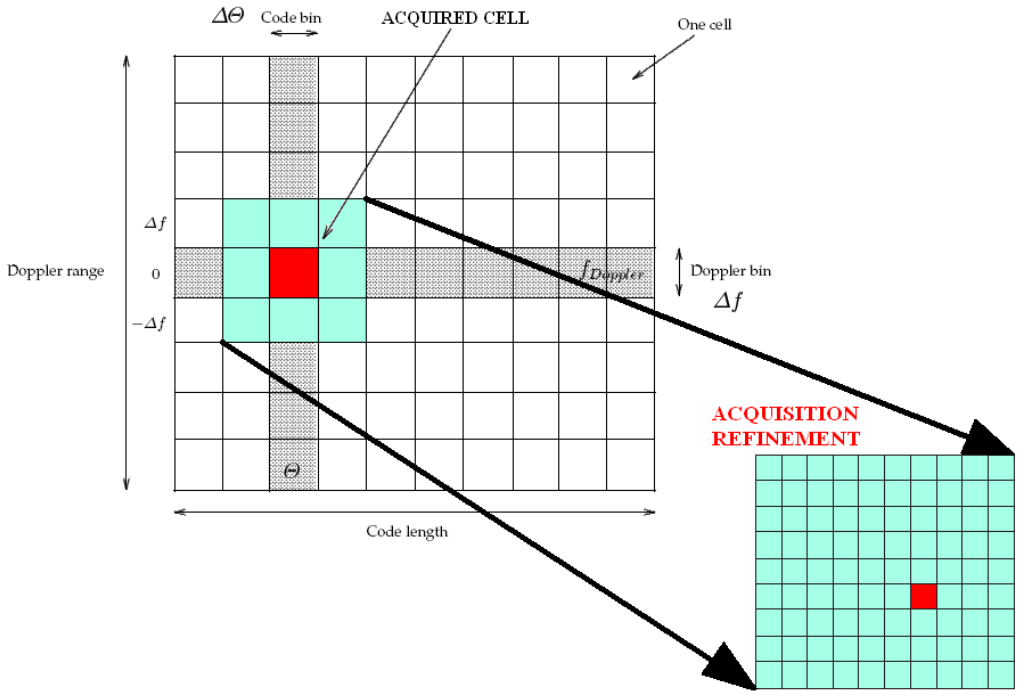

Figura 11: Spazio di ricerca per la tecnica di acquisizione progressiva

replica locale del codice secondario che deve essere acquisito. A questo punto la fase di tracking può iniziare, dato che il ricevitore è in grado di generare in modo corretto l'intero codice, composto dal codice primario e dal secondario, e quindi di demodulare i dati.

Nel testo completo della tesi è anche presente una discussione dettagliata di tutti i parametri dei ricevitori AltBOC che possono influenzare le prestazioni della sezione di acquisizione (frequenza di campionamento f_{Sample}, frequenza intermedia f_{IF}, ampiezza e risoluzione dello spazio di ricerca, integrazioni coerenti e non coerenti, caratteristiche dei filtri), ma questo esula i limiti di spazio di questo sommario.

• Blocchi di acquisizione per i ricevitori AltBOC

Dopo aver presentato e discusso le tecniche di acquisizione adatte per il segnale AltBOC, in questa sezione queste considerazioni sono applicate alle architetture dei ricevitori AltBOC discusse in precedenza, suggerendo il blocco di acquisizione adatto per ogni ricevitore (si faccia riferimento al precedente schema in Figura 10).

Per quanto riguarda il *ricevitore a banda singola*, può essere usata l'acquisizione SSB, sfruttando solo il codice pilota (ad esempio *E5a-Q*). L'implementazione di questa tecnica risulta particolarmente semplice, dato che i campioni all'uscita dell'ADC del ricevitore corrispondono proprio al segnale BPSK

presente nella banda laterale (ad esempio *E5a*), spostato alla frequenza intermedia f_{IF}. La sezione di acquisizione del ricevitore deve quindi traslare il segnale dalla frequenza intermedia alla banda base e cercare il corretto spostamento Doppler (l'NCO che controlla la frequenza della portante locale viene impostato con una frequenza pari a $f_{IF} + f_{Doppler}$) e il ritardo del codice, analogamente a quanto viene fatto in un comune ricevitore GPS.

Con il *ricevitore non coerente a due bande* invece si può scegliere di usare un'acquisizione a banda singola (SSB) o su due bande separate (DSB), dato che l'hardware del ricevitore è costruito in modo da convertire separatamente a frequenza intermedia entrambe le bande laterali. La prima tecnica è però consigliata, perché richiede una implementazione più semplice e si possono sfruttare in parallelo tutti i canali di correlazione del ricevitore per cercare un singolo codice, velocizzando il tempo di acquisizione.

Per il *ricevitore coerente a due bande* sono possibili diversi approcci di acquisizione ma, come discusso in precedenza, anche in questo caso è consigliato l'uso della tecnica di acquisizione SSB (ad esempio usando solo il codice pilota *E5a-Q*). Vanno però fatte alcune considerazioni aggiuntive, dato che con questa architettura i campioni all'uscita dell'ADC corrispondono all'intero segnale a banda larga AltBOC, traslato a frequenza intermedia. La sezione di acquisizione deve quindi operare uno spostamento di frequenza opportuno, in modo da spostare in banda base solo una banda laterale del segnale: l'NCO che controlla la frequenza della portante locale deve essere impostato con una frequenza pari a $f_{IF} - f_{sub} + f_{Doppler}$, dove f_{sub} è la frequenza delle sottoportanti ($f_{sub} = R_{S,E5} = 15.345\,\text{MHz}$) e i filtri della sezione di acquisizione devono selezionare solo la banda *E5a*.

Inoltre, dato che questo ricevitore funziona con una frequenza di campionamento elevata (ad esempio $f_{Sample} \cong 120\,\text{MHz}$, cioè con 12 campioni/chip per la fase di tracking), è anche necessario applicare un **sotto-campionamento** all'interno della sezione di acquisizione (ad esempio decimando i campioni del segnale da 12 campioni/chip a 2 campioni/chip). In questo modo si può applicare la tecnica dell'**acquisizione progressiva** precedentemente illustrata, che consiste in un'acquisizione iniziale a bassa risoluzione, seguita da una fase di raffinamento della stima dei parametri $\widetilde{\Theta}$ e $\widetilde{f}_{Doppler}$, in cui i campioni ricevuti non sono più decimati.

Lo stesso schema di acquisizione (cioè SSB con la tecnica dell'acquisizione progressiva) può essere sfruttato anche per il *ricevitore con il correlatore-discriminatore* e per tutte le altre architetture derivate dal *ricevitore coerente a due bande*.

• Simulazioni e risultati ottenuti

Gli schemi di acquisizione precedentemente introdotti per il segnale AltBOC sono stati implementati in un simulatore digitale in modo da validarli, verificandone il corretto funzionamento. Per simulare le operazioni svolte dalla sezione di acquisizione del ricevitore è stato scritto un programma in linguaggio *C*, in grado di eseguire le seguenti operazioni:

- la **generazione** dei campioni del segnale ricevuto all'uscita dell'ADC della sezione a frequenza intermedia (f_{IF}), introducendo un ritardo a piacere per il codice (Θ), uno spostamento Doppler ($f_{Doppler}$) ed un *rumore gaussiano bianco additivo* (AWGN);
- le **operazioni di acquisizione** svolte dal ricevitore, implementando tutte le tecniche adatte al segnale AltBOC discusse in precedenza (acquisizione SSB con il codice *E5a-Q* o acquisizione DSB con i codici *E5a-Q* ed *E5b-Q*, acquisizione progressiva).

Va notato che tutti i parametri di questo simulatore possono essere modificati a piacere, simulando diverse configurazioni del ricevitore e diverse condizioni operative. Ad esempio è possibile variare la potenza del rumore all'ingresso dell'acquisitore e quindi il rapporto segnale-rumore (SNR).

Sono state quindi eseguite diverse simulazioni, in particolare per verificare il corretto funzionamento della tecnica dell'acquisizione progressiva e l'effetto delle accumulazioni non coerenti sulle prestazioni del ricevitore. Si è avuto conferma del fatto che, in presenza di rumore, un aumento del numero di accumulazioni non coerenti rende più distinguibile il picco di correlazione rispetto al livello del rumore. Questo però implica anche un maggiore peso computazionale e quindi un maggiore tempo di acquisizione. Il numero di accumulazioni non coerenti quindi deve essere scelto come un compromesso tra la velocità di acquisizione e le prestazioni in presenza di rumore.

Il programma di simulazione sviluppato nel corso di questa tesi potrà essere utilizzato anche per futuri studi riguardanti i sistemi di acquisizione per il segnale AltBOC (ad esempio per la validazione di algoritmi innovativi di acquisizione, l'analisi delle probabilità di falso allarme e della probabilità di rilevamento, l'introduzione di algoritmi di miglioramento statistico, ecc.), che esulano dagli obiettivi di questa tesi.

Tecniche di mitigazione dei cammini multipli

L'effetto dei **cammini multipli** (detti in inglese *multipath*) è una delle più importanti cause di errore nei comuni ricevitori GPS, quindi deve essere preso in considerazione anche per i futuri ricevitori Galileo. I cammini multipli

implicano la presenza di molteplici repliche sovrapposte del segnale, che raggiungono il ricevitore in istanti di tempo diversi: queste repliche sono dovute alle riflessioni sulle superfici vicine all'antenna del ricevitore. La presenza dei cammini multipli di solito provoca errori nella stima della posizione, dato che i segnali riflessi possono causare uno spostamento del punto di aggancio del PLL e del DLL del ricevitore. In particolare l'effetto sul PLL consiste in un errore nella stima della fase della portante (*carrier multipath*), mentre il DLL può subire uno spostamento del punto di aggancio del codice (*code multipath*), che si traduce direttamente in un errore nella stima delle distanze tra il ricevitore e i satelliti.

Va notato che esistono numerose tecniche per mitigare l'effetto dei cammini multipli, sia per il PLL sia per il DLL degli attuali ricevitori GPS. Tipicamente l'effetto sul DLL è quello che può causare i maggiori errori, dunque la sua mitigazione è di primaria importanza. A questo scopo vengono di solito usate delle tecniche basate sul discriminatore usato nel DLL del ricevitore: infatti, scegliendo con cura la forma della funzione di discriminazione, si possono ridurre notevolmente gli effetti dei cammini multipli.

Sebbene le tecniche di mitigazione dei cammini multipli siano ampiamente discusse in numerosi articoli per i ricevitori GPS e per i segnali BOC, per quanto riguarda la modulazione AltBOC il materiale attualmente presente in letteratura è scarso. In questa tesi è quindi presente uno studio completo delle prestazioni dei futuri ricevitori per il segnale AltBOC in presenza di cammini multipli, considerando le architetture proposte in precedenza e adattando al segnale AltBOC le principali tecniche di mitigazione attualmente conosciute.

L'effetto dei cammini multipli (inteso come *code multipath*) è legato a diversi parametri del segnale trasmesso e del ricevitore. In particolare vi sono tre parametri che sono legati all'ambiente circostante il ricevitore:

- il numero di segnali riflessi; di solito, per studiare in modo semplice e simulare l'effetto dei cammini multipli, si considera una sola componente riflessa, oltre alla componente diretta, che è anche chiamata segnale *Line Of Sight* (LOS) e che si assume che sia sempre presente;
- il ritardo relativo tra i vari cammini multipli e la componente diretta; i segnali riflessi arrivano sempre dopo il segnale diretto, in quanto devono percorrere un cammino più lungo;
- il livello di potenza relativo dei vari segnali; normalmente i segnali riflessi hanno una potenza inferiore rispetto alla componente diretta e nelle simulazioni si considera tipicamente un'attenuazione pari ad $\alpha = 0.5$ (che corrisponde a $SMR = 6\,\text{dB}$, il cosiddetto *Signal-to-Multipath power Ratio*), ossia una componente riflessa con un'ampiezza pari alla metà di quella della componente diretta.

I seguenti parametri invece sono legati alle proprietà del segnale trasmesso e all'architettura del ricevitore:

- il tipo di segnale ricevuto (ad esempio BPSK, BOC o AltBOC) e quindi la forma della funzione di correlazione; va notato che, come accennato in diversi articoli, la modulazione AltBOC permetterà di raggiungere migliori prestazioni in presenza di cammini multipli rispetto alle altre modulazioni previste per il sistema Galileo;

- la frequenza di chip dei codici PRN ($R_C = 10.23\,\text{Mchip/s}$); infatti per la banda E5 verranno usati dei codici più lunghi e con una velocità dieci volte maggiore rispetto a quelli usati per il segnale C/A del GPS, ottenendo minori errori per l'effetto dei cammini multipli;

- la banda del ricevitore, dato che la banda del segnale ricevuto e le caratteristiche dei filtri del ricevitore possono implicare delle distorsioni del segnale, alterando i risultati dei calcoli di correlazione e peggiorando le prestazioni del ricevitore;

- il tipo di discriminatore usato nel DLL (ad esempio il cosiddetto *narrow correlator* ™ o il *double delta correlator*); come accennato in precedenza, è infatti possibile migliorare le prestazioni del ricevitore in presenza di cammini multipli usando più correlatori e combinando le loro uscite in modo da ottenere una funzione di discriminazione con una forma opportuna;

- la spaziatura tra i correlatori del discriminatore, che influenza la pendenza della funzione di discriminazione.

In particolare, la **banda del ricevitore** è uno dei parametri più importanti per quanto riguarda le prestazioni dei futuri ricevitori AltBOC: solo usando una banda larga si può ottenere una funzione di discriminazione particolarmente ripida nel punto di tracking e quindi maggiormente resistente all'effetto dei cammini multipli, ma questo implica anche una maggiore complessità ed un costo più alto del ricevitore ed una sua maggiore vulnerabilità rispetto a possibili segnali interferenti. Dopo un'attenta analisi, si è quindi scelto un valore ottimale pari a 30 MHz per la banda del *ricevitore a banda singola* ed una banda di 51.150 MHz per il *ricevitore coerente a due bande* e per il *ricevitore con il correlatore-discriminatore*, che sono le architetture di cui sono state analizzate le prestazioni in presenza di cammini multipli.

Va infatti notato che il *ricevitore a banda singola* e il *ricevitore non coerente a due bande* (introdotti in precedenza) avranno le stesse prestazioni in presenza di cammini multipli, dato che entrambi sfruttano un'elaborazione di segnali BPSK e quindi una funzione di correlazione triangolare. Quindi le prestazioni di questi due ricevitori sono state valutate considerando un generico **ricevitore BPSK** e le si è confrontate con quelle del *ricevitore coerente a due bande*, di seguito chiamato **ricevitore AltBOC**, in quanto è l'unico che sfrutta la funzione di correlazione complessa combinata del segnale AltBOC.

Le prestazioni dei due ricevitori sono state valutate usando diverse tecniche di mitigazione e sfruttando due tipi di grafici: gli inviluppi degli errori dei cammini multipli (*multipath error envelopes*) e le medie mobili di tali inviluppi (*running average of multipath error envelopes*). Questi due approcci sono comunemente usati negli articoli riguardanti i cammini multipli, perché permettono di confrontare in modo semplice e veloce le prestazioni di diversi segnali e diverse configurazioni dei ricevitori, senza richiedere una complessità di calcolo eccessiva per le simulazioni.

In Figura 12 sono presentate le prestazioni del ricevitore BPSK e del ricevitore AltBOC, considerando i grafici delle medie mobili (*running average of multipath error envelopes*) per confrontare in modo semplice l'effetto delle varie tecniche di mitigazione. Le prestazioni dei ricevitori nelle varie configurazioni sono state valutate usando degli appositi programmi di simulazione, scritti in linguaggio MATLAB® per questa tesi.

In particolare, le prestazioni del ricevitore BPSK e del ricevitore AltBOC sono state valutate adattando per queste due architetture le principali tecniche di mitigazione dei cammini multipli attualmente utilizzate nei comuni ricevitori GPS (*wide correlator*, *narrow correlator* ™, *double delta correlator*, *Early-Late Slope technique* ed *E1/E2 tracking technique*). Sono state prese in considerazione ed analizzate anche due tecniche emergenti, proposte recentemente per mitigare gli effetti dei cammini multipli: l'approccio basato sullo *shaping* della funzione di discriminazione e la tecnica di *gating*. Il primo approccio in pratica richiede un'architettura con molteplici correlatori ed ottiene una funzione di discriminazione sagomata usando una combinazione lineare e coerente delle uscite dei diversi correlatori. Invece la tecnica di *gating* è basata su una funzione di riferimento (*gated reference function*) che opera una cancellazione su una parte del segnale ricevuto, con lo scopo di ridurre gli errori dovuti ai cammini multipli.

Per quanto riguarda il ricevitore BPSK, in Figura 12(a) è evidente il fatto che tutte le tecniche di mitigazione comunemente usate nei ricevitori GPS possono essere facilmente adattate per questa architettura, ottenendo un miglioramento delle prestazioni rispetto al caso del ricevitore senza mitigazione dei cammini multipli (usando il *wide correlator*). In particolare, le migliori prestazioni sono state ottenute usando la tecnica ELS (*Early-Late Slope*), che però richiede l'uso di quattro correlatori aggiuntivi. Delle buone prestazioni sono state ottenute anche con la tecnica E1/E2 (*Early1/Early2*), che sembra un buon compromesso tra la mitigazione dei cammini multipli e la complessità del ricevitore (sono necessari solo due correlatori).

Invece, se si considera il ricevitore AltBOC, si può notare che esso ottiene delle prestazioni in presenza di cammini multipli che sono intrinsecamente buone, usando il *wide correlator* (senza tecniche di mitigazione). Tuttavia, le tecniche di mitigazione precedentemente elencate non riescono a migliorare di molto queste prestazioni intrinseche, come si vede in Figura 12(b): solo

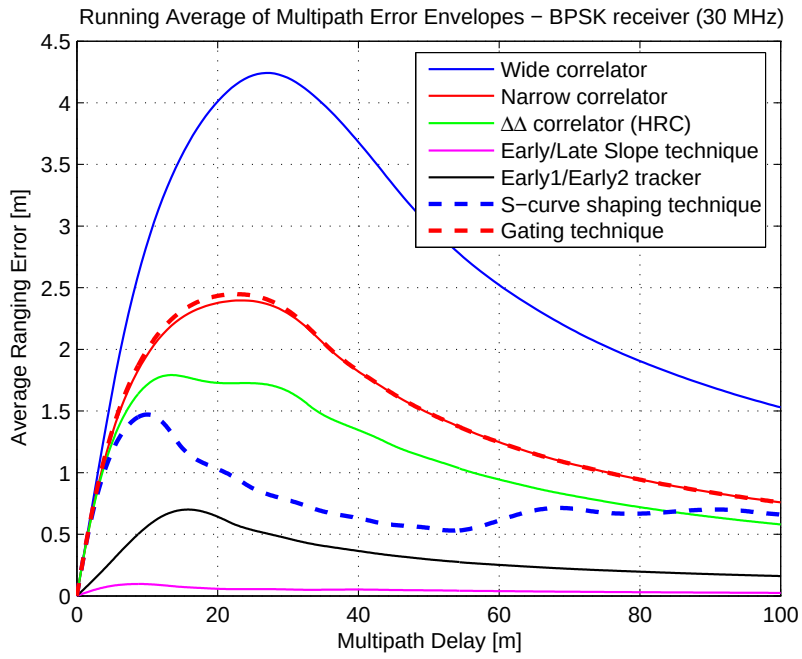

(a)

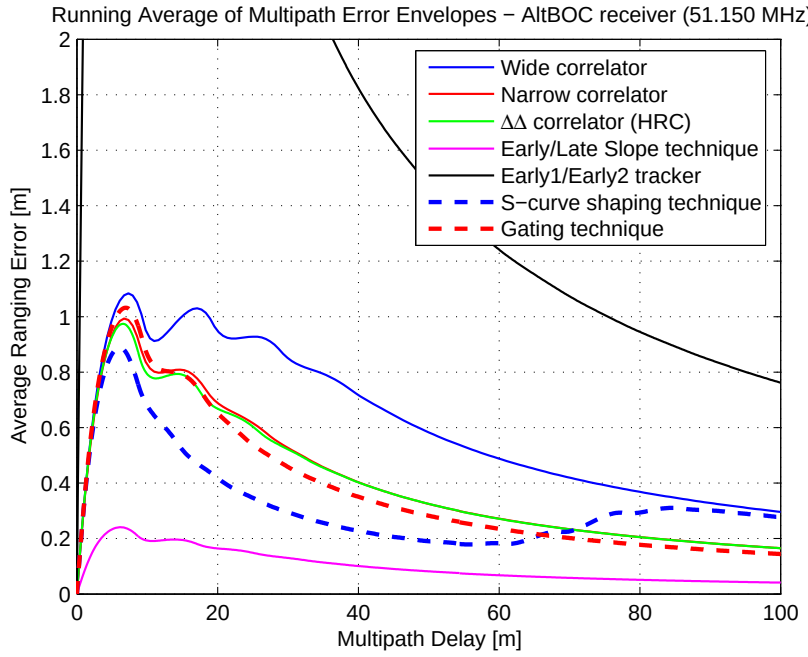

(b)

Figura 12: Confronto delle prestazioni in presenza di cammini multipli, usando le varie tecniche di mitigazione (tecniche comuni ed emergenti) per il ricevitore BPSK con una banda di 30 MHz (a) e per il ricevitore AltBOC con una banda di 51.150 MHz (b)

la tecnica ELS permette un significativo miglioramento, ma il risultato ottenuto è comunque peggiore di quello raggiunto dal ricevitore BPSK con la stessa tecnica (ELS). Nel caso della tecnica E1/E2 addirittura si è verificato un netto peggioramento nelle prestazioni. Questo è dovuto al fatto che le prestazioni delle tecniche di mitigazione con il ricevitore AltBOC sono fortemente influenzate dalla posizione e dalla spaziatura scelta per i correlatori: una loro piccola variazione può portare ad inviluppi degli errori dei cammini multipli notevolmente diversi, dato che la funzione di correlazione complessa del segnale AltBOC presenta una forma oscillante e diversi attraversamenti dello zero. Risulta quindi difficile trovare una spaziatura ottimale per i correlatori del ricevitore AltBOC e, in ogni caso, le tecniche di mitigazione analizzate non sembrano particolarmente adatte a questo tipo di ricevitore, perché forniscono migliori risultati se applicate al ricevitore BPSK.

Va inoltre notato che le tecniche emergenti (*shaping* e *gating*), indicate con delle linee tratteggiate in Figura 12, non hanno fornito dei risultati particolarmente interessanti. Infatti per entrambi i ricevitori la tecnica di *gating* ha fornito prestazioni vicine a quelle ottenute con il *narrow correlator* ^{TM}, mentre la tecnica di *shaping* ha permesso un leggero miglioramento delle prestazioni, ottenendo comunque un risultato peggiore rispetto alle altre tecniche.

Sono poi state analizzate anche le prestazioni del *ricevitore con il correlatore-discriminatore*. Questa architettura innovativa permette un considerevole risparmio nell'hardware del ricevitore, come discusso in precedenza. Le sue prestazioni in presenza di cammini multipli sono state simulate in condizioni analoghe a quelle usate per i precedenti ricevitori e sono rappresentate in Figura 13. Si può notare che questo ricevitore presenta delle buone prestazioni intrinseche, senza usare le tecniche di mitigazione.

Per quanto riguarda la mitigazione dell'effetto dei cammini multipli, va invece notato che solo le tecniche emergenti accennate in precedenza (*shaping e gating*) possono essere applicate a questo ricevitore. Invece le tecniche comuni, che si basano su molteplici correlatori e su un opportuno discriminatore per ridurre l'effetto dei cammini multipli, non sono adatte a questa architettura innovativa, in cui è presente un solo correlatore modificato e non è presente il blocco di discriminazione. In questo modo un piccolo miglioramento delle prestazioni in presenza di cammini multipli è stato ottenuto sia con la tecnica di *gating*, sia con la tecnica di *shaping* (ma solo per ritardi dei cammini multipli inferiori a 58.65 metri, cioè all'interno della zona in cui è stata eseguita l'interpolazione lineare della funzione di discriminazione). In ogni caso queste due tecniche di mitigazione non sembrano convenienti per il ricevitore con il correlatore-discriminatore, se si considera il fatto che esse non portano a miglioramenti delle prestazioni particolarmente significativi, ma implicano un costo aggiuntivo per il ricevitore. Inoltre, entrambe queste due tecniche possono portare ad un peggioramento delle prestazioni del ricevitore in presenza di rumore, come accennato nel testo completo della tesi, quindi sono sconsigliate.

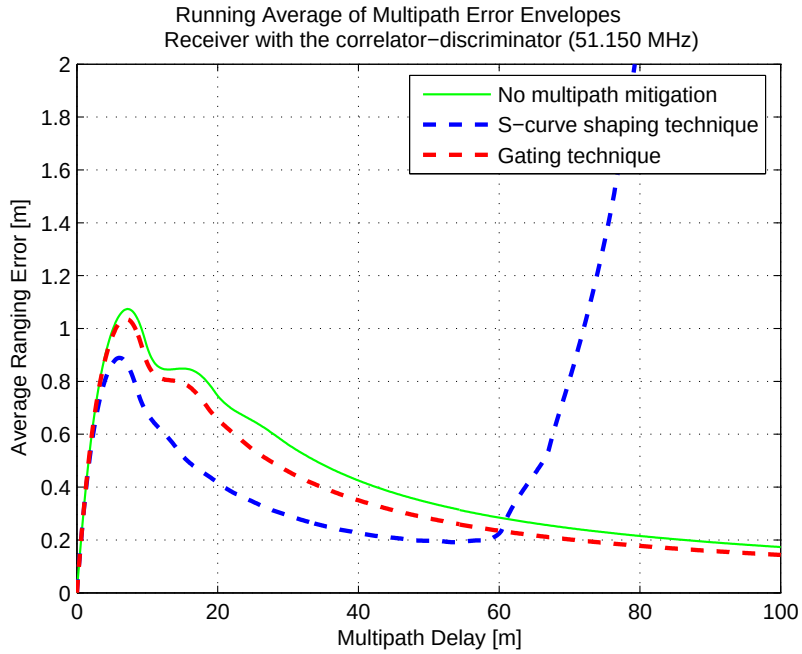

Figura 13: Confronto delle prestazioni in presenza di cammini multipli ottenute con il ricevitore con il correlatore-discriminatore con una banda di 51.150 MHz, usando le tecniche di mitigazione ad esso applicabili

Alla fine di questa analisi, si è svolto un confronto tra le prestazioni ottenute dalle tre architetture analizzate (il ricevitore BPSK, il ricevitore AltBOC ed il ricevitore con il correlatore-discriminatore), considerandole senza tecniche di mitigazione (prestazioni intrinseche dei ricevitori) ed usando la migliore tecnica per ogni ricevitore, ossia quella che ha portato al maggiore miglioramento delle prestazioni. I risultati sono riportati in Figura 14.

In particolare in Figura 14(a) si può notare come il ricevitore con il correlatore-discriminatore ottenga buone prestazioni intrinseche, migliori rispetto a quelle degli altri due ricevitori senza tecniche di mitigazione. Esso presenta anche dei considerevoli vantaggi in termini di hardware, dato che permette un notevole risparmio per i componenti necessari.

Tuttavia, considerando le tecniche di mitigazione, le migliori prestazioni in assoluto sono state ottenute dal ricevitore BPSK con la tecnica ELS, come si vede nella Figura 14(b). In particolare è risultato evidente che le tecniche di mitigazione attualmente esistenti non sono particolarmente adatte per il ricevitore AltBOC e per il ricevitore con il correlatore-discriminatore, che non traggono da queste tecniche dei vantaggi paragonabili a quelli ottenuti dal ricevitore BPSK. Probabilmente in futuro verranno scoperte delle nuove tecniche di mitigazione, *ad-hoc* per queste due architetture innovative, ottenendo così considerevoli miglioramenti delle loro prestazioni.

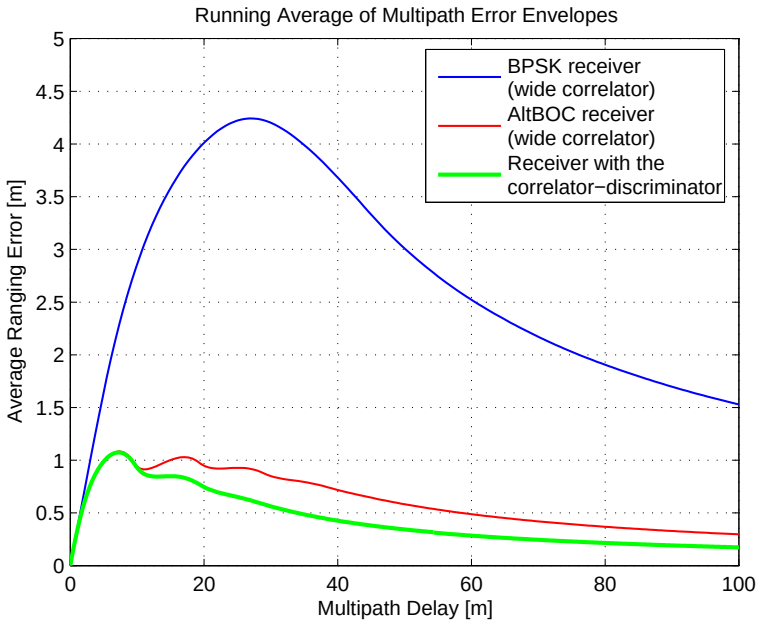

(a)

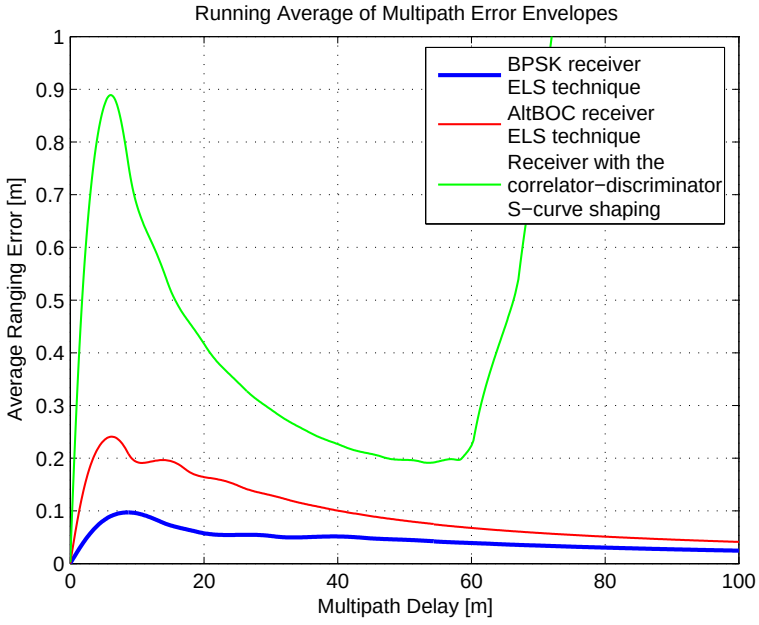

(b)

Figura 14: Prestazioni in presenza di cammini multipli ottenute con le tre architetture dei ricevitori: il ricevitore BPSK (30 MHz), il ricevitore AltBOC (51.150 MHz) ed il ricevitore con il correlatore-discriminatore (51.150 MHz). Confronto tra le prestazioni ottenute dai tre ricevitori senza tecniche di mitigazione dei cammini multipli (a) ed usando la migliore tecnica per ogni ricevitore (b)

In conclusione, si può affermare che attualmente le migliori prestazioni per la ricezione del segnale AltBOC in presenza di cammini multipli possono essere ottenute solo con un ricevitore BPSK, usando un hardware costoso ed abbastanza complicato (è necessaria la tecnica ELS). Invece il ricevitore innovativo basato sul correlatore-discriminatore al momento non è in grado di raggiungere simili prestazioni, ma è un'architettura interessante e promettente che implica un notevole risparmio di hardware e sembra un buon compromesso tra le prestazioni ed il costo del ricevitore.

Conclusioni

Nel corso di questa tesi è stato svolta una trattazione completa ed approfondita della modulazione AltBOC, che attualmente è discussa in modo generico e sintetico solo in pochi articoli. In particolare sono state studiate le caratteristiche del segnale AltBOC, le possibili architetture dei ricevitori, le strategie di acquisizione e le tecniche di mitigazione dei cammini multipli adatte a tale segnale.

Per svolgere le analisi necessarie ed esaminare le proprietà di tale segnale, sono stati scritti diversi programmi in linguaggio *C* e MATLAB® in grado di simulare la generazione dei campioni del segnale AltBOC, le procedure di acquisizione per i vari ricevitori e le prestazioni in presenza di cammini multipli, usando varie tecniche di mitigazione.

Inoltre nel corso di questa tesi sono anche state proposte ed analizzate alcune soluzioni innovative per i ricevitori del segnale AltBOC: il *sideband translator* (per cui si sta valutando la possibilità di un brevetto) all'interno del ricevitore coerente a due bande, l'architettura innovativa del ricevitore con il *correlatore-discriminatore* e la tecnica di *acquisizione progressiva*.

Rimangono ancora alcuni problemi aperti, che potranno essere l'oggetto di futuri lavori riguardanti la modulazione AltBOC. In particolare i programmi di simulazione realizzati nel corso di questa tesi potranno essere utilizzati per ulteriori analisi delle prestazioni delle tecniche di acquisizione (ad esempio l'analisi delle probabilità di falso allarme e della probabilità di rilevamento, l'introduzione di algoritmi di miglioramento statistico, ecc.) o per la validazione di altri algoritmi innovativi di acquisizione. Inoltre si potranno analizzare le prestazioni di nuove tecniche di mitigazione dei cammini multipli, che probabilmente verranno proposte in futuro, confrontandole con quelle discusse in questa tesi.

Un'altro interessante campo di attività sarà l'analisi delle prestazioni in presenza di rumore delle architetture dei ricevitori e delle tecniche di mitigazione dei cammini multipli discusse in questa tesi. Infine, si potranno testare e validare queste tecniche anche utilizzando i segnali provenienti dal satelliti sperimentale GIOVE-A e dal futuro satellite GIOVE-B del sistema Galileo.

Summary

This thesis is motivated by the emerging interest on the future global navigation satellite system, the GALILEO system, due to the possibility to develop innovative receivers, taking advantage of new Galileo signals that will be transmitted in next years. In detail, the most promising signal of the Galileo system is the **AltBOC** (*Alternative BOC*) modulated signal, that will be transmitted in the E5 band (1164-1215 MHz). As pointed out in some articles in literature, the AltBOC signal could lead to formidable performances in terms of tracking noise and multipath (the major error sources in actual GPS receivers), for a receiver able to process the entire E5 band. Therefore the AltBOC demodulation and tracking is one of most interesting problem in Galileo receiver design.

It must be noted that at the moment the AltBOC signal is briefly discussed only in few papers, that often result difficult to understand. Besides, the future receiver architectures for the AltBOC signal are only highlighted and a complete discussion and comparison between all possible arrangements is not present in literature. In addition, also the acquisition operations and the multipath mitigation techniques that are suitable for the AltBOC signal are not exhaustively discussed.

Accordingly, the subject of this thesis is a complete discussion of the AltBOC signal, that will be transmitted in the E5 band of the future Galileo system. The features of this modulation, the possible receiver architectures, the acquisition strategies and the multipath mitigation techniques that are suitable for the AltBOC signal are analyzed in detail in the following dissertation, comparing the performances obtained with different arrangements and introducing some innovative solutions for the future AltBOC receivers.

In detail, the *sideband translator* block (that is patent pending) for the *coherent dual band receiver*, the innovative architecture with the *correlator-discriminator* and the *progressive acquisition* technique are proposed for the first time in this thesis and are analyzed from the analytical point of view and by means of simulations, comparing them with other alternative arrangements for the Galileo AltBOC receivers.

Acknowledgments

Foremost, I would like to thank my tutor Paolo Mulassano for his guidance, continuous encouragement and support during my research. I learned a lot of things from him and I am sure I will keep doing it.

A special thank goes also to prof. Fabio Dovis and prof. Letizia Lo Presti. I was their student at the Polytechnic of Turin and from them I learned a lot of notions about the satellite navigation systems; subsequently, they helped me to choose the subject of my thesis and they guided me during the work.

I am also sincerely grateful to the staff of the Navigation Lab of the ISMB (*Istituto Superiore Mario Boella*) for the possibility they have given to me to develop this work in an advanced and helpful environment. In detail, I would like to express my gratitude to Gianluca Marucco, Manuela Gianola, Maurizio Fantino, Andrea Tomatis, Massimiliano Spelat and all the great people who supported me.

On my personal side, I would like to thank my classmates and all my friends: we spent unforgettable moments together, not only during our studies at the Polytechnic, and I hope to keep in touch also in future.

Finally, I would like to thank my mother Marilena and my brother Flavio. They have believed in me and supported me in different ways: it would not be possible to go through all the hard times without their continuous love and affection.

Table of contents

List of acronyms

ADC	Analog to Digital Converter
AGC	Automatic Gain Control
AltBOC	Alternative Binary Offset Carrier
ARNS	Aeronautical Radio Navigation Services
AWGN	Additive White Gaussian Noise
BB	BaseBand
BER	Bit-Error-Rate
BOC	Binary Offset Carrier
BPSK	Binary Phase Shift Keying
BRW	Bipolar Reference Waveform
C/A	Clear/Acquisition or Coarse/Acquisition
C/N_0	Carrier-to-Noise-Density Ratio
CC	Central-Carrier
CCRW	Code Correlation Reference Waveforms
CDMA	Code Division Multiple Access
COSPAS-	COsmicheskaya Systyema Poiska Avariynich Sudov -
-SARSAT	Search And Rescue Satellite Aided Tracking
CRC	Cyclic Redundancy Check
CS	Commercial Service
DLL	Delay Lock Loop
DFT	Discrete Fourier Transform
DME	Distance Measurement Equipment
DSB	Double Side-Band
DSP	Digital Signal Processor
EC	European Commission
EGNOS	European Geostationary Navigation Overlay Service
EIRP	Equivalent Isotropic Radiated Power
ELS	Early/Late Slope
ENC	European Navigation Conference
ESA	European Space Agency
EU	European Union
FEC	Forward Error Correction
FFT	Fast Fourier Transform
FLL	Frequency Lock Loop
FOC	Full Operational Capability

GCS	Ground Control Segment
GJU	Galileo Joint Undertaking
GLONASS	Global Orbiting Navigation Satellite System
GMS	Ground Mission Segment
GNSS	Global Navigation Satellite System
GPS	Global Positioning System
GSS	Ground Sensor Station
GST	Galileo System Time
GSTB	Galileo System Test Bed
HPA	High Power Amplifier
HRC	High Resolution Correlator
I	In-Phase Component
I/O	Input/Output
ICD	Interface Control Document
ID	Identification
IDS	Integrity Determination System
IEEE	International Electrical and Electronic Engineers
IF	Intermediate Frequency
IFFT	Inverse Fast Fourier Transform
ION	Institute of Navigation
IOV	In-Orbit Validation
ITM	International Technical Meeting
ITU	International Telecommunications Union
JTIDS	Joint Tactical Information Distribution System
LAN	Local Area Network
LNA	Low Noise Amplifier
LOS	Line Of Sight
LUT	Look-Up Table
MEO	Medium Earth Orbit
MIDS	Multifunctional Information Distribution System
MPI	MultiPath Invariance
NASA	National Aeronautical and Space Administration
NAVSTAR	NAVigation System with Timing And Ranging
NCO	Numerically Controlled Oscillator
NRZ	Non-Return to Zero
NTM	National Technical Meeting
OC	Offset-Carrier
OS	Open Service
PAC	Pulse Aperture Correlator
PLL	Phase Lock Loop
PN	Pseudo Noise
PR	Pseudo-Range
PRN	Pseudo-Random Noise
PRS	Public Regulated Service
PSD	Power Spectral Density
PSK	Phase Shift Keying

PVT	Position, Velocity and Time
Q	Quadrature Component
QPSK	Quadrature Phase Shift Keying
RF	Radio Frequency
RHCP	Right-Hand Circular Polarization
RNSS	Radio Navigation Satellite System
RX	Receiver
S/A	Selective Availability
SAR	Search-and-Rescue
SIS	Signal-In-Space
SISA	Signal in Space Accuracy
SMR	Signal-to-Multipath power Ratio
SNR	Signal-to-Noise Ratio
SoL	Safety-of-Life service
SSB	Single Side-Band
STF	Signal Task Force
SV	Satellite Vehicle
SVN	Satellite Vehicle Number
TACAN	Tactical Air Navigation
TOA	Time Of Arrival
US	United States
UTC	Universal Time Coordinated

Chapter 1

Introduction

In this introductory Chapter the Galileo system is briefly presented, discussing the scope and the functioning of this future global navigation satellite system.

The frequency allocation and the signal that will be used in the Galileo system are also outlined in Section 1.2: in the following of this thesis only the AltBOC (*Alternative Binary Offset Carrier*) signal in the E5 band will be exhaustively discussed, considering the issues related to the architecture and the functioning of an AltBOC receiver.

Finally, the motivation of the thesis and the organization of the following Chapters are outlined in Section 1.3.

1.1 Overview of the Galileo System

More and more often, it will become necessary to ascertain one's precise position in space and time in a reliable manner. In a few years time this will be possible with the **GALILEO** satellite radio navigation system. Galileo is an initiative of the *European Union* (EU), in collaboration with the *European Space Agency* (ESA) and European Industries, to launch a European financed *Global Navigation Satellite System* (GNSS) under civilian control.

Satellite radio navigation is an advanced technology, which has been developed over the last thirty years or so, essentially for military purposes originally. It enables anyone with a receiver capable of picking up signals emitted by a constellation of satellites to quickly determine their position in time and space very accurately.

The operating principle is simple: the satellites orbit around the earth, composing a constellation, and they are equipped with an atomic clock that measures time very accurately. The satellites emit personalized signals indicating the precise time the signal leaves the satellite. The ground receiver, incorporated for example into a mobile phone, has in its memory the precise details

Figure 1.1: Illustration of the constellation of satellites for the GALILEO European Satellite Navigation System [1]

of the orbits of all the satellites in the constellation (these data are also broadcasted by the satellites). By reading the incoming signal, it can thus recognize the particular satellite, determine the time taken by the signal to arrive and calculate the distance from the satellite. Once the ground receiver receives the signals from at least four satellites simultaneously, it can synchronize its local clock with the satellite clock and it can calculate its position, with a typical precision within one meter.

Galileo is Europe's initiative for a state-of-the-art global navigation satellite system, providing a highly accurate, guaranteed global positioning service under civilian control. It is the second step of the Europe to develop its own GNSS capability, after the *European Geostationary Navigation Overlay Service* (EGNOS, operational from 2004), the Europe's first foray into satellite navigation [2].

In detail, in the *European Commission* (EC) policy paper leading to the Galileo Resolution at the Transport Council Meeting (see Reference [3]) it was stated:

"Galileo must be an open, global system,
fully compatible with GPS, but independent from it".

While providing autonomous navigation and positioning services, Galileo will at the same time be inter-operable with the United States' *Global Positioning System* (GPS) and also with the Russia's *Global Orbiting Navigation Satellite System* (GLONASS), the two other global satellite navigation systems. An user will be able to take a position with the same receiver from any of the

satellites in any combination. By offering dual frequencies as standard, however, Galileo will deliver real-time positioning accuracy down to the meter range, which is unprecedented for a publicly available system. It will guarantee availability of the service under all but the most extreme circumstances and will inform users within seconds of a failure of any satellite (*integrity*). This will make it suitable for applications where safety is crucial, such as running trains, guiding cars and landing aircraft. The combined use of Galileo and other GNSS systems will offer much improved performances for all kinds of user communities all over the world [2].

The Galileo system architecture, similarly to other satellite radio navigation systems (GPS and GLONASS), will be composed by three segments (as shown in Figure 1.2):

1. the **space segment**, corresponding to in-orbit satellites;
2. the **ground segment**, composed by the control centers and up-link stations that control the space segment;
3. the **user segment**, consisting of all the users of the Galileo system.

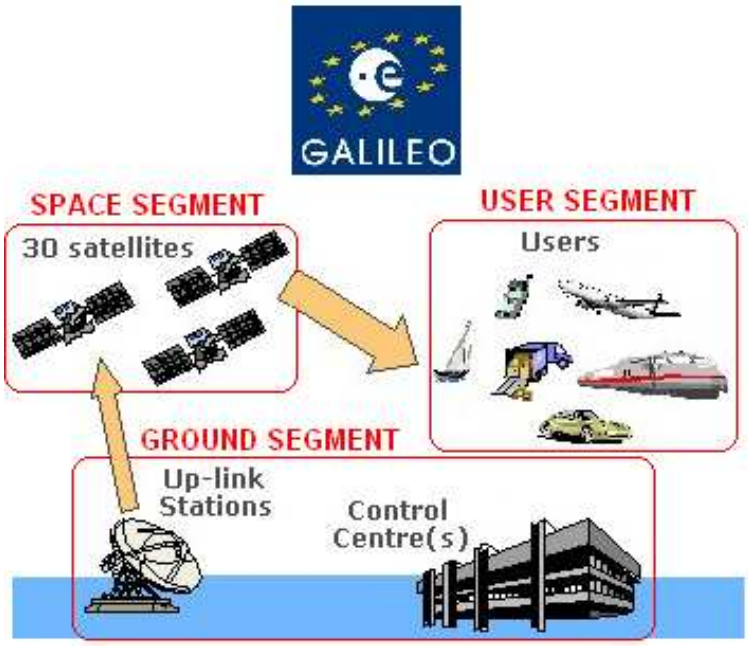

Figure 1.2: Architecture of the GALILEO system

In detail, the fully deployed Galileo system should be operational by 2011 and its **space segment** will consist of a constellation of 30 satellites (27 operational + 3 spares), positioned in three circular *Medium Earth Orbit* (MEO) planes at a nominal average orbit semi-major axis of 29601.297 Km, and at an inclination of the orbital planes of 56° with reference to the equatorial

plane. Once this is achieved, the Galileo navigation signals will provide a good coverage even at latitudes up to 75° north and 75° south [4].

The Galileo **ground segment** comprises the control segment for operation as well as orbit and time determination (GCS or *Ground Control Segment*) and the system for integrity monitoring (IDS or *Integrity Determination System*). The GCS will consist of reference stations, up-link stations and control centers. The IDS will include monitor stations, up-link stations for integrity data and central stations for integrity computations. In the European area the integration with the EGNOS ground segment plays an important role [5].

The information provided by the two other segments will be used by the **user segment**, consisting of all users on land, on water, in the air and in space. In detail, numerous applications are planned for Galileo, including positioning and derived value-added services concerning many sectors, such as transport (vehicle location, route searching, speed control, guidance systems, etc.), social services (e.g. aid for the disabled or elderly), the justice system and customs services (location of suspects, border controls), public works (geographical information systems), search and rescue systems, or leisure (direction-finding at sea or in the mountains, etc.) [2].

The Galileo programme is being carried out in three phases:

- **definition**;
- **development** and **in-orbit validation**;
- **full deployment** and **operations**.

The first phase has been recently completed, with the definition of the Galileo system architecture, the frequency plan and the modulation format to be used for the signals transmitted to the satellites (up-link, taking advantage of the S-band) and from the satellites (down-link, taking advantage of the L-band, as discussed in next Section).

After the definition phase, the development and *In-Orbit Validation* (IOV) phase is already well under way, with GIOVE-A, the first test satellite (see Figure 1.3) launched on 28 December 2005 aboard a Soyuz-Fregat rocket from the Baikonur Cosmodrome. The GIOVE-A satellite is in good health and started transmitting the first Galileo signals from medium Earth orbit on 12 January 2006 [1].

GIOVE-A's mission (formerly known as GSTB-V2/A) is to secure use of the frequencies allocated by the *International Telecommunications Union* (ITU) for the Galileo system, demonstrate critical technologies for the navigation payloads of future operational Galileo satellites, characterize the radiation environment of the orbits planned for the Galileo constellation and test the receivers on the ground.

Figure 1.3: Artist's impression of GIOVE-A satellite in orbit [1]

A second demonstrator satellite, GIOVE-B, built by the European consortium Galileo Industries (Germany), is currently being tested and will be launched later.

Until year-end 2008, four operational satellites will be launched to validate the basic Galileo space and related ground segments. Once this *In-Orbit Validation* (IOV) phase is completed, the remaining satellites will be launched to achieve *Full Operational Capability* (FOC), in order to have the Galileo system fully operational worldwide by 2011. In detail, the full deployment phase will cover the manufacture and launch of the remaining 26 satellites plus the completion of the ground segment, comprising a worldwide network of stations and service centers [1].

1.2 Galileo frequency plan and services

The Galileo frequency structure and signal design has been developed by the *Signal Task Force* (STF) of the *European Commission* (EC). The Signal Task Force was a working group involved in the design of the Galileo frequency and signal plan, during the definition phase [6].

Galileo will provide 10 navigation signals with *Right-Hand Circular Polarization* (RHCP) in the so-called L-band [7]. In detail, these signals will be transmitted in four frequency bands: the **E5a** band (1164-1191.795 MHz), the **E5b** band (1191.795-1215 MHz), the **E6** band (1260-1300 MHz) and the **L1** band (1559-1591 MHz). The latest frequency band (L1) is also called **E1**, in the terminology of the Galileo system.

In Figure 1.4, the beginning and ending frequencies of each band and the corresponding central carrier frequencies are reported. The frequency bands that are common to Galileo and to GPS (Ea/L5 and E1/L1) are also highlighted.

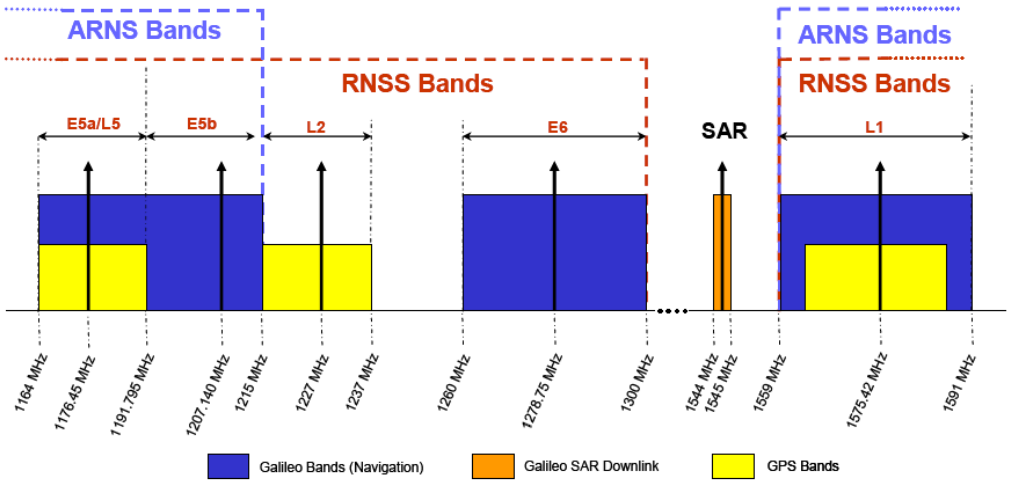

Figure 1.4: Galileo frequency plan [4]

The frequency bands for the Galileo system have been selected in the allocated spectrum for *Radio Navigation Satellite Systems* (RNSS) and, in addition to that, E5a, E5b and L1 bands are included in the allocated spectrum for *Aeronautical Radio Navigation Services* (ARNS), employed by Civil-Aviation users, and allowing dedicated safety-critical applications. It must be noted that also the band allocated for the downlink signals for the *Search-and-Rescue* (SAR) service is depicted in Figure 1.4. In fact, Galileo will provide enhanced distress localization and call features for the provision of a *Search-and-Rescue* (SAR) service inter-operable with the COSPAS-SARSAT system [4].

All Galileo transmitting satellites will share the same frequency bands, making use of *Code Division Multiple Access* (CDMA) technique. Spread Spectrum signals will be transmitted including different (quasi-orthogonal) ranging codes per signal component, per signal, per frequency and per Galileo satellites [4]. In this way, a future Galileo receiver will be able to distinguish the different signals coming from different Galileo satellites.

In addition, different modulation types will be used for the Galileo signals in E5, E6 and E1 bands, allowing different services mapped on these bands. Figure 1.5 illustrates the baseline Galileo signals' spectral characteristics as well as modulation, chip rate and data rate for each Galileo signal (except for the PRS service signals, that are classified).

In detail, 10 signals will be transmitted and 4 of them will be data-free channels, so-called **pilot channels** (ranging codes not modulated by data): these channels will offer an aid in the recovery of the data channels, providing robust tracking of the satellite signal.

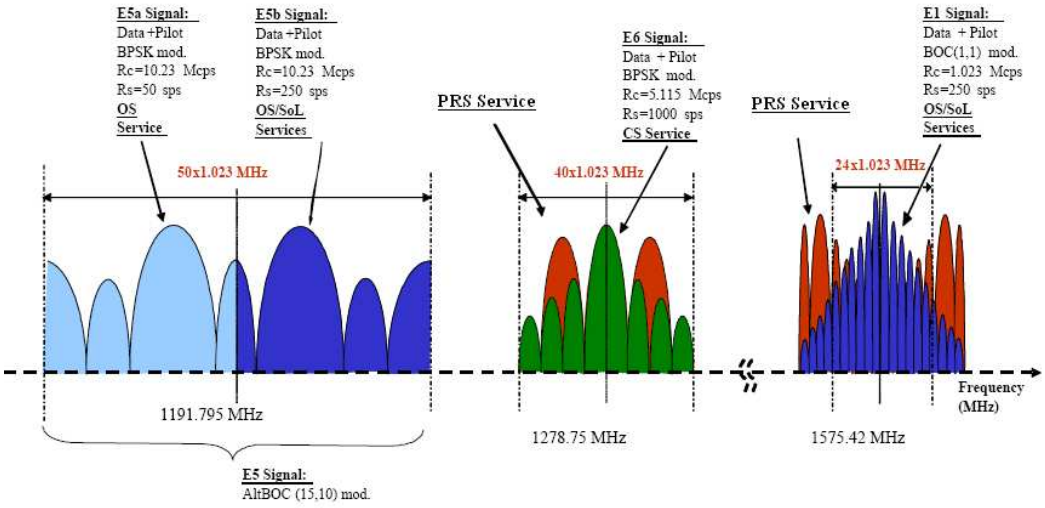

Figure 1.5: Galileo signals and mapping to services [4]

The **data channels** will provide the following categories of services (as stated in References [4], [6] and [7]):

- the **Open Service** (OS) signals will use un-encrypted ranging codes and un-encrypted navigation data messages on the E5a, E5b and E1 carriers, providing a freely accessible navigation message (F/NAV). OS data will be accessible to all users and will include mainly navigation data and SAR (*Search-and-Rescue*) data;

- the **Safety-of-Life** (SoL) service signals will use the OS ranging codes and navigation data messages on E5b and E1 carriers, providing extended system integrity information with an integrity navigation message (I/NAV). SoL data will include mainly integrity and *Signal in Space Accuracy* (SISA) data;

- the **Commercial Service** (CS) signals will use the OS ranging codes and navigation data messages, with an additional commercial navigation message (C/NAV) on the E6 carrier, using an encrypted CS ranging code and navigation data message. All CS data will be encrypted and will be provided by some service providers that interface with the Galileo Control Center. Access to those commercial data will be provided directly to the users by the service providers;

- the **Public Regulated Service** (PRS) signals will use the encrypted PRS ranging code and navigation data messages on the E6 and E1 carriers, providing governmental navigation message (G/NAV). The PRS signals will be accessible only to authorized users (police forces, military users, etc.) and information about these signals are classified.

A synthesis of the modulations and the signal parameters that will be used for the Galileo system is provided in Table 1.1, where all the signals that will be used for OS, SoL and CS services are presented (PRS signals are not illustrated, because they are classified). It must be noted that the power sharing between pilot and data channels of each carrier will be always 50% [4].

Signal name	Channel	Modulation Type	Chip Rate [Mcps]	Symbol Rate [sps]	User min. received power above 10° elevation [dBW] (based on an ideally matched and isotropic 0 dBi antenna and lossless atmosphere)
E5	E5a data	AltBOC(15,10)	10.23	50	-155
	E5a pilot			N/A	
	E5b data			250	-155
	E5b pilot			N/A	
E6	E6-B data	BPSK(5)	5.115	1000	-155
	E6-C pilot			N/A	
E1	E1-B data	BOC(1,1)	1.023	250	-157
	E1-C pilot			N/A	

Table 1.1: Main Galileo navigation signal parameters, for the signals used for OS/SoL/CS services (PRS signals are not presented) [4]

Furthermore, a 1/2 rate Viterbi convolutional coding scheme will be used for all the data channels [7]. This means that the true data rates (in bits per second) will be the half of the symbol rates (in symbols per second) presented in Table 1.1.

Considering the signals in the E5 band (that will be the subject of this thesis), the E5a and E5b signals will be modulated onto a single E5 carrier using a technique known as **AltBOC** (*Alternative BOC*). The composite of the E5a and E5b signals is denoted as the E5 signal and can be processed as a single large bandwidth signal with an appropriate user receiver implementation [4].

1.3 Motivation and contents of the thesis

This thesis is motivated by the emerging interest on the Galileo signals, due to the possibility to develop innovative receivers, taking advantage of new Galileo signals that will be transmitted in next years.

In detail, the interest of Galileo receivers is motivated by the following differences, between the future Galileo system and the current global navigation satellite systems (e.g. GPS):

- a **larger number of signals** will be transmitted by the Galileo system, using different frequency bands (E5, E6, E1): this implies an increased complexity and computational capability for the future Galileo receivers, with respect to current GPS receivers;

- **new modulation and multiplexing schemes** will be used (BOC, AltBOC) and only a little know how in terms of signal processing could be adapted to the new receivers: innovative architectures and signal processing techniques could be developed;
- **larger bandwidths** (equal or larger than 10 times the bandwidth of the current GPS C/A signal) will be used: the future Galileo receivers must use high sampling frequencies, but this could lead to better accuracy in the position estimation;
- **new services** will be provided by the Galileo system (SoL, CS, PRS), in addition to the *Open Service* (OS) navigation signals: multi-function and multi-band receivers are foreseeable;
- four **pilot channels** will also be transmitted in E5a, E5b, E6 and E1 bands: the acquisition process and the tracking operations can take advantage of these data-free channels, achieving improved performances;
- considering the signal **acquisition**, longer codes will be used in Galileo system (with respect of the current GPS C/A code) and the correlation functions obtained with the new modulation schemes (BOC, AltBOC) will present multiple correlation peaks, implying an ambiguity issue: different acquisition strategies must be investigated and innovative approaches could be discovered;
- new **tracking** techniques, that are suitable to the future Galileo signals could also be developed: improved tracking performances are foreseeable with respect of GPS receivers, both in presence of noise and multipath effect, considering the new modulation formats and the wide bandwidth of the signals; however, the danger of false acquisition and tracking, due to the ambiguity issue of the BOC and AltBOC signals, must be considered and ad-hoc unambiguous techniques must be employed.

In particular, the most promising signal that will be transmitted by the Galileo system is the **AltBOC** (*Alternative BOC*) modulated signal in the E5 band (E5a + E5b sidebands). Some articles in literature point out that the AltBOC modulation could lead to formidable performances in terms of tracking noise and multipath, for a receiver able to process the entire E5 band. Therefore the AltBOC demodulation and tracking is one of most interesting problem in Galileo receiver design.

It must be noted that at the moment the AltBOC signal is discussed only in few papers, that often result difficult to understand. Besides, the future receiver architectures for the AltBOC signal are only highlighted and a complete discussion and comparison between all possible arrangements is not present in literature at the moment. In addition, also the acquisition operations and the multipath mitigation techniques that are suitable for the AltBOC signal are not exhaustively discussed.

A complete study of the receivers for Galileo E5 AltBOC signal is then the subject of this thesis, that is organized in seven Chapters:

Chapter 1: the first Chapter (that you have just read) is an introduction of the field of studies where this thesis is inserted: the Galileo system is briefly presented, pointing out the different signals that will be transmitted in the assigned frequency bands;

Chapter 2: the AltBOC modulation, that will be transmitted in Galileo E5 band, is studied in deep in this Chapter, presenting all the signal components used for this modulation. An explanation of the derivation of the E5 AltBOC modulation from conventional BOC modulations is also presented;

Chapter 3: the AltBOC signal features are then exhaustively discussed in the third Chapter, where it is explained the modulation complexity and the advantages that this implies. In addition, the correlation proprieties of the AltBOC signals are pointed out, introducing a complex correlation scheme, that could be used to track the AltBOC signal;

Chapter 4: the fourth Chapter concerns the AltBOC receiver architectures; some possibile arrangements that could be used for the reception of the AltBOC signal are introduced, considering the signal tracking functioning and comparing the implementation complexity and the foreseeable performances of each arrangement;

Chapter 5: a complete study of possible acquisition strategies for the AltBOC signal, that at the moment is not present in literature, is done in this Chapter. The receiver architectures presented in previous Chapter are considered and the differences between the acquisition techniques used in current GNSS receivers and those needed with the proposed AltBOC architectures are pointed out;

Chapter 6: in this Chapter the code multipath mitigation problem is discussed for the AltBOC signal, trying to adapt to the AltBOC receivers the well-known discriminator-based techniques used in common GPS receivers and considering also two emerging mitigation techniques. The performances of each arrangement is then evaluated and compared;

Chapter 7: in this final Chapter, the results obtained are summarized, pointing out the innovative concepts presented in this thesis and listing also the open problems and the future activities about the AltBOC receivers.

At the end of this thesis, two Appendixes are included: the first (**Appendix A**) discuss the cross-correlation effect between the PRN codes that will be used in E5 band, whereas the other (**Appendix B**) contains a demonstration for one of the multipath mitigation techniques illustrated in Chapter 6 (the ELS technique).

Chapter 2

Galileo AltBOC signal in E5 band

The AltBOC modulation (*Alternative BOC*) will be used for Galileo signals in E5 band. This modulation scheme is an extension of the BOC modulation (*Binary Offset Carrier*) and has a similar signal spectrum.

However the AltBOC modulation used in Galileo navigation system is the result of an optimization process, done to meet the *Signal In Space* (SIS) requirements defined by the *European Space Agency* (ESA) and the other institutions involved in satellites and receivers design. In fact, for the E5 band it is necessary a constant envelope modulation that combines two separate sidebands (E5a and E5b), each consisting itself of two binary signals (in I and Q channels).

The AltBOC modulation offers the advantage that the E5a and E5b bands can be processed independently, as traditional BPSK signals, in low cost receivers, or together with an appropriate wide band demodulation scheme, leading to formidable performances in terms of tracking noise and multipath. Therefore the AltBOC demodulation and tracking is one of most interesting problem in Galileo receiver design.

In this Chapter it is presented the AltBOC modulation, with the signal components transmitted in E5 band. Indeed for the AltBOC modulation it is necessary the generation of subcarriers, ranging codes and navigation data, and all these components are analytically described in the following Sections. In the last part of this Chapter the concept of the constant envelope AltBOC modulation is introduced, after a brief preamble about the BOC modulations, that permits to understand how the modulation that will be used in E5 band has been derived from the BOC modulations.

All the notations used in this Chapter and subsequent ones are coherent with the following conventions, used in SIS-ICD [4]. The signal parameters are defined in Table 2.1, with the indices:

- *'X'* accounting for the respective signal (*E5*, *E5a* or *E5b*);
- *'Y'* accounting for the respective signal component (S or P for subcarrier) or signal channel (I or Q) within the signal *'X'*.

Parameter	**Explanation**	**Unit**
f_X	Carrier frequency	Hz
P_X	RF-Signal power	W
$L_{X\text{-}Y}$	Ranging code repetition period	chips
$T_{C,X\text{-}Y}$	Ranging code chip length	s
$T_{S,X\text{-}Y}$	Subcarrier period	s
$T_{D,X\text{-}Y}$	Navigation message symbol duration	s
$R_{C,X\text{-}Y}$	$= 1/T_{C,X\text{-}Y}$; Code chip rate	Hz
$R_{S,X\text{-}Y}$	$= 1/T_{S,X\text{-}Y}$; Subcarrier frequency	Hz
$R_{D,X\text{-}Y}$	$= 1/T_{D,X\text{-}Y}$; Navigation message symbol rate	Hz
$C_{X\text{-}Y}(t)$	Binary (NRZ modulated) ranging code	
$D_{X\text{-}Y}(t)$	Binary (NRZ modulated) navigation message signal	
$sc_{X\text{-}Y}(t)$	Subcarrier waveform	
$e_{X\text{-}Y}(t)$	Binary NRZ modulated navigation signal component including code and navigation message data (if available); $e_{X\text{-}Y}(t) = C_{X\text{-}Y}(t) \cdot D_{X\text{-}Y}(t)$	
$s_X(t)$	$= s_{X\text{-}I}(t) + \mathrm{j} \cdot s_{X\text{-}Q}(t)$ Normalized baseband signal (unit mean power);	
$S_X(t)$	$= \sqrt{2 \cdot P_X} \cdot [s_{X\text{-}I}(t) \cdot \cos(2\pi f_X t) - s_{X\text{-}Q}(t) \cdot \sin(2\pi f_X t)]$ Signal pass-band representation;	
$c_{X\text{-}Y,k}$	'k^{th}' Chip of the ranging code	
$d_{X\text{-}Y,k}$	'k^{th}' Symbol of the navigation message	
$DC_{X\text{-}Y}$	$= T_{D,X\text{-}Y}/T_{C,X\text{-}Y}$; Number of code chips per symbol	
$\lvert i \rvert_L$	'i' modulo L	
$[i]_{DC}$	Integer part of (i/DC)	
$\mathrm{rect}_T(t)$	Function "rectangle", which is equal to 1 for $0 < t < T$, and it is equal to 0 elsewhere	

Table 2.1: Signal description parameters [4]

2.1 E5 signal components

Galileo satellites shall transmit the navigation signals in E5 band using the AltBOC modulation. The modulated signal will be transmitted over a bandwidth of 92.07 MHz in Right-Hand Circular Polarization (RHCP), around a carrier frequency (f_{E5}) of 1191.795 MHz [4].

The E5 band is subdivided in two sidebands, as shown in Figure 2.1:

- **E5a** band, with a central frequency (f_{E5a}) of 1176.45 MHz;
- **E5b** band, with a central frequency (f_{E5b}) of 1207.14 MHz.

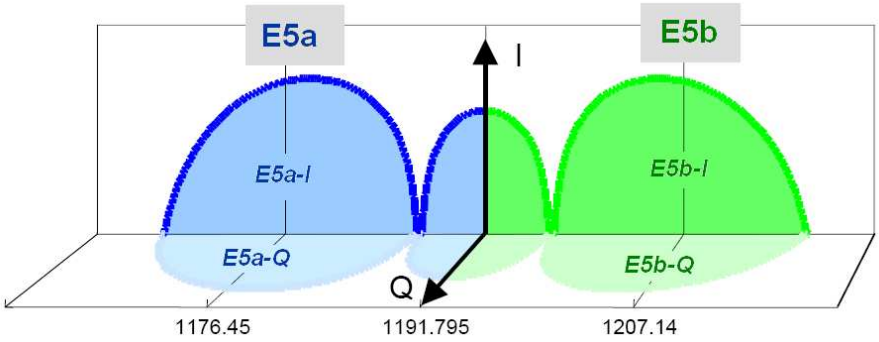

Figure 2.1: Spectral scheme for Galileo E5 band

The transmitted signal is composed by four different components. Two of them (*E5a-I* and *E5b-I*) are in phase components and will carry navigation messages, respectively for the *Open Service* (F/NAV) and the *Safety-of-Life Service* (I/NAV), whilst the other two signals (*E5a-Q* and *E5b-Q*) are in quadrature dataless channels (the so-called *pilot* channels), useful for the receiver during the acquisition and tracking operations. In Table 2.2 there are summarized the features of these signal components and the provided services.

Signal component	Channel	Code Chip Rate [Mchip/s]	Symbol Rate [symbols/s]	Service
E5a	I	10.23	50	F/NAV
	Q	10.23	No data	Pilot
E5b	I	10.23	250	I/NAV
	Q	10.23	No data	Pilot

Table 2.2: E5 AltBOC signals: chip-rates, symbol-rates and services mapped for each signal

Each component is modulated with a different PRN (*Pseudo-Random Noise*) code, that works like a spreading code in a CDMA (*Code Division Multiple Access*) system. In effect these codes are assigned to Galileo satellites so as the receiver can recognize separately each signal component transmitted from each satellite. They are also called *ranging codes*, because they are used by the receiver to determine its distance from the transmitting satellite. A general description of the PRN codes used in E5 band can be found in Section 2.1.2.

The two in phase signals carry distinct navigation data, with different symbol-rate. *E5a-I* channel is used for Open Service (F/NAV), whilst *E5b-I* carry

information for Safety-of-Life Service (I/NAV). Conversely the quadrature channels don't carry data (pilot channels), and are useful for receiver synchronization and tracking.

The four channels are modulated using the AltBOC modulation (for details see Section 2.2.4), that produces the signal spectrum schematized in Figure 2.1. This modulation scheme features a power spectrum with two sidebands (E5a and E5b). Each transmitted channel is shifted in the corresponding sideband using the subcarrier waveforms, that are analyzed in the next Section.

2.1.1 Subcarriers generation

The subcarriers used in the AltBOC modulation are the two four-valued functions $sc_{E5\text{-}S}(t)$ and $sc_{E5\text{-}P}(t)$ shown in Figure 2.2, where the index S and P denote respectively the function used for the so-called **Signal components** and for the **Product signals** in the AltBOC modulation (to understand the reason of this terminology, see Section 3.2).

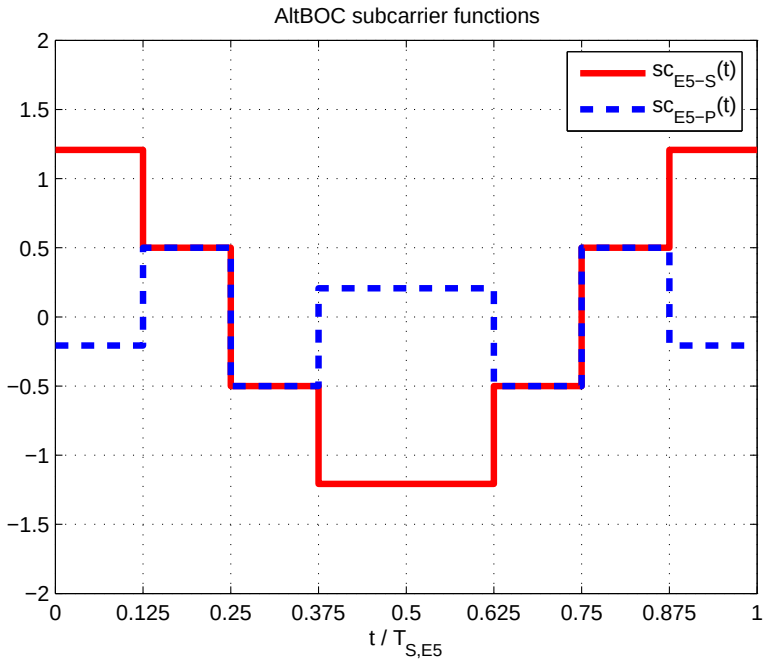

Figure 2.2: One period of the two AltBOC subcarrier functions

It must be observed that the $sc_{E5\text{-}S}(t)$ waveform resemble to a sampled cosine waveform, whereas the $sc_{E5\text{-}P}(t)$ has an irregular waveform with a lower amplitude. The reason of these waveforms will be explained in Chapter 3 (see Section 3.3), where the signal features of the modulated signal are presented.

These waveforms are generated with a subcarrier rate $R_{S,E5} = 1/T_{S,E5} = 15.345\,\text{MHz}$ $(15 \times 1.023\,\text{MHz})$ and can be represented with the following

expressions, where each subcarrier period $T_{S,E5}$ is partitioned in 8 equals sub-periods, indicated by the i index:

$$sc_{E5\text{-}S}(t) = \sum_{i=-\infty}^{+\infty} AS_{|i|_8} \cdot \mathrm{rect}_{\frac{T_{S,E5}}{8}}\left(t - i \cdot \frac{T_{S,E5}}{8}\right) \tag{2.1}$$

$$sc_{E5\text{-}P}(t) = \sum_{i=-\infty}^{+\infty} AP_{|i|_8} \cdot \mathrm{rect}_{\frac{T_{S,E5}}{8}}\left(t - i \cdot \frac{T_{S,E5}}{8}\right) \tag{2.2}$$

$$\text{where } \mathrm{rect}_T(t) = \begin{cases} 1 & \text{for } 0 < t < T \\ 0 & \text{otherwise} \end{cases}$$

The coefficients AS_i and AP_i are listed in Table 2.3.

i	**0**	**1**	**2**	**3**	**4**	**5**	**6**	**7**
AS_i	$\frac{\sqrt{2}+1}{2}$	$\frac{1}{2}$	$-\frac{1}{2}$	$\frac{-\sqrt{2}-1}{2}$	$\frac{-\sqrt{2}-1}{2}$	$-\frac{1}{2}$	$\frac{1}{2}$	$\frac{\sqrt{2}+1}{2}$
AP_i	$\frac{-\sqrt{2}+1}{2}$	$\frac{1}{2}$	$-\frac{1}{2}$	$\frac{\sqrt{2}-1}{2}$	$\frac{\sqrt{2}-1}{2}$	$-\frac{1}{2}$	$\frac{1}{2}$	$-\frac{\sqrt{2}+1}{2}$

Table 2.3: AltBOC subcarrier coefficients

To simulate the AltBOC modulation, both for the transmitter and the receiver, it is necessary to locally generate the subcarrier waveforms. In detail, with a digital system it is necessary to produce a sampled version of the subcarrier functions. Obviously the accuracy of the simulation strongly depends on the sampling frequency.

For example, choosing to represent each subcarrier period with 16 samples, in each of the 8 sub-periods there are 2 samples. The result is shown in Figure 2.3.

In Figure 2.4 the correlation proprieties of the two subcarriers waveforms are represented, simulating only one period of the subcarriers. The purpose of these graphs is to study the subcarrier waveforms, evaluating their correlation. Both the auto-correlation curves have a peak, but the one related to $sc_{E5\text{-}P}(t)$ is lower than the other, because the relative power of the two signals is:

$$P_{rel} = \frac{\left[\left(\sqrt{2}-1\right)^2 + 1\right]}{8} \cong 15\% \tag{2.3}$$

In fact the subcarrier with greater amplitude $sc_{E5\text{-}S}(t)$ is used in the AltBOC modulation for the **signal components**, whilst $sc_{E5\text{-}P}(t)$ is necessary for **product signals** that don't carry information, but are necessary to obtain a constant envelope signal (see Section 2.2.4).

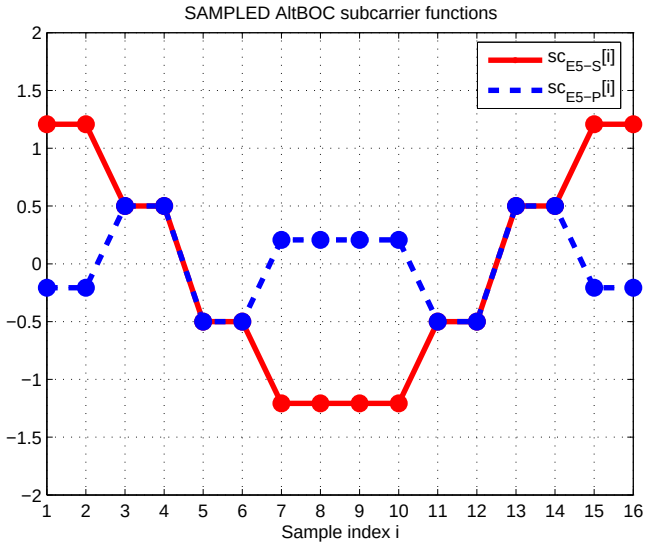

Figure 2.3: Sampled AltBOC subcarriers, with 16 samples per period

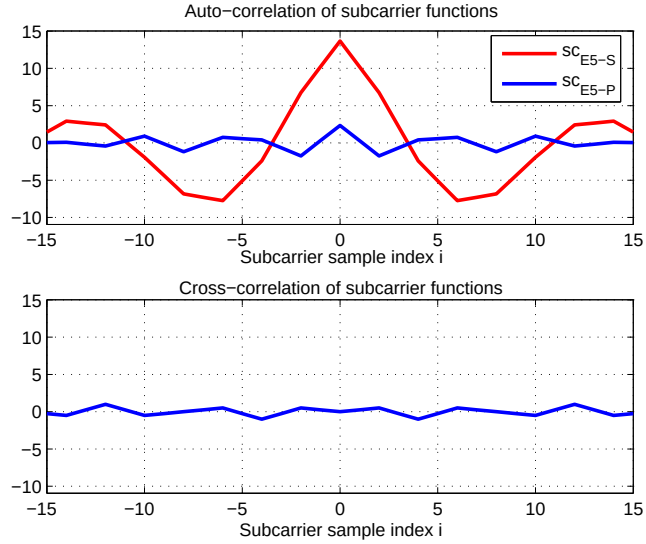

Figure 2.4: Subcarrier correlation proprieties (correlation functions evaluated with only one period of subcarriers)

2.1.2 Ranging codes generation

The code structure for Galileo spreading codes is currently in the process of being defined. The current status of system development foresees a **tiered code structure**, with a primary and a secondary code for each E5 channel. The general idea of this code structure is that successive repetitions of a primary code period are overlaid with a secondary code such that one chip of the secondary code corresponds to the entire period of the primary code. In this way long spreading codes could be generated, simply composing the

primary and the secondary codes. This concept is explained in Figure 2.5.

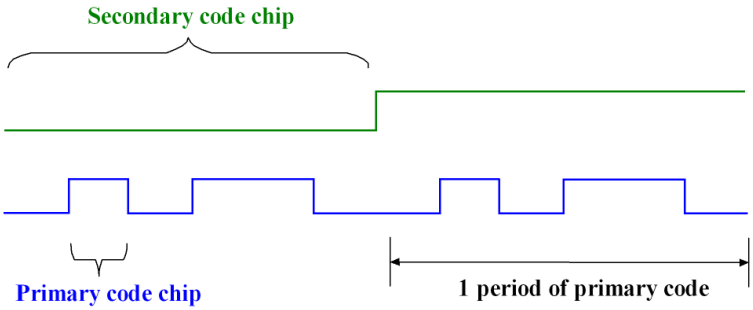

Figure 2.5: Illustration of the tiered code structure

On E5 band there are four different code types: two for E5a (I and Q channel) and two for E5b (I and Q channel). For convention, the four ranging codes are denoted with: $c_{E5a\text{-}I}$, $c_{E5a\text{-}Q}$, $c_{E5b\text{-}I}$ and $c_{E5b\text{-}Q}$. These codes are generated with a chip rate $R_C = 1/T_C = 10.23\,\text{Mchip/s}$ ($10\times1.023\,\text{Mchip/s}$). They are raging codes, used to determine pseudo-ranges between receiver and satellites, and work also like spreading codes, to discriminate satellite signals. Each satellite will use different codes and, in addition, everyone of channels in E5 band will use quasi-orthogonal codes.

The code assignment for each satellite must still to be defined, but it is known that every satellite will use four codes generated in similar manner for the four transmitted channels. These codes have different lengths, because the secondary codes differ between pilot and data channels. The primary codes have always a period of 1 ms (10230 chips), whilst secondary code length can vary from 4 to 100 ms. Table 2.4 illustrate code lengths used for each channel.

Channel	**Code length [ms]**	**Code length [chips]**	
		Primary	**Secondary**
E5a-I	20	10230	20
E5a-Q	100	10230	100
E5b-I	4	10230	4
E5b-Q	100	10230	100

Table 2.4: E5 spreading code lengths

The primary codes can be used for fast acquisitions, aiming at typical integration times for acquisition of 1 ms or a few ms, while the entire code (primary and secondary code) can be used for tracking.

The pilot channels use longer tiered codes (with a period of 100 ms) to allow the receiver to obtain excellent tracking performances. The data channels *E5a-I* and *E5b-I* use shorter codes with different lengths, since they have

different symbol-rates (see Table 2.2) and one code period corresponds exactly to one symbol duration.

The **primary codes** either can be considered as memory stored binary sequences or can be generated with linear feedback shift registers [4].

The first approach implies that the code is stored in a ROM and the code generation is straightforward, because code chips are simply read from the memory. This representation is useful for the satellite and the receiver design, because simplifies the code generation and allows more flexibility.

Instead for the second approach the primary codes are generated considering that they are truncated and combined Gold sequences. In this case the code generation can be described using a *shift register* model with 14 taps. The feedbacks are described using register polynomials, with order 14. Two parallel shift registers are used for primary code generation, the so-called base register 1 and base register 2. The primary output sequence is the exclusive OR of register 1 and 2 outputs, as well as shown in Figure 2.6.

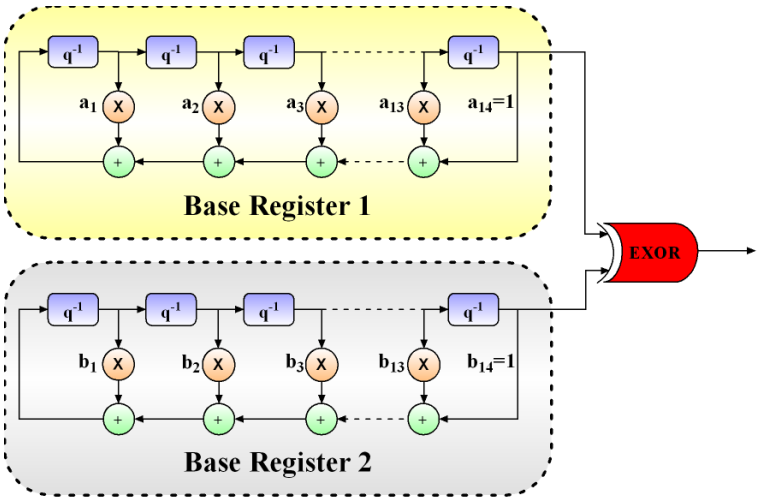

Figure 2.6: Primary code generation, with two shift registers

The primary codes for the four transmitted channels are generated using different base register polynomials and different register initializations (see the SIS-ICD [4]), to ensure low cross-correlation between channels. In detail base register 1 cells are initialized with all '1', in logic level notation, whilst base register 2 start values are different for each primary code number (1-50).

The **secondary codes** are fixed sequences (*random codes*) that cannot be generated with shift registers, but must be stored in a memory in the satellite and in the receiver. As well as shown in Table 2.4, the four channels use different secondary codes, with a different length. The secondary code sequences can be found in SIS-ICD [4].

Combining primary and secondary code chips, generated with a proper clock

frequency, long spreading codes shall be generated. The correspondence between the logic level of the code chips and the generated signal level shall be according the values stated in Table 2.5. Therefore the obtained signals are BPSK modulated.

Logic levels	Signal levels
1	−1.0
0	+1.0

Table 2.5: Logic to signal level assignment

Code correlation proprieties

After an overview of the spreading codes used in E5 band, it is then possible to examine the **correlation proprieties** of this codes. Using an arbitrary choice of two possible codes[1], the normalized auto-correlation and cross-correlation follow the shape shown in Figure 2.7. These graphs are obtained evaluating the correlation of two sequences of 10230 chips, which corresponds to one entire period of the **primary code**, and normalizing the result with the length of one code sequence. In this way the auto-correlation peak is normalized to one.

It is self-evident the quasi-orthogonality between the two codes, and the strong auto-correlation peak. The codes aren't perfectly orthogonal because, as mentioned before, they are truncated Gold sequences.

Using any other arbitrary choice of Galileo E5 codes, similar correlation figures can be obtained. Obviously the cross-correlation values may change using different codes, but their maximum value remains small compared to the auto-correlation peaks.

The non null cross-correlation could produce a small **bias** in the tracking loop of the receiver, using a locally generated code to despread the received signal (as stated in [8]). In fact each channel is tracked taking advantage of the auto-correlation peak of its PRN code, but the presence of the other codes can affect the tracking point. Typically this problem is neglected in common GPS receivers, because the induced offset is very small and is overcome by noise and other error sources. Besides, this effect is time varying because depends on the number of satellites that are in view and on their relative positions.

[1]For the simulation the first *E5a-I* code and the first *E5a-Q* code, obtained with the parameters in SIS-ICD [4], have been used. In fact in SIS-ICD [4] there are defined 50 primary codes for each E5 channel. With another arbitrary choice the results are similar, with negligible differences. In fact it must be noted that the code assignment for each satellite must still to be defined.

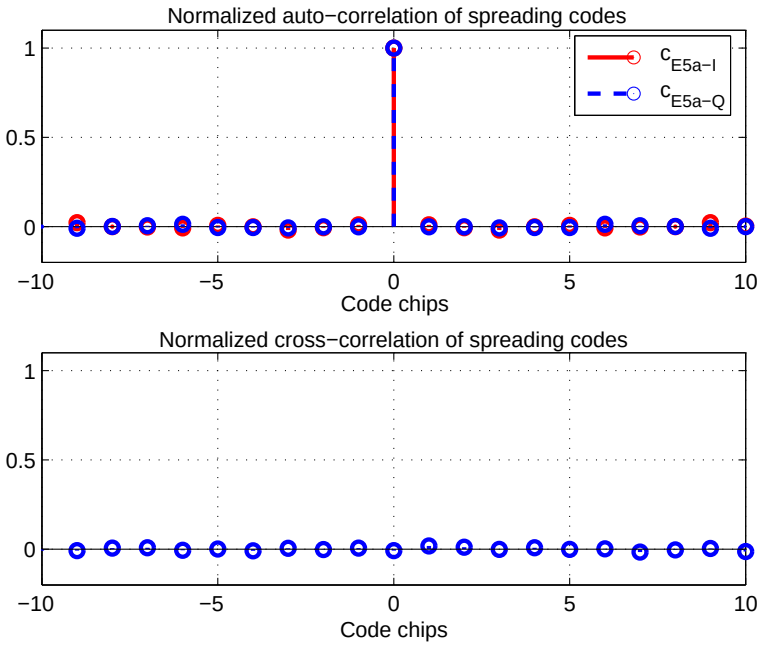

Figure 2.7: Correlation proprieties of two spreading codes used in E5 band

As demonstrated by the detailed analysis performed in Appendix A, the error caused by the non null cross-correlation is negligible also for the E5 AltBOC signal. Then for the receiver design it is acceptable to consider orthogonal the E5 PRN codes.

2.1.3 Navigation data generation

As outlined in Section 2.1, the two in phase (I) signals carry distinct navigation data, with different symbol-rates:

- *E5a-I* channel is used for *Open Service* (F/NAV) and broadcasts d_{E5a-I} navigation data to receivers at 50 symbols/s (satellite ephemeris, timing data, corrections, satellite constellation health status, and so on);
- *E5b-I* carry integrity information in d_{E5b-I} data, transmitted at 250 symbols/s, for *Safety-of-Life Service* (I/NAV).

It must be noted that a 1/2 rate Viterbi convolutional coding scheme will be used for all the data channels of the Galileo system [7]. This means that the true data rates (in bits/s) will be the half of the symbol rates (in symbols/s). A detailed description of data message generated by satellites can be found in SIS-ICD [4].

The purpose of this document is not a detailed system performance evaluation, but the goal is to analyze the signal features and the feasibility of

different demodulation schemes for the AltBOC signals. Accordingly it is possible to assume that **random data bits** are transmitted, neglecting the message structure and the coding scheme used for the data.

For more detailed simulations, the assumption of random data bits generation may also be suitable to obtain approximate *Bit-Error-Rate* (BER) values. Besides it will be necessary to take in account the positive effect in performances produced by the Viterbi convolutional coding, that is employed for all transmitted channels, adding an appropriate coding gain to the performances obtained simulating random data bits.

2.2 AltBOC modulation

All the signal components presented in previous Sections, that are the subcarriers, the ranging codes and the navigation data, are combined to obtain the AltBOC modulated wide band signal, transmitted from Galileo satellites in E5 band around the carrier frequency (f_{E5}) of 1191.795 MHz.

The *Alternative Binary Offset Carrier* (AltBOC) modulation scheme aims at generating a subcarrier signal adopting a source coding similarly to the one involved in a classical *Binary Offset Carrier* (BOC) modulation. Therefore it is possible to consider the AltBOC as an extension of the BOC modulation scheme.

In the following Section (2.2.1) the *BOC* modulations are briefly introduced, then they are used as a starting point for the derivation of the *Complex-BOC* modulation (see Section 2.2.2). This modulation scheme will be further extended in Section 2.2.3, transmitting more than one channel, and obtaining the so-called *Standard AltBOC* modulation. At the end of this Chapter (see Section 2.2.4), the true *E5 AltBOC* modulation that will be adopted for the Galileo E5 band is presented. It differs from the standard AltBOC essentially because it is a constant envelope modulation.

2.2.1 General BOC approach

The standard **Binary Offset Carrier** (BOC) is a square subcarrier modulation, that will also be used for Galileo signals transmitted in E1 and E6 bands.

To illustrate the general BOC modulation scheme, it is necessary to define a generic baseband signal component $s(t)$, modulated with square waves and with nominal power P_s, that means:

$$s(t) = \sqrt{2 \cdot P_s} \cdot e(t) \quad \text{with } e(t) \in \{+1, -1\} \tag{2.4}$$

In detail this component $e(t)$ contains the binary data $d(t)$, transmitted with a symbol rate R_D, multiplied by the chips of a PRN code $c(t)$, with a chip rate R_C (with $R_C > R_D$):

$$\begin{aligned} e(t) &= d(t) \cdot c(t) \\ &\text{with } d(t),\, c(t) \in \{+1, -1\} \end{aligned} \tag{2.5}$$

Then the baseband signal component $s(t)$ appears similar to a BPSK modulated signal and its *Power Spectral Density* (PSD) $S(f)$ has the shape of a *sinc*, as shown on the top of Figure 2.9. Obviously the width of the main lobe of this spectrum depends on the chip rate R_C of the spreading code.

The *BOC* modulated signal $s_{BOC}(t)$ is then obtained multiplying the signal $s(t)$ by a rectangular subcarrier, shown in Figure 2.8, with frequency f_{sub} (assuming $f_{sub} \geq R_C$):

$$s_{BOC}(t) = s(t) \cdot \text{sign}[\sin(2\pi f_{sub} t)] \tag{2.6}$$

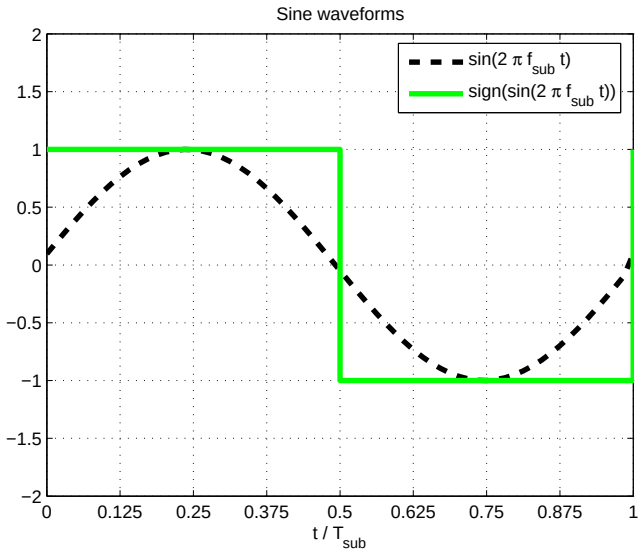

Figure 2.8: Subcarrier function for BOC modulation

This corresponds to use modified transmission pulses, with the shape of a truncated square wave and with a number of cycles equal to f_{sub}/R_C.

The Power Spectral Density $S_{BOC}(f)$ of the modulated signal could be expressed in frequency domain, neglecting high order harmonics, with the following expression:

$$S_{BOC}(f) \cong \alpha \cdot S(f) \otimes [\delta(f - f_{sub}) - \delta(f + f_{sub})] \tag{2.7}$$

$$= \alpha \cdot S(f - f_{sub}) - \alpha \cdot S(f + f_{sub}) \tag{2.8}$$

As shown in Figure 2.9, this operation splits the spectrum of the signal $S(f)$ into two symmetrical parts, located at the left and right side of the carrier frequency. It must be noted that both the sidebands of the spectrum $S_{BOC}(f)$ contain information about the transmitted baseband signal $s(t)$.

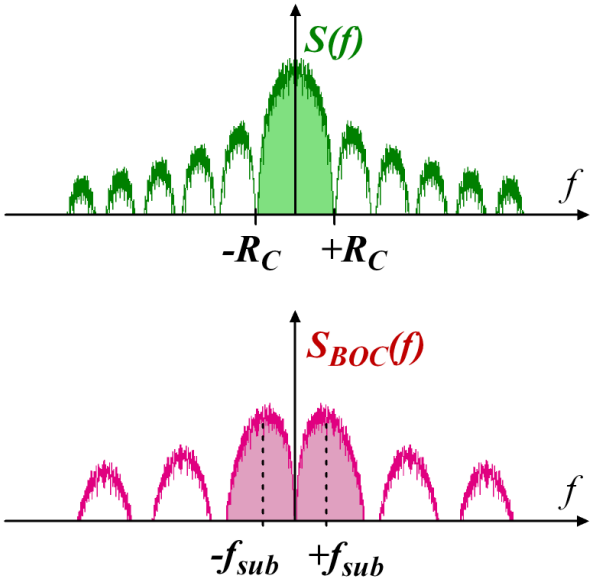

Figure 2.9: BOC modulation scheme

In literature typically this modulation is denoted as BOC(f_{sub},R_C), to point out the main parameters of the modulation, while for Galileo system this modulation is conventionally denoted BOC(m,n), with $m \geq n$, where:

- m denotes the subcarrier frequency f_{sub}, normalized by the reference frequency $f_0 = 1.023\,\text{MHz}$ (it is the chip rate of the GPS C/A code);
- n denotes the chip rate R_C of the spreading code, normalized by $f_0 = 1.023\,\text{MHz}$.

In Figure 2.9 a BOC(1,1) was simulated, whereas in Figure 2.10 it is possible to see the spectrum of BOC modulations with different m and n, compared with the current GPS signals (C/A and P codes).

It must be noticed that the shape of the spectrum of the modulated signal depends on the values m and n, and in detail on the ratio m/n (or f_{sub}/R_C). In fact in Figure 2.10 it is evident that increasing the ratio m/n the distance between the two main lobes increases; simultaneously the power around the carrier frequency decreases, then the spectrum appears more selective, allowing to manage in different way the available bandwidth.

This means that with a proper choice of the BOC parameters it is possible (with some limitations) to share the same frequency band between different systems (e.g. GPS and Galileo) or to allocate in a single band more than one

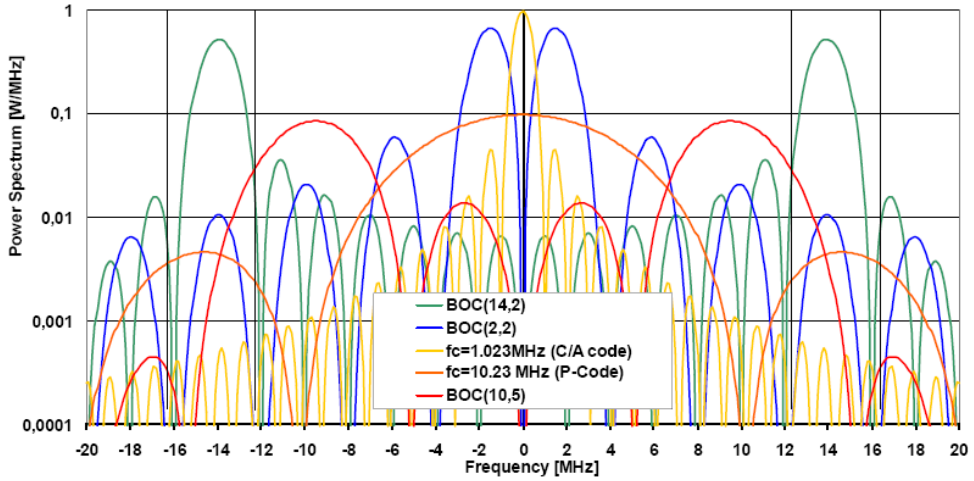

Figure 2.10: Comparison of different BOC modulations and the GPS BPSK signals (C/A and P codes) [6]

signal of the same system, allowing more services with a negligible signal loss and interference.

2.2.2 General AltBOC approach (Complex-BOC)

The idea of the *Alternative BOC* (AltBOC) modulation is to operate a similar process than that performed for the BOC modulation, but multiplying a base band signal $s(t)$ by a "complex" rectangular subcarrier. To understand this concept, it is necessary first to introduce the **Complex-BOC** modulation. In the following Sections this modulation scheme will be further extended, to derive the true AltBOC modulation that will be adopted for Galileo system.

In agreement to previous Section (2.2.1), the generic BPSK baseband signal $s(t)$ to be transmitted is defined with the following expression:

$$s(t) = \sqrt{2 \cdot P_s} \cdot d(t) \cdot c(t) \quad \text{with } d(t),\, c(t) \in \{+1, -1\} \tag{2.9}$$

where P_s is the nominal power of $s(t)$, $d(t)$ are the binary data, transmitted with a symbol rate R_D, and $c(t)$ is the PRN code, with a chip rate R_C (with $R_C > R_D$).

The *Complex-BOC* modulation is then performed multiplying $s(t)$ with two rectangular subcarrier waveforms, following the expression:

$$s_{Complex\text{-}BOC}(t) = s(t) \cdot \{\text{sign}[\cos(2\pi f_{sub} t)] + \text{j} \cdot \text{sign}[\sin(2\pi f_{sub} t)]\} \tag{2.10}$$

In literature (see [8]) this modulation scheme is called *Complex-BOC* because

it is an extension of the BOC modulation, employing a complex exponential obtained with two rectangular subcarrier waveforms (shown in green in Figure 2.11).

In some articles the *Complex-LOC* modulation is also discussed. It differs from the Complex-BOC for the subcarrier waveforms, that are continuous cosine and sine waveforms (shown with dashed black lines in Figure 2.11). These two modulations have similar spectral proprieties, then for shortness only the Complex-BOC modulation is discussed in the following.

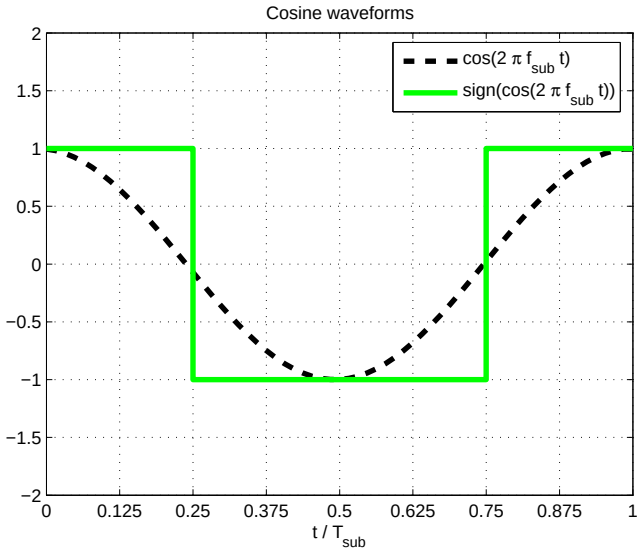

(a)

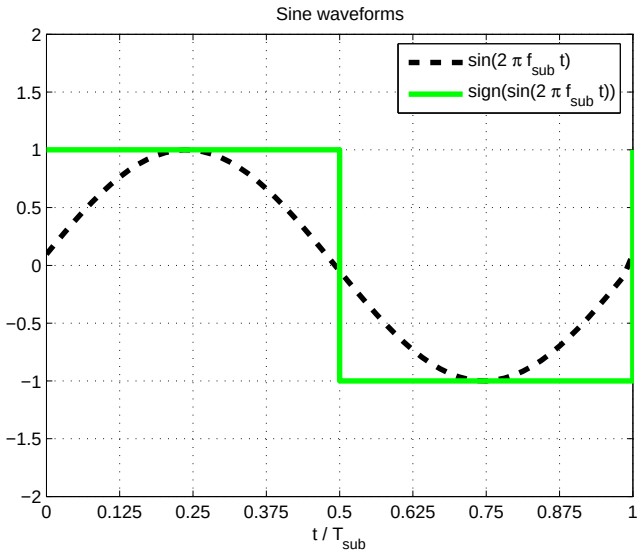

(b)

Figure 2.11: Subcarrier functions for Complex-LOC and Complex-BOC modulations: cosine waveforms (a) and sine waveforms (b)

Using the following notations to represent the rectangular subcarriers:

$$cr(t) = \text{sign}[\cos(2\pi f_{sub} t)] \tag{2.11}$$
$$sr(t) = \text{sign}[\sin(2\pi f_{sub} t)] \tag{2.12}$$

it is then possible to define the following "complex" exponentials, obtained composing the rectangular subcarriers:

$$er(t) = cr(t) + \mathrm{j} \cdot sr(t) \tag{2.13}$$
$$er^*(t) = cr(t) - \mathrm{j} \cdot sr(t) \tag{2.14}$$

They performs in a similar way than complex exponentials defined with the continuous waveforms $\cos(2\pi f_{sub} t)$ and $\sin(2\pi f_{sub} t)$:

$$exp(\mathrm{j} \cdot 2\pi f_{sub} t) = \cos(2\pi f_{sub} t) + \mathrm{j} \cdot \sin(2\pi f_{sub} t) \tag{2.15}$$
$$exp(\mathrm{j} \cdot 2\pi f_{sub} t)^* = \cos(2\pi f_{sub} t) - \mathrm{j} \cdot \sin(2\pi f_{sub} t) \tag{2.16}$$
$$\text{with } exp(\mathrm{j} \cdot 2\pi f_{sub} t)^* = exp(-\mathrm{j} \cdot 2\pi f_{sub} t)$$

The only difference dealing with the rectangular subcarriers is in the spectrum: the power spectral density of the ideal exponential $exp(\mathrm{j} \cdot 2\pi f_{sub} t)$ is a delta centered on the frequency of the cosine and the sine (f_{sub}), whereas the complex exponential $er(t) = cr(t) + \mathrm{j} \cdot sr(t)$ has the power spectral density shown in Figure 2.12.

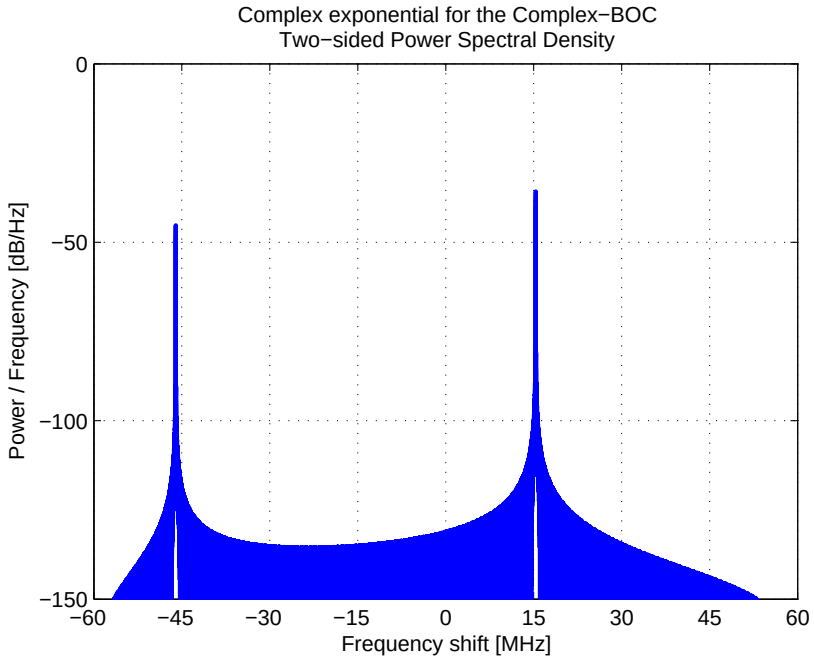

Figure 2.12: Spectrum of the complex exponential $er(t)$, used in the Complex-BOC modulation

It should be noted that the main peak of $er(t)$ is centered to the subcarrier frequency f_{sub} (= 15.345 MHz, in this case), and there is a secondary peak centered around $-3 \cdot f_{sub}$ (= −46.035 MHz). For $er^*(t)$ the same considerations are valid, obviously inverting the signs.

Equation (2.10) of the Complex-BOC modulation can then be rewritten pointing out the complex exponential $er(t)$:

$$s_{Complex\text{-}BOC}(t) = s(t) \cdot er(t) \tag{2.17}$$

In this way the signal spectrum is not split up as in BOC modulation, but only shifted to higher frequencies. In fact, the main peak of the spectrum of the exponential (see Figure 2.12) produces a frequency shift in the modulated signal spectrum, whereas the secondary peak centered around $-3 \cdot f_{sub}$ could be neglected. Accordingly, the baseband BPSK signal $s(t)$ is shifted around the frequency of the complex exponential ($+f_{sub}$), as illustrated in Figure 2.13. A secondary component is also present around $-3 \cdot f_{sub}$, but it is negligible.

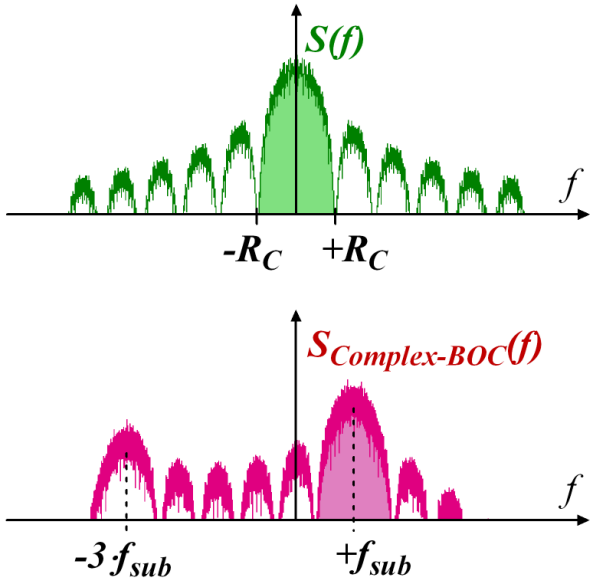

Figure 2.13: Complex BOC modulation scheme

The signal spectrum of the modulated signal $s_{Complex\text{-}BOC}(t)$, neglecting higher order harmonics, can then be approximated with:

$$S_{Complex\text{-}BOC}(f) \cong \alpha \cdot S(f) \otimes \delta(f - f_{sub}) \tag{2.18}$$

$$= \alpha \cdot S(f - f_{sub}) \tag{2.19}$$

2.2.3 Standard AltBOC modulation

The technique described in previous Section allows to shift a baseband BPSK signal $s(t)$ to a higher frequency ($+f_{sub}$). Obviously the Complex-BOC could

also be used to shift the signal to lower frequencies, using the complex conjugate exponential $er^*(t)$. A different BPSK signal, containing a different ranging code and navigation data message, can then be shifted to the lower frequency range. By this principle the two typical side lobes of the spectrum of a BOC signal can carry different information.

The **Standard AltBOC** modulation take advantage of this idea, transmitting information using four channels (*E5a-I*, *E5a-Q*, *E5b-I* and *E5b-Q*) that are shifted in two separate sidebands (*E5a* and *E5b*): in this way each sideband contains two channels, that are allocated in quadrature (I and Q). In detail, the four signal components to be transmitted are defined with the following expressions, where every signal has unit mean power:

$$
\begin{aligned}
e_{E5a\text{-}I}(t) &= d_1(t) \cdot c_1(t) && (2.20)\\
e_{E5a\text{-}Q}(t) &= d_2(t) \cdot c_2(t) && (2.21)\\
e_{E5b\text{-}I}(t) &= d_3(t) \cdot c_3(t) && (2.22)\\
e_{E5b\text{-}Q}(t) &= d_4(t) \cdot c_4(t) && (2.23)\\
&\text{with } d_i(t),\, c_i(t) \in \{+1, -1\}\\
&\text{for } i \in \{1,2,3,4\}
\end{aligned}
$$

The different PRN codes $c_i(t)$ must be orthogonal and in this way every channel could transmit different data $d_i(t)$.

The four channels are combined in accord with the following equation, for the *Standard AltBOC* modulation:

$$
\begin{aligned}
s_{Standard\ AltBOC}(t) &= [e_{E5a\text{-}I}(t) + \mathrm{j} \cdot e_{E5a\text{-}Q}(t)] \cdot er^*(t) +\\
&\quad +[e_{E5b\text{-}I}(t) + \mathrm{j} \cdot e_{E5b\text{-}Q}(t)] \cdot er(t) \qquad (2.24)
\end{aligned}
$$

Recalling previous Section, it is evident that this operation shift to lower frequency (*E5a* sideband) the two components $e_{E5a\text{-}I}(t)$ and $e_{E5a\text{-}Q}(t)$, whereas $e_{E5b\text{-}I}(t)$ and $e_{E5b\text{-}Q}(t)$ are shifted to higher frequency (*E5b* sideband).

The resulting spectrum of the modulated signal $s_{Standard\ AltBOC}(t)$ is shown in Figure 2.14, where the two sidebands are pointed out. This figure has been obtained simulating a Standard AltBOC(15,10), that means assuming a subcarrier frequency $f_{sub} = 15.345\,\mathrm{MHz}$, and a chip rate of the spreading code $R_C = 10.23\,\mathrm{Mchip/s}$, according to the notation previously introduced for the BOC modulations (see Section 2.2.1).

Expanding the two complex exponentials, Equation (2.24) becomes:

$$
\begin{aligned}
s_{Standard\ AltBOC}(t) &= \{[e_{E5a\text{-}I}(t) + e_{E5b\text{-}I}(t)] \cdot cr(t) +\\
&\quad +[e_{E5a\text{-}Q}(t) - e_{E5b\text{-}Q}(t)] \cdot sr(t)\} +\\
&\quad +\mathrm{j} \cdot \{[e_{E5a\text{-}Q}(t) + e_{E5b\text{-}Q}(t)] \cdot cr(t) +\\
&\quad +[e_{E5b\text{-}I}(t) - e_{E5a\text{-}I}(t)] \cdot sr(t)\} \qquad (2.25)
\end{aligned}
$$

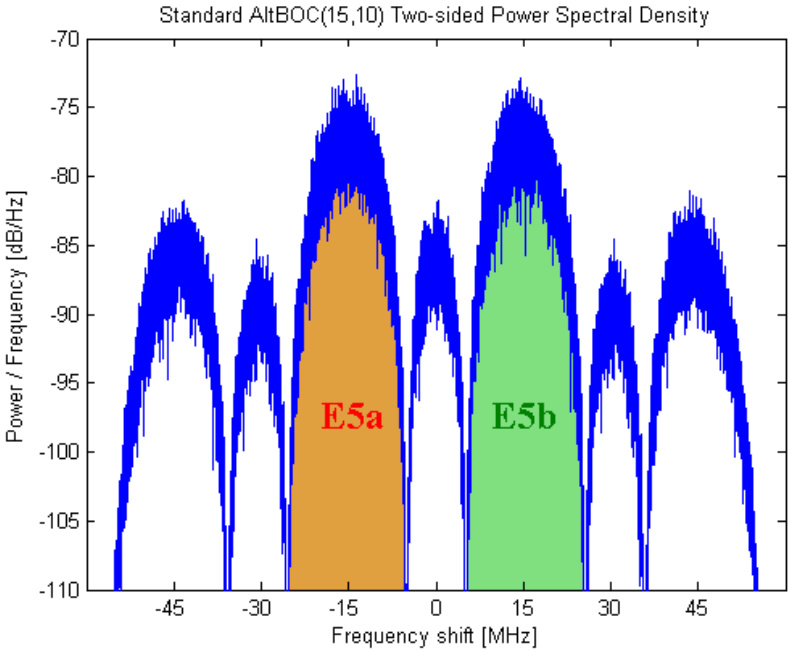

Figure 2.14: Standard AltBOC(15,10) signal spectrum

It is possible to demonstrate [9] that this signal can take 9 different values, which can be written by the following formula, where k defines the scattered plot number as in Figure 2.15:

$$s_{Standard\ AltBOC}(t) = A_k \cdot e^{j k \frac{\pi}{4}} \tag{2.26}$$

$$\text{with} \begin{cases} k \in \{0,1,2,3,4,5,6,7,8\} & \\ A_k = 0 & \text{for } k = 0 \\ A_k = 2\sqrt{2} & \text{for } k = \text{odd} \\ A_k = 4 & \text{for } k = \text{even} \end{cases}$$

It is clearly seen that the *Standard AltBOC* is not a constant envelope modulation. The I and Q channels can even be zero at the same time and some portions of the signal may be at null power (this peculiarity will be discussed in Section 3.2).

Having a non-constant envelope signal is a real issue when considering the satellite amplifiers. Indeed, to optimize the link budget and the power efficiency on-board the satellite, these amplifiers need to work at saturation. If this is the case, a non-constant envelope signal would suffer some distortions that will affect the tracking performances of the receiver [10]. In conclusion the *Standard AltBOC* is not suitable for the Galileo system.

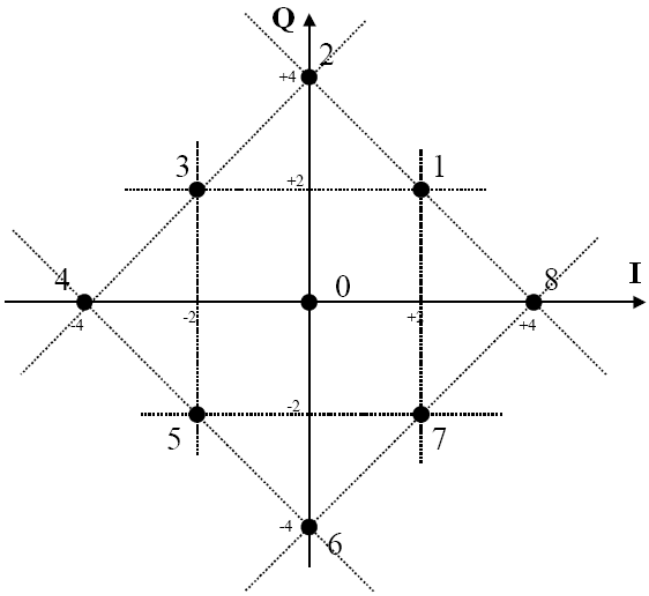

Figure 2.15: Scattered plots for standard AltBOC modulation [9]

2.2.4 Constant envelope AltBOC (E5 AltBOC)

The true modulation scheme that will be adopted for Galileo E5 transmissions is a modified version of the Standard AltBOC, with similar spectral features (BOC-like spectrum) and some adjustments to obtain a constant envelope signal (8-PSK like signal). In detail the subcarriers are not simple square waves, but are more complicated waveforms (see Section 2.1.1). Moreover in the signal expression it is necessary to add some others terms (called *product signals* in equations below) to meet the requirement for a constant envelope.

This modulation is conventionally denoted **E5 AltBOC(15,10)**. In particular the notation used in Galileo system is $AltBOC(m,n)$, where:

- $m = 15$ denotes the subcarrier frequency, that is $f_{sub} = R_{S,E5} = 15.345\,\text{MHz}$, normalized by the reference frequency $f_0 = 1.023\,\text{MHz}$;
- $n = 10$ denotes the chip rate of the spreading code $R_C = 10.23\,\text{Mchip/s}$, normalized by $f_0 = 1.023\,\text{MHz}$.

The E5 signal will be modulated combining the four unencrypted ranging codes $c_{E5a\text{-}I}(t)$, $c_{E5a\text{-}Q}(t)$, $c_{E5b\text{-}I}(t)$ and $c_{E5b\text{-}Q}(t)$ (previously presented in Section 2.1.2) with the navigation data streams $d_{E5a\text{-}I}(t)$ and $d_{E5b\text{-}I}(t)$ (see Section 2.1.3), as shown in Figure 2.16.

To illustrate the constant envelope AltBOC modulation, first it is necessary to define the following four base band signal components:

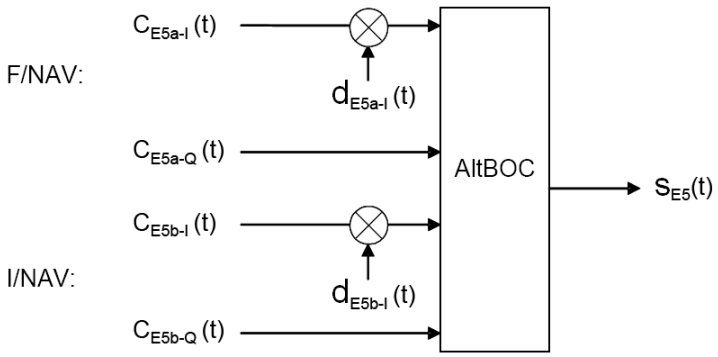

Figure 2.16: Modulation scheme for the E5 AltBOC signal [4]

- $\mathbf{e_{E5a\text{-}I}}(t)$, obtained from the F/NAV navigation data stream $d_{E5a\text{-}I}(t)$, modulated with the unencrypted ranging code $c_{E5a\text{-}I}(t)$;
- $\mathbf{e_{E5a\text{-}Q}}(t)$, that is a data-less component (pilot channel) obtained with the unencrypted ranging code $c_{E5a\text{-}Q}(t)$;
- $\mathbf{e_{E5b\text{-}I}}(t)$, obtained from the I/NAV navigation data stream $d_{E5b\text{-}I}(t)$, modulated with the unencrypted ranging code $c_{E5b\text{-}I}(t)$;
- $\mathbf{e_{E5b\text{-}Q}}(t)$, that is a data-less component (pilot channel) obtained with the unencrypted ranging code $c_{E5b\text{-}Q}(t)$.

The analytical expressions of the four signal components are presented in the following, with the notations used in SIS-ICD [4]:

$$e_{E5a\text{-}I}(t) = \sum_{i=-\infty}^{+\infty} \left[c_{E5a\text{-}I,|i|_{L_{E5a\text{-}I}}} \cdot d_{E5a\text{-}I,[i]_{DC_{E5a\text{-}I}}} \cdot \mathrm{rect}_{T_{c,E5a\text{-}I}}(t - i \cdot T_{c,E5a\text{-}I}) \right] \quad (2.27)$$

$$e_{E5a\text{-}Q}(t) = \sum_{i=-\infty}^{+\infty} \left[c_{E5a\text{-}Q,|i|_{L_{E5a\text{-}Q}}} \cdot \mathrm{rect}_{T_{c,E5a\text{-}Q}}(t - i \cdot T_{c,E5a\text{-}Q}) \right] \quad (2.28)$$

$$e_{E5b\text{-}I}(t) = \sum_{i=-\infty}^{+\infty} \left[c_{E5b\text{-}I,|i|_{L_{E5b\text{-}I}}} \cdot d_{E5b\text{-}I,[i]_{DC_{E5b\text{-}I}}} \cdot \mathrm{rect}_{T_{c,E5b\text{-}I}}(t - i \cdot T_{c,E5b\text{-}I}) \right] \quad (2.29)$$

$$e_{E5b\text{-}Q}(t) = \sum_{i=-\infty}^{+\infty} \left[c_{E5b\text{-}Q,|i|_{L_{E5b\text{-}Q}}} \cdot \mathrm{rect}_{T_{c,E5b\text{-}Q}}(t - i \cdot T_{c,E5b\text{-}Q}) \right] \quad (2.30)$$

Accordingly, the wide band E5 signal generated by the **E5 AltBOC(15,10)** modulation can be represented with the following expression:

$$\begin{aligned} s_{E5}(t) = {} & \frac{1}{2 \cdot \sqrt{2}} \cdot [e_{E5a\text{-}I}(t) + \mathrm{j} \cdot e_{E5a\text{-}Q}(t)] \cdot [sc_{E5\text{-}S}(t) - \mathrm{j} \cdot sc_{E5\text{-}S}(t - T_{s,E5}/4)] + \\ & + \frac{1}{2 \cdot \sqrt{2}} \cdot [e_{E5b\text{-}I}(t) + \mathrm{j} \cdot e_{E5b\text{-}Q}(t)] \cdot [sc_{E5\text{-}S}(t) + \mathrm{j} \cdot sc_{E5\text{-}S}(t - T_{s,E5}/4)] + \\ & + \frac{1}{2 \cdot \sqrt{2}} \cdot [\overline{e}_{E5a\text{-}I}(t) + \mathrm{j} \cdot \overline{e}_{E5a\text{-}Q}(t)] \cdot [sc_{E5\text{-}P}(t) - \mathrm{j} \cdot sc_{E5\text{-}P}(t - T_{s,E5}/4)] + \\ & + \frac{1}{2 \cdot \sqrt{2}} \cdot [\overline{e}_{E5b\text{-}I}(t) + \mathrm{j} \cdot \overline{e}_{E5b\text{-}Q}(t)] \cdot [sc_{E5\text{-}P}(t) + \mathrm{j} \cdot sc_{E5\text{-}P}(t - T_{s,E5}/4)] \end{aligned} \quad (2.31)$$

where the signal $s_{E5}(t)$ is represented with its complex envelope and the two subcarrier waveforms $sc_{E5\text{-}S}(t)$ and $sc_{E5\text{-}P}(t)$ are recalled in Figure 2.17.

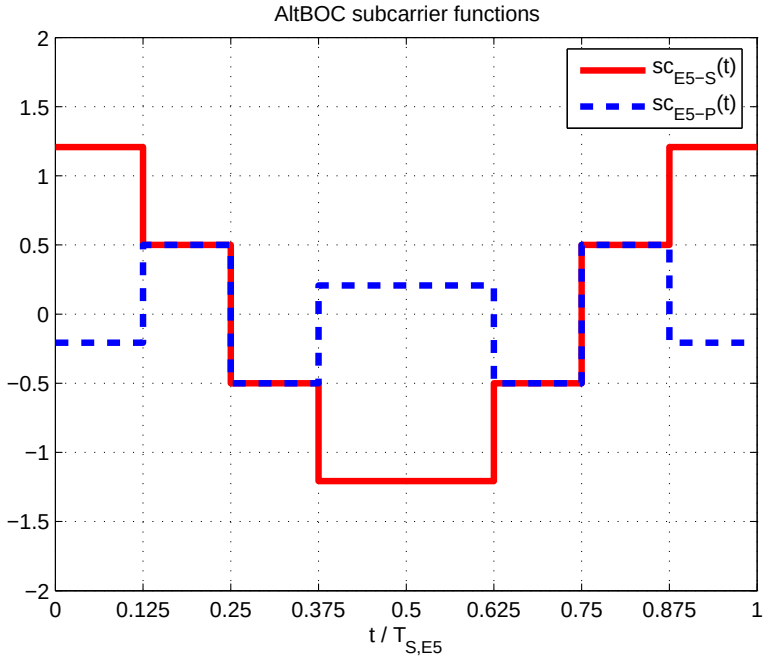

Figure 2.17: One period of the two AltBOC subcarrier functions

The first two terms of Equation (2.31) contains the **signal components** $e_{E5a\text{-}I}(t)$, $e_{E5a\text{-}Q}(t)$, $e_{E5b\text{-}I}(t)$ and $e_{E5b\text{-}Q}(t)$. All these terms have a *sinc* spectrum, with main lobe width determined by two times the spreading codes chip rate ($R_C = 10.23\,\text{Mchip/s}$).

They are multiplied by "complex" exponentials, obtained using the $sc_{E5\text{-}S}(t)$ waveform. In detail the two *E5b* channels ($e_{E5b\text{-}I}(t)$ and $e_{E5b\text{-}Q}(t)$, in the second term) are multiplied by the exponential defined by:

$$sc_{E5\text{-}S}(t) + \mathrm{j} \cdot sc_{E5\text{-}S}\left(t - \frac{T_{s,E5}}{4}\right)$$

This exponential has the power spectral density shown in Figure 2.18, and produces a frequency shift that moves the two channels to the *E5b* central frequency.

Similarly the first exponential in Equation (2.31):

$$sc_{E5\text{-}S}(t) - \mathrm{j} \cdot sc_{E5\text{-}S}\left(t - \frac{T_{s,E5}}{4}\right)$$

downshift the two *E5a* channels from the baseband to the *E5a* central frequency.

In that way the four channels are correctly shifted to their respective frequency band. The frequency shifts are both exactly equals to the subcarriers

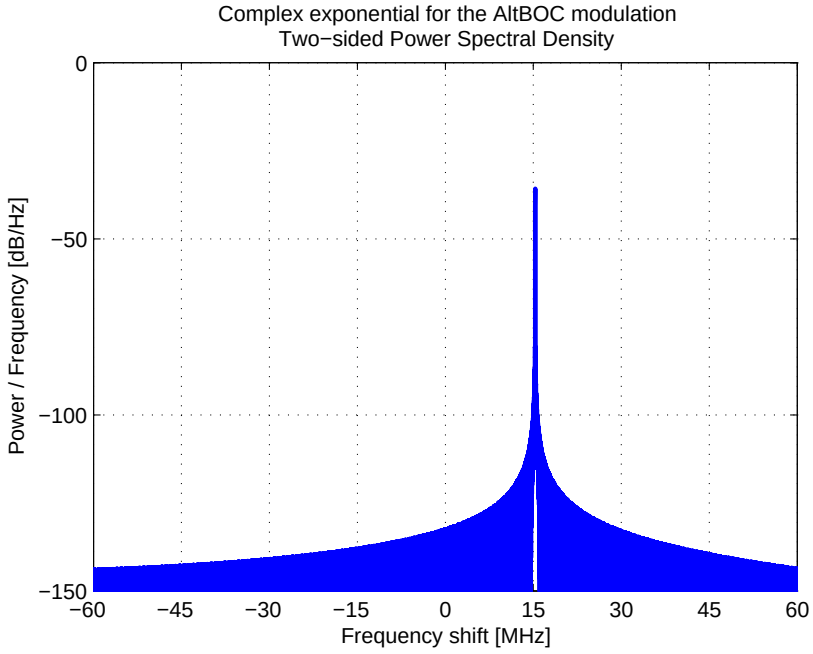

Figure 2.18: Spectrum of the complex exponential, used in the AltBOC modulation

frequency (15.345 MHz). The obtained signal spectrum is shown in Figure 2.19, where the typical AltBOC(15,10) spectrum could be observed, with two main lobes centered respectively at -15.345 and $+15.345$ MHz.

The last two terms in Equation (2.31) contain the dashed components $\overline{e}_{E5a\text{-}I}(t)$, $\overline{e}_{E5a\text{-}Q}(t)$, $\overline{e}_{E5b\text{-}I}(t)$ and $\overline{e}_{E5b\text{-}Q}(t)$, that represent the so-called **product signals**:

$$\overline{e}_{E5a\text{-}I}(t) = e_{E5a\text{-}Q}(t) \cdot e_{E5b\text{-}I}(t) \cdot e_{E5b\text{-}Q}(t) \quad (2.32)$$

$$\overline{e}_{E5a\text{-}Q}(t) = e_{E5a\text{-}I}(t) \cdot e_{E5b\text{-}I}(t) \cdot e_{E5b\text{-}Q}(t) \quad (2.33)$$

$$\overline{e}_{E5b\text{-}I}(t) = e_{E5a\text{-}I}(t) \cdot e_{E5a\text{-}Q}(t) \cdot e_{E5b\text{-}Q}(t) \quad (2.34)$$

$$\overline{e}_{E5b\text{-}Q}(t) = e_{E5a\text{-}I}(t) \cdot e_{E5a\text{-}Q}(t) \cdot e_{E5b\text{-}I}(t) \quad (2.35)$$

The presence of these product terms in the AltBOC expression is necessary to satisfy the requirement of a constant envelope signal (an exhaustive explanation can be found in the following Chapter, in Section 3.2).

Separating the signal $s_{E5}(t)$ in Equation (2.31) in phase and quadrature terms (real and imaginary parts), the following expressions, that are further utilized (see Section 3.4) to describe the received signal, are finally obtained:

$$s_{E5}(t) = s_{E5\mathbf{I}}(t) + \mathrm{j} \cdot s_{E5\mathbf{Q}}(t) \quad (2.36)$$

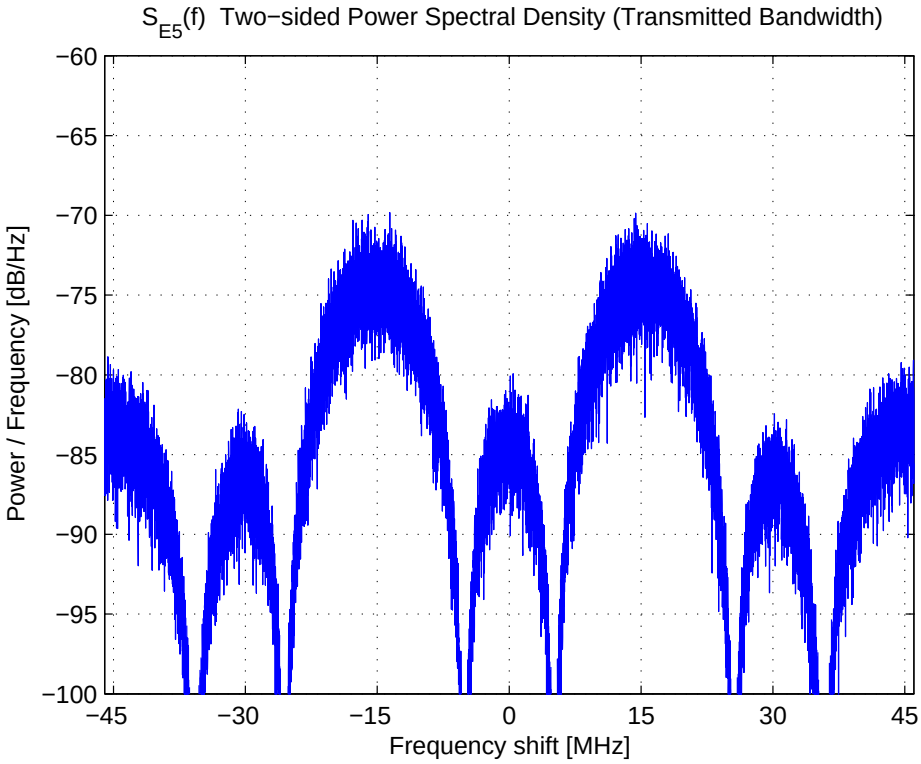

Figure 2.19: E5 AltBOC(15,10) signal spectrum

$$
\begin{aligned}
s_{E5\mathbf{I}}(t) \;=\; & \frac{1}{2\cdot\sqrt{2}}\cdot\left[e_{E5a\text{-}I}(t)+e_{E5b\text{-}I}(t)\right]\cdot sc_{E5\text{-}S}(t)+ \\
& +\frac{1}{2\cdot\sqrt{2}}\cdot\left[e_{E5a\text{-}Q}(t)-e_{E5b\text{-}Q}(t)\right]\cdot sc_{E5\text{-}S}\left(t-\frac{T_{s,E5}}{4}\right)+ \\
& +\frac{1}{2\cdot\sqrt{2}}\cdot\left[\overline{e}_{E5a\text{-}I}(t)+\overline{e}_{E5b\text{-}I}(t)\right]\cdot sc_{E5\text{-}P}(t)+ \\
& +\frac{1}{2\cdot\sqrt{2}}\cdot\left[\overline{e}_{E5a\text{-}Q}(t)-\overline{e}_{E5b\text{-}Q}(t)\right]\cdot sc_{E5\text{-}P}\left(t-\frac{T_{s,E5}}{4}\right) \qquad (2.37) \\
s_{E5\mathbf{Q}}(t) \;=\; & \frac{1}{2\cdot\sqrt{2}}\cdot\left[e_{E5a\text{-}Q}(t)+e_{E5b\text{-}Q}(t)\right]\cdot sc_{E5\text{-}S}(t)+ \\
& +\frac{1}{2\cdot\sqrt{2}}\cdot\left[e_{E5b\text{-}I}(t)-e_{E5a\text{-}I}(t)\right]\cdot sc_{E5\text{-}S}\left(t-\frac{T_{s,E5}}{4}\right)+ \\
& +\frac{1}{2\cdot\sqrt{2}}\cdot\left[\overline{e}_{E5a\text{-}Q}(t)+\overline{e}_{E5b\text{-}Q}(t)\right]\cdot sc_{E5\text{-}P}(t)+ \\
& +\frac{1}{2\cdot\sqrt{2}}\cdot\left[\overline{e}_{E5b\text{-}I}(t)-\overline{e}_{E5a\text{-}I}(t)\right]\cdot sc_{E5\text{-}P}\left(t-\frac{T_{s,E5}}{4}\right) \qquad (2.38)
\end{aligned}
$$

An intuitive explanation

To understand more clearly the frequency shift operated by the subcarriers, it is necessary to make some approximations in the AltBOC expression.

First of all, it is possible to neglect the product signals, because these terms are multiplied by the subcarrier $sc_{E5\text{-}P}(t)$, that has smaller amplitude than $sc_{E5\text{-}S}(t)$ subcarrier (see Figure 2.17).

Equations (2.37) and (2.38) can then be approximated with the following expressions, where the terms multiplied by $sc_{E5\text{-}P}(t)$ are neglected:

$$\begin{aligned} s_{E5\mathbf{I}}(t) \cong\ & \frac{1}{2\cdot\sqrt{2}}\cdot[e_{E5a\text{-}I}(t)+e_{E5b\text{-}I}(t)]\cdot sc_{E5\text{-}S}(t)+ \\ & +\frac{1}{2\cdot\sqrt{2}}\cdot[e_{E5a\text{-}Q}(t)-e_{E5b\text{-}Q}(t)]\cdot sc_{E5\text{-}S}\left(t-\frac{T_{s,E5}}{4}\right) \end{aligned} \tag{2.39}$$

$$\begin{aligned} s_{E5\mathbf{Q}}(t) \cong\ & \frac{1}{2\cdot\sqrt{2}}\cdot[e_{E5a\text{-}Q}(t)+e_{E5b\text{-}Q}(t)]\cdot sc_{E5\text{-}S}(t)+ \\ & +\frac{1}{2\cdot\sqrt{2}}\cdot[e_{E5b\text{-}I}(t)-e_{E5a\text{-}I}(t)]\cdot sc_{E5\text{-}S}\left(t-\frac{T_{s,E5}}{4}\right) \end{aligned} \tag{2.40}$$

Then, it is possible to combine again the in phase and quadrature terms of the modulated signal $s_{E5}(t)$:

$$\begin{aligned} s_{E5}(t) \cong\ & \frac{1}{2\cdot\sqrt{2}}\cdot\left\{[e_{E5a\text{-}I}(t)+e_{E5b\text{-}I}(t)]\cdot sc_{E5\text{-}S}(t)+\right. \\ & \left.+[e_{E5a\text{-}Q}(t)-e_{E5b\text{-}Q}(t)]\cdot sc_{E5\text{-}S}\left(t-\frac{T_{s,E5}}{4}\right)\right\}+ \\ & +\mathrm{j}\cdot\frac{1}{2\cdot\sqrt{2}}\cdot\left\{[e_{E5a\text{-}Q}(t)+e_{E5b\text{-}Q}(t)]\cdot sc_{E5\text{-}S}(t)+\right. \\ & \left.+[e_{E5b\text{-}I}(t)-e_{E5a\text{-}I}(t)]\cdot sc_{E5\text{-}S}\left(t-\frac{T_{s,E5}}{4}\right)\right\} \end{aligned} \tag{2.41}$$

The subcarrier waveform $sc_{E5\text{-}S}(t)$ resemble to a sampled cosine waveform, and its shifted version $sc_{E5\text{-}S}(t-T_{s,E5}/4)$ is similar to a sampled sine. Therefore it is possibile to write a further approximation of the AltBOC signal, using continuous sine and cosine waveforms (*Complex-LOC* approximation, see Section 2.2.2):

$$\begin{aligned} s_{E5}(t) \cong\ & \frac{1}{2\cdot\sqrt{2}}\cdot\{[e_{E5a\text{-}I}(t)+e_{E5b\text{-}I}(t)]\cdot\cos(2\pi f_{sub}t)+ \\ & +[e_{E5a\text{-}Q}(t)-e_{E5b\text{-}Q}(t)]\cdot\sin(2\pi f_{sub}t)\}+ \\ & +\mathrm{j}\cdot\frac{1}{2\cdot\sqrt{2}}\cdot\{[e_{E5a\text{-}Q}(t)+e_{E5b\text{-}Q}(t)]\cdot\cos(2\pi f_{sub}t)+ \\ & +[e_{E5b\text{-}I}(t)-e_{E5a\text{-}I}(t)]\cdot\sin(2\pi f_{sub}t)\} \end{aligned} \tag{2.42}$$

$$\text{with } f_{sub}=R_{S,E5}=\frac{1}{T_{S,E5}}$$

The terms in Equation (2.42) can be reordered in the following manner:

$$s_{E5}(t) \cong \frac{1}{2\cdot\sqrt{2}}\cdot\{[e_{E5a\text{-}I}(t)+\mathrm{j}\cdot e_{E5a\text{-}Q}(t)]\cdot[\cos(2\pi f_{sub}t)-\mathrm{j}\cdot\sin(2\pi f_{sub}t)]+ \\ +[e_{E5b\text{-}I}(t)+\mathrm{j}\cdot e_{E5b\text{-}Q}(t)]\cdot[\cos(2\pi f_{sub}t)+\mathrm{j}\cdot\sin(2\pi f_{sub}t)]\} \quad (2.43)$$

Then it is possible to substitute the continuous cosine and sine waveforms with complex exponentials:

$$s_{E5}(t) \cong \frac{1}{2\cdot\sqrt{2}}\cdot[e_{E5a\text{-}I}(t)+\mathrm{j}\cdot e_{E5a\text{-}Q}(t)]\cdot\mathrm{e}^{-\mathrm{j}\cdot 2\pi f_{sub}t}+ \\ +\frac{1}{2\cdot\sqrt{2}}\cdot[e_{E5b\text{-}I}(t)+\mathrm{j}\cdot e_{E5b\text{-}Q}(t)]\cdot\mathrm{e}^{+\mathrm{j}\cdot 2\pi f_{sub}t} \quad (2.44)$$

An expression similar to the Equation (2.24) of the *Standard AltBOC* has been finally obtained. Observing this expression it is possible to understand the frequency shift performed by the complex exponentials, obtained using the subcarrier waveforms. The $e_{E5a\text{-}I}(t)$ and $e_{E5a\text{-}Q}(t)$ signals are left shifted in E5a band, as $e_{E5b\text{-}I}(t)$ and $e_{E5b\text{-}Q}(t)$ go to E5b band, coherently with the scheme in Figure 2.20.

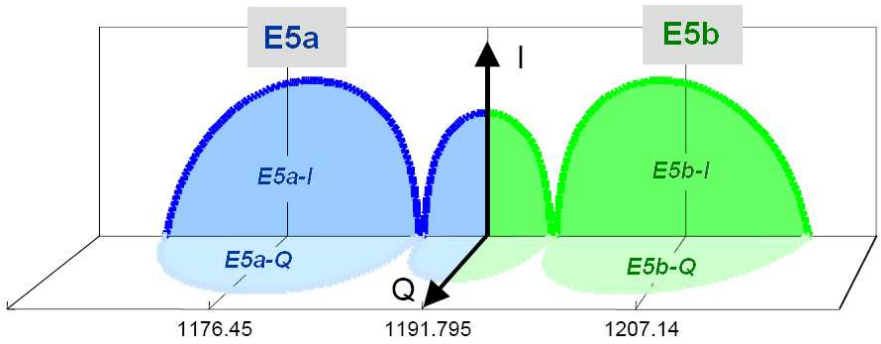

Figure 2.20: Spectral scheme for Galileo E5 band

Generation of the modulated signal using a LUT

In conclusion of this Section, it must be reported that the rather complex scheme presented for the Constant envelope AltBOC modulation can be easily implemented in a digital transmitter, simplifying the satellite on-board signal generator. In fact, as reported in [4] and [9], the E5 AltBOC modulated signal could be generated using a simple **Look-Up Table** (LUT) for the phase assignments (see Table 2.6).

As noticed above, the E5 AltBOC features an 8-PSK constellation. Then the modulated signal could be expressed with the following formula:

$$s_{E5}(t) = \mathrm{e}^{\mathrm{j}\cdot\frac{\pi}{4}\cdot k(t)} \quad (2.45)$$

$$\text{with } k(t)\in\{1,2,3,4,5,6,7,8\}$$

	Input Quadruples															
$e_{E5a\text{-}I}$	-1	-1	-1	-1	-1	-1	-1	-1	1	1	1	1	1	1	1	1
$e_{E5b\text{-}I}$	-1	-1	-1	-1	1	1	1	1	-1	-1	-1	-1	1	1	1	1
$e_{E5a\text{-}Q}$	-1	-1	1	1	-1	-1	1	1	-1	-1	1	1	-1	-1	1	1
$e_{E5b\text{-}Q}$	-1	1	-1	1	-1	1	-1	1	-1	1	-1	1	-1	1	-1	1
i_{Ts}	$k(t)$ (according to $s_{E5}(t) = e^{j\cdot\frac{\pi}{4}\cdot k(t)}$)															
0	5	4	4	3	6	3	1	2	6	5	7	2	7	8	8	1
1	5	4	8	3	2	3	1	2	6	5	7	6	7	4	8	1
2	1	4	8	7	2	3	1	2	6	5	7	6	3	4	8	5
3	1	8	8	7	2	3	1	6	2	5	7	6	3	4	4	5
4	1	8	8	7	2	7	5	6	2	1	3	6	3	4	4	5
5	1	8	4	7	6	7	5	6	2	1	3	2	3	8	4	5
6	5	8	4	3	6	7	5	6	2	1	3	2	7	8	4	1
7	5	4	4	3	6	7	5	2	6	1	3	2	7	8	8	1

Table 2.6: Look-up table for AltBOC phase states in dependency of input quadruples and time [4]

The index $k(t)$ defines the scattered plot number as in Figure 2.21.

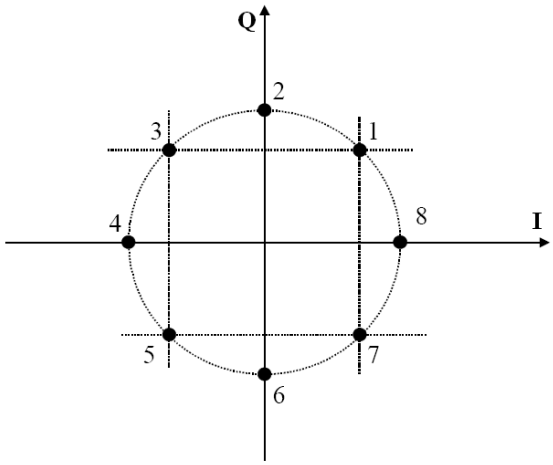

Figure 2.21: 8-PSK phase-state diagram of E5 AltBOC signal [9]

The idea is here to allocate any of the 4 codes and 8 subcarrier phases combinations to a phase spot in the constellation, using a look-up table, and then to generate the corresponding I and Q signals prior to digital-to-analog conversion. The value of the constellation spot is a function of the value of the 4

codes (-1 or +1) and depends also on time. Therefore, time is partitioned first in subcarrier intervals $T_{S,E5}$ and further sub-divided in 8 equal sub-periods. The index i_{T_s} of the actual sub-period is given by:

$$i_{T_s} = \text{integer part}\left[\frac{8}{T_{S,E5}} \cdot (t \text{ modulo } T_{S,E5})\right] \quad (2.46)$$

$$\text{with } i_{T_s} \in \{0,1,2,3,4,5,6,7\}$$

There are 4 binary codes, resulting in 16 (2^4) code combinations: this means that there are a total of 128 different phase plots, whose value may vary between 1 and 8. In fact the look-up table is composed by 16 $\times$ 8 values, that can easily be stored in a memory and used for the signal modulation.

This efficient technique based on a LUT will be used for the signal generation sections on board of the Galileo satellites, obtaining a significative simplification for the necessary hardware and computational burden. A similar approach could also be used for the simulations: for this thesis an AltBOC signal generator has been implemented in C and MATLAB® languages, taking advantage of the LUT approach to speed up the simulation time. In addition, also a signal generator based on the previous equations (see Section 2.2.4), with the separate generation of all the signal components, has been implemented: this generator results less efficient from a computational point of view, but is more flexible and allows to generate single components of the AltBOC signal, useful for the study of the AltBOC features.

Observing the values in Table 2.6, it should also be noted that choosing an input quadruple and observing one column of the table (that is one sub-carrier period), the modulated signal change the phase state in the scatter diagram, moving like a square wave, from one point of the 8-PSK constellation to the opposite. This alternative motion and others signal features are analyzed in detail in the following Chapter.

Chapter 3

AltBOC signal features

The modulation and multiplexing schemes for all the transmitted signals of the Galileo system are resulting from a compromise between the following criteria (as stated in Reference [7]):

- minimization of the implementation losses in the Galileo satellites, making use of the current state of the art of the related equipments;
- minimization of the level of interference induced by the Galileo signals in GPS receivers, and in all other signals inside and outside the transmitted band;
- maximization of the power efficiency in the Galileo satellites;
- optimization of the performance and associated complexity of future Galileo user receivers.

For the Galileo E5 band it is foreseen the constant envelope AltBOC modulation scheme, that produce a wide band signal, transmitted around the carrier frequency (f_{E5}) of 1191.795 MHz.

This choice implies the following advantages:

- simplification of the base-band generator on board of the satellite, because there will be only a wideband AltBOC modulator for the entire E5 band instead of two separate QPSK modulators for E5a and E5b bands;
- efficient use of the saturated amplifier on board of the satellite, since the modulated AltBOC signal has constant envelope;
- optimization of the receiver architecture because, receiving the wide band AltBOC signal, the receiver could demodulate simultaneously the navigation data in E5a and E5b sidebands;

- excellent receiver performances in presence of noise and multipath, using the wide band AltBOC demodulation scheme. In fact it is commonly acknowledged [10] that wide band signals perform better than narrow band (like the C/A GPS signal), because using the secondary lobes it is possible to build a sharp correlation function, taking advantage of the narrow correlation techniques. Besides, the AltBOC signal features a steep correlation function, leading to good tracking performances.

The AltBOC modulation features are described in following Sections, where it is explained the modulation complexity and the advantages that this implies. In the last Section the correlation proprieties of the signals are analyzed and there is proposed the complex correlation scheme, that could be used to track the AltBOC signal.

3.1 Constant envelope and alternative transitions

As mentioned in Section 2.2.4, the *E5 AltBOC* modulation provides a **constant envelope** signal.

The scattering diagram of the modulated signal $s_{E5}(t)$ is shown in Figure 3.1(a), and is similar to an 8-PSK constellation, with some differences. In detail, it is possible to see signal transitions (represented with blue lines) that can also cross the null amplitude point, but the signal samples theoretically[1] never have null power. In fact the points of the constellation (indicated with red stars) lies on a circle, like 8-PSK signals, and have always unitary energy.

This constant envelope signal could be obtained only assuming an ideal transmission, that is an infinite bandwidth for the satellite and the receiver. Reducing the bandwidth to realistic values (e.g. 51.150 MHz, see Section 6.3.2), the signal is slightly distorted and becomes a *quasi-constant envelope* constellation. For the moment this band limiting effect could be neglected, then a 8-PSK constellation is considered in the following dissertation.

As observed discussing the signal generation using a LUT (see pag. 38), the **transitions** on the scattering diagram are due to the subcarriers and to the spreading code chip transitions. For the AltBOC(15,10) signal it must be reminded that if $T_{C,E5}$ is the duration of a chip and $T_{S,E5}$ the subcarrier period, the two values are related with the following expression:

$$T_{C,E5} = 1.5 \cdot T_{S,E5} \tag{3.1}$$

Therefore, during the length of one chip, the subcarrier phase value (i.e. the argument of $sc_{E5\text{-}S}$ and $sc_{E5\text{-}P}$) cycle 1.5 times through a full period.

[1] With an ideal infinite bandwidth transmission. The simulations for the AltBOC signal generation have been done without consider any signal filtering.

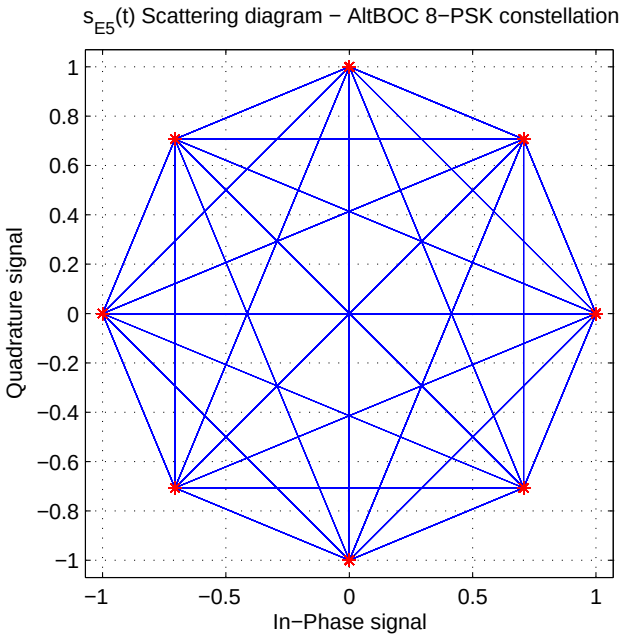

(a)

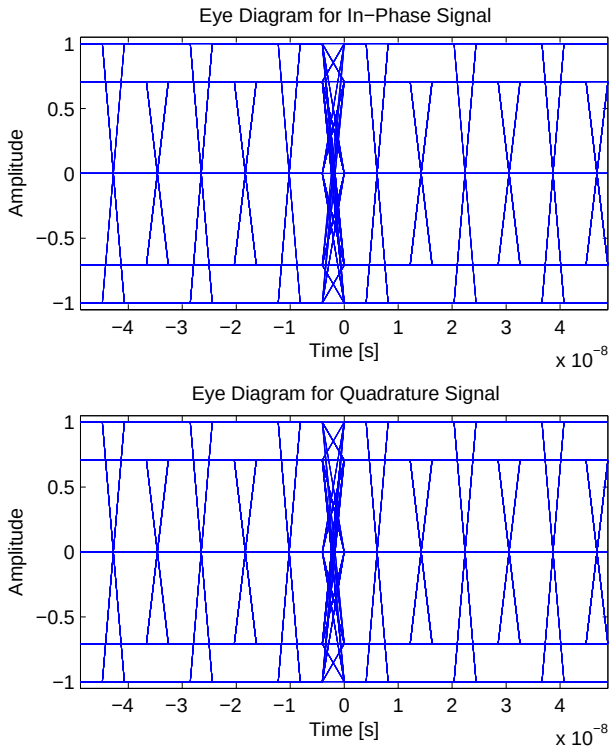

(b)

Figure 3.1: E5 AltBOC(15,10) scattering diagram (a) and eye diagram (b)

This results that in the eye diagram (shown in Figure 3.1(b)) during the length of one chip there are transitions corresponding to 1.5 subcarrier period. In the scattering diagram, within a chip length, the subcarrier transitions causes alternate changes of position of the signal in the constellation, shifting from one position to the opposite. At the end of the chip time, a code transition causes the change of the starting point, choosing between one of the 8 positions in the constellation. After this, the subcarriers produce again the alternate changes of position, during the successive chip time.

This effect can be seen simulating sample by sample the $s_{E5}(t)$ signal, and displaying its evolution with the scattering and the eye diagrams.
In Figure 3.2 there are the diagrams obtained with three different code chips. It is possible to see the alternative movements of the signal in the scattering diagram, caused by the subcarriers. During the length of a chip the signal changes its position in the constellation crossing the zero, with diagonal, vertical or horizontal movements, that can be understood observing the corresponding in-phase and the quadrature eye diagrams. In effect the subcarriers produce a square wave oscillation in one or both the eyes of the signal, that are the reason of the alternative movement. This oscillation of the signal lasts for an entire chip time.
When the chip time ends, a new quadruple of chips for the four E5 channels can change the direction of the oscillation and, in the transition from one chip time to the successive, it is possibile to see in the scattering diagram a transition that does not cross the zero.

In conclusion it is possible to affirm that in the scattering diagram the transitions crossing the zero (vertical, horizontal and diagonals) are due to the subcarriers, and all others transitions are caused by chip code transitions.

3.2 Product signals in the AltBOC expression

Another importante feature of the *E5 AltBOC(15,10)* is the presence of the **product signals** in the signal expression (see Equation (2.31), that is recopied here for the sake of clarity):

$$\begin{aligned} s_{E5}(t) \quad = \quad & \frac{1}{2\cdot\sqrt{2}}\cdot[e_{E5a\text{-}I}(t)+\mathrm{j}\cdot e_{E5a\text{-}Q}(t)]\cdot[sc_{E5\text{-}S}(t)-\mathrm{j}\cdot sc_{E5\text{-}S}(t-T_{s,E5}/4)]+ \\ & +\frac{1}{2\cdot\sqrt{2}}\cdot[e_{E5b\text{-}I}(t)+\mathrm{j}\cdot e_{E5b\text{-}Q}(t)]\cdot[sc_{E5\text{-}S}(t)+\mathrm{j}\cdot sc_{E5\text{-}S}(t-T_{s,E5}/4)]+ \\ & +\frac{1}{2\cdot\sqrt{2}}\cdot[\overline{e}_{E5a\text{-}I}(t)+\mathrm{j}\cdot \overline{e}_{E5a\text{-}Q}(t)]\cdot[sc_{E5\text{-}P}(t)-\mathrm{j}\cdot sc_{E5\text{-}P}(t-T_{s,E5}/4)]+ \\ & +\frac{1}{2\cdot\sqrt{2}}\cdot[\overline{e}_{E5b\text{-}I}(t)+\mathrm{j}\cdot \overline{e}_{E5b\text{-}Q}(t)]\cdot[sc_{E5\text{-}P}(t)+\mathrm{j}\cdot sc_{E5\text{-}P}(t-T_{s,E5}/4)] \end{aligned} \tag{3.2}$$

These product signals, denoted with the dashed terms in Equation (3.2), are necessary to meet the requirements for a constant envelope [11].

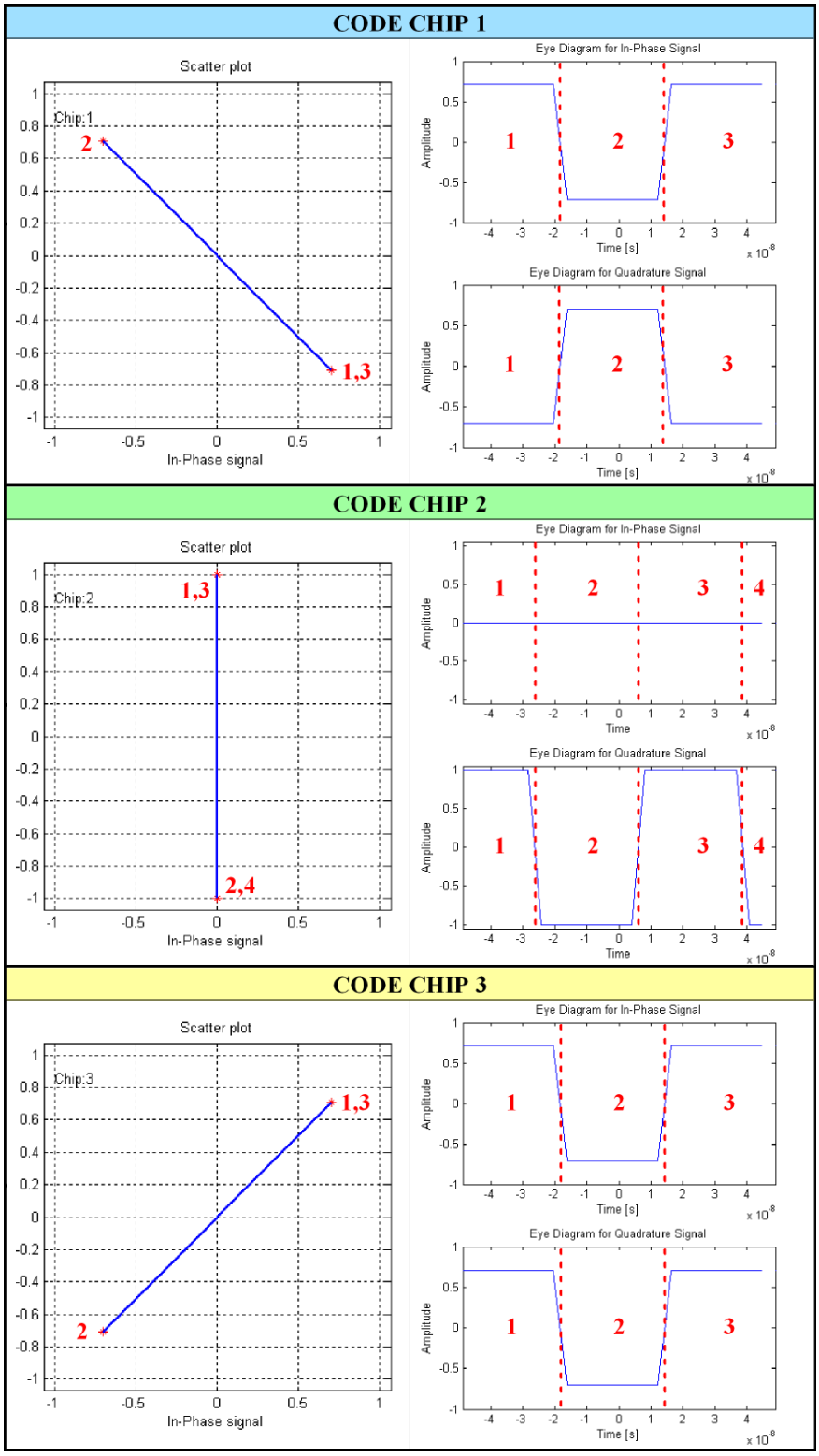

Figure 3.2: Illustration of the transitions during three code chips, caused by the subcarriers, in the scattering diagram and in the eye diagram of the AltBOC modulated signal

In effect, considering the *Standard AltBOC* (previously presented, in Section 2.2.3), the scattering diagram has a non-constant envelope (as affirmed in [10]), as shown in Figure 3.3.

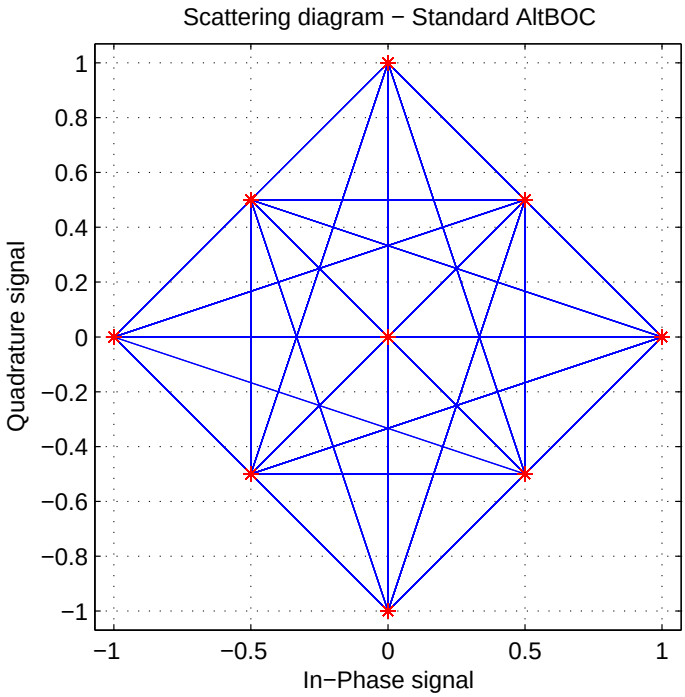

Figure 3.3: Standard AltBOC(15,10) scattering diagram

With this modulation scheme, that has not the product signals and is obtained with different subcarrier waveforms (simple squared waves), the signal will have oscillations at subcarrier frequency, either along the horizontal and the vertical axis of the constellation, or along the diagonals. The vertical and horizontal oscillations of the subcarrier in the constellation have higher amplitudes than the diagonal ones. Moreover, they take a zero amplitude.

Having a non-constant envelope signal is a real issue when considering the satellite amplifiers. Indeed, to optimize the link budget and the power efficiency on-board the satellite, these amplifiers need to work at saturation. If this is the case, a non-constant envelope signal would suffer some distortions that will affect the tracking performances of the receiver.

Therefore the modulation that will be used in Galileo E5 band can be considered a modified version of the *Standard AltBOC*, aiming to obtain a signal with similar spectral features, but with constant envelope. Indeed, it is possibile to modify the *Standard AltBOC* constellation in order to make the envelope constant, varying the subcarriers waveforms and adding the additional product terms.

The product signals in the *E5 AltBOC(15,10)* expression can also be explained like **intermodulation products** [12].

In the AltBOC signal spectrum, shown in the left side of Figure 3.4, there are evident the two main lobes, centered in E5a and E5b band.

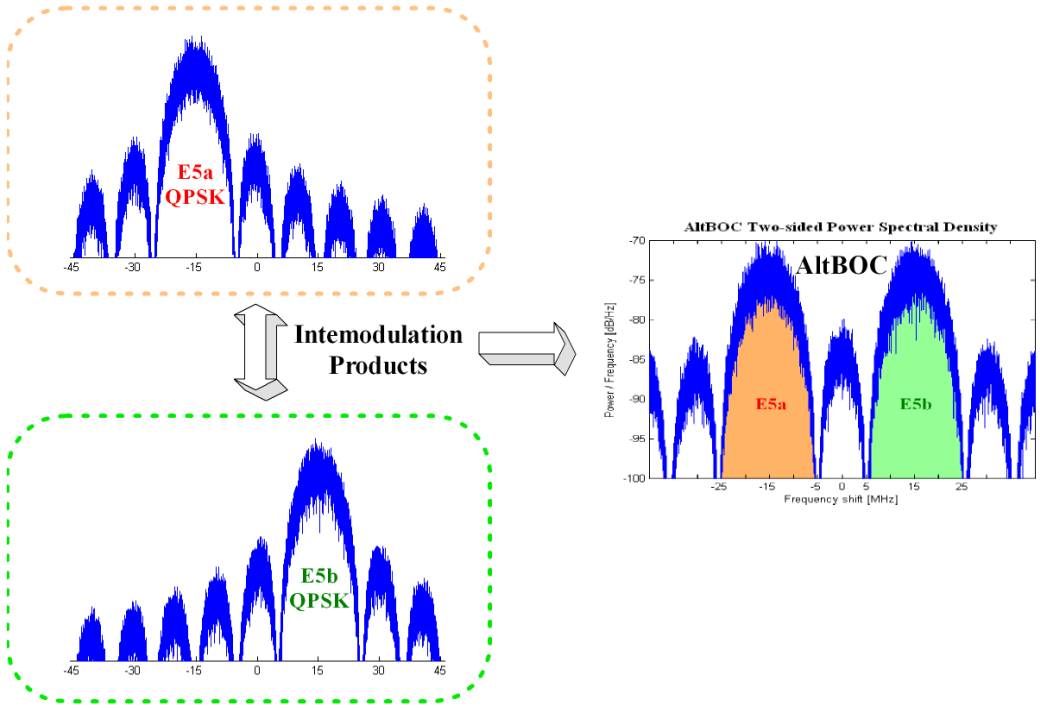

Figure 3.4: Illustration of AltBOC signal spectrum, like a multiplexing of two separate QPSK modulations

The AltBOC modulation is a multiplexing technique that allow to transmit two adjacent signals in E5a and E5b band, without using two separate QPSK modulators. This has the advantage that permits to transmit the four E5 channels with one single chain, obtaining a coherent wide band signal with spectral characteristics similar to a BOC(15,10) signal. The coherence is intended like a stable phase coherence between the two band emissions. Obviously the wide bandwidth of the AltBOC signal permits to achieve a lower error bound, in terms of tracking performances and multipath mitigation [10], than two separate narrow band QPSK transmissions. It is however necessary a more complex implementation for the wide band transmission chain and for the receiver (see Section 4.3).
Anyway the AltBOC modulation scheme allow to design less complex receivers (low cost), based on separate sideband processing. The E5a and E5b bands can be received separately, demodulating simple QPSK signals, but with worse performances (see Section 4.2).

Therefore the product signals in the *E5 AltBOC* expression can be considered intermodulation products, interferences between the two adjacent sideband

QPSK modulations. It is then necessary to add these terms in the *Standard AltBOC* expression to obtain a constant envelope signal, similar to that obtained with two multiplexed QPSK modulations.

3.3 Multi-level square wave subcarriers

In literature there are proposed other variants of the AltBOC modulation scheme. All these modified modulations have a BOC-like spectrum, but with some differences. A particular variant is the **3-state AltBOC** (outlined in [10]) that was introduced in order to reduce the amount of energy transmitted in the secondary lobes. The idea is to smooth the subcarrier, replacing the square wave with a 3 level wave, so as to reduce its harmonics. A continuation of the 3-state process to 4 or more states is possible and further reduces the harmonic energy, without degrade the amplitude of the main lobes (E5a and E5b) of the signal spectrum.

The AltBOC modulation that will be used in Galileo E5 band is the result of an **optimization process** and can be understood considering a multi-level AltBOC.

The starting point of the optimization was the *Standard AltBOC*. This modulation scheme has been modified altering the subcarrier waveforms, choosing a 4-level quantized cosine for the $sc_{E5\text{-}S}(t)$ subcarrier, in order to reduce the secondary lobes.
Secondly it was necessary to add the product signals, with the subcarriers $sc_{E5\text{-}P}(t)$, in order to obtain a constant envelope, without zero amplitude samples. But the introduction of these intermodulation products causes a worsening of secondary lobes, increasing their power.

In fact comparing the signal spectrum of the *E5 AltBOC* signal, in Figure 3.5(a), with that one of the *Standard AltBOC*, in Figure 3.5(b), it is possible to see a similar shape for the main lobes (in E5a and E5b bands) and the adjacent secondary lobes. Only for high order secondary lobes there are slight differences. The relative power difference between the main and secondary lobes is however identical. Anyway the secondary lobes of the *E5 AltBOC* signal results to be not worse than these of the *Standard AltBOC*.

In conclusion, the *E5 AltBOC* modulation has been optimized, starting from the *Standard AltBOC*, in order to obtain a constant envelope modulated signal, without degrade the spectral features of the *Standard AltBOC*.

3.4 Correlation proprieties

The modulated signal $s_{E5}(t)$ contains the four channels $e_{E5a\text{-}I}(t)$, $e_{E5a\text{-}Q}(t)$, $e_{E5b\text{-}I}(t)$ and $e_{E5b\text{-}Q}(t)$. Taking advantage of the AltBOC correlation proprieties and the quasi-orthogonality of the four codes, it is possibile to coherently

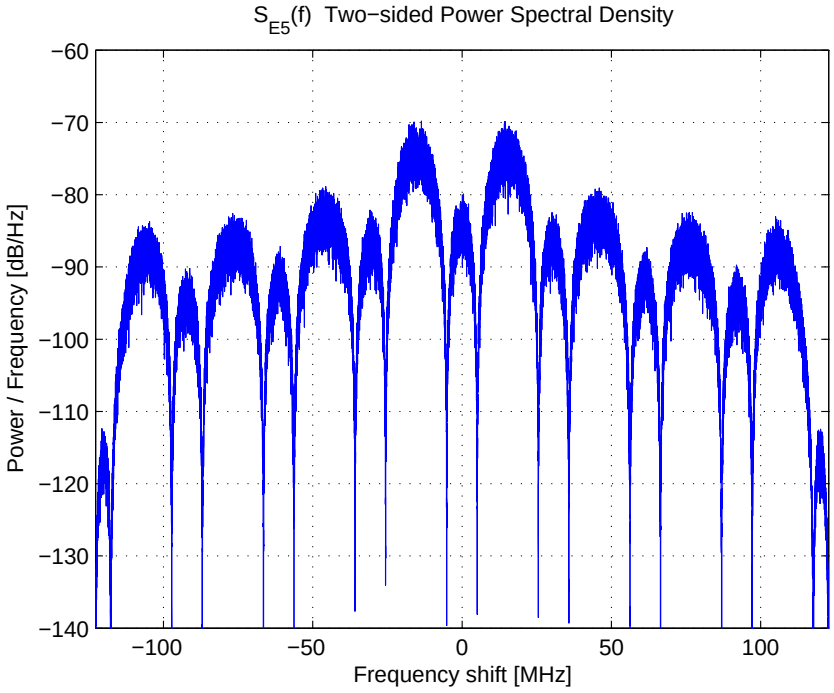

(a)

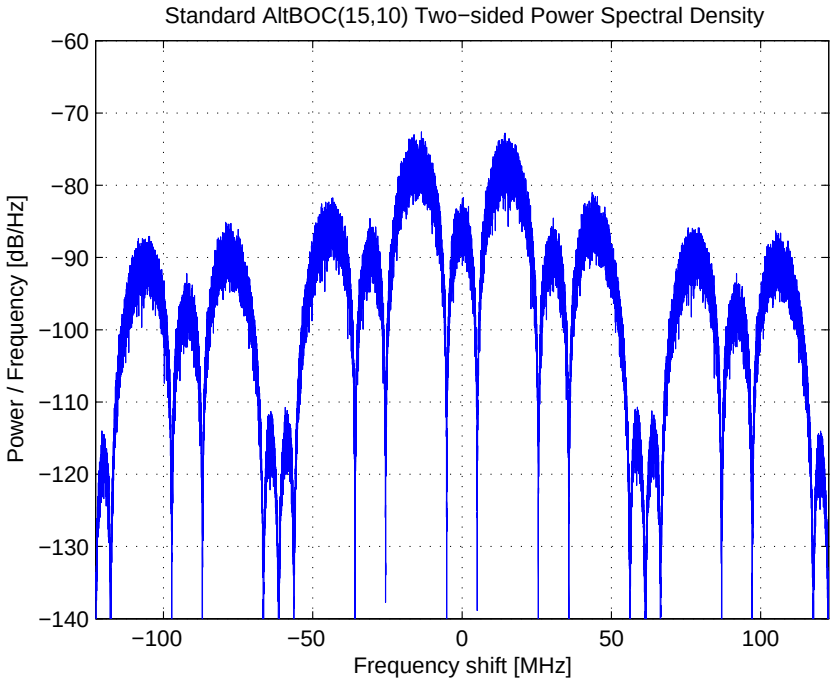

(b)

Figure 3.5: Comparison between the E5 AltBOC(15,10) signal spectrum (a) and the Standard AltBOC(15,10) signal spectrum(b)

track the two quadrature pilot channels $e_{E5a\text{-}Q}(t)$ and $e_{E5b\text{-}Q}(t)$, and then to demodulate the navigation data contained in the other two channels. In fact, it is possible to use the synchronism, recovered tracking the two pilot channels, for the demodulation of the other two channels, without the need of a bit estimation process (this idea will be illustrated in detail in Section 4.3).

Otherwise, if it is necessary to track also the data channels, their data bits have to be wiped off. This bit estimation process makes the tracking of the data channels less robust, especially at low C/N_0, where the probability of bit error is high.

Therefore it advisable to track only the two pilot channels $e_{E5a\text{-}Q}(t)$ and $e_{E5b\text{-}Q}(t)$. For the sake of clarity the expression of the modulated signal $s_{E5}(t)$ is rewritten here, pointing out the two pilot channels[2]:

$$\begin{aligned} s_{E5}(t) \;=\; & \frac{1}{2\cdot\sqrt{2}}\cdot[e_{E5a\text{-}I}(t)+\mathrm{j}\cdot\mathbf{e_{E5a\text{-}Q}(t)}]\cdot[sc_{E5\text{-}S}(t)-\mathrm{j}\cdot sc_{E5\text{-}S}(t-T_{s,E5}/4)]+\\ & +\frac{1}{2\cdot\sqrt{2}}\cdot[e_{E5b\text{-}I}(t)+\mathrm{j}\cdot\mathbf{e_{E5b\text{-}Q}(t)}]\cdot[sc_{E5\text{-}S}(t)+\mathrm{j}\cdot sc_{E5\text{-}S}(t-T_{s,E5}/4)]+\\ & +\frac{1}{2\cdot\sqrt{2}}\cdot[\overline{e}_{E5a\text{-}I}(t)+\mathrm{j}\cdot\overline{e}_{E5a\text{-}Q}(t)]\cdot[sc_{E5\text{-}P}(t)-\mathrm{j}\cdot sc_{E5\text{-}P}(t-T_{s,E5}/4)]+\\ & +\frac{1}{2\cdot\sqrt{2}}\cdot[\overline{e}_{E5b\text{-}I}(t)+\mathrm{j}\cdot\overline{e}_{E5b\text{-}Q}(t)]\cdot[sc_{E5\text{-}P}(t)+\mathrm{j}\cdot sc_{E5\text{-}P}(t-T_{s,E5}/4)] \end{aligned} \tag{3.3}$$

As previously done, the $s_{E5}(t)$ signal could be decomposed in its real and imaginary components:

$$s_{E5}(t) = s_{E5\mathbf{I}}(t) + \mathrm{j}\cdot s_{E5\mathbf{Q}}(t) \tag{3.4}$$

$$\begin{aligned} s_{E5\mathbf{I}}(t) \;=\; & \frac{1}{2\cdot\sqrt{2}}\cdot[e_{E5a\text{-}I}(t)+e_{E5b\text{-}I}(t)]\cdot sc_{E5\text{-}S}(t)+\\ & +\frac{1}{2\cdot\sqrt{2}}\cdot[\mathbf{e_{E5a\text{-}Q}(t)}-\mathbf{e_{E5b\text{-}Q}(t)}]\cdot sc_{E5\text{-}S}\left(t-\frac{T_{s,E5}}{4}\right)+\\ & +\frac{1}{2\cdot\sqrt{2}}\cdot[\overline{e}_{E5a\text{-}I}(t)+\overline{e}_{E5b\text{-}I}(t)]\cdot sc_{E5\text{-}P}(t)+\\ & +\frac{1}{2\cdot\sqrt{2}}\cdot[\overline{e}_{E5a\text{-}Q}(t)-\overline{e}_{E5b\text{-}Q}(t)]\cdot sc_{E5\text{-}P}\left(t-\frac{T_{s,E5}}{4}\right) \end{aligned} \tag{3.5}$$

$$\begin{aligned} s_{E5\mathbf{Q}}(t) \;=\; & \frac{1}{2\cdot\sqrt{2}}\cdot[\mathbf{e_{E5a\text{-}Q}(t)}+\mathbf{e_{E5b\text{-}Q}(t)}]\cdot sc_{E5\text{-}S}(t)+\\ & +\frac{1}{2\cdot\sqrt{2}}\cdot[e_{E5b\text{-}I}(t)-e_{E5a\text{-}I}(t)]\cdot sc_{E5\text{-}S}\left(t-\frac{T_{s,E5}}{4}\right)+\\ & +\frac{1}{2\cdot\sqrt{2}}\cdot[\overline{e}_{E5a\text{-}Q}(t)+\overline{e}_{E5b\text{-}Q}(t)]\cdot sc_{E5\text{-}P}(t)+\\ & +\frac{1}{2\cdot\sqrt{2}}\cdot[\overline{e}_{E5b\text{-}I}(t)-\overline{e}_{E5a\text{-}I}(t)]\cdot sc_{E5\text{-}P}\left(t-\frac{T_{s,E5}}{4}\right) \end{aligned} \tag{3.6}$$

[2]Actually the two pilot channels are also included in product signals (the dashed components), but this information can be neglected because the smaller amplitude of the $sc_{E5\text{-}P}$ subcarrier.

The two components $s_{E5\mathbf{I}}(t)$ and $s_{E5\mathbf{Q}}(t)$ can be considered as the ideal received signals in the I and Q branch of the receiver. In fact, assuming the correct synchronization of the receiver (PLL and DLL correctly locked) and neglecting the noise, the distortions and other propagation effects, the received signal $s_{E5}(t)$ is partitioned in the I and Q branch of the receiver, separating correctly its real and imaginary parts, that corresponds to $s_{E5\mathbf{I}}(t)$ and $s_{E5\mathbf{Q}}(t)$.

In the modulated signal the two pilot channels are multiplied by the subcarrier $sc_{E5\text{-}S}$, that shifts them in the two sidebands, with an operation similar to a complex exponential multiplication.

In principle each component could be demodulated by correlating $s_{E5}(t)$ with the desired code sequence multiplied by the complex conjugate of the corresponding subcarrier "exponential" [11].

Then a **sideband complex correlation function** could be defined, for example for the *E5a-Q* channel:

$$\mathcal{C}_{E5a\text{-}Q}(\tau) = \int_0^{T_{int}} s_{E5}(t) \cdot g_{E5a\text{-}Q}(t-\tau)\, dt \tag{3.7}$$

where:

- $s_{E5}(t)$ is the received signal, expressed like a baseband signal in the complex envelope notation:

$$s_{E5}(t) = s_{E5\mathbf{I}}(t) + \mathrm{j} \cdot s_{E5\mathbf{Q}}(t)$$

- $g_{E5a\text{-}Q}(t)$ is the locally generated signal, multiplied by the subcarrier "exponential". It corresponds to the complex conjugate of the term for $e_{E5a\text{-}Q}(t)$ in the AltBOC expression in Equation (3.3):

$$g_{E5a\text{-}Q}(t) = -\mathrm{j} \cdot e_{E5a\text{-}Q}(t) \cdot \left[sc_{E5\text{-}S}(t) + \mathrm{j} \cdot sc_{E5\text{-}S}\left(t - \frac{T_{s,E5}}{4}\right)\right]$$

  It could also be rewritten in the following manner:

$$g_{E5a\text{-}Q}(t) = e_{E5a\text{-}Q}(t) \cdot \left[sc_{E5\text{-}S}\left(t - \frac{T_{s,E5}}{4}\right) - \mathrm{j} \cdot sc_{E5\text{-}S}(t)\right]$$

- τ is the delay between the received signal $s_{E5}(t)$ and the local signal $g_{E5a\text{-}Q}(t)$;
- T_{int} is the so-called *integration time* (typically 1 ms).

The signs in the local signal $g_{E5a\text{-}Q}(t)$ are justified because it must be complex conjugate with respect of that used $s_{E5}(t)$: the sign of the imaginary part must result opposite.

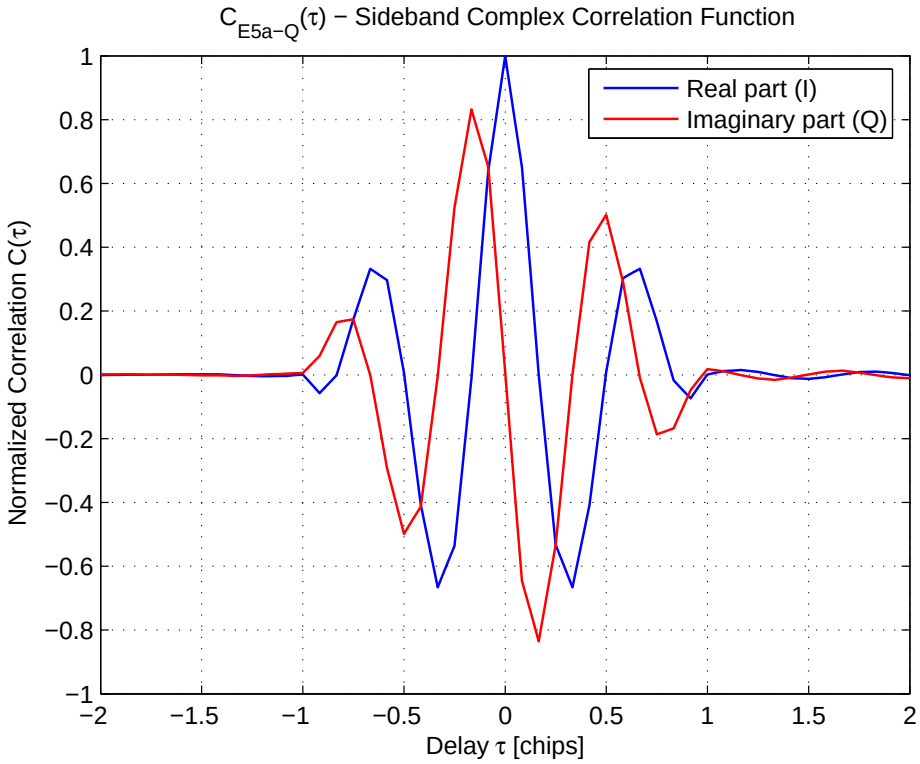

Figure 3.6: Sideband complex correlation function $\mathcal{C}_{E5a\text{-}Q}(\tau)$, for the pilot channel of the E5a band

The resulting function $\mathcal{C}_{E5a\text{-}Q}(\tau)$ is then a complex function. Its real and imaginary parts are depicted[3] in Figure 3.6.

Considering the pilot channel in the other sideband of the AltBOC signal (*E5b-Q*), the following expression is obtained and this **sideband complex correlation function** is presented in Figure 3.7:

$$\mathcal{C}_{E5b\text{-}Q}(\tau) = \int_0^{T_{int}} s_{E5}(t) \cdot g_{E5b\text{-}Q}(t-\tau)\, dt \tag{3.8}$$

where $$g_{E5b\text{-}Q}(t) = -\mathrm{j} \cdot e_{E5b\text{-}Q}(t) \cdot \left[sc_{E5\text{-}S}(t) - \mathrm{j} \cdot sc_{E5\text{-}S}\left(t - \frac{T_{s,E5}}{4}\right)\right]$$

Accordingly with that done for the *E5a-Q* channel, the locally generated

[3]The correlation functions in Figures 3.6, 3.7, 3.8 and 3.9 has been obtained simulating the *E5 AltBOC(15,10)* signal oversampled with 16 samples per subcarrier period, that are 24 samples per code chip, with infinite bandwidth (without any signal filtering), and correlating the signals with an integration time of 1 ms (1 primary code period). The functions appear with some edges, that cannot be reduced increasing the sampling frequency. They are due to the square wave subcarriers. Filtering the simulated signal with a pass-band filter, it is possible to obtain a smoothed correlation function.
The ordinate axis of the graphs are normalized with the peak of the correlation function, so that the amplitude of the function is independent on the sampling frequency.

signal could be rewritten in the following manner:

$$g_{E5b\text{-}Q}(t) = e_{E5b\text{-}Q}(t) \cdot \left[-sc_{E5\text{-}S}\left(t - \frac{T_{s,E5}}{4}\right) - \mathrm{j} \cdot sc_{E5\text{-}S}(t) \right]$$

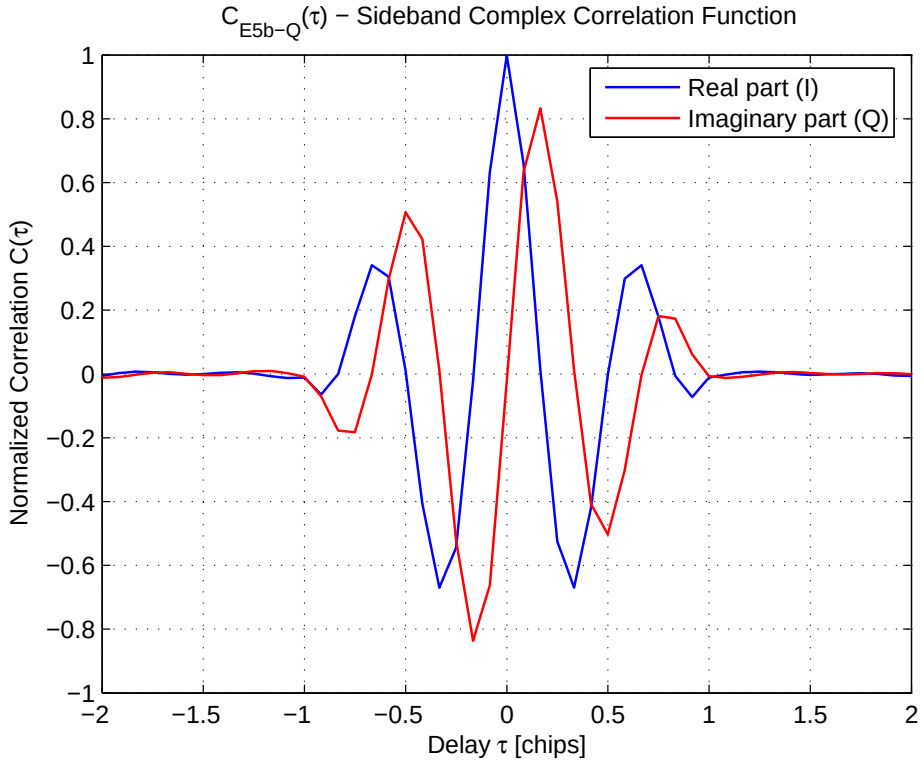

Figure 3.7: Sideband complex correlation function $\mathcal{C}_{E5b\text{-}Q}(\tau)$, for the pilot channel of the E5b band

These complex correlations in Equations (3.7) and (3.8) are only analytical expressions: to design a demodulation scheme for the *E5 AltBOC* signal it is necessary to adapt them.

Firstly, the receiver will work with sampled signals, then the signals must be expressed in the discrete time domain. If $F_s = 1/T_s$ is the sampling frequency, a signal $x(t)$ is expressed in the discrete time domain using the notation:

$$x[n] = x\left(t = n \cdot T_s\right) \tag{3.9}$$

Moreover the integrals become sums of discrete values, converting the integration time T_{int} to the corresponding number of samples N:

$$N = \frac{T_{int}}{T_s} = T_{int} \cdot F_s \tag{3.10}$$

Then Equations (3.7) and (3.8) can be rewritten, using the discrete time

notation:

$$\mathcal{C}_{E5a\text{-}Q}[m] = \sum_{n=0}^{N} s_{E5}[n] \cdot g_{E5a\text{-}Q}[n-m] \tag{3.11}$$

$$\mathcal{C}_{E5b\text{-}Q}[m] = \sum_{n=0}^{N} s_{E5}[n] \cdot g_{E5b\text{-}Q}[n-m] \tag{3.12}$$

$$\text{where} \quad m = \frac{\tau}{T_s}$$

A complex correlation operation between the two complex signals $s_{E5}[n]$ and $g_{E5a\text{-}Q}[n]$ (or $g_{E5b\text{-}Q}[n]$) could be implemented with four conventional correlators, using the following expressions:

$$\mathcal{C}_X[m] = \{C_1^X[m] + C_2^X[m]\} + \mathrm{j} \cdot \{C_3^X[m] + C_4^X[m]\} \tag{3.13}$$

where $X =$ *E5a-Q* or *E5b-Q*

$$C_1^X[m] = \sum_{n=0}^{N} \mathrm{Re}\{s_{E5}[n]\} \cdot \mathrm{Re}\{g_X[n-m]\} \tag{3.14}$$

$$C_2^X[m] = \sum_{n=0}^{N} \mathrm{j} \cdot \mathrm{Im}\{s_{E5}[n]\} \cdot \mathrm{j} \cdot \mathrm{Im}\{g_X[n-m]\} \tag{3.15}$$

$$C_3^X[m] = \sum_{n=0}^{N} \mathrm{Re}\{s_{E5}[n]\} \cdot \mathrm{Im}\{g_X[n-m]\} \tag{3.16}$$

$$C_4^X[m] = \sum_{n=0}^{N} \mathrm{Im}\{s_{E5}[n]\} \cdot \mathrm{Re}\{g_X[n-m]\} \tag{3.17}$$

Remembering that the received signal $s_{E5}[n]$ could be partitioned in its in phase and quadrature components, that correspond to its real and imaginary part:

$$s_{E5}[n] = s_{E5\mathbf{I}}[n] + \mathrm{j} \cdot s_{E5\mathbf{Q}}[n] \tag{3.18}$$

it is then possible to substitute $s_{E5\mathbf{I}}[n]$ and $s_{E5\mathbf{Q}}[n]$ in previous expressions

for the four correlation components:

$$C_1^X[m] = \sum_{n=0}^{N} s_{E5\mathbf{I}}[n] \cdot \mathrm{Re}\{g_X[n-m]\} \tag{3.19}$$

$$C_2^X[m] = \sum_{n=0}^{N} -s_{E5\mathbf{Q}}[n] \cdot \mathrm{Im}\{g_X[n-m]\} \tag{3.20}$$

$$C_3^X[m] = \sum_{n=0}^{N} s_{E5\mathbf{I}}[n] \cdot \mathrm{Im}\{g_X[n-m]\} \tag{3.21}$$

$$C_4^X[m] = \sum_{n=0}^{N} s_{E5\mathbf{Q}}[n] \cdot \mathrm{Re}\{g_X[n-m]\} \tag{3.22}$$

$$\text{where} \qquad X = \textit{E5a-Q} \text{ or } \textit{E5b-Q}$$

The negative sign inside of the $C_2^X[m]$ component is due to the fact that this term is obtained multiplying two imaginary parts ($\mathrm{j} \cdot \mathrm{j} = -1$).

Substituting Equation (3.13) in Equation (3.11) for $\mathcal{C}_{E5a\text{-}Q}[m]$ and in Equation (3.12) for $\mathcal{C}_{E5b\text{-}Q}[m]$, it is possible to obtain the following expressions:

$$\begin{aligned} \mathcal{C}_{E5a\text{-}Q}[m] = {} & \{C_1^{E5a\text{-}Q}[m] + C_2^{E5a\text{-}Q}[m]\} + \\ & + \mathrm{j} \cdot \{C_3^{E5a\text{-}Q}[m] + C_4^{E5a\text{-}Q}[m]\} \end{aligned} \tag{3.23}$$

$$\begin{aligned} \mathcal{C}_{E5b\text{-}Q}[m] = {} & \{C_1^{E5b\text{-}Q}[m] + C_2^{E5b\text{-}Q}[m]\} + \\ & + \mathrm{j} \cdot \{C_3^{E5b\text{-}Q}[m] + C_4^{E5b\text{-}Q}[m]\} \end{aligned} \tag{3.24}$$

To evaluate the two complex correlation functions $\mathcal{C}_{E5a\text{-}Q}[m]$ and $\mathcal{C}_{E5b\text{-}Q}[m]$ (presented before in Figures 3.6 and 3.7), it is necessary to calculate separately their respective C_1, C_2, C_3 and C_4 components, as result of real correlation operations. The behavior of these components is shown in Figure 3.8(a) for $\mathcal{C}_{E5a\text{-}Q}[m]$, and in Figure 3.8(b) for $\mathcal{C}_{E5b\text{-}Q}[m]$.

Expanding the correlation components, the following final expressions could

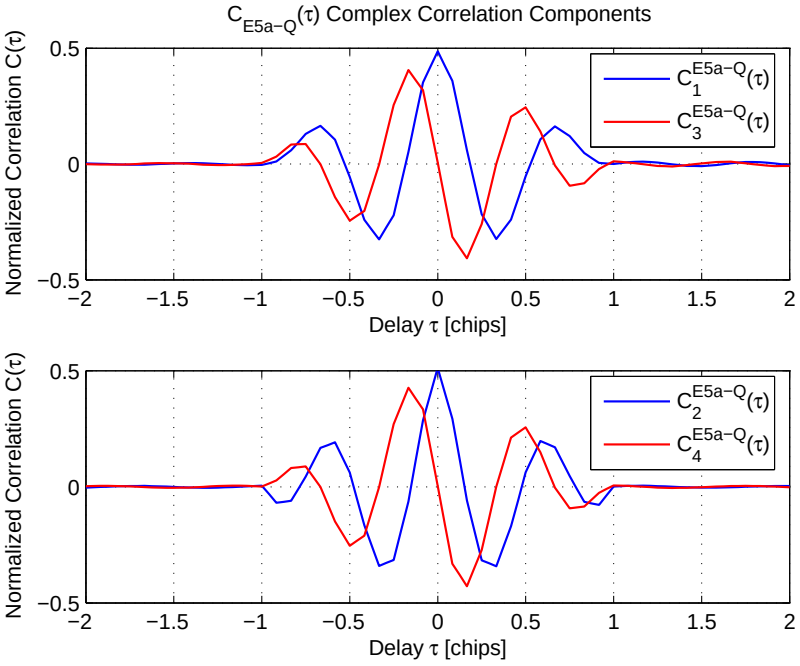

(a)

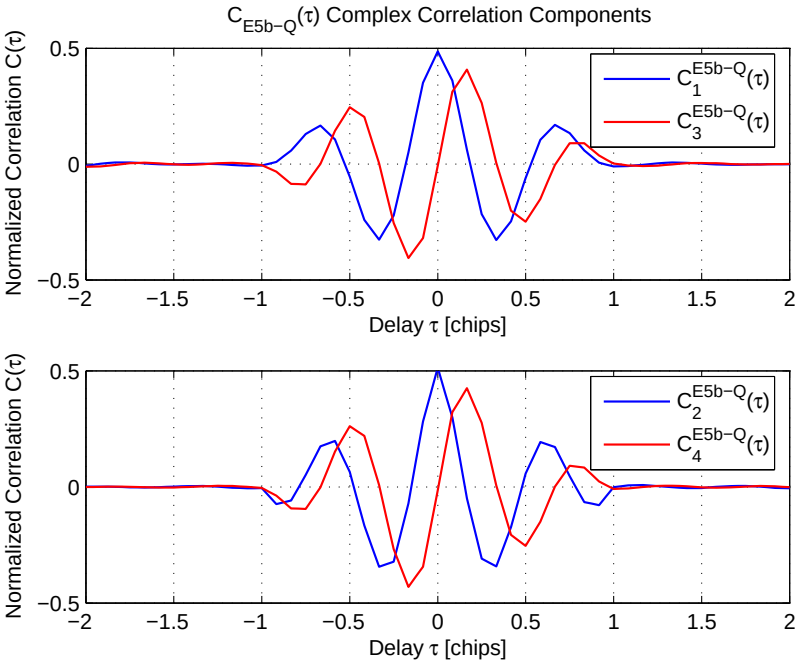

(b)

Figure 3.8: Components for the sideband complex correlation functions: in (a) the four components for $\mathcal{C}_{E5a\text{-}Q}(\tau)$, and in (b) the four components for $\mathcal{C}_{E5b\text{-}Q}(\tau)$

be obtained:

$$\begin{aligned}\mathcal{C}_{E5a\text{-}Q}[m] \;=\; & \sum_{n=0}^{N} s_{E5\mathbf{I}}[n]\cdot e_{E5a\text{-}Q}[n-m]\cdot sc^{off}_{E5\text{-}S}[n-m] + \\ & + \sum_{n=0}^{N} s_{E5\mathbf{Q}}[n]\cdot e_{E5a\text{-}Q}[n-m]\cdot sc_{E5\text{-}S}[n-m] + \\ & + \mathrm{j}\cdot\left\{ - \sum_{n=0}^{N} s_{E5\mathbf{I}}[n]\cdot e_{E5a\text{-}Q}[n-m]\cdot sc_{E5\text{-}S}[n-m] + \right. \\ & \left. + \sum_{n=0}^{N} s_{E5\mathbf{Q}}[n]\cdot e_{E5a\text{-}Q}[n-m]\cdot sc^{off}_{E5\text{-}S}[n-m] \right\} \end{aligned} \tag{3.25}$$

$$\begin{aligned}\mathcal{C}_{E5b\text{-}Q}[m] \;=\; & - \sum_{n=0}^{N} s_{E5\mathbf{I}}[n]\cdot e_{E5b\text{-}Q}[n-m]\cdot sc^{off}_{E5\text{-}S}[n-m] + \\ & + \sum_{n=0}^{N} s_{E5\mathbf{Q}}[n]\cdot e_{E5b\text{-}Q}[n-m]\cdot sc_{E5\text{-}S}[n-m] + \\ & + \mathrm{j}\cdot\left\{ - \sum_{n=0}^{N} s_{E5\mathbf{I}}[n]\cdot e_{E5b\text{-}Q}[n-m]\cdot sc_{E5\text{-}S}[n-m] + \right. \\ & \left. - \sum_{n=0}^{N} s_{E5\mathbf{Q}}[n]\cdot e_{E5b\text{-}Q}[n-m]\cdot sc^{off}_{E5\text{-}S}[n-m] \right\} \end{aligned} \tag{3.26}$$

It must be noticed that in these expressions the subcarrier waveform $sc_{E5\text{-}S}(t)$ and its delayed version $sc_{E5\text{-}S}\left(t - T_{s,E5}/4\right)$ have been denoted respectively with $sc_{E5\text{-}S}[n]$ and $sc^{off}_{E5\text{-}S}[n]$, in the discrete time domain.

The two sideband complex correlation functions $\mathcal{C}_{E5a\text{-}Q}[m]$ and $\mathcal{C}_{E5b\text{-}Q}[m]$, if considered individually, are difficult to be used for the tracking, because they are complex functions.

They become useful only defining the **combined complex correlation function** $\mathcal{C}_{\mathbf{E5Q}}[m]$ (see [11]), obtained summing the two complex correlations:

$$\mathcal{C}_{\mathbf{E5Q}}[m] = \mathcal{C}_{E5a\text{-}Q}[m] + \mathcal{C}_{E5b\text{-}Q}[m] \tag{3.27}$$

This correlation function is plotted in Figure 3.9. It presents a sharp peak and some decreasing oscillations. This is the typical shape of the AltBOC correlation that is presented in several articles in literature. It is similar in shape to that obtainable with a BOC(15,10) on the entire E5 band, but its main peak is steeper, leading to better tracking performances [11].

It can be seen that the combined E5a/E5b correlation in Equation (3.27) is a **real** function of the code delay m. In fact the real components $C_1^{E5a\text{-}Q}[m]$ and $C_2^{E5a\text{-}Q}[m]$ of $\mathcal{C}_{E5a\text{-}Q}[m]$ and the corresponding components $C_1^{E5b\text{-}Q}[m]$

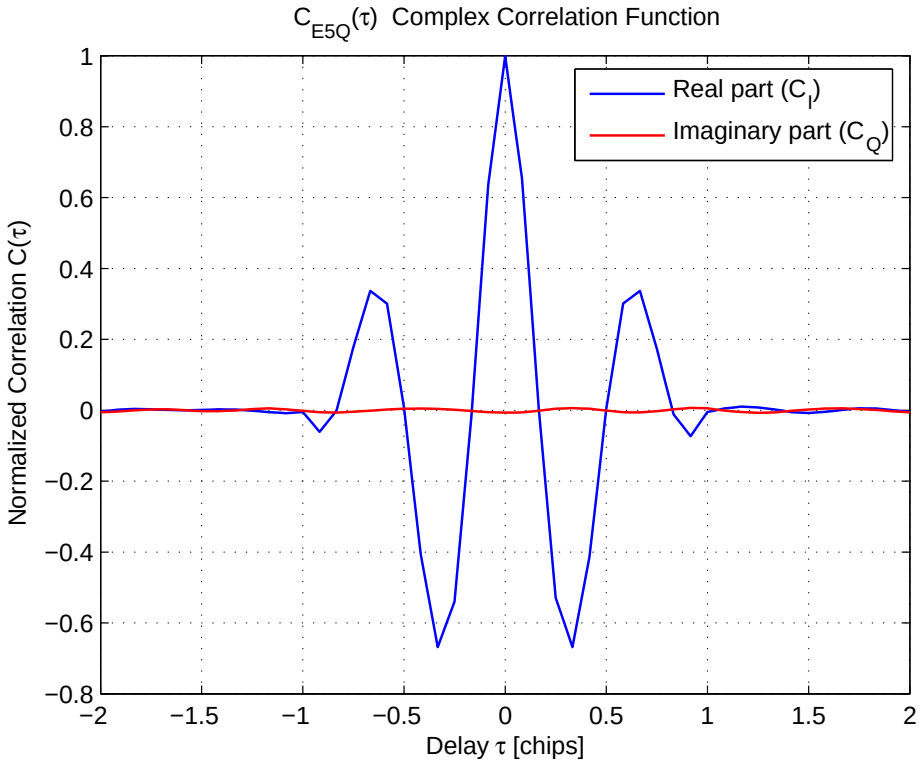

Figure 3.9: Combined complex correlation function $\mathcal{C}_{\mathbf{E5Q}}(\tau)$

and $C_2^{E5b\text{-}Q}[m]$ of $\mathcal{C}_{E5b\text{-}Q}[m]$ have similar shapes (see Figure 3.8). Then, in the $\mathcal{C}_{\mathbf{E5Q}}[m]$ expression, they combine coherently to obtain an higher correlation peak, that is the real part of $\mathcal{C}_{\mathbf{E5Q}}[m]$ (the blue line in Figure 3.9).

The other components ($C_3^{E5a\text{-}Q}[m]$, $C_4^{E5a\text{-}Q}[m]$, $C_3^{E5b\text{-}Q}[m]$ and $C_4^{E5b\text{-}Q}[m]$), that correspond to the imaginary parts of the sideband complex correlations $\mathcal{C}_{E5a\text{-}Q}[m]$ and $\mathcal{C}_{E5b\text{-}Q}[m]$, cancel them. In effect the imaginary part of $\mathcal{C}_{\mathbf{E5Q}}[m]$ (the red line in Figure 3.9) is practically null: this is true only if the carrier is correctly tracked by the PLL of the receiver and the DLL in correctly locked (for more details, see Section 4.3). Then the four imaginary components ($C_3^{E5a\text{-}Q}[m]$, $C_4^{E5a\text{-}Q}[m]$, $C_3^{E5b\text{-}Q}[m]$ and $C_4^{E5b\text{-}Q}[m]$), that individually are unusable for tracking, become useful if summed in the combined correlation expression $\mathcal{C}_{\mathbf{E5Q}}[m]$, because its imaginary part could be used to detect tracking errors.

At last, the expressions of the real and the imaginary parts of $\mathcal{C}_{\mathbf{E5Q}}[m]$ could be written:

$$\mathcal{C}_{\mathbf{E5Q}}[m] = \mathcal{C}_{\mathbf{I}}[m] + \mathrm{j} \cdot \mathcal{C}_{\mathbf{Q}}[m] \tag{3.28}$$

$$
\begin{aligned}
\mathcal{C}_{\mathbf{I}}[m] \;=\; & \sum_{n=0}^{N} s_{E5\mathbf{I}}[n] \cdot e_{E5a\text{-}Q}[n-m] \cdot sc^{off}_{E5\text{-}S}[n-m] + \\
& + \sum_{n=0}^{N} s_{E5\mathbf{Q}}[n] \cdot e_{E5a\text{-}Q}[n-m] \cdot sc_{E5\text{-}S}[n-m] + \\
& - \sum_{n=0}^{N} s_{E5\mathbf{I}}[n] \cdot e_{E5b\text{-}Q}[n-m] \cdot sc^{off}_{E5\text{-}S}[n-m] + \\
& + \sum_{n=0}^{N} s_{E5\mathbf{Q}}[n] \cdot e_{E5b\text{-}Q}[n-m] \cdot sc_{E5\text{-}S}[n-m] \qquad (3.29) \\
\mathcal{C}_{\mathbf{Q}}[m] \;=\; & - \sum_{n=0}^{N} s_{E5\mathbf{I}}[n] \cdot e_{E5a\text{-}Q}[n-m] \cdot sc_{E5\text{-}S}[n-m] + \\
& + \sum_{n=0}^{N} s_{E5\mathbf{Q}}[n] \cdot e_{E5a\text{-}Q}[n-m] \cdot sc^{off}_{E5\text{-}S}[n-m] + \\
& - \sum_{n=0}^{N} s_{E5\mathbf{I}}[n] \cdot e_{E5b\text{-}Q}[n-m] \cdot sc_{E5\text{-}S}[n-m] + \\
& - \sum_{n=0}^{N} s_{E5\mathbf{Q}}[n] \cdot e_{E5b\text{-}Q}[n-m] \cdot sc^{off}_{E5\text{-}S}[n-m] \qquad (3.30)
\end{aligned}
$$

In conclusion, the real part $\mathcal{C}_{\mathbf{I}}[m]$ of the combined complex correlation function $\mathcal{C}_{\mathbf{E5Q}}[m]$ can be used for code tracking and this seems to be the best way to take advantage of the coherence of the two sideband *E5a-Q* and *E5b-Q* signals.

The final expressions in Equations (3.29) and (3.30) will be used in Section 4.3.2, where the combined complex correlation function will be implemented as a component of the AltBOC receiver.

Chapter 4

AltBOC receiver architectures

The wideband AltBOC signal processing is challenging for the receiver for two main reasons:

- to process the AltBOC(15,10) signal, the whole E5 band has to be downconverted through the same RF/IF chain. The minimal signal bandwidth is approximatively 50 MHz (processing only the main lobes E5a and E5b, as shown in Figure 4.1). This leads to sampling rates and clocking frequencies higher than currently used in GPS receivers;
- the baseband signal processing is difficult, due to the complex nature of the AltBOC baseband signal: to perform one complex correlation it is necessary to use at least four conventional correlators.

Some different receiver architectures are foreseen, depending on the type of correlators used and the capability to process a single band only (E5a or E5b) or to operate in coherent dual band mode (E5a + E5b).

The future receiver architectures can be classified in the following three types:

1. **single band receiver**, based on a BPSK demodulator for the E5a band. This arrangement could be used in simple low-cost receivers, without high precision;
2. **separate dual band receiver**, with non-coherent reception of E5a and E5b bands. It works with two separate BPSK demodulators and offer slightly better performance than the first one;
3. **coherent dual band receiver**, based on the combined AltBOC correlation of E5a and E5b. This receiver achieves the best performance, but is more complex than the others.

In the following Sections these proposed receiver architectures are presented in detail, analyzing their performances and the implementation complexity.

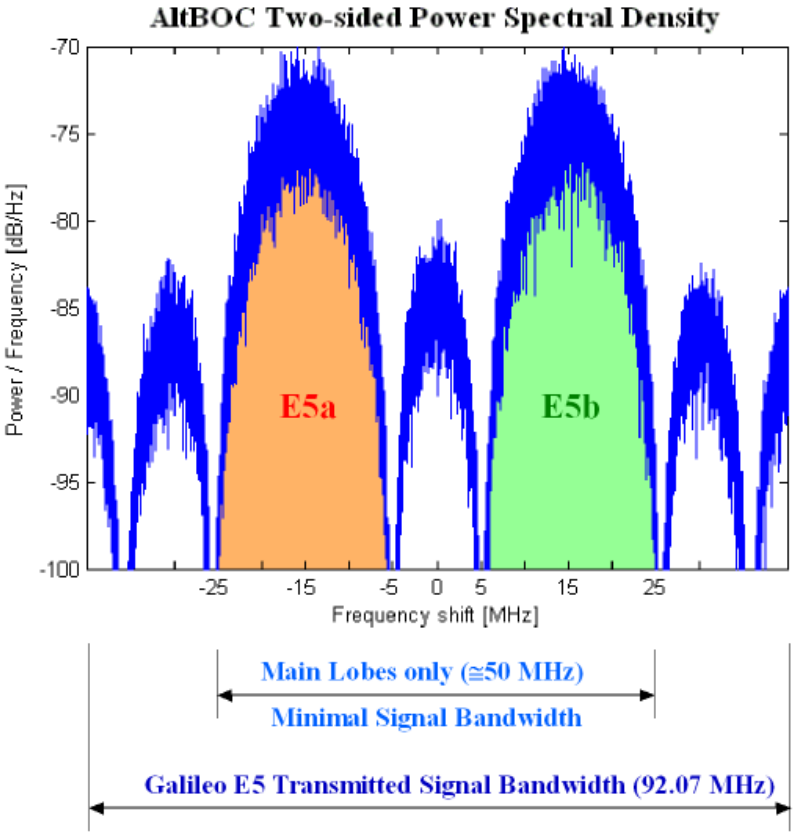

Figure 4.1: Galileo E5 AltBOC(15,10) signal bandwidth

These receiver architectures are considered here only for the signal tracking functioning, neglecting for the moment the acquisition process, that requires different operations for each receiver type and will be exhaustively discussed in next Chapter.

At the end of this Chapter, three further receiver architectures are also presented and compared with previous schemes:

- an AltBOC receiver protected by a patent (see Reference [13]);
- the *Offset-Carrier Single Side Band Tracking* (OC SSB) receiver;
- the coherent dual band receiver with a *correlator-discriminator*.

The first two receivers are quite similar to the coherent dual band receiver, whereas the last one (the *receiver with the correlator-discriminator*) is an innovative architecture that features interesting implementation solutions, proposed in this dissertation for the first time.

4.1 Single band receiver

This architecture, also known as *Central-Carrier Single Side Band Tracking* (CC SSB [8]), is the simplest receiver model. It works using only a single sideband (for example E5a) of the Galileo E5 signal, processing it like a simple QPSK modulated signal.

The demodulation of the received signal is performed tracking the center frequency of the sideband (1176.45 MHz, for E5a band), as shown in Figure 4.2. In this way the receiver down-converts to the baseband the received signal, and then select the signal of interest using an appropriate baseband low-pass filter (e.g. with a filter bandwidth of about 20 MHz, to select only the main lobe of E5a).

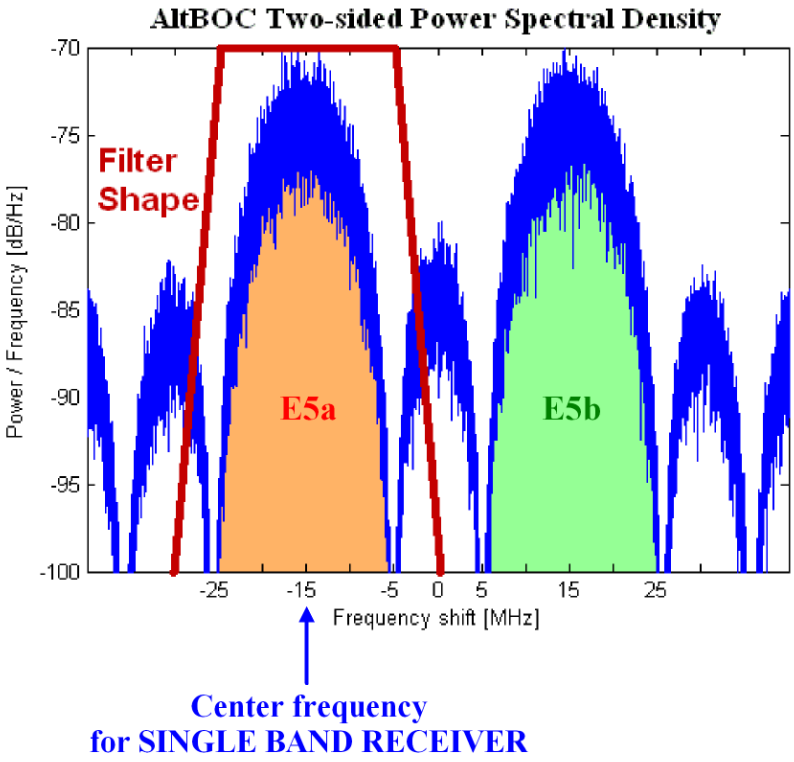

Figure 4.2: Signal bandwidth selection for a single band receiver

The block diagram of this receiver architecture is presented in Figure 4.3. Its functional blocks are:

RF front end: the satellite signal is received using an appropriate antenna, and is firstly processed at radio-frequency in the analog domain, using a low noise amplifier and a band-pass filter;

IF section: using a single stage heterodyne, the received signal is down-converted to the intermediate frequency. It is necessary a stable frequency reference for the local oscillator. After the mixer, the signal

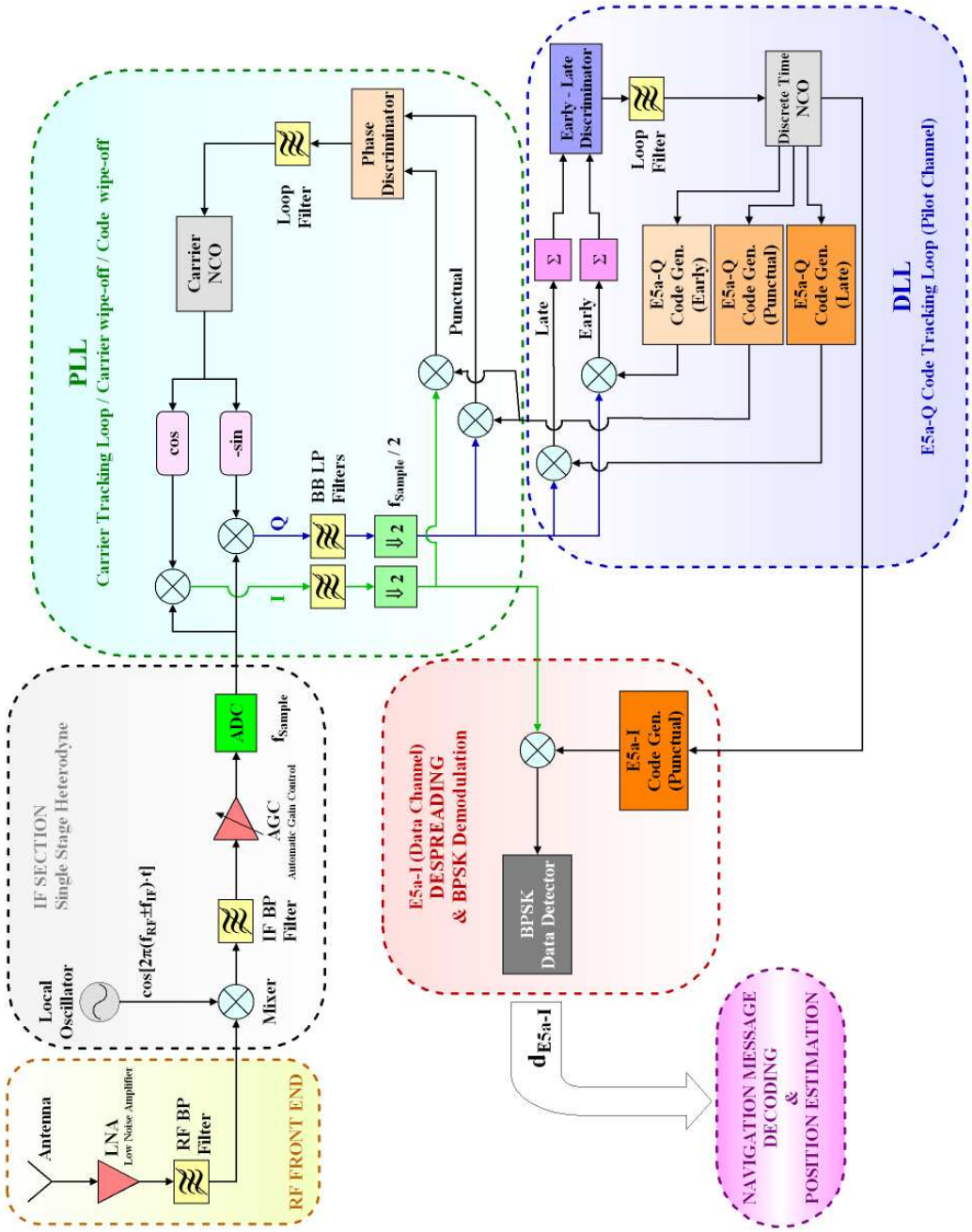

Figure 4.3: Block diagram of a single band receiver architecture

is conditioned using a filter, to remove high-order harmonics, and an automatic gain control amplifier, to control the dynamic at the input of the *Analog to Digital Converter*. The ADC operates with an appropriate sampling frequency (f_{Sample}) and converts the signal to the digital domain;

FLL/PLL: the *Phase Locked Loop* (PLL) is used to coherently track the central carrier of the sideband, separating the in-phase and the quadrature

channel. This loop, during the transition phase between the acquisition and the tracking, works like a *Frequency Locked Loop* (FLL), to refine the estimation of the Doppler frequency. After the convergence of the FLL, the PLL is installed and locks on the carrier phase. In the two branches of the PLL, after the baseband filtering, the signals are down-sampled, halving the sampling frequency. The loop works using the punctual channel of the correlator, obtained from the DLL;

DLL: the *Delay Locked Loop* operates on the quadrature channel, tracking the code of the pilot channel (*E5a-Q*). The tracking can be done using different types of discriminator: in Figure 4.3 it is presented the simplest one, the Early-Late discriminator. The goal of this code tracking loop is to synchronize a discrete time *Numerically Controlled Oscillator* (NCO) to the chip transitions of the spreading code. Indeed the NCO is used like a time reference for the code generators of the pilot and the data channels; in detail, for the pilot channel three time shifted replicas of the code are generated, respectively for the early, the punctual and the late correlators. The three correlation values are evaluated multiplying the received signal (Q channel) with the three local signals and then applying an integrate and dump operation (denoted with the $\sum$ symbol in the scheme);

Despreading and Demodulation: the in-phase channel, that contains the modulated data, is firstly multiplied with a local code, generated using the time reference provided by the NCO. This operation produces the despreading of the data channel. After this, the data could be easily recovered using a BPSK data detector, that performs an integrate and dump operation and compares the result with a decision threshold;

Data processing: at last the demodulated data are used to decode the navigation message of the satellites and to estimate the position of the receiver, measuring the pseudoranges (like in a GPS receiver).

Considering the implementation of the PLL, the design of old GNSS receivers (GPS, GLONASS) has traditionally been limited to the use of *Costas Loop* PLL discriminators, that are insensitive to 180° phase reversals due to data modulation. One of the key features of the proposed Galileo signal structure is the use of pilot signals. Since the pilot signals have no data modulation, and therefore no 180° phase reversals, a true *four-quadrant arctangent* PLL discriminator can be used (as stated in Reference [14]). This means the receiver performances could be significantly improved taking advantage of the presence of the pilot codes (the pre-detection integration period can be extended beyond the data period and the tracking error threshold of the full 360° PLL is double that of the Costas PLL).

After the PLL, the received signal results down-converted, with the sideband of interest centered to the baseband. The purpose of the baseband filters on

the two I and Q channels is to select only the main lobe of the sideband, obtaining a result similar to that one shown in Figure 4.4. Obviously the bandwidth of the filters must be optimized, in order to remove the adjacent interfering signals, but without excessively degrade the correlation proprieties of the filtered signal.

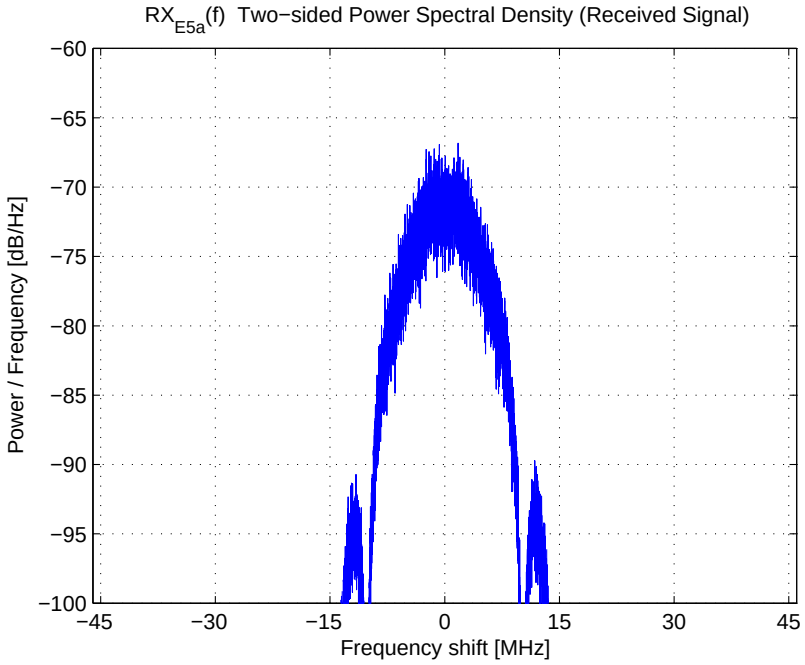

Figure 4.4: Filtered signal spectrum for a single band receiver

After the filtering, the scattering diagram of the signal is similar to that one shown in Figure 4.5.

This demonstrates that a single sideband of the AltBOC signal could be considered like a QPSK modulation, that could be demodulated considering two BPSK signals. In fact the BPSK channel in quadrature contains the spreading code of the pilot channel, and the in-phase channel includes the spreading code and the symbols of the data channel. The chip transitions of both the channels are evident in the eye diagrams in Figure 4.6.

This Central Carrier Single Side Band Tracking architecture presents the advantage that requires a simple and low-cost signal processing. In fact there are only ordinary components for the BPSK demodulation and for the decorrelation of the spreading codes. Moreover, in the receiver the reference signal generation is the simplest one, because does not require the generation of the AltBOC subcarrier waveforms. This architecture implies also the advantage of lower necessary sampling rate and bandwidth: the analog and digital sections have to down-convert only a sideband, not the entire E5 band.

The drawbacks of this simple and low-cost receiver are lower performances

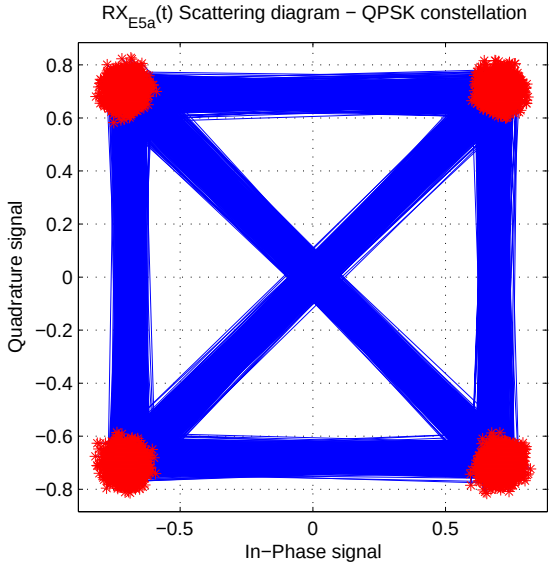

Figure 4.5: QPSK scattering diagram for a single band receiver

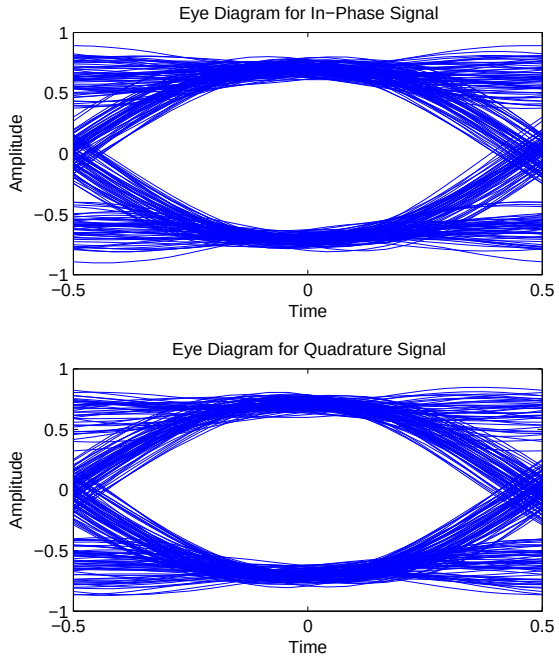

Figure 4.6: Received signal eye diagram for a single band receiver

than other wide-band arrangements, in terms of precision of measurement in presence of noise, multipath and other typical error sources.

4.2 Separate dual band receiver

The *separate dual band receiver architecture* (also called *non-coherent dual band receiver*) is just an extension of the single band receiver, obtained duplicating the functional blocks after the radio-frequency front end. In this way the two sidebands E5a and E5b are separately down-converted, tracking their respective central frequencies, and the receiver is able to recover both the data channels transmitted in the Galileo E5 band.

The block diagram of this receiver architecture is presented in Figure 4.7.

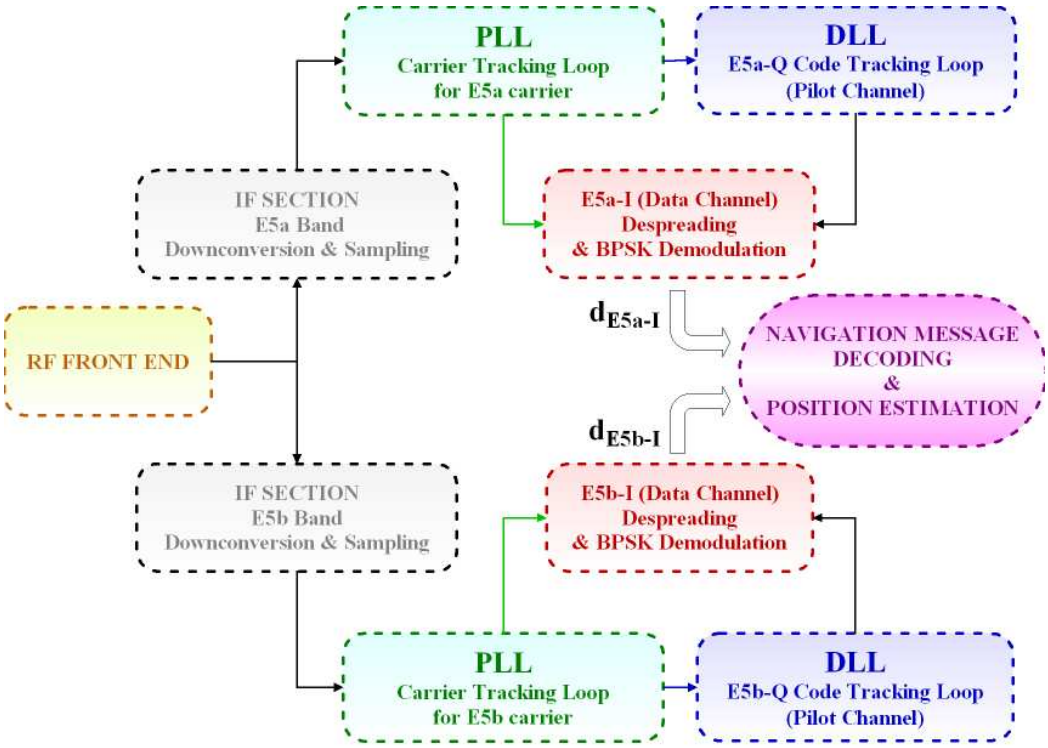

Figure 4.7: Block diagram of the separate dual band receiver architecture

There are two branches that separately receive the two sidebands. For each sideband, the functional blocks are the same of those ones used in the single band receiver. The bandwidth and the sampling frequency for the components of the two branches are similar (suitable to receive only a single sideband). The unique difference is in the RF front-end, because in the separate dual band architecture these analog components (antenna, LNA, band-pass filter) must be able to receive the entire E5 band, not only a single sideband.

The PLLs and the DLLs of the two branches can work independently, in simple implementations, or can interact, co-operating to achieve the synchronism to track the two signals, taking advantage of the coherence between the signals in the two sidebands. In fact the edges of code chips are synchronous, without relative bias or relative chip-slip, for all signal components

within the same AltBOC signal transmitted from a satellite (as stated in Reference [4]). Obviously for the second arrangement (with co-operating PLLs and DLLs) there are foreseeable improved performances, but with a more complex implementation.

The principal advantage of the separate dual band receiver is the possibility to correct the **ionospheric error** (that causes different delays for signals at different frequencies). In fact, using the two separate sidebands, the receiver could process two signals at different frequencies, estimating the ionospheric error from the delay between the two received signals.

Of course the use of the two sidebands in this non coherent arrangement can lead to significant improvements in measurement precision with respect of the single band arrangement. In fact it is possible to obtain a combined position estimation, averaging the pseudoranges measured from the two sidebands.

Anyway this architecture obtains performances worse than the coherent dual band receiver (see next Section) and it is the most expensive architecture in terms of hardware, because there are two PLLs and two DLLs. The implementation of the necessary components, however, is as simple as in single band receiver.

4.3 Coherent dual band receiver

The coherence between the two E5 sidebands, due to the AltBOC modulation, could be fully exploited using a *coherent dual band receiver architecture*. This leads to improved performances for the precision of the position estimation and in presence of the typical error sources.

The block diagram of this receiver architecture is shown in Figure 4.8. The main differences between this arrangement and the previous ones are essentially in the DLL and in the demodulation functional block.

The DLL works similarly to the previous arrangements, using an Early-Late discriminator to track the two pilot channels (*E5a-Q* and *E5b-Q*).
The main difference is that each correlation operation is implemented with a **complex correlator** block (subsequently presented in detail), instead of the simple multiplication operator used in previous architectures. There are three complex correlators, respectively for the evaluation of the early, the punctual and the late correlation. Each of these correlators has two complex inputs: the received signal ($s_{E5\mathbf{I}}$ and $s_{E5\mathbf{Q}}$) and a complex local signal, that is a local replica of the pilot codes, modulated with the subcarriers. In detail, each correlator requires the generation of four local signal components: the two pilot codes ($c_{E5a\text{-}Q}$ and $c_{E5b\text{-}Q}$) and the samples of the subcarrier waveform, with the correct timing ($sc_{E5\text{-}S}$) and in its delayed version ($sc^{off}_{E5\text{-}S}$). As depicted in Figure 4.8, these signals are generated using three **code generators** (early, punctual and late) and three **subcarrier generators**, controlled by the time

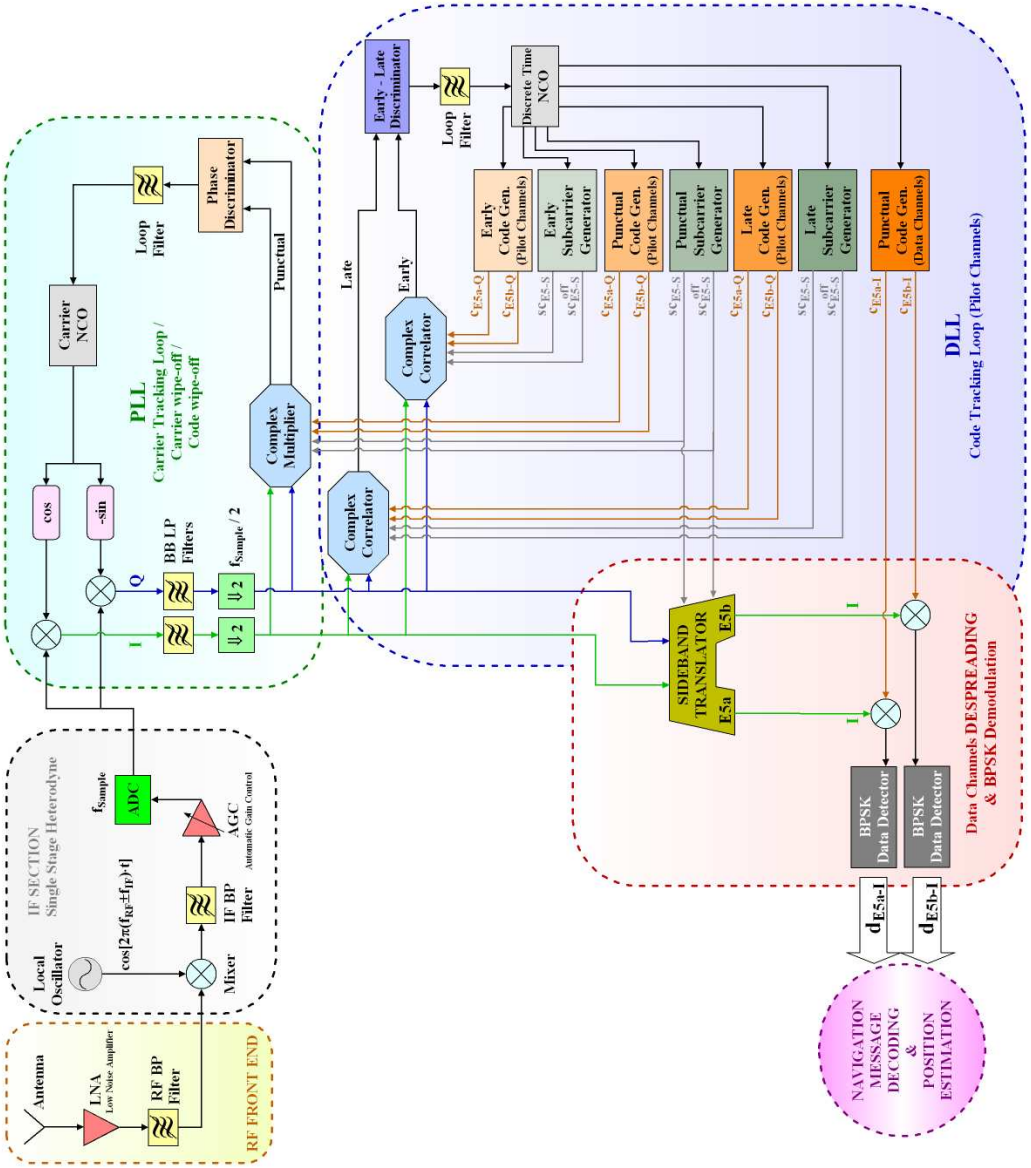

Figure 4.8: Block diagram of the coherent dual band receiver architecture

reference provided by the NCO. There is another code generator, that produces the two codes ($c_{E5a\text{-}I}$ and $c_{E5b\text{-}I}$) for data channels, that are used in the despreading and demodulation block.

It must also be noticed the presence of the **sideband translator** in the despreading and demodulation block of the receiver. This sideband translator is a patent pending functional block, introduced for the first time in this thesis (see Section 4.3.3), that performs a "*translation operation*": the two separate in-phase signals containing the navigation data (*E5a-I* and *E5b-I*) are recovered from the received complex baseband signal $s_{E5}(t)$. This means that the two sideband signals, located in frequency around the center frequency of E5a and E5b sidebands, are shifted to the baseband. The correct

components (in phase) are then selected and passed to the subsequent BPSK data detector blocks.

The coherent dual band architecture could be considered the best way to take advantage of the correlation proprieties of the AltBOC signal. Actually with this arrangement it is possible to obtain a sharp correlation peak (the *combined complex correlation function*, previously discussed in Section 3.4), that could be tracked obtaining better performances than with the previous architectures, in presence of noise, multipath and other typical error sources. In fact previous arrangements are based on a BPSK signal processing, then the correlation function has a simple triangular shape, leading to worse performances.

The drawback of the coherent dual band architecture is the implementation complexity, because requires some new functional blocks (see next Sections), not included in common GPS receivers. Moreover it requires the largest bandwidth and sampling frequency, because the entire Galileo E5 band must be down-converted and processed.

4.3.1 Subcarrier generator block

It must be noticed that in the coherent dual band receiver, to generate the complex local signal, it is necessary the **subcarrier generator** block, absent in previous architectures.

Different options are foreseeable for the waveform produced by the subcarrier generator:

- a sampled cosine waveform (the black line, in Figure 4.9), obtaining a complex-LOC signal;
- a squared cosine (the green line), to generate a complex-BOC signal;
- the four-valued subcarrier function $sc_{E5\text{-}S}(t)$ (the red line), that is the correct waveform used in Galileo satellites to modulate the AltBOC SIS (*Signal In Space*).

These choices for the waveform generator lead to different performances in terms of correlation losses (see [8]). The last one clearly seems to be the best way to generate a local signal, coherent with the transmitted signal, and then this waveform is used in the following. The other two could also be used because they are easy to generate, but they lead to a correlation loss.

4.3.2 Complex correlator block

The **complex correlator** is a direct implementation of the complex correlation function $\mathcal{C}_{\mathbf{E5Q}}[m]$ (presented in Section 3.4), obtained combining the

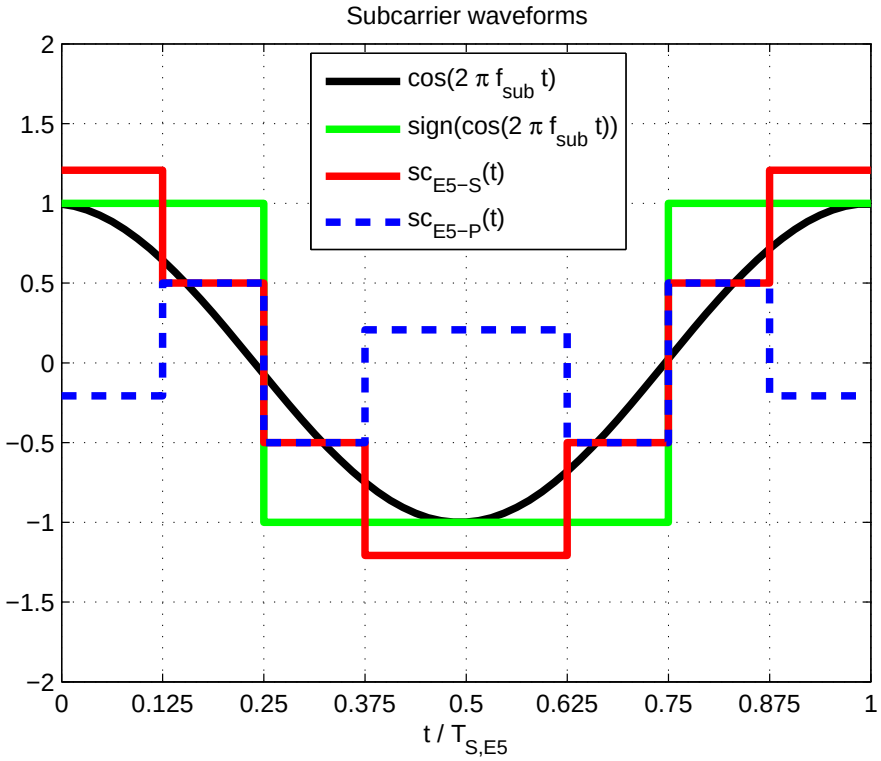

Figure 4.9: Different subcarrier functions for tracking options

correlation proprieties of the two pilot channels in E5a and E5b sidebands. For the sake of clarity, the final expressions obtained for the real and imaginary part of $\mathcal{C}_{\mathbf{E5Q}}[m]$ is rewritten here:

$$\mathcal{C}_{\mathbf{E5Q}}[m] = \mathcal{C}_{\mathbf{I}}[m] + \mathrm{j} \cdot \mathcal{C}_{\mathbf{Q}}[m] \tag{4.1}$$

$$\begin{aligned}
\mathcal{C}_{\mathbf{I}}[m] \;=\; & \sum_{n=0}^{N} s_{E5\mathbf{I}}[n] \cdot e_{E5a\text{-}Q}[n-m] \cdot sc^{off}_{E5\text{-}S}[n-m] + \\
& - \sum_{n=0}^{N} s_{E5\mathbf{I}}[n] \cdot e_{E5b\text{-}Q}[n-m] \cdot sc^{off}_{E5\text{-}S}[n-m] + \\
& + \sum_{n=0}^{N} s_{E5\mathbf{Q}}[n] \cdot e_{E5a\text{-}Q}[n-m] \cdot sc_{E5\text{-}S}[n-m] + \\
& + \sum_{n=0}^{N} s_{E5\mathbf{Q}}[n] \cdot e_{E5b\text{-}Q}[n-m] \cdot sc_{E5\text{-}S}[n-m]
\end{aligned} \tag{4.2}$$

$$\begin{aligned}\mathcal{C}_{\mathbf{Q}}[m] \;=\; & -\sum_{n=0}^{N} s_{E5\mathbf{I}}[n]\cdot e_{E5a\text{-}Q}[n-m]\cdot sc_{E5\text{-}S}[n-m]+ \\ & -\sum_{n=0}^{N} s_{E5\mathbf{I}}[n]\cdot e_{E5b\text{-}Q}[n-m]\cdot sc_{E5\text{-}S}[n-m]+ \\ & +\sum_{n=0}^{N} s_{E5\mathbf{Q}}[n]\cdot e_{E5a\text{-}Q}[n-m]\cdot sc^{off}_{E5\text{-}S}[n-m]+ \\ & -\sum_{n=0}^{N} s_{E5\mathbf{Q}}[n]\cdot e_{E5b\text{-}Q}[n-m]\cdot sc^{off}_{E5\text{-}S}[n-m] \end{aligned} \tag{4.3}$$

The functional diagram of the complex correlator is illustrated in Figure 4.10. It is possible to see that the expressions of the combined correlation could be efficiently implemented using only four multiplier, instead of eight (four for the $\mathcal{C}_{\mathbf{I}}[m]$ and the others for $\mathcal{C}_{\mathbf{Q}}[m]$). In fact, for the linearity of the correlation operation, it is possibile to combine the two codes ($c_{E5a\text{-}Q}$ and $c_{E5b\text{-}Q}$) before the multiplication and the sum, halving the required multipliers. Adding and subtracting the two binary codes (as shown in Figure 4.10), it is possible to obtain two 3-level signals, that could be used to evaluate the correlation.

In this arrangement it must be noticed that only one output of the correlator block is used. In detail the complex correlator evaluate the real ($\mathcal{C}_{\mathbf{I}}[m]$) and the imaginary part ($\mathcal{C}_{\mathbf{Q}}[m]$) of the complex correlation, but only the first component is suitable for the code tracking.

The imaginary part $\mathcal{C}_{\mathbf{Q}}[m]$, if the received signal is undistorted and correctly tracked by the PLL and the DLL, exhibits a null amplitude ($\mathcal{C}_{\mathbf{Q}}[m] \cong 0$, as stated in [11]). Otherwise this signal could be used to detect tracking errors, for example in presence of ionospheric error.

4.3.3 Sideband translator block

In the despreading and demodulation block of the coherent dual band receiver, the main difference with respect of previous architectures is the presence of the **sideband translator**. This block performs a double frequency shift, taking the two in phase data channels ($e_{E5a\text{-}I}$ and $e_{E5b\text{-}I}$) and moving them from the sidebands of the E5 AltBOC spectrum to the baseband, as illustrated by the red arrows in the scheme in Figure 4.11.

It must be remarked that the idea and the implementation of this block is **patent pending**. A patent is already present for an AltBOC receiver architecture (as discussed in Section 4.4.1), similar to the coherent dual band receiver, but the data are recovered from the two in-phase channels (*E5aI* and *E5bI*) using a different technique. Then the sideband translator is an innovative arrangement, presented for the first time in this thesis, that could be used to demodulate the navigation data in the AltBOC signal.

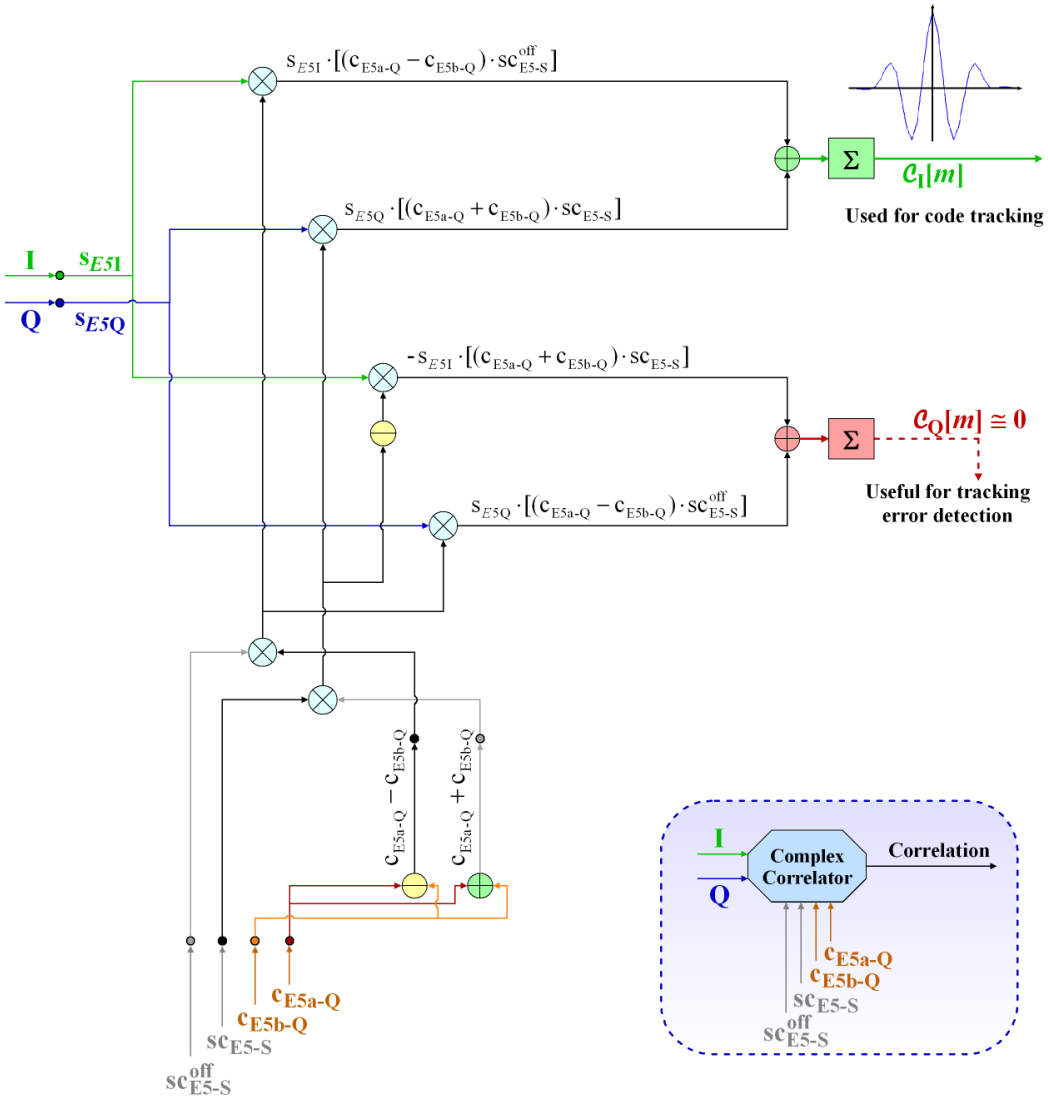

Figure 4.10: Block diagram of the complex correlator

To understand the operations performed by the sideband translator, it is useful to consider a simpler situation, for example a BOC receiver. The signal to be transmitted with a BOC modulation is multiplied with a rectangular subcarrier: this operation causes a frequency shift, that leads to the two typical sidebands of the BOC spectrum (similar to the spectrum of the E5 AltBOC signal). To demodulate this split-spectrum signal, once the received signal is correctly tracked by the DLL and the PLL of the BOC receiver (the local PRN code is synchronized), a simple technique is to multiply the received BOC signal again with a local rectangular subcarrier, generated in accord to the punctual channel of the DLL. This operation translates the two sidebands of the BOC signal again to the baseband: in this way, the signal becomes again a baseband signal and the information contained in it could be easily recovered (after the despreading with the local PRN code),

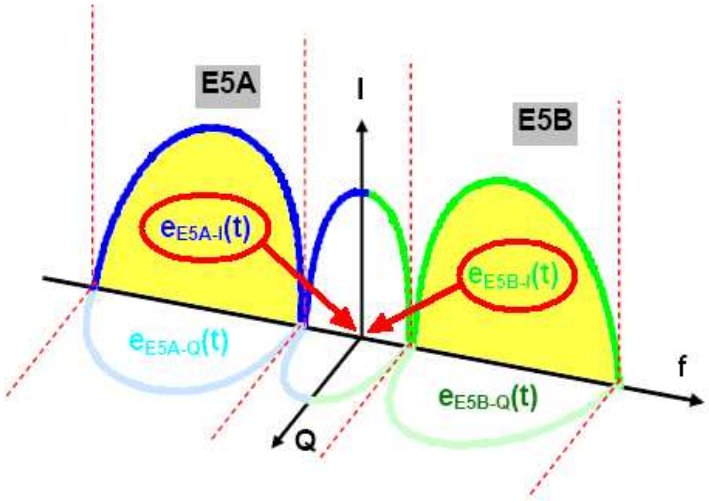

Figure 4.11: Illustration of the operations performed by the sideband translator block, in the E5 AltBOC spectrum

with a BPSK data detector. Then, with a BOC modulation, the sideband translation is a simple multiplication with a local subcarrier, that reconverts the received signal in a baseband signal.

On the contrary, with the E5 AltBOC signal this operation is more complicated, because there are four transmitted channels (instead of one) and the frequency shifts of the channels in the two sidebands are performed taking advantage of complex exponentials. Then the sideband translator block must choose the correct channels (only the in phase channels, that contain the navigation data) and needs to use complex exponential operations to move these channels to the baseband, as depicted in Figure 4.11.

The block diagram of the sideband translator is presented in Figure 4.12. It extracts from the received complex baseband signal $s_{E5}(t)$ the two separate in-phase signals $e_{E5a\text{-}I}(t)$ and $e_{E5b\text{-}I}(t)$, useful for the subsequent despreading and BPSK data detection.

To explain the operations performed by this block, it is necessary to remember the received baseband signal expression:

$$s_{E5}(t) = s_{E5\mathbf{I}}(t) + \mathrm{j} \cdot s_{E5\mathbf{Q}}(t) \tag{4.4}$$

$$\begin{aligned} = {} & \frac{1}{2 \cdot \sqrt{2}} \cdot [e_{E5a\text{-}I}(t) + \mathrm{j} \cdot e_{E5a\text{-}Q}(t)] \cdot [sc_{E5\text{-}S}(t) - \mathrm{j} \cdot sc_{E5\text{-}S}(t - T_{s,E5}/4)] + \\ & + \frac{1}{2 \cdot \sqrt{2}} \cdot [e_{E5b\text{-}I}(t) + \mathrm{j} \cdot e_{E5b\text{-}Q}(t)] \cdot [sc_{E5\text{-}S}(t) + \mathrm{j} \cdot sc_{E5\text{-}S}(t - T_{s,E5}/4)] + \\ & + \frac{1}{2 \cdot \sqrt{2}} \cdot [\overline{e}_{E5a\text{-}I}(t) + \mathrm{j} \cdot \overline{e}_{E5a\text{-}Q}(t)] \cdot [sc_{E5\text{-}P}(t) - \mathrm{j} \cdot sc_{E5\text{-}P}(t - T_{s,E5}/4)] + \\ & + \frac{1}{2 \cdot \sqrt{2}} \cdot [\overline{e}_{E5b\text{-}I}(t) + \mathrm{j} \cdot \overline{e}_{E5b\text{-}Q}(t)] \cdot [sc_{E5\text{-}P}(t) + \mathrm{j} \cdot sc_{E5\text{-}P}(t - T_{s,E5}/4)] \end{aligned} \tag{4.5}$$

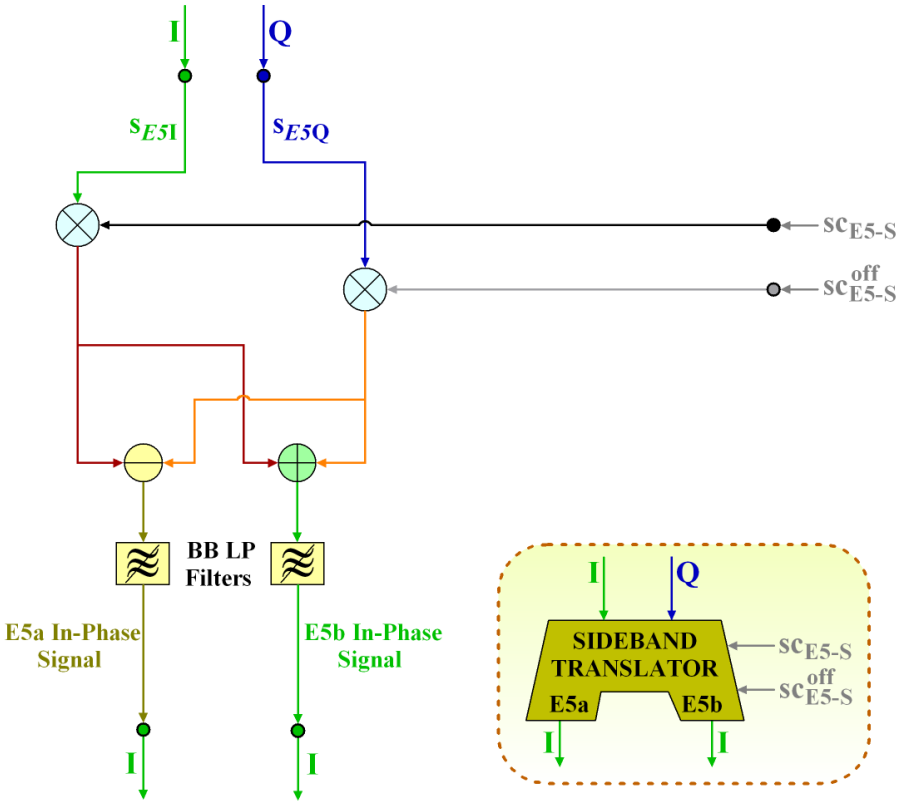

Figure 4.12: Block diagram of the sideband translator (**patent pending**)

As discussed in Section 2.2.4, the E5 AltBOC modulation shifts the four channels $e_{E5a\text{-}I}$, $e_{E5a\text{-}Q}$, $e_{E5b\text{-}I}$ and $e_{E5b\text{-}Q}$ in the two sidebands of the power spectrum. This is achieved using the subcarrier signal $sc_{E5\text{-}S}(t)$ and its delayed version $sc_{E5\text{-}S}\left(t - T_{s,E5}/4\right)$, denoted respectively $sc_{E5\text{-}S}$ and $sc^{off}_{E5\text{-}S}$ in previous diagrams, to create two complex exponentials:

- the first exponential

$$sc_{E5\text{-}S}(t) - \mathrm{j} \cdot sc_{E5\text{-}S}\left(t - \frac{T_{s,E5}}{4}\right)$$

  downshifts the two E5a channels, from the center of the E5 band to the correct frequency;

- the second exponential

$$sc_{E5\text{-}S}(t) + \mathrm{j} \cdot sc_{E5\text{-}S}\left(t - \frac{T_{s,E5}}{4}\right)$$

  upshifts the two E5b channels.

The sideband translator take advantage of this idea, performing the opposite operation, to extract the two in-phase channels $e_{E5a\text{-}I}(t)$ and $e_{E5b\text{-}I}(t)$ from the baseband received signal $s_{E5}(t)$.

To obtain the $e_{E5a\text{-}I}(t)$ channel it is necessary to upshift the received signal spectrum, multiplying it for the second exponential. In this way the E5a band becomes centered to the baseband, and it is possible to recover the $e_{E5a\text{-}I}(t)$ signal selecting the in-phase (real) component of the result, as shown in the following equations:

$$\begin{aligned} e_{E5a\text{-}I}(t) &\cong \mathrm{Re}\{[s_{E5\mathbf{I}}(t) + \mathrm{j} \cdot s_{E5\mathbf{Q}}(t)] \cdot [sc_{E5\text{-}S}(t) + \mathrm{j} \cdot sc_{E5\text{-}S}(t - T_{s,E5}/4)]\} && (4.6) \\ &= \mathrm{Re}\{s_{E5\mathbf{I}}(t) \cdot sc_{E5\text{-}S}(t) - s_{E5\mathbf{Q}}(t) \cdot sc_{E5\text{-}S}(t - T_{s,E5}/4) + \\ &\quad + \mathrm{j} \cdot [s_{E5\mathbf{I}}(t) \cdot sc_{E5\text{-}S}(t - T_{s,E5}/4) + s_{E5\mathbf{Q}}(t) \cdot sc_{E5\text{-}S}(t)]\} && (4.7) \\ &= s_{E5\mathbf{I}}(t) \cdot sc_{E5\text{-}S}(t) - s_{E5\mathbf{Q}}(t) \cdot sc_{E5\text{-}S}(t - T_{s,E5}/4) && (4.8) \end{aligned}$$

In previous equations the product signals, that are the dashed terms in Equation (4.5), are neglected[1]. In fact the product signals can be ignored because they are multiplied by $sc_{E5\text{-}P}(t)$ subcarrier waveform, that has smaller amplitude (see Figure 4.9).

Similarly to that done for the $e_{E5a\text{-}I}(t)$ channel, it is possible to recover the $e_{E5b\text{-}I}(t)$ signal, downshifting the received signal $s_{E5}(t)$ with the following operations:

$$\begin{aligned} e_{E5b\text{-}I}(t) &\cong \mathrm{Re}\{[s_{E5\mathbf{I}}(t) + \mathrm{j} \cdot s_{E5\mathbf{Q}}(t)] \cdot [sc_{E5\text{-}S}(t) - \mathrm{j} \cdot sc_{E5\text{-}S}(t - T_{s,E5}/4)]\} && (4.9) \\ &= \mathrm{Re}\{s_{E5\mathbf{I}}(t) \cdot sc_{E5\text{-}S}(t) + s_{E5\mathbf{Q}}(t) \cdot sc_{E5\text{-}S}(t - T_{s,E5}/4) + \\ &\quad + \mathrm{j} \cdot [s_{E5\mathbf{Q}}(t) \cdot sc_{E5\text{-}S}(t) - s_{E5\mathbf{I}}(t) \cdot sc_{E5\text{-}S}(t - T_{s,E5}/4)]\} && (4.10) \\ &= s_{E5\mathbf{I}}(t) \cdot sc_{E5\text{-}S}(t) + s_{E5\mathbf{Q}}(t) \cdot sc_{E5\text{-}S}(t - T_{s,E5}/4) && (4.11) \end{aligned}$$

The results, shown in Equation (4.8) and in Equation (4.11), are directly implemented in the sideband translator block (see Figure 4.12), with multiplications and sums between the received signal and the locally generated subcarriers.

As shown in the block diagram, the results of the two equations could be filtered, with two baseband low-pass filters, to reduce the interference and the cross-correlation caused by the adjacent channels. The shape and the bandwidth of the filters must be optimized, because a narrow band filtering can reduce the performances, worsening the correlation proprieties of the data channels.

[1]The product signals contain also the navigation message of the two data channels $e_{E5a\text{-}I}(t)$ and $e_{E5b\text{-}I}(t)$, but to take advantage of this information it would be necessary to know the transmitted data before the demodulation. This is achievable only with two additional non coherent correlators for the data channels, or with a bit estimation process. But using these arrangements the receiver will be more vulnerable to errors (as stated in [11]). Then it is recommended to neglect the product signals during the demodulation of the AltBOC signal.

4.4 Other proposed architectures

The three receiver architectures presented in previous Sections are not the only arrangements that could be used to receive the AltBOC signal. Some other receiver architectures are discussed in this Section and compared with the previous ones:

- an AltBOC receiver protected by a patent;
- the *Offset-Carrier Single Side Band Tracking* (OC SSB) receiver;
- the coherent dual band receiver with a *correlator-discriminator*.

In detail, the first two receivers can be considered quite similar to the coherent dual band receiver, with some differences but with worse performances, then they are only presented here and are not further investigated in following Chapters.

On the contrary, the receiver with the correlator-discriminator is an innovative architecture proposed in this dissertation for the first time. It features a lower hardware complexity than the coherent dual band receiver and its performances will be further analyzed.

4.4.1 Patented AltBOC receiver

During the writing of this Chapter about the future AltBOC receivers, an existing patent was found (see Reference [13] in the Bibliography). This patent claims an hardware architecture of a receiver for use with a *Global Navigation Satellite System* (GNSS) that transmits AltBOC signals.

In detail, this patented receiver is quite similar to the *coherent dual band receiver* described in Section 4.3 of this thesis, but some remarkable differences can be highlighted:

1. the modulation described in the patent is not the true E5 AltBOC modulation (*Constant envelope AltBOC*) that will be used in Galileo GNSS, but corresponds to the *Standard AltBOC*;
2. the tracking of the two pilot codes (*E5aQ* and *E5bQ*) is performed in the DLL using local subcarriers that are simple rectangular waveforms, instead of the four-valued subcarrier function $sc_{E5\text{-}S}(t)$ (see Section 4.3.1);
3. the data are recovered from the two in-phase channels (*E5aI* and *E5bI*) using a technique that is different from that one used in the *coherent dual band receiver*.

About the first point, it is evident that this patent, filed on 8 October 2003 and published on 26 July 2005, refers to early hypothesis about the *Signal In Space* (SIS) for the E5 band: in fact in old articles the *Standard AltBOC* modulation (previously presented in Section 2.2.3) is supposed to be used. But the true modulation that will be used in Galileo system is the E5 AltBOC (*Constant envelope AltBOC*, see Section 2.2.4), as reported in the *Galileo OS SIS ICD* [4].

The Standard AltBOC modulation is an extension of the *Complex BOC* and has remarkable differences with respect of the true E5 AltBOC modulation:

- the Standard AltBOC is not a constant envelope modulation, like the E5 AltBOC;
- simple rectangular subcarrier waveforms are used, instead of the four-valued subcarrier functions $sc_{E5\text{-}S}(t)$ and $sc_{E5\text{-}P}(t)$ needed for the E5 AltBOC modulation;
- the *product signals* (see Section 2.2.4) are not present in the signal expression of the Standard AltBOC modulated signal; these terms are necessary to produce the constant envelope in E5 AltBOC signal.

Considering the implementation of the DLL in the scheme described in the patent, the tracking of received signal is performed with similar operations with respect of the coherent dual band receiver. The two pilot codes (*E5aQ* and *E5bQ*) are tracked with an early-minus-late approach, evaluating the complex correlation values between the received signal (I and Q components) and the local signals (early, prompt and late complex signals) and operating in a known manner to produce the associated DLL error signal (discrimination function). The operations needed for the complex correlation are discussed and derived in a different way with respect of that done in this thesis (in Section 3.4), but the final operations performed by the correlator subsystem of the patented receiver are exactly the same as in the coherent dual band receiver.

The only remarkable difference is that the local subcarriers used for the local signal generation are the simple rectangular waveforms $\text{sign}[\cos(2\pi f_{sub}t)]$ and $\text{sign}[\sin(2\pi f_{sub}t)]$, instead of the four-valued subcarrier function $sc_{E5\text{-}S}(t)$ and its delayed version $sc_{E5\text{-}S}\left(t - T_{s,E5}/4\right)$, used in the coherent dual band receiver. This leads to a **correlation loss**, as stated in Reference [8]: in fact in the patented architecture the received AltBOC signal is correlated with a local Complex BOC signal, instead of a true AltBOC signal. Accordingly, the proposed architecture for the coherent dual band receiver leads to improved performance with respect of the scheme discussed in the patent [13].

At last, it is necessary to remark the differences between the data demodulation sections of the two receivers. In the coherent dual band receiver the data are recovered from the two in-phase channels (*E5aI* and *E5bI*) taking

advantage of the *sideband translator* (previously presented in Section 4.3.3): this block selects and separately downconverts the two data channels, that subsequently are multiplied with the local PRN codes (for the despreading) and finally the data can be BPSK demodulated.

On the contrary, the patented receiver use a different technique: the first and second codes used in the data channels ($c_{E5a\text{-}I}$ and $c_{E5b\text{-}I}$, called respectively c_2 and c_1 in the paper) and the corresponding square waves are generated, and they are combined in order to obtain the real and imaginary components of $(R_1 + R_2)$ and $(R_2 - R_1)$, that are respectively the sum and the difference between the autocorrelation functions of the two codes (for more details see the demonstration in Reference [13], that is not reported here for the sake of shortness). In this way, with quite complex operations performed in an additional correlator subsystem, it is possible to demodulate the sum and the difference between the data bits of the two data channels, that must be further processed to recover the transmitted data, in accord with the chart in Table 4.1.

R_1	-1	1	-1	1
R_2	-1	-1	1	1
$R_1 + R_2$	-2	0	0	2
$R_2 - R_1$	0	-2	2	0

Table 4.1: Chart of idealized correlation values, used in the patented receiver to decode the transmitted data [13]

Comparing the two arrangements, the demodulation technique adopted in the patented receiver is not recommended, because is more complicated. The technique proposed for the coherent dual band receiver could be implemented easily and requires less hardware and software resources: the data are directly recovered and further calculations to decode the two data from their sum and difference (as in the patented receiver) are not necessary. Besides, since the two data channels are separately processed, the demodulation technique proposed for the coherent dual band receiver seems more robust: an error in a data bit of one channel (e.g. caused by a strong interference on the E5a sideband) does not affect the correct demodulation of the data of the other channel, whereas with the technique of the patented receiver a bit error in one data channel could affect also the other channel.

In conclusion, the receiver architecture presented in the patent [13] is quite similar to the coherent dual band receiver, but could lead to worse performances (correlation losses, demodulation errors in presence of interfering signals), then it is not recommended and will not be discussed in the following.

4.4.2 Offset-carrier single-sideband tracking receiver

The **offset-carrier single-sideband tracking receiver**, introduced in Reference [8], is a simplified and flexible version of the coherent dual band receiver, that can track only a single sideband of the AltBOC signal, but using the same front-end and signal down-conversion. This means the demodulation of the input signal to the E5-band carrier frequency (1191.795 MHz) using reference signals including respective (complex) SSB subcarrier functions, corresponding to one of the side-bands of Complex-LOC, Complex-BOC or AltBOC signals. This idea is illustrated in Figure 4.13.

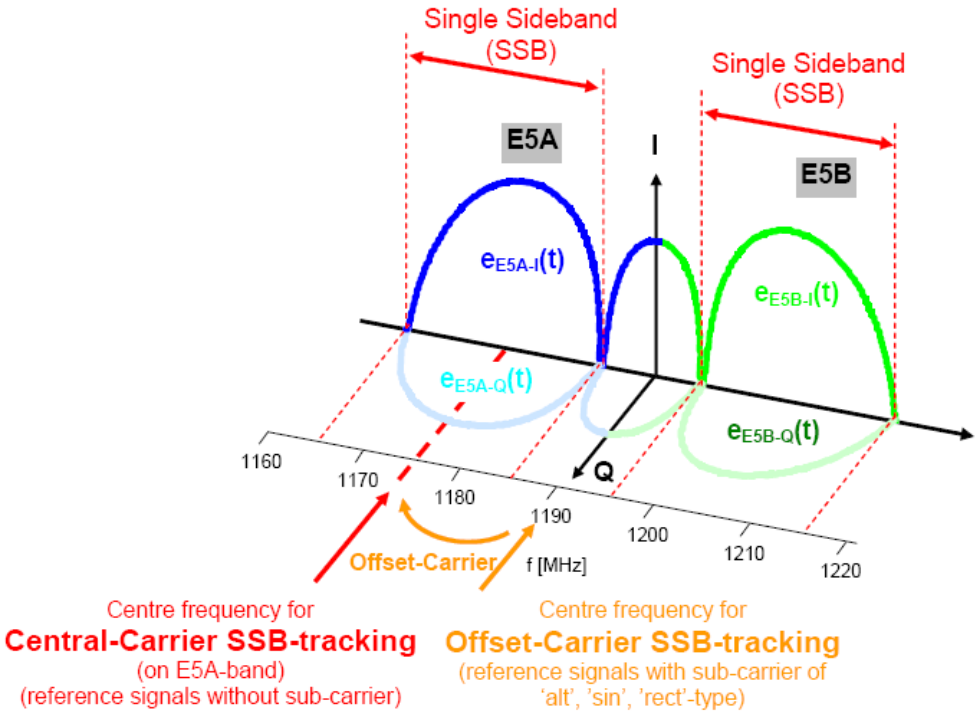

Figure 4.13: Different E5-band tracking options [8]

The advantage with the Offset-Carrier SSB tracking method is that a single fixed RF-front-end can be used for tracking arbitrary signal components in one or the other sideband. In this way the tracking operation has lower computational complexity than in the coherent dual band receiver, but produces lower tracking performances, similar to those of the single band receiver.

In synthesis this flexible receiver is interesting only for research purposes, because needs the same wide band front-end and high sampling frequency of the coherent dual band architecture, but could reach only the noise and multipath performances of the single band receiver.

4.4.3 Receiver with the correlator-discriminator

The **receiver with the correlator-discriminator** is an innovative receiver architecture, that could also be considered like a variant of the coherent dual band receiver. Actually, the receiver with the correlator-discriminator is not present in literature for the AltBOC signal and is proposed in this dissertation for the first time.

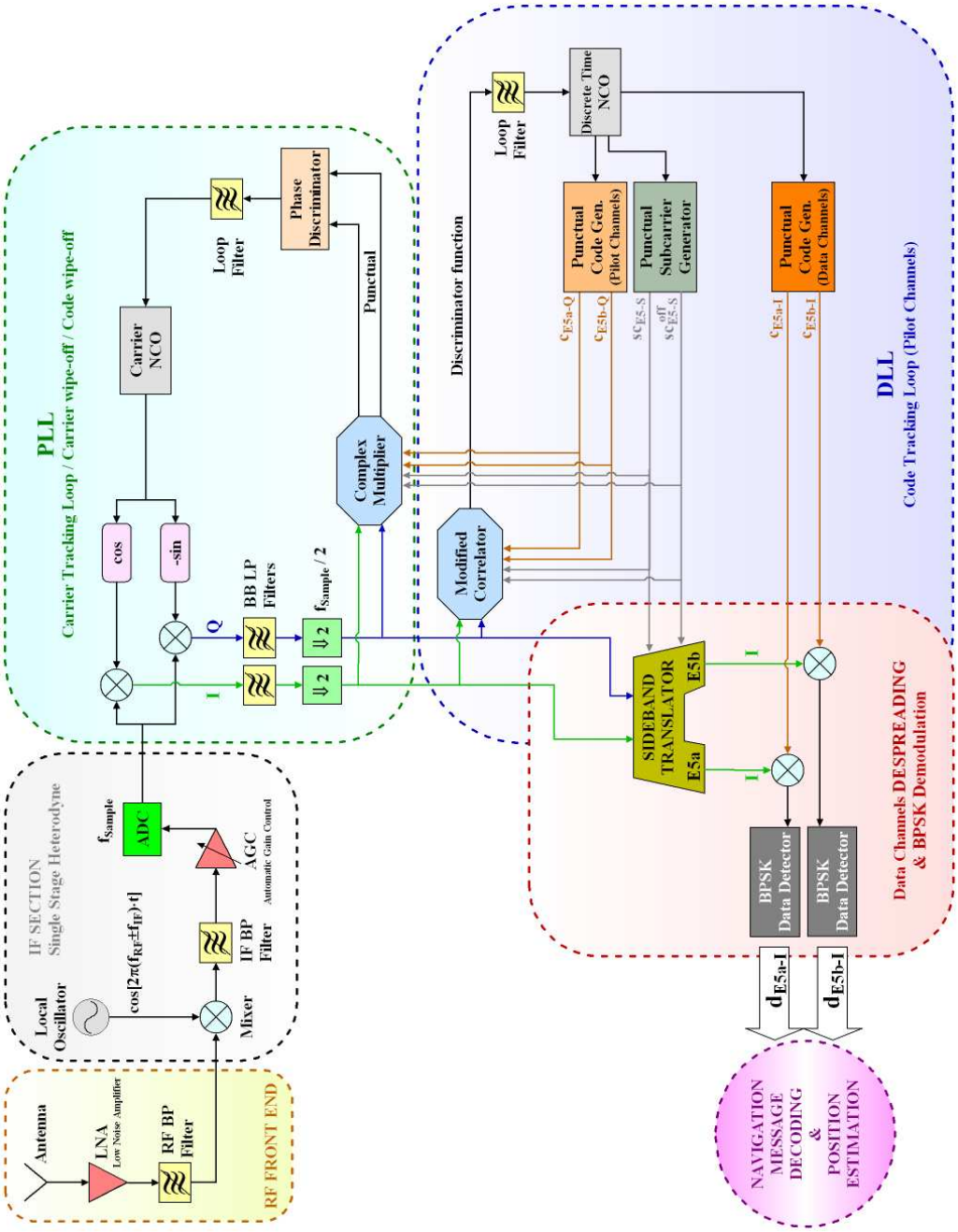

Figure 4.14: Block diagram of the innovative receiver architecture with the correlator-discriminator

The main difference with respect of previous architectures is the presence of a **modified correlator** (presented in Figure 4.15), that directly evaluates a discrimination function.

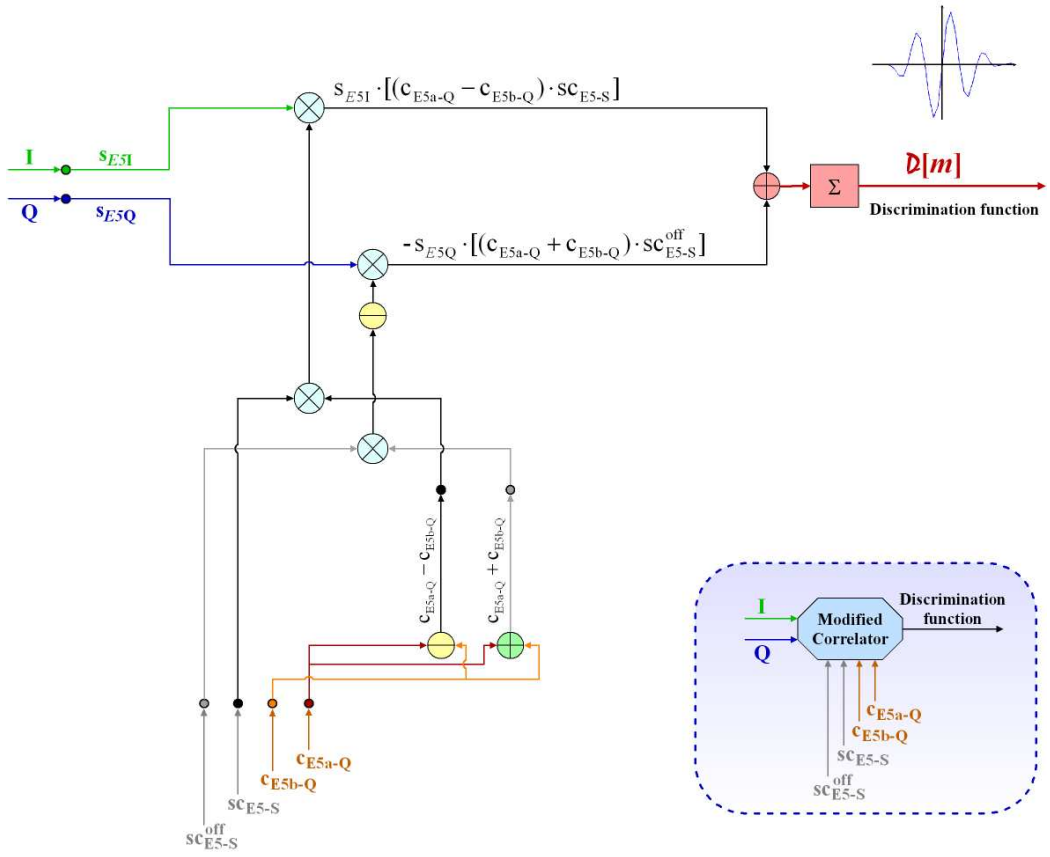

Figure 4.15: Block diagram of the correlator-discriminator

This idea is derived from the article in Reference [15], where an innovative receiver architecture was introduced for the Galileo BOC(n,n) signals. This receiver uses a modified DLL where the discrimination function is directly evaluated with a single operation, that is equivalent to a standard Early-Late structure, but saves both hardware and software resources.

It is possible to take advantage of this idea also for the AltBOC signal, but with some complications due to the difference between the BOC and the Alt-BOC modulations. In detail, it is necessary to take in account the difficulties related to the implementation of the complex correlation.

The coherent dual band receiver could be modified using a modified correlator, that combines in a different way the AltBOC complex correlation components: only the punctual channel of the receiver is used, to obtain an output function that could be directly utilized like a discrimination function. This idea is illustrated in the block diagram of the receiver in Figure 4.14.

This innovative receiver architecture has considerable advantages in terms of required hardware, with respect of the coherent dual band receiver, because

the discriminator is no longer necessary. In fact the operations previously performed by two complex correlators (early and late) and the discriminator, with this arrangement are carried out by the modified correlator, that evaluates the discriminator function using less hardware.

Furthermore, also the local signal generation section of the receiver is strongly simplified, since only the punctual codes and subcarrier waveforms must be generated, whereas the early and late code and subcarrier generators are now unnecessary.

However, a single complex correlator is still necessary for the PLL, as shown in Figure 4.14, to correctly track the carrier of the punctual channel.

The derivation and the operation performed by the modified correlator are illustrated in the following.

The complex correlator, previously discussed for the coherent dual band architecture (see Figure 4.10), could be modified combining in a different way the components used to obtain the $\mathcal{C}_{\mathbf{Q}}[m]$ value; its expression is recalled here for the sake of clarity:

$$\begin{aligned}\mathcal{C}_{\mathbf{Q}}[m] \;=\; & -\sum_{n=0}^{N} s_{E5\mathbf{I}}[n]\cdot e_{E5a\text{-}Q}[n-m]\cdot sc_{E5\text{-}S}[n-m] + \\ & -\sum_{n=0}^{N} s_{E5\mathbf{I}}[n]\cdot e_{E5b\text{-}Q}[n-m]\cdot sc_{E5\text{-}S}[n-m] + \\ & +\sum_{n=0}^{N} s_{E5\mathbf{Q}}[n]\cdot e_{E5a\text{-}Q}[n-m]\cdot sc^{off}_{E5\text{-}S}[n-m] + \\ & -\sum_{n=0}^{N} s_{E5\mathbf{Q}}[n]\cdot e_{E5b\text{-}Q}[n-m]\cdot sc^{off}_{E5\text{-}S}[n-m] \end{aligned} \tag{4.12}$$

Changing the signs of the first and the third component of $\mathcal{C}_{\mathbf{Q}}[m]$, the following expression of the discrimination function $\mathcal{D}[m]$ is obtained:

$$\begin{aligned}\mathcal{D}[m] \;=\; & \sum_{n=0}^{N} s_{E5\mathbf{I}}[n]\cdot e_{E5a\text{-}Q}[n-m]\cdot sc_{E5\text{-}S}[n-m] + \\ & -\sum_{n=0}^{N} s_{E5\mathbf{I}}[n]\cdot e_{E5b\text{-}Q}[n-m]\cdot sc_{E5\text{-}S}[n-m] + \\ & -\sum_{n=0}^{N} s_{E5\mathbf{Q}}[n]\cdot e_{E5a\text{-}Q}[n-m]\cdot sc^{off}_{E5\text{-}S}[n-m] + \\ & -\sum_{n=0}^{N} s_{E5\mathbf{Q}}[n]\cdot e_{E5b\text{-}Q}[n-m]\cdot sc^{off}_{E5\text{-}S}[n-m] \end{aligned} \tag{4.13}$$

In fact with these adjustments, the result is no longer null as in $\mathcal{C}_{\mathbf{Q}}[m]$, but becomes the odd discrimination function $\mathcal{D}[m]$ that is shown in Figure 4.16.

Then this function could be directly used for the tracking loop: the steep shape of the curve in the tracking point allows to conjecture a good tracking performance.

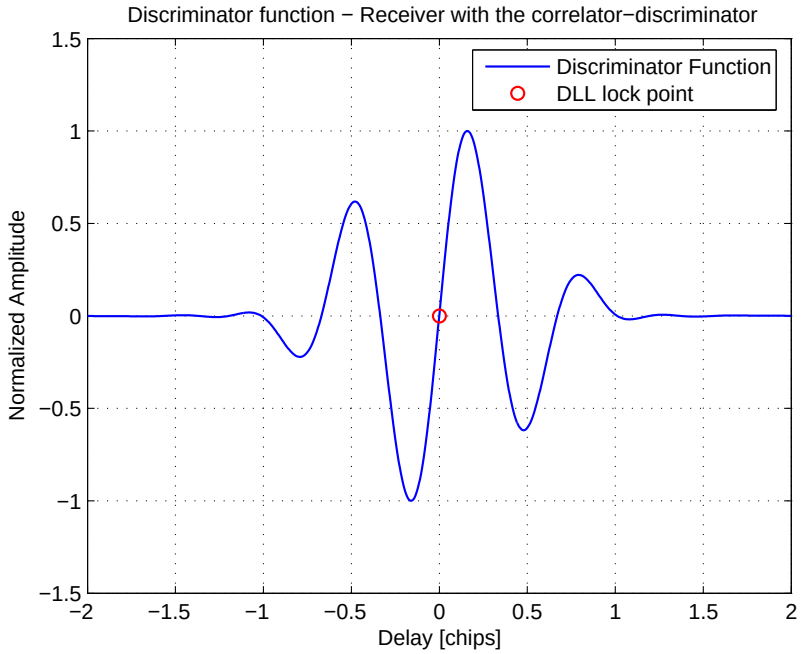

Figure 4.16: Discriminator function obtained using the receiver architecture with the correlator-discriminator (with a pre-correlation bandwidth of 51.150 MHz)

The block diagram of the modified complex correlator is presented in Figure 4.15. In this scheme, Equation (4.13) has been implemented in a similar way than that done for the complex correlator, combining the two codes ($c_{E5a\text{-}Q}$ and $c_{E5b\text{-}Q}$) before the multiplications and the sums, so that the hardware complexity is reduced, halving the number of required multipliers.

In conclusion, with this interesting receiver architecture there are considerable advantages for the hardware complexity, because the discrimination function is evaluated using simplified operations and reducing the number of necessary local signals. However its performances must be evaluated and compared with those ones of other receiver architectures, as will be done in Chapter 6 (see Section 6.6).

Chapter 5

Acquisition strategies for the AltBOC signal

In previous Chapter, the receiver architectures for the AltBOC signal have been presented and discussed only for the signal tracking functioning. But before to track the signal and to estimate the satellite pseudoranges, the receiver must acquire the received signal.

The **acquisition** process (already performed by the current GNSS receivers) aims to estimate the unknown code phase and the *Doppler* frequency shift of the received signal: a two-dimensional search of all possible code phases and Doppler frequencies is performed to acquire the signal coming from one satellite, using a decision threshold to obtain an estimate of the parameters of the received signal. Once the receiver has estimated these two unknowns with enough precision, the tracking process could start.

In spite of fact that the acquisition strategies are discussed in several articles and have been studied in detail both for the GPS signals (see for example [16], [17], [18], [19], [20], [21]) and for the BOC modulated signals (see [22], [23], [24], [25], [26]), also with exhaustive theoretical analysis, the acquisition of the signals in the Galileo E5 band is discussed only in few articles, considering only conventional receiver architectures (see [27], [28], [29], [30]).

Thus, a complete study of acquisition strategies for the AltBOC signal, that at the moment is not present in literature, is done in this Chapter. The receiver architectures previously presented in Chapter 4 are considered and the differences between the acquisition techniques used in current receivers and those needed with the proposed AltBOC architectures are highlighted.

In addition, an innovative acquisition strategy (the **progressive acquisition**), tailored to the *coherent dual band receiver*, is also introduced in Section 5.1.4.

5.1 Basics of the acquisition process

Considering the typical operative conditions of a GNSS receiver, two situations are considered for the acquisition process:

- the so-called **cold start**, when the user's position is completely unknown or no data on the satellites positions and time of the day are available;
- the so-called **warm start**, when an estimate of the receiver location or of the time of the day or some other a priori knowledge are available.

In first case, that is the typical situation at the first startup of a GNSS receiver, all the satellites of the constellation have to be searched for and this process is very time consuming. In order to face this problem typically the receivers performs a parallel search of different satellites. Accordingly, the signal acquisition process in this case becomes a three-dimensional search in time (code phase), Doppler frequency and satellite-specific PRN code, since each satellite uses a different PRN code for each transmitted channel.

However, in the *warm start* conditions, it is possible to select the subset of the available satellites from an external source or from a recently updated almanac broadcast. This solution needs to search for few satellites, so that it is very fast.

In the following, only the acquisition of the code of a single satellite of the Galileo constellation is considered, for simplicity. In this case, the acquisition stage of the AltBOC receiver has to perform a two-dimensional search in code delay and Doppler domain, as shown in Figure 5.1.

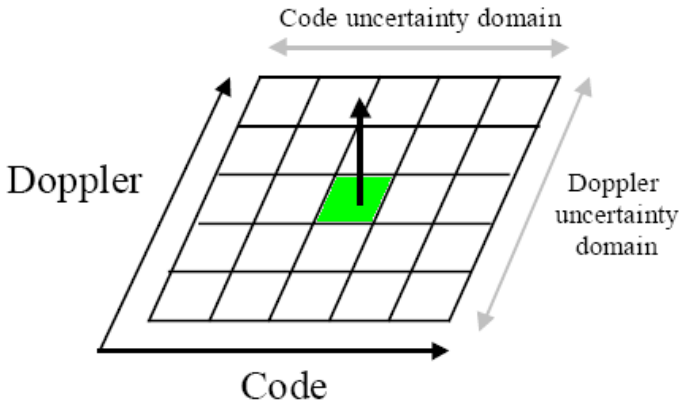

Figure 5.1: Search space for the acquisition system [22]

In fact the receiver must estimate the phase of the received code Θ with respect to the local replica and the Doppler frequency shift $f_{Doppler}$ of the

carrier of the received signal and compensate this shift with an opposite local frequency shift. The code delay and the Doppler shift are two independent unknowns: they are the output parameters estimated by the acquisition system, if the satellite signal is detected and acquired.

The acquisition process is then performed searching for energy in the time-frequency (or code-Doppler) domain. To do this, the receiver correlates one block of received samples with a local signal and makes the local code position sweeping the uncertainty time domain and varies the local frequency inside the Doppler uncertainty domain, until energy is detected, which means a correlation peak is present at the output of the correlators. This sweeping is typically performed step by step, digitizing the two variables and subdividing the search space in a grid: each couple of digitized variables in the grid is called *bin* and the combination of one Doppler bin (Δf) and one code bin ($\Delta\Theta$) is a *cell*, as denoted in Figure 5.2.

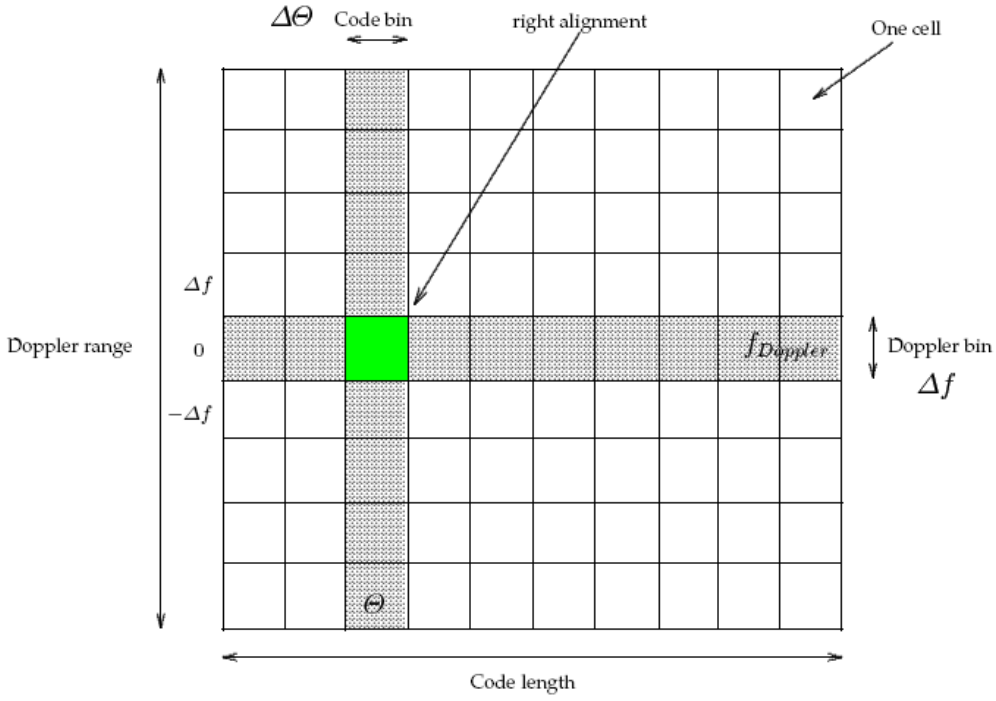

Figure 5.2: Terminology for the search space

The acquisition strategies could be classified essentially in two categories, depending on the way used to perform the energy search:

- **linear search** (also called *sequential* search), when each cell of the search space is separately tested;
- **parallel search**, when multiple cells are simultaneously searched.

Current GNSS receivers typically use a parallel search, because with this method a shorter acquisition time is achieved, but using a more complicated hardware (e.g. with matched filters or a DSP that performs the FFT, as discussed in Section 5.1.3).

The linear search is not used in practice, but it allows a simple explanation of the operations performed during the acquisition. Then the linear search method will be used in the following to present the acquisition strategies for the AltBOC signal, from the functional point of view, whereas the parallel approaches needed to speed up the acquisition will be highlighted in Section 5.1.3.

Another advantage of the linear search is that the operations performed by the acquisition section could be explained reusing the hardware of the receiver architectures illustrated in previous Chapter. As depicted in Figure 5.3 for the single band receiver, the RF front end and the IF section of the receiver remains unchanged: the signal processing in the analog domain is the same as for the tracking. The digital samples at the output of the Analog to Digital Converter (ADC) are then processed in a different way in the **acquisition section**, reusing the hardware of the PLL and the DLL.

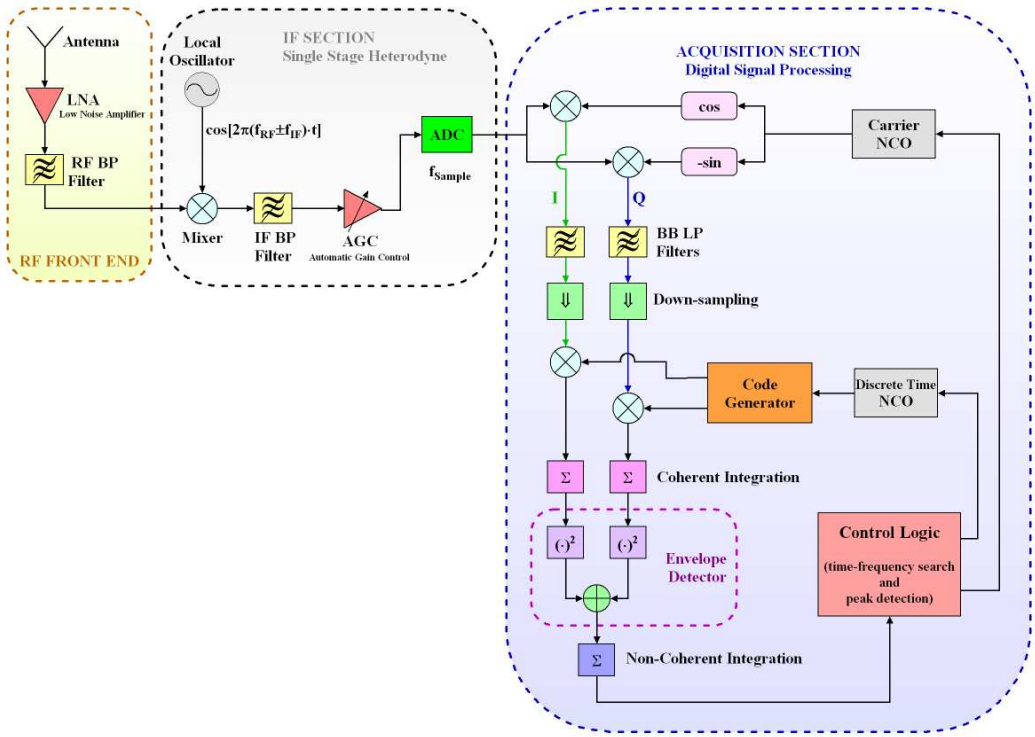

Figure 5.3: Example of acquisition section in the block diagram of the receiver architecture (single band receiver)

In detail, the hardware of the two loops is rearranged in an *open loop* configuration and the two NCOs are commanded by a **control logic**, that sweeps the frequency of the carrier NCO in the Doppler range and controls also the

other NCO, searching all the code phases. It must be noted that the frequency used for the carrier NCO is the sum of the intermediate frequency (f_{IF}) and the searched Doppler frequency ($f_{Doppler}$): this is necessary to down-convert to the baseband the received signal, that at the output of the IF section is centered around the chosen f_{IF}, and to compensate the Doppler effect on the received signal.

After the multiplication by the local digital carrier, the in-phase samples (I) and the quadrature samples (Q) are then filtered with two baseband filters, to remove interfering signals adjacent to the useful signal, and down-sampled, reducing the sampling frequency and then the computational burden of the acquisition section. Both signals are then multiplied by the local code and the results are summed, obtaining a **coherent integration** operation. Typically an integration period of 1 ms is used to evaluate each correlation value: this means every block of 1 ms of received samples is correlated with one period of the local primary code. The results of the I and Q correlations are then squared and summed in the **envelope detector**. Its outputs are accumulated to obtain a **non-coherent integration** of successive correlation values, corresponding to the same code bin and Doppler bin. This method is necessary in presence of noise, because the correct correlation peak between the local code and the received signal becomes more evident with these non-coherent accumulations. The result of the coherent and non-coherent integrations for each cell of the search space is then evaluated and returned to the control logic.

Once a correlation peak is detected by the control logic, the signal of the satellite is declared acquired and the estimated code phase $\widetilde{\Theta}$ and Doppler shift $\widetilde{f}_{Doppler}$ are used to start the subsequent tracking operations, closing the two loops. At the beginning the carrier tracking loop works like a FLL, to refine the estimation of the Doppler frequency. After the convergence of the FLL, the PLL is installed and locks on the carrier phase. Also the DLL during the transition phase between the acquisition and the tracking typically works with a coarse configuration, to accept the uncertainty in the code phase estimated by the acquisition section. After the code convergence, it selects a precise configuration, reducing the tracking gate width of the code discriminator, for optimal noise performances (as done for the acquisition & tracking state machine of the receiver in Reference [31]).

In following Sections, the methods that could be used for the acquisition of the AltBOC signal and the main issues are presented and discussed.

5.1.1 Methods for performing the correlation search

As previously mentioned, the acquisition process is based on the search of the correlation peak in a two-dimensional search domain. As stated in References [25] and [26], current GNSS receivers generally perform the correlation between the received code and the local one in two different ways:

- the **circular correlation**;
- the **window correlation**.

With the *circular correlation*, the same number of received and local code samples are correlated, performing a circular shift on the local samples to test all the possible code phases, whereas with the *window correlation* a moving window is used to correlate the local samples with a portion of the received samples, as depicted in Figure 5.4.

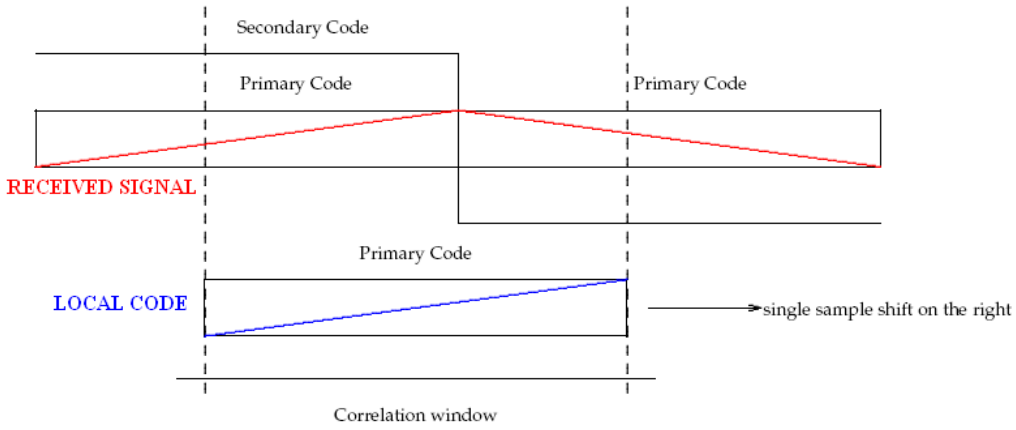

Figure 5.4: Correlation search scheme in presence of secondary codes [26]

Due to the presence of the **secondary codes** in the signal transmitted in the E5 band (as previously noticed in Section 2.1.2), only the *window correlation* approach could be used to acquire the received signal. In fact, as shown in Figure 5.4, the secondary codes can cause a sign reversal in the correlation operation over the integration interval. Accordingly, only one single period of the primary code (that corresponds to one chip of the secondary code) must be locally generated and correlated with the window correlation: in this way the acquisition scheme results practically insensitive to the secondary code transitions (as demonstrated in [26]).

The window correlation technique could be efficiently implemented using a parallel technique, based on the *Fast Fourier Transform* (FFT), as will be discussed in Section 5.1.3.

Considering the shape of the code correlation function, it must be noticed that the receiver architectures previously proposed in Chapter 4 for the AltBOC signal use two types of correlation function:

- a **BPSK-like correlation function**;
- the **AltBOC combined complex correlation function**.

The first function has a triangular shape and is obtained both with the *single band receiver* (*CC-SSB tracking*) and the *separate dual band receiver* (the first two architectures presented in Chapter 4), because both process the received signal as two adjacent BPSK modulations in E5a and E5b sidebands.

On the contrary, the true AltBOC correlation function is achieved only with the *coherent dual band receiver* (the third architecture in Chapter 4), that fully exploits the complex correlation function of the AltBOC using a wide-band setup.

The two correlation functions are plotted in Figure 5.5, assuming to use ideal receivers with infinite bandwidth[1].

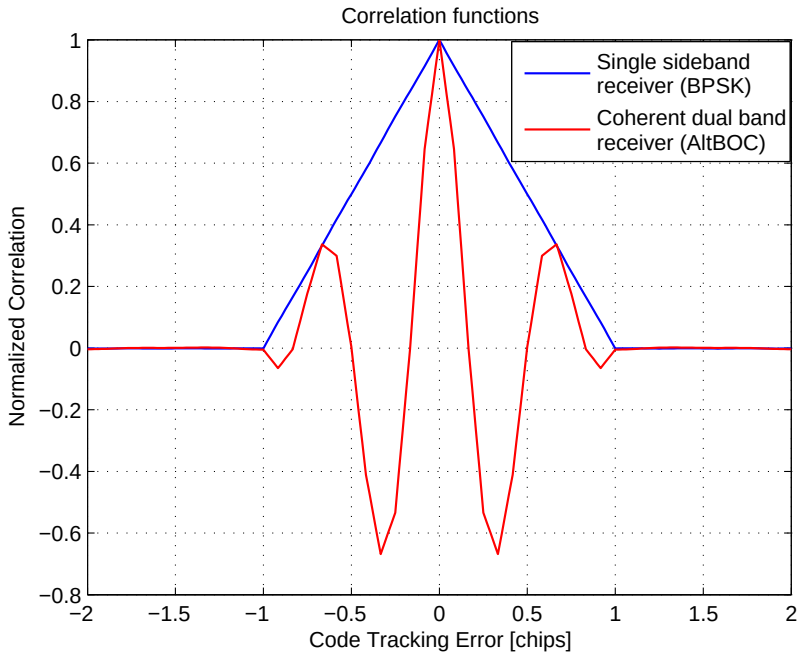

Figure 5.5: Comparison of the correlation functions for the single sideband and the dual band receivers, simulated with infinite bandwidth

The BPSK-like correlation function could be acquired with conventional acquisition strategies, already used in current GPS receivers: the resulting triangular code correlation function is unambiguous and the position of its correlation peak could be easily estimated.

However the presence of multiple peaks in the AltBOC correlation function implies an **ambiguity** issue for the acquisition: in presence of noise or multipath effect (see next Chapter), it could be difficult to distinguish the main

[1]The normalized correlation functions has been obtained simulating the E5 AltBOC(15,10) signal oversampled with 48 samples per code chip, with infinite bandwidth (without any signal filtering), and correlating the signals with an integration time of 1 ms (1 primary code period). The ordinate axis of the graphs are normalized with the peak of the correlation function, so that the amplitude of the function is independent on the sampling frequency.

correlation peak from the secondary peaks and there is the risk of a *false lock*, that could lead to a bias in the pseudorange estimation.

A similar problem is also present for the acquisition of BOC modulated signal and is discussed in several articles in literature. One solution is the so-called **bump-jumping technique**, presented in Reference [32] for the BOC signals. This approach could be adapted to the AltBOC correlation function and consists in measuring and comparing the received power of adjacent peaks with respect to currently tracked peak and jumping left or right depending on the comparison result, until maximum is found. This technique uses two additional correlation channels positioned on each side of the main correlation peak and an additional decision logic. Accordingly, the *bump-jumping* technique requires a considerable hardware increase and high computational resources to accomplish the acquisition in a short time. Then it is not recommended for the acquisition of the AltBOC signal, but could be useful during the tracking operations, to detect *false lock* problems.

For the acquisition of the multi-peak correlation function of the AltBOC signal, obtained with the *coherent dual band receiver*, some alternative techniques could be used instead of the *bump-jumping* approach, as discussed in following Section.

5.1.2 Direct or side-band acquisition

The acquisition in the *coherent dual band receiver* could be performed using two different techniques, already approached in the literature for the BOC signals (see Reference [22]):

- the **direct acquisition**;
- the **side-band acquisition** (called *BPSK-like method* in [22]).

The first technique tries to directly acquire the main peak of the multi-peak AltBOC correlation function. An over-sampling of the code sequence is necessary, and the *bump-jumping* approach (outlined in previous Section) could be used to solve the ambiguity problem of the multi-peak correlation function, in order to be sure to find the correct position of the main peak. But this choice implies an high sampling frequency (f_{Sample}) and then the computational complexity of this technique is very heavy, inducing drastically augmented acquisition time. Besides, the correlation function for the AltBOC signal is defined as a complex function (as previously discussed in Section 3.4) that could be evaluated only generating local complex signals, composed by spreading codes multiplied by local subcarriers. Thus, the implementation of a direct acquisition for the AltBOC signal results very complicated.

On the contrary the *side-band acquisition* is a promising technique for fast, simple and robust acquisition of correlation functions with multiple peaks

(BOC-like signals). This method only consists in considering the received AltBOC signal as the sum of BPSK signals with carrier frequency symmetrically positioned on each side of the central frequency of the Galileo E5 band. Thus each side-lobe of the AltBOC spectrum could be treated independently, down-converted to the baseband and correlated only with the corresponding local code, as a BPSK signal, providing an unambiguous triangular correlation function that could be acquired using at least 2 samples for each code chip (as in traditional GPS receivers). In this way a low sampling frequency is required in the acquisition phase, leading to low computational complexity. Besides, the acquisition section is also simplified with respect to previous arrangement, because it is not necessary to locally generate the four-valued subcarrier waveforms of the E5 AltBOC (see Section 2.1.1): the side-band is down-converted to the base-band, then the local code could be directly correlated without the subcarrier multiplication.

Since the AltBOC modulated signal contains two pilot channels (*E5a-Q* and *E5b-Q*) and two data channels (*E5a-I* and *E5b-I*), transmitted in two side-lobes in the E5 band (*E5a* and *E5b*), it is possible to perform the acquisition with the side-band technique in two different ways:

- **Single Side-Band** (SSB) acquisition, using only one sideband of the received signal;
- **Double Side-Band** (DSB) acquisition, with a separate reception of the two sidebands (like in the *separate dual band receiver*).

Choosing to acquire only one side-band of the AltBOC spectrum (e.g. *E5a*), it is possible to use only the pilot code (*E5a-Q*) or both the codes (*E5a-I* and *E5a-Q*) transmitted in the side-band (as done in the analysis performed in [27], [28] and [29]). In the second case, the received signal must be separately correlated with two local codes, typically with an integration time of one primary code period (1 ms), using two separate correlation channels. Then the outputs of the correlators must be non-coherently combined, obtaining a doubled correlation peak. It is not possible to perform a coherent combination of the correlations of the two codes (that generally implies more advantages, as will be explained in Section 5.2.5) because a similar operation could lead to a null correlation result: this is due to the presence of the navigation data (in the data channel) and the secondary codes, that are different for each transmitted channel.

Considering the acquisition performances in presence of noise, it must be noted that the SSB acquisition of the two codes (e.g. *E5a-I* and *E5a-Q*) non-coherently combined leads to the same performances of a SSB acquisition of one code, with a doubled number of non-coherent integrations: the resulting correlation peak has the same amplitude. The computational burden with the two arrangements is nearly the same, but the latter one is preferable, since only one local code must be generated, whereas the acquisition of the

two codes requires a more expensive hardware (two code generators and two separate correlation channels).

On the other hand, the *double side-band* acquisition allows to acquire the received signal taking advantage of all the codes (four) contained in the AltBOC signal of one satellite, obviously increasing the number of correlation channels. The amplitude of the resulting correlation peak is four time that obtainable with a single code correlation. But the same result can be achieved increasing the number of non-coherent accumulations in a SSB arrangement. The only advantage of the DSB acquisition is the major robustness against interferences: if a jamming signal is present only in one side-band, the SSB technique applied to this side-band could not be able to acquire the code, whereas the DSB technique seems more robust because take advantage of both side-bands.

In conclusion, for the *coherent dual band receiver* the SSB acquisition using only one pilot code (e.g. *E5a-Q*) seems a good compromise between the implementation complexity and the acquisition performances. In fact this technique could obtain the same performances in presence of noise than other techniques (it is sufficient to increase the number of non-coherent integrations) and implies a simpler implementation (only one local code must be generated and correlated). The DSB acquisition has a better interference robustness, but requires a major implementation complexity, then it is not recommended.

As a final remark, the SSB acquisition technique allows to roughly estimate the code phase, with a typical resolution of 2 samples per chip. But for the successive tracking operations of the AltBOC complex correlation, a better resolution is needed. A solution to this problem is the **progressive acquisition** method, that will be presented and discussed in Section 5.1.4.

5.1.3 Receiver implementation

In current GNSS receivers the acquisition operations are not typically implemented with the *linear search* approach (see Section 5.1): the only advantage of this approach is that it does not use any specific hardware resources for the acquisition, but reuses the same correlators that are used later for the tracking of the signal. However, this approach leads to excessive acquisition time.

To speed up the acquisition, current GNSS receivers typically use a dedicated acquisition hardware. In fact, the acquisition operations are often efficiently implemented taking advantage of two *parallel techniques*, depending on the type of architecture that is used:

- the **matched filters**, that are frequently used to implement correlator channels with a fast and simple hardware structure (see e.g. Reference [20]);

- the **Fast Fourier Transform** (FFT), that on the contrary are used in receiver architectures where the acquisition process is performed as a software task (see [17]).

Obviously, it is possible to take advantage of these techniques also for the previously discussed acquisition strategies for the AltBOC signal.

The **matched filters** are devices which continuously compute correlation between a known (reference) signal and a signal to be measured, and give maximal output when the correlation between the reference signal and the incoming signal is strongest. By definition, they are optimum detectors for signals embedded in *Additive White Gaussian Noise* (AWGN). Thus a matched filter is an useful device to be used in the acquisition phase of spread spectrum receiver operation to search the correct timing for the replica code. The acquisition can be performed passing the received signal samples as an input for a tapped delay line, as depicted in Figure 5.6.

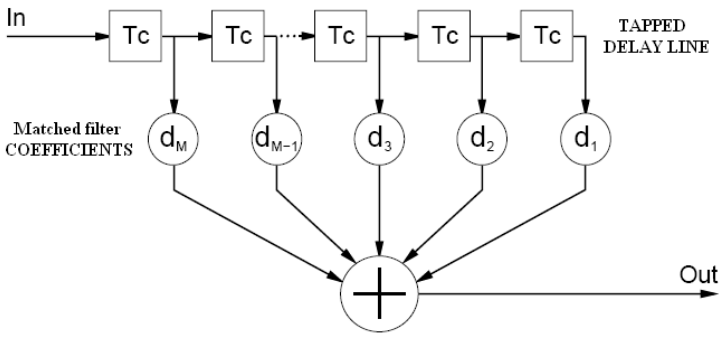

Figure 5.6: A tapped delay line implementation of a matched filter for the acquisition of a PRN code sequence [20]

The M coefficients of the filter are matched with the ideal samples of the desired PRN code sequence. In this way, when a new received sample is inserted in the delay line, the old samples are shifted and the received signal is correlated with a local code. If the received code is correctly aligned, the output of the matched filter is maximum.

Therefore, the matched filter is a valid approach to implement an hardware correlation channel for the acquisition, because it performs a rapid search in the code delay domain. The Doppler domain could be explored varying the frequency of the local carrier and performing a search with a matched filter for each Doppler frequency.

The **Fast Fourier Transform** on the contrary is used in software receivers, where the acquisition and tracking operations are performed using a *Digital Signal Processor* (DSP). Several existing acquisition algorithms taking advantage of the FFT are discussed in literature for the GPS receivers and could be easily adapted to the acquisition of the AltBOC signal. In detail, there are

two typical approaches that perform a parallel acquisition taking advantage of the FFT:

- a **parallel acquisition in time delay domain**, obtained with a FFT operation on the received signal and the local code, followed by an IFFT (*Inverse Fast Fourier Transform*); these operations (shown in Figure 5.7) are equivalent to a circular correlation, but imply a considerable reduction of the computational burden;
- a **parallel acquisition in Doppler domain**, where a parallel search in the Doppler frequency domain is obtained using a FFT operation.

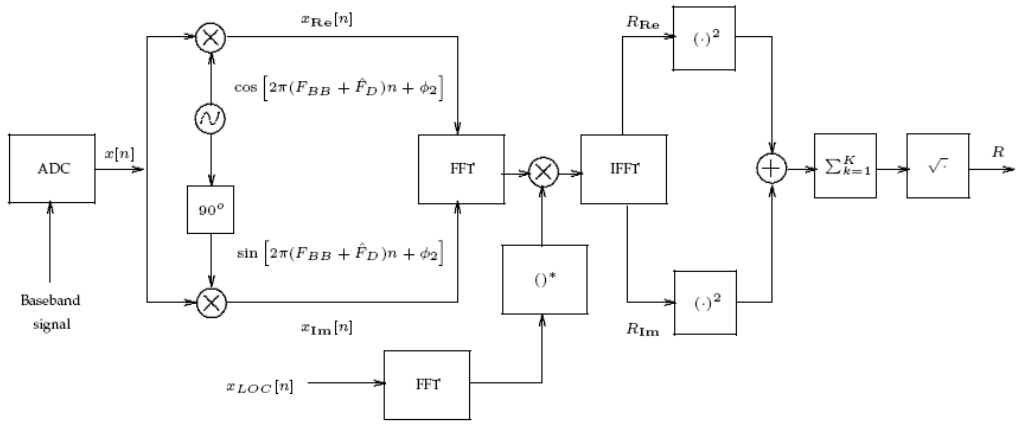

Figure 5.7: Non-coherent correlator implemented with a parallel search in the time delay domain [26]

Both these techniques are presented and explained in detail in References [25] and [26]. It must be noticed that the first technique, schematized in Figure 5.7, is more often used than the other: typically the number of the searched code bins is higher than the number of the Doppler bins, then a parallel search in the time domain could lead a major advantage for the computational burden and for the reduction of the acquisition time.

Accordingly, the parallel FFT acquisition in time delay domain is the technique most frequently used by software receivers. The architecture of these receivers must include a *Digital Signal Processor* (DSP) able to perform the FFT.

Another useful application of the FFT technique is for the simulation of an acquisition system: in this way it is possible to strongly reduce the simulation time with respect of a direct implementation of a serial search (each cell of the search space evaluated separately). Then the FFT approach in the time domain will be used in Section 5.4, to simulate the discussed acquisition schemes for the AltBOC signal.

Considering the features of the codes that will be used in the Galileo E5 band, it is necessary to notice that the standard FFT approach must be modified, to tolerate the **secondary code transitions**. In fact, as previously noticed, the standard FFT approach in the time domain corresponds to a circular correlation. If this technique is applied using a coherent integration time corresponding to a single period of the primary code, the secondary code chips can cause a sign reversal within the correlation window, affecting the result of the correlation, that becomes unreliable.

A possible solution to this problem (as discussed in References [19], [26] and [29]) is to conduct a window correlation on two primary code periods with a **zero-padding approach**, as shown in Figure 5.8.

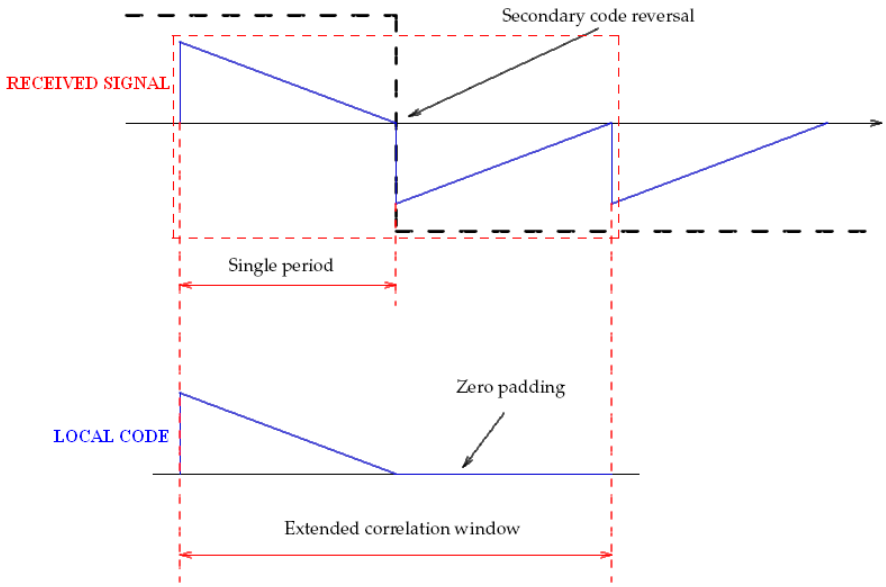

Figure 5.8: Correlation search scheme in presence of secondary codes, using the zero padding approach [26]

A block of received signal samples, corresponding to two primary code periods, is correlated with a single period of the local primary code, zero-padded to fit the correlation window. The zero terms in the second period does not introduce any advantage in terms of noise reduction (as generally achieved with a longer coherent integration time). In conclusion, the zero-padding approach is insensitive to secondary code transitions, but the price to be paid is to increase the computational burden, because the FFT must be evaluated on block of samples with doubled length.

As a final remark, it must be noticed that some receivers (e.g. new Septentrio's GPS/Galileo receiver products, as affirmed in [30]) use an acquisition technique that combines the two previously discussed approaches, the matched filters and the FFT, in a highly efficient manner. In detail, the matched filters are used to perform the code delay search with a simple and

fast hardware, and an FFT processor is used to search the Doppler frequency shift (parallel FFT acquisition in Doppler domain). This is the current state of art for the implementation of the acquisition section in a GNSS receiver, with fast and efficient hardware.

5.1.4 Transition phase to tracking

During the acquisition phase, the receiver estimates the code delay and the Doppler frequency shift of the received signal, with the previously discussed techniques. After that operations, the receiver must be able to lock the carrier loop (PLL) and the code loop (DLL) and to generate the local signals, in order to correctly track the signal transmitted from one satellite. But a **transition phase** between the acquisition and the tracking operations is needed, because two issues must be handled:

- the acquisition is typically performed using the primary code, but also the **secondary code** must be acquired;
- the estimated code delay and Doppler shift must have a sufficient **resolution**, to allow the correct lock.

The first issue is peculiar of the Galileo system, because its codes will have a *tiered code structure* (as previously discussed in Section 2.1.2), with a secondary code superimposed to a primary code. The short primary codes are used during the acquisition, because in this way the computational burden is not excessive. But for the successive tracking operations, it is necessary to locally generate the entire code structure, also with the secondary codes, then the secondary code synchronization must be performed during the transition phase.

This can be done using for example the approach suggested in Reference [29], where both the primary and the secondary codes and simultaneously acquired with a technique equivalent to a two-dimensional cross-correlation search (with size primary code x secondary code), performed using a two-dimensional FFT/IFFT algorithm.

Otherwise, a more simple approach is to first acquire the primary code of a pilot channel and then to demodulate the secondary code chips, storing them in a vector. The secondary code synchronization can be easily obtained, performing a circular correlation between the vector with the estimated chips and a local replica of the secondary code.

The second problem that must be handled in the transition phase is due to the rough **resolution** for the code bin and the Doppler bin, used in the acquisition phase to reduce the computational burden and to speed up the acquisition time. This problem is generally solved in current GNSS receivers with a *convergence phase*, where the carrier loop is a FLL, to refine the Doppler

frequency estimation and to the allow the successive phase lock (PLL), and the DLL works in a coarse configuration to tolerate the initial code phase errors.

A similar approach for the estimation refinement could be used for the acquisition of the AltBOC signal, with the *single band receiver* and the *separate dual band receiver* (introduced in previous Chapter), that process the received signal in a BPSK-like manner, similarly to a current GPS receiver.

On the other hand, for the *coherent dual band receiver* the transition to tracking is a critical problem, because an uncertainty in the code code phase estimation could lead to a *false lock* on a secondary peak of the AltBOC correlation function. In this case, as discussed in Section 5.1.2, the multi-peak correlation function could be directly acquired, using a *bump-jumping* approach to solve the ambiguity problem due to the multiple correlation peaks. But this approach is not recommended, because implies an high sampling frequency and an enormous computational burden.

A suitable acquisition approach for the *coherent dual band receiver* is the *side-band acquisition*, that is based on a BPSK-like signal processing of a single side-band (SSB) or both the side-band (DSB) of the AltBOC signal spectrum (see Section 5.1.2). In this way the code phase is roughly estimated, with a typical resolution of 2 samples per chip. But for the successive tracking operations of the AltBOC complex correlation, a better resolution is needed.

A possible solution to this problem is the **progressive acquisition** method. This acquisition technique, not present in literature at the moment and proposed in this thesis for the first time, is based on a simple idea: the acquisition could be performed in two or more successive steps, refining the estimation of the code delay and the Doppler shift, as schematized in Figure 5.9.

A initial acquisition with a rough resolution for the code length (typically 2 samples per chip) and for the Doppler range could be performed, obtaining a first estimate of the peak position (acquired cell). After that, the acquisition search could be performed only around this estimated position, increasing the resolution, primarily for the code delay (e.g. with 12 o more samples per chip). In this way the acquisition time and the computational burden are not excessively increased, since only a small portion of the search space must be explored with high resolution, and a sufficient precision for the code delay and the Doppler shift estimation is achieved. Then this technique seems suitable for the *coherent dual band receiver* and will be used for its acquisition section (see Section 5.3.3).

5.1.5 Statistical improvement algorithms

As discussed in Reference [25], the performance of the acquisition section in current GNSS receivers is improved using **statistical improvement algorithms**, that reduce the risk of *false alarms* and to improve the *detection*

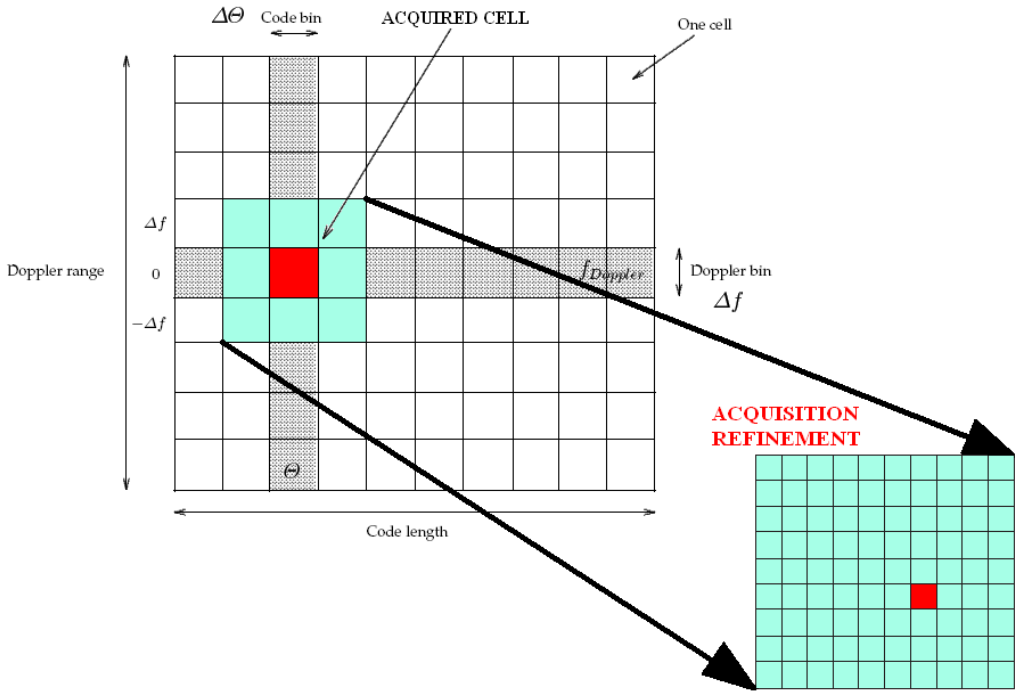

Figure 5.9: Progressive acquisition scheme

probability.

The acquisition algorithms proposed in literature can be classified in two different ways: *fixed dwell time* versus *variable dwell time* acquisition techniques and *single trial* versus *multiple trial* acquisition methodologies.

The so-called *dwell time* is the time needed to analyze a cell of the acquisition search space: in the *fixed dwell time* acquisition techniques, the correlation of the incoming code with its local replica is calculated over a number of code periods that can be one or more than one, but that is fixed for each search cell. According to the *variable dwell time* techniques, the dwell time duration depends on the characteristics of the analyzed cell.

For the *single trial* detection criterion, a binary decision on the presence or absence of the satellite signal in a certain cell is taken after a dwell time, without any successive check; in the *multiple trial* acquisition methodology, the final decision is taken only after more than one dwell time.

Two interesting statistical improvement algorithms, discussed in detail in Reference [25], are:

- the **M of N search algorithm** (fixed dwell time, multiple trial)
- the **Tong search algorithm** (variable dwell time, multiple trial)

They could also be used with the AltBOC receiver architectures, to improve their acquisition performances and no modifications are needed with respect

of the algorithms used in current GPS receivers. Then, these algorithms are not further discussed in this Chapter, because only the differences between the current receivers and the proposed AltBOC architectures are highlighted.

5.2 Parameters involved in acquisition

After the discussion of the acquisition techniques that are suitable to the AltBOC receiver architectures, the main parameters that influence the acquisition performance are then discussed in following Sections.

5.2.1 Sampling frequency

An important receiver parameter that influences the acquisition performances is the **sampling frequency** (f_{Sample}) used for the *Analog to Digital Converter* (ADC).

In current GNSS receivers the sampling frequency is often chosen as an *incommensurable* (prime) value with respect to the ranging code rate (as stated in Reference [26]). This is an optimal choice for the tracking performance of the receiver, since with an incommensurable sample frequency the tracking loop could obtain a fine code synchronization, improving the pseudorange estimation.

A typical value for the sampling frequency in GPS receivers (see [25]) is:

$$f_{Sample} = 2.11 \cdot R_C \tag{5.1}$$

where R_C is the ranging code chip rate. In this way the sampling rate is slightly greater than two times the chipping rate and then in some chips three samples fall. This fact is not useful for the acquisition section, but it is justified by the improvement for the tracking performances: the tracking loop works on these "special chips" with three samples for the code fine synchronization.

Since the chipping rate for the codes in E5 band will be 10.23 Mchip/s, a sampling frequency of 21.5853 MHz may be used. This choice is suitable for the *single band receiver* and the *separate dual band receiver* (introduced in previous Chapter), that process the received signal in a BPSK-like manner, similarly to a current GPS receiver. In fact two samples per chip are sufficient to estimate the position of a triangular BPSK correlation peak.

On the contrary, for the *coherent dual band receiver* architecture an higher sampling frequency is required, because not only the ranging code must be tracked, but also the subcarriers. Since the AltBOC modulated signal features four-valued subcarrier waveforms, with 12 subcarrier samples per chip, a sampling frequency of at least $12 \cdot R_C$ (122.76 MHz) is required to locally

generate subcarrier waveforms aligned with those present in the received signal. Besides, a sampling performed with 12 samples per chip is suitable for the direct acquisition of the multi-peak AltBOC correlation function. An incommensurable frequency (e.g. $12.11 \cdot R_C$) could also be used, to further improve the precision of the tracking loop.

But it must be noted that a similar sampling frequency ($f_{Sample} \cong 120$ MHz) is impractical for the acquisition operations, because it leads to an enormous computational burden for the evaluation of each correlation value. Then the proposed solution for the acquisition of the multi-peak AltBOC correlation is the use of BPSK-like techniques, performing a *side-band acquisition* (as previously discussed in Section 5.1.2). In this way the correlation function that must be acquired has again a triangular shape and two samples per chip are sufficient for the correct acquisition of the correlation peak. Thus, a **down-sampling** could be applied to the received signal before the acquisition, obtaining a reduction of the acquisition time. In this way a sampling frequency of about 20 MHz could be used in the acquisition section.

Then, to achieve a sufficient resolution in the code delay and Doppler frequency estimation, the **progressive acquisition** technique (previously introduced in Section 5.1.4) could be used in the transition phase between the acquisition and the tracking with the *coherent dual band receiver*. For example, the code delay could be roughly estimated with a resolution of 2 samples per chip during the acquisition, and then refined investigating a only a portion of the search space, adjacent to the first estimate, with a resolution of 12 samples per chip.

In this way, the acquisition in the *coherent dual band receiver* could be performed with an initial rough acquisition, performed on a down-sampled signal, followed by a refinement during the transition phase to the tracking.

5.2.2 Intermediate frequency

In block diagrams of the receiver architectures previously presented in Chapter 4, a *single stage heterodyne* was used. This means that the satellite signal, centered around a *Radio-Frequency* carrier (denoted as f_{RF}), is received by the RF front end of the receiver and then is down-converted to an appropriate **intermediate frequency** (f_{IF}) in the IF section, before the sampling performed by the ADC, as schematized in Figure 5.10.

In must be noted that for the *single band receiver* only one sideband of the AltBOC signal spectrum is down-converted (e.g. f_{RF} is the central frequency of the *E5a* sideband), whereas the *separate dual band receiver* uses two separate IF section for the separate down-conversion of the two sidebands (as previously discussed in Section 4.2). On the contrary, the *coherent dual band receiver* operates a down-conversion of the entire *E5* band (f_{RF} is the central frequency of the *E5* band).

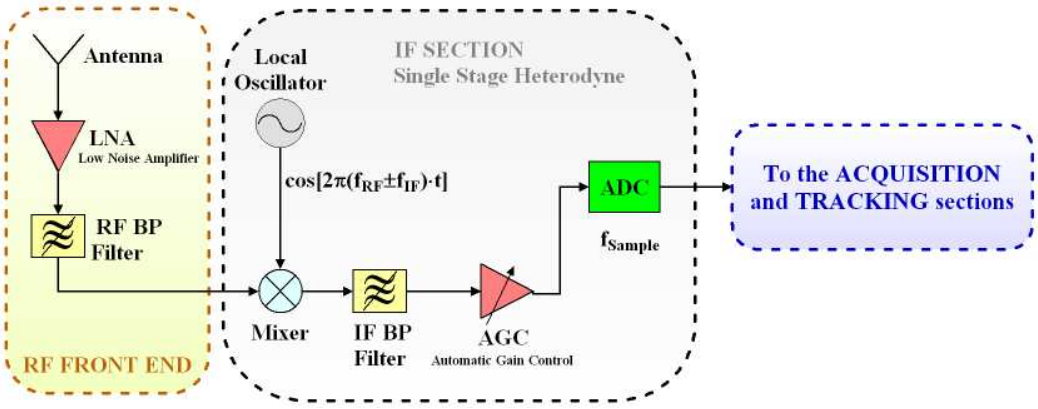

Figure 5.10: Block diagram of the RF front end and the IF section of previous receiver architectures

In all the receiver architectures, the down-conversions are obtained using a mixer, that multiplies the received analog signal with a local carrier, with frequency equal to $(f_{RF} \pm f_{IF})$. In this way the resulting signal is centered around the desired working frequency (f_{IF}).

Instead of a *single stage heterodyne*, the down-conversion could be performed in two or more stages, shifting the central frequency of the received signal in more steps. The only difference is the receiver implementation (different cost and complexity of the required components, different noise performances).

It must also be noted that in conventional GNSS receivers the working frequency could be chosen of the order of the MegaHertz (MHz) or some KiloHertz (kHz). In first case the working frequency is properly called **intermediate frequency** (f_{IF}), whereas the other choice is conventionally called **baseband frequency** (f_{BB}). But experimental results (as stated in Reference [26]) show that with these two choices the receiver presents the same performances in terms of *Signal-to-Noise Ratio* (SNR), after the digitization performed by the ADC. Accordingly, one or the other choice could be indifferently used for the receiver implementation and in the following the terminology of *intermediate frequency* (f_{IF}) is used to indicate the both arrangements, without losing generality.

But it must be noted that the second arrangement (f_{BB}) allows the possibility to use a lower sampling rate and then a lower processing capability required by the hardware used for the receiver implementation (as noted in [26]). Then it is preferable a low working frequency.

However, the working frequency could not be chosen too low, because some issues must be considered. In detail, the down-conversion of the RF signal to a zero center frequency $(f_{IF} = 0)$ is not used in GNSS receivers, primarily for two reasons (see [26]):

- the *ambiguity* in the determination of the Doppler frequency shift in the acquisition system;

- the *variation* of the envelope detector output due to the initial carrier phase.

The first problem means that the acquisition stage is unable to distinguish negative and positive Doppler frequency shifts, if the working frequency is chosen near to zero, then it is necessary to use an intermediate frequency (f_{IF}) greater than the maximum foreseeable Doppler shift ($f_{Doppler}^{MAX}$):

$$f_{IF} > f_{Doppler}^{MAX} \tag{5.2}$$

Obviously, the value of $f_{Doppler}^{MAX}$ depends on the relative speed between the receiver and the Galileo satellite. For example, in References [25] and [30], the maximum amount of the Doppler shift is assumed $f_{Doppler}^{MAX} = 5\,\text{kHz}$, for a low-speed user.

The second issue implies that the minimal residual carrier, after the compensation of the Doppler shift in the acquisition stage (performed by the carrier NCO), should be high enough to minimize the variation of the envelope detector output. Accordingly, the minimum value of the working frequency must be further increased (e.g. in [26] it is demonstrated that a residual carrier greater than 2 kHz is already sufficient to neglect this influence).

In conclusion, considering the previous issues for the GNSS receivers, the intermediate frequency must be greater than 7 kHz, to ensure a correct acquistion. Then a working frequency of $f_{IF} = 10\,\text{kHz}$ has been chosen for the AltBOC receiver architectures and will be used in Section 5.4 to simulate the behavior of their acquisition sections.

5.2.3 Amplitude and resolution of the search space

The acquisition time is strongly conditioned by the amplitude and the resolution chosen for the search space (see Figure 5.11), because these parameters determine the number of cells to be searched and then the computational burden.

Considering the **amplitude** of the search space for a *cold start* acquisition, it must be noted that the entire primary code length (10230 chips) must be searched, and the Doppler range could be considered as $f_{Doppler} = \pm 5\,\text{kHz}$ (as done in References [25] and [30]).

Besides, the **resolution** of the search space must be carefully chosen. In fact, using a high resolution the code delay and the Doppler shift are estimated with high precision, but the computational burden could be enormous, whereas if a coarse resolution for each code bin and Doppler bin is used, the tracking section of the receiver could not be able to follow the acquired signal. Then the resolution of the search space must be chosen as a compromise between the acquisition speed and the precision and the reliability of the estimated values.

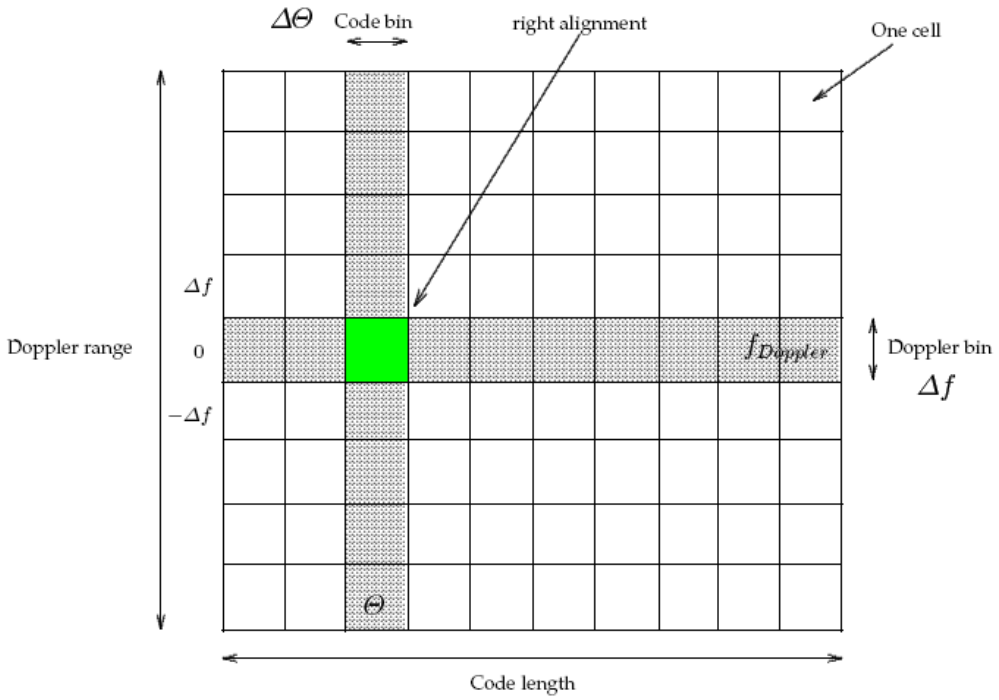

Figure 5.11: Illustration of amplitude and resolution of the acquisition search space

For the acquisition sections in the previously discussed receiver architectures it is possible to use the same search resolution as in References [25] and [30]:

- a resolution of $\Delta f = 500\,\text{Hz}$ could be used for the Doppler frequency range;
- the code uncertainty domain could be digitized with a resolution of $\Delta\Theta = 0.5\,\text{chip}$ (that means a sampling with 2 samples/chip).

This means that 21 Doppler bins and 20460 code bins must be searched to acquire the code of one satellite, resulting in a search space with 429660 cells (21×20460). To perform this acquisition search is acceptable time, the parallel implementation strategies discussed in Section 5.1.3 must be used, to speed-up the acquisition.

It must also be recalled that a code resolution of $\Delta\Theta = 0.5\,\text{chip}$ is not sufficient for the acquisition with the *coherent dual band receiver*. With this architecture, as previously discussed in Section 5.1.4, the **progressive acquisition** approach must be adopted, to refine with a sufficient resolution the estimated code phase (and eventually also the Doppler shift).

5.2.4 Coherent integration

Current GPS receivers typically use a **coherent integration** of multiple code periods to improve the *Signal-to-Noise Ratio* (SNR) at the output of the envelope detector in the acquisition section, as previously outlined in Section 5.1. The block diagram of the acquisition section, illustrated by a functional point of view, is recalled in Figure 5.12 for the sake of clarity.

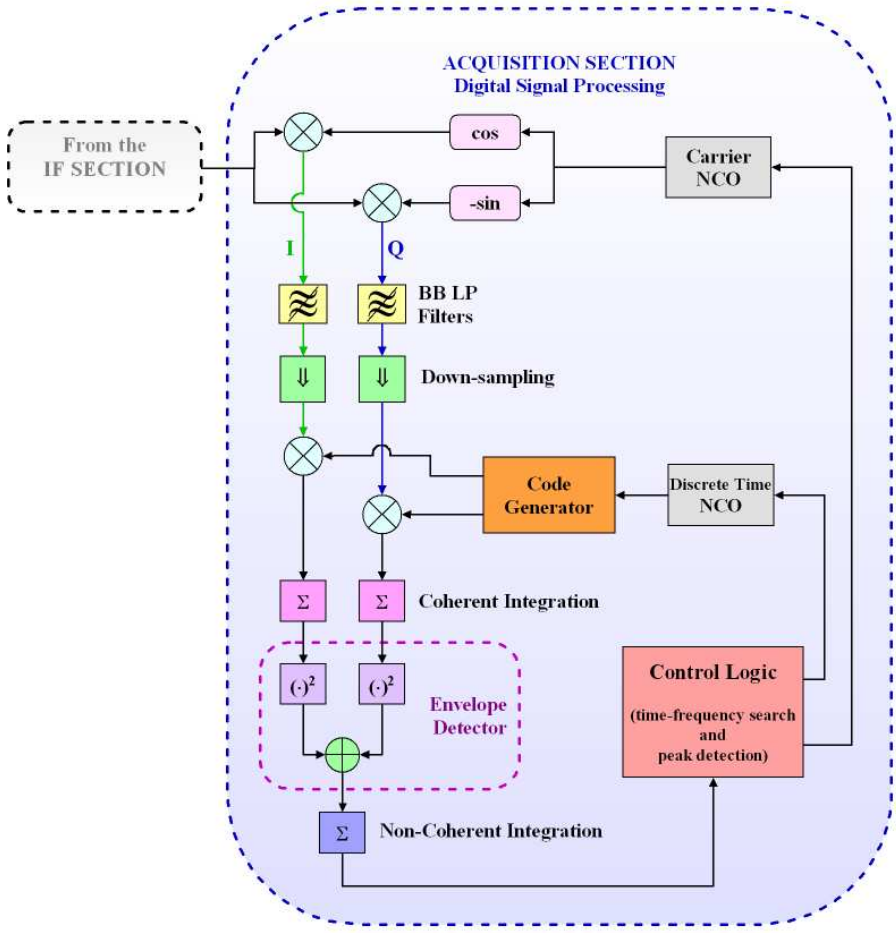

Figure 5.12: Block diagram of the acquisition section

The coherent integration is a coherent summation, in the sense that it performs an average on different correlated samples: if more samples are summed, the noise contribution at the output of the envelope detector is reduced, since the noise is zero mean, while the signal contribution is increased (as stated in [25]). The values of the cells in the search space that contain only noise are therefore reduced and the value of the cell containing the signal is increased: the result is that the envelope detector output is more and more similar to the correlation matrix in the absence of noise as the number of summed code periods increases. In detail, it is possible to affirm that doubling the coherent

integration time, also the SNR at the output of the envelope detector results doubled (this corresponds to an increase of 3 dB of the SNR).

Obviously, the maximum number of coherently integrated code periods in GPS receivers is limited by the following effects:

- the *Doppler effect on the code*; in fact, if a too long coherent summation is performed, the residual Doppler (due to the chosen resolution for the acquisition search) could affect the result, degrading the correlation peak amplitude;
- the *data transitions*, due to the navigation data modulated over the code; if a data transition fall in the coherent integration window, the resulting correlation value is reduced;
- the *computational burden*, that depends on the length of the coherent integration operation and conditions the acquisition time.

Considering the acquisition of the AltBOC signal, in addition to previous issues, also the presence of the **secondary codes** must be highlighted. In fact, as previously discussed in Section 5.1.1, the secondary codes can cause a sign reversal in the correlation operation over the coherent integration interval. Accordingly, only one single period of the primary code (that corresponds to one chip of the secondary code) must be locally generated and correlated with a window correlation method: in this way the acquisition scheme results practically insensitive to the secondary code transitions.

Accordingly, for the acquisition of the Galileo E5 codes, the coherent integration time is forced to be 1 ms (one primary code period). This is a limit for the achievable SNR at the output of the envelope detector, and then for the acquisition performances. However, the SNR could be improved with **non-coherent integrations**, as discussed in the following Section.

5.2.5 Non-coherent integration

As schematized in Figure 5.12, a non-coherent summation, which is also called **non-coherent integration**, could be performed after the envelope detector: in that case both the signal and the noise power are increased. In particular, if a non-coherent summation over two code periods is carried out, the signal power increases by a factor of 2 and the noise by a factor of $\sqrt{2}$: the SNR then increases by $\sqrt{2}$, or 1.5 dB (as stated in [25]).

It must be noted that comparing coherent and non-coherent integrations over the same number of multiple code periods, the obtained gain in terms of SNR for the non-coherent integration is of a less amount. This is due to the fact that the noise after the envelope detector is no more zero mean, as with the coherent integration. Then an increase of the non-coherent integration time is

less effective to improve the SNR than an increase of the coherent integration time.

For the acquisition of the AltBOC signal, as noticed in previous Section, the coherent integration time is limited to 1 ms by the secondary code transitions. Thus, only the number of non-coherent summations could be increased, aiming to improve the resulting SNR.

The previous statement is not completely true, because a technique that allows to use a coherent integration time higher than 1 ms is present in literature (the *partial correlation technique* proposed in Reference [29]). But it must be noted that this acquisition technique requires a quite complicated implementation and expensive hardware (it is equivalent to a two-dimensional FFT/IFFT search), then it is not recommended.

In conclusion, for the AltBOC acquisition the standard approach is recommended, with a coherent integration of only one primary code period and multiple non-coherent accumulations to increase the resulting SNR (e.g. as done in Reference [30]).

5.2.6 Filter characteristics

The acquisition performances of the receiver could also be affected by the filter characteristics. In detail, several filters are present in the block diagram of the receiver:

- in the RF front end and in the IF section, two band pass (BP) filters are used (see the previous scheme in Figure 5.10);
- two baseband (BB) filters are also present after the multiplication by the local digital carrier, in the I and Q branches of the acquisition section (see the previous scheme in Figure 5.12).

These filters are necessary to avoid unwanted replicas in the signal spectrum (*anti-aliasing*) and to reduce the amount of noise and interference signals (*interference rejection*).

In detail, the effects of a filter on the received signal, that must be taken in account in the acquisition section, are:

- the **group delay** of the filtered signal, with respect of the received signal;
- the **correlation loss**, due to the reduction of the signal energy at the output of the filter.

The first effect could lead to a wrong estimate of the code delay. But this problem could be easily handled, since the delay inserted by a filter is a constant value that can be easily determined (is depends on the filter type and its order) and subtracted, to obtain the correct estimation of the code delay.

The other effect is the correlation loss caused by the filter: the filtered signal shows a rounded code correlation peak, with a lower amplitude with respect of the infinite bandwidth case. Accordingly, this effect could be easily considered equal to a reduction of the *Signal-to-Noise Ratio* (SNR), neglecting the distortion of the correlation peak.

Typically, the effects of the filters are non considered in the articles where the acquisition performances are discussed and simulated. It is frequently assumed to receive an ideal signal with infinite bandwidth.

This choice is primarily motivated by the need to speed-up the simulation time, reducing the needed signal processing. Secondly, this choice is necessary to avoid the lose of generality. In fact the effect of each filter depends on the type of filter, its order and bandwidth, then each different filter implementation could lead to different acquisition performances. To take in account the effect of each filter, it is sufficient to study the correlation loss on the filtered code correlation peak, and then to consider an equivalent SNR reduction with respect of the infinite bandwidth case.

Accordingly, an ideal acquisition system could be simulated, without signal filtering, and the filter impact on the acquisition performances could be separately considered, reducing the effective SNR at the input of the acquisition section. Then, in the following of this Chapter, the effects of the filters are no more considered and the simulations in Section 5.4 will be performed without any filter.

5.3 Acquisition methods for AltBOC receiver architectures

After the discussion of the acquisition strategies that are suitable for the AltBOC signal and the considerations about the parameters involved in acquisition, in this Section the acquisition strategies are then applied to the receiver architectures previously proposed in Chapter 4.

In detail, for each receiver architecture a suitable acquisition method is discussed, considering only the block diagrams of the acquisition sections from a functional point a view, reusing the hardware needed for the tracking operations. Obviously, in a real receiver a dedicated acquisition hardware is typically used, taking advantage of the parallel techniques previously discussed in Section 5.1.3. The choice of reuse the hardware needed for the

tracking (illustrated in previous Chapter) has been done for the sake of simplicity, because in this way the acquisition operations and the required signal processing can be easily understood.

In addition, it must be remarked that at the moment a complete discussion of acquisition methods for the proposed AltBOC receiver architectures is not present in literature and is done in this thesis for the first time.

5.3.1 Acquisition with the single band receiver

Considering the *single band receiver architecture* (introduced in Section 4.1), the acquisition of the received signal could be performed with the **Single Side-Band** (SSB) acquisition strategy, previously discussed in Section 5.1.2. In fact with this architecture, the received signal is processed like a BPSK modulated signal, then the acquisition operations are not substantially different from these performed in a conventional GPS receiver.

This acquisition strategy is illustrated in Figure 5.13, where the acquisition section has been inserted in the block diagram of the single band receiver.

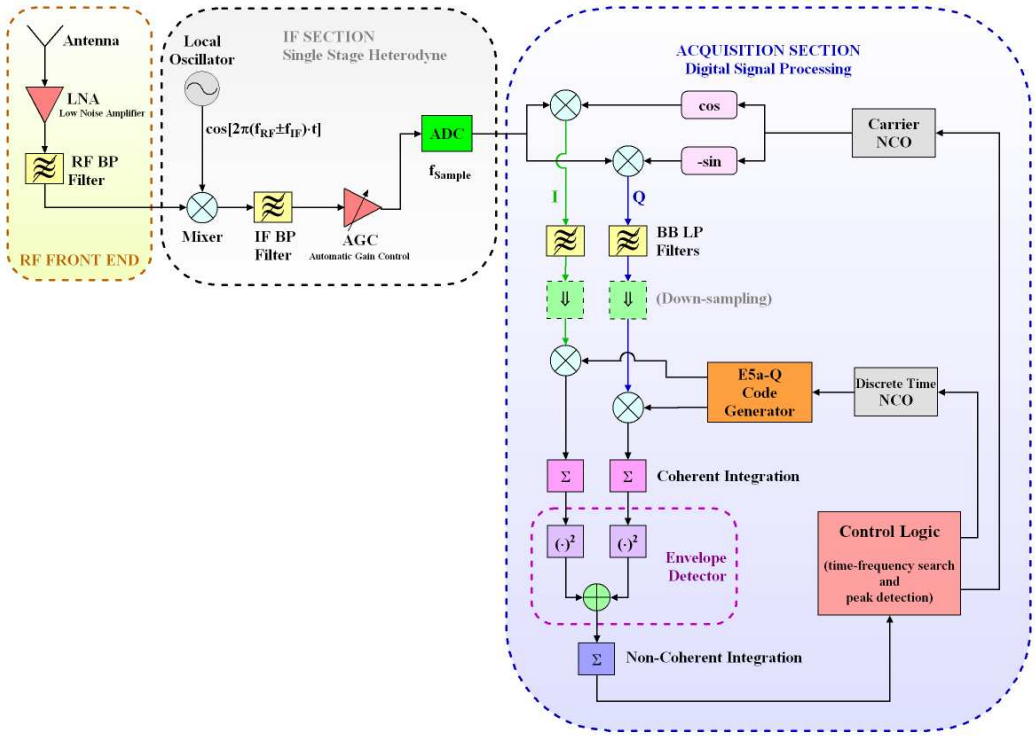

Figure 5.13: Block diagram of the single band receiver architecture, with the SSB (*E5a* sideband) acquisition section

As previously outlined, the RF and the IF sections of the receiver remain unchanged and perform the same operations as during the tracking. Since with this receiver architecture only one sideband (e.g. the *E5a* sideband)

of the AltBOC signal is received and down-converted, the received signal is shifted in the frequency domain accordingly to the scheme in Figure 5.14, where the spectrum of the signal is represented in the three sections of the receiver (*RF section*, *IF section* and *Acquisition section*).

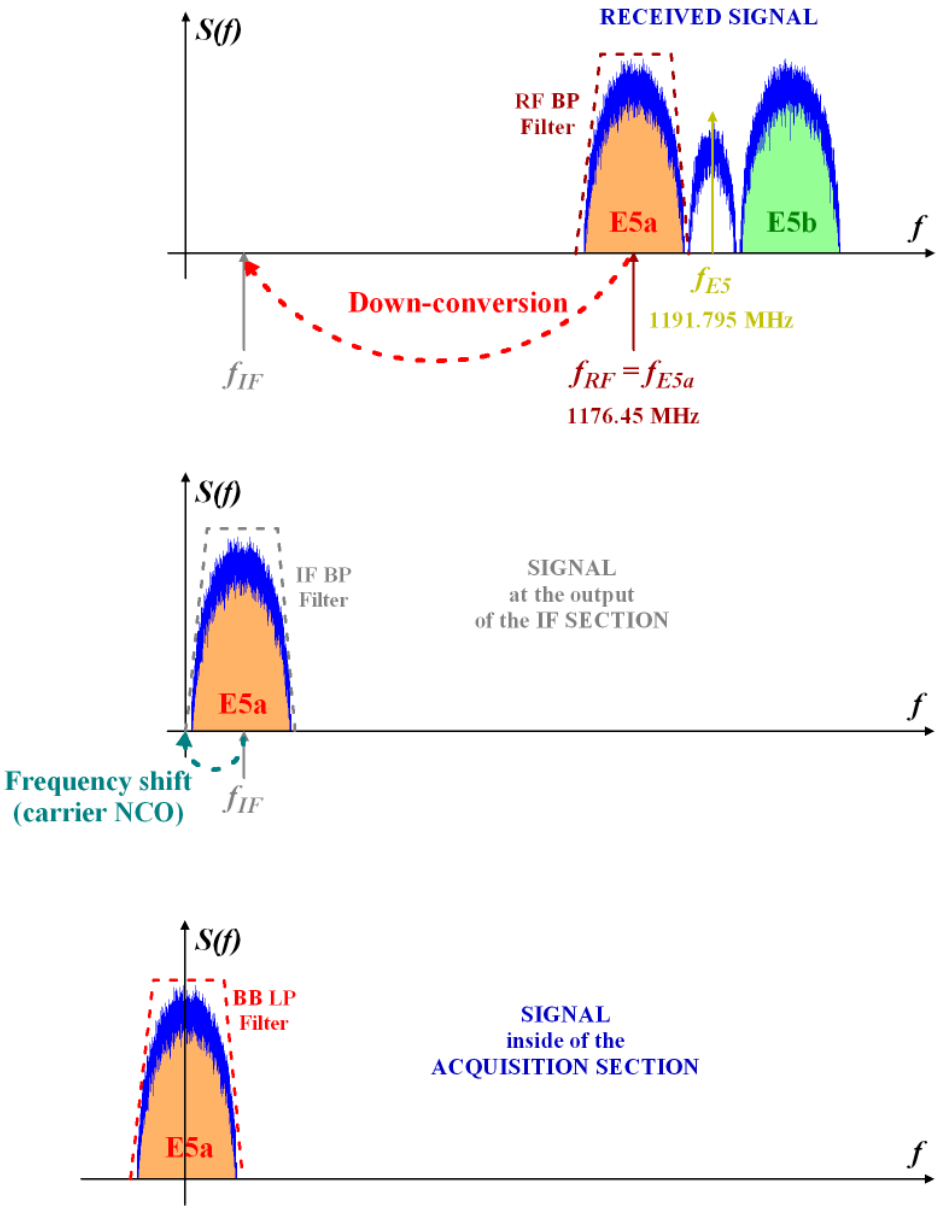

Figure 5.14: Signal bandwidth selection for the SSB (*E5a* sideband) acquisition with the single band receiver

The Band Pass (BP) filter in the RF front end selects only the *E5a* sideband, that is down-converted from its RF center frequency ($f_{RF} = f_{E5a}$) to the desired intermediate frequency (f_{IF}). The down-conversion is performed in the IF section with a mixer, that multiplies the received signal with a local

sinusoid with appropriate frequency ($f_{RF} \pm f_{IF}$). It must be noted that the value of f_{IF} could be chosen of the order of the MHz, or a working frequency of some kHz (f_{BB}) could also be used, as previously discussed in Section 5.2.2. Then in Figure 5.14 a generic f_{IF} value is represented, without losing generality.

After the mixer, another band pass filter in the IF section ensures that unwanted replicas in the signal spectrum are not present. Next, the signal is sampled by the ADC, with the chosen sampling frequency (e.g. $f_{Sample} = 21.5853$ MHz, as stated in Section 5.2.1). At the output of the IF section, the spectrum of the digitized signal results equal to the *E5a* side-lobe, centered to f_{IF}, as depicted in Figure 5.14.

At last, the acquisition section performs a frequency shift of the received signal from f_{IF} to the baseband ($f = 0$). This is done multiplying the received signal with the local frequency synthesized by the carrier NCO. In detail, the control logic of the acquisition section sets up the carrier NCO with a frequency that is the sum of the intermediate frequency and the desired Doppler shift ($f_{IF}+f_{Doppler}$): in this way the whole Doppler frequency domain could be searched, varying $f_{Doppler}$. The search in the code delay domain is performed controlling the code NCO, that controls the local code generation (only the pilot code *E5a-Q* is generated and correlated, as recommended in Section 5.1.2). It must be noted that with this receiver architecture a *down-sampling* inside the acquisition section is not necessary, because the chosen sampling frequency f_{Sample} is suitable for the acquisition and implies a feasible computational burden.

In this way, the two-dimensional acquisition domain could be entirely explored, performing coherent and non-coherent integrations, with the parameters previously discussed. The Doppler shift and the code delay are then estimated and, after the *transition phase* (see Section 5.1.4), the tracking of the BPSK correlation peak of the *E5a-Q* code could start, closing the PLL and the DLL.

5.3.2 Acquisition with the separate dual band receiver

The acquisition with the *separate dual band receiver* could be performed with two different strategies (previously discussed in Section 5.1.2):

- with a **Single Side-Band** (SSB) acquisition, using only one sideband of the received signal;
- with a **Double Side-Band** (DSB) acquisition, with a separate reception of the two sidebands.

The first technique is exactly the same as that used in previous Section (for the *single band receiver*). In fact, the separate dual band architecture separately

receives the two sidebands of the AltBOC signal with two IF sections. At the output of these two sections, each sideband results filtered an down-converted around the chosen intermediate frequency f_{IF}: the output of the upper IF section in the block diagram Figure 5.15 is then the same as the IF section of the single band receiver (the *E5a* sideband results centered around f_{IF}), whereas the lower IF section performs a similar operation for the other sideband (the *E5b* sideband results centered around f_{IF}).

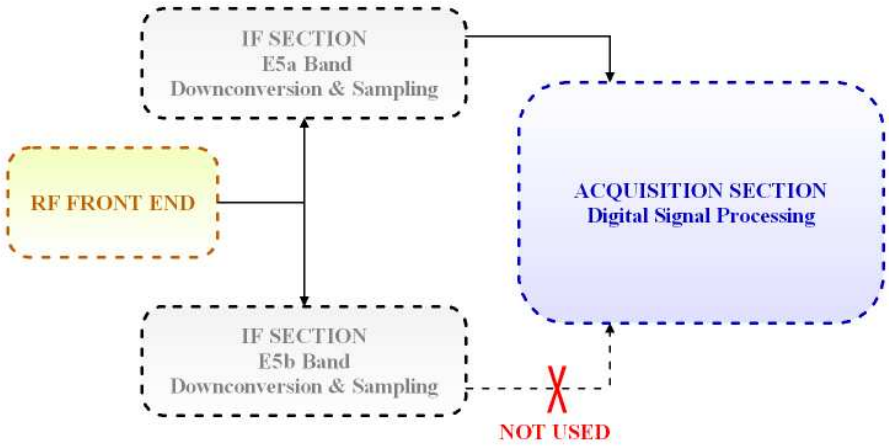

Figure 5.15: Block diagram of the separate dual band receiver architecture, with the acquisition section

If the output of the IF section for the *E5b* sideband is not used during the acquisition, as pointed out in Figure 5.15, the digital signal processing performed by the acquisition section is exactly the same as with the single band receiver. After this single sideband acquisition, the receiver could start the tracking operations of the received signal, using both the outputs of the IF sections (as previously discussed in Section 4.2): in fact the synchronism acquired taking advantage of one code of a single sideband could be easily used also to track the other sideband, because the edges of code chips are synchronous, without relative bias or relative chip-slip, for all signal components within the same AltBOC signal transmitted from a satellite (as stated in Reference [4]) and the frequency shift between one sideband to the other is known (equals to two times the subcarrier frequency).

Otherwise, the *Double Side-Band* (DSB) acquisition strategy could also be used, as previously stated in Section 5.1.2. In this case the acquisition section must use both the sampled signals produced by the two IF section, correlating each signal with the corresponding spreading code (*E5a-Q* or *E5b-Q*). The correlation results for the two codes must be non-coherently combined in the acquisition section.

It must be remarked that the double sideband acquisition technique shows a better interference robustness than the single band approach, but it implies

also a more complex implementation (two local codes must be generated and the correlation channels are doubled), then it is not recommended.

In conclusion, the Single Side-Band (SSB) acquisition is suitable for the separate dual band receiver, because this acquisition strategy allows to correctly estimate the code delay and the Doppler shift of the received signal and implies a simple implementation.

5.3.3 Acquisition with the coherent dual band receiver

Considering the *coherent dual band receiver architecture* (previously proposed and described in Section 4.3), three acquisition techniques could be applied:

- a **direct acquisition** of the AltBOC complex correlation function;
- a **Single Side-Band** (SSB) acquisition, taking advantage of the BPSK-like correlation function of one side-lobe of the received signal;
- a **Double Side-Band** (DSB) acquisition, using the BPSK-like correlation function obtained combining the two side-lobes, that are separately received.

As stated in Section 5.1.2, the *direct acquisition* is not recommended, because this choice implies an enormous computational burden and additional hardware to handle the ambiguity problem, due to the multiple peaks of the AltBOC complex correlation function.

The other two approaches (SSB and DSB acquisition) are *BPSK-like techniques*, because the AltBOC received signal is processed during the acquisition like two separate BPSK signals. In this way, the same statements discussed in previous Section can be done: the single sideband (SSB) acquisition is preferable, because implies a more simple implementation.

The resulting block diagram of the single sideband (SSB) acquisition section adapted to the coherent dual band receiver is then depicted in Figure 5.16.

This acquisition section is nearly the same as that previously introduced for the single band receiver and the separate dual band receiver: the acquisition is performed with the same procedure, searching the Doppler shift and the code delay of a single sideband of the received signal and considering the pilot code ($E5a$-Q), but the **down-conversion** is performed in a different way (see Figure 5.17) and it is also necessary a **down-sampling**, to reduce the computational burden.

In detail, considering the **down-conversion** of the desired single sideband ($E5a$) for the acquisition with this architecture, it is necessary to recall that in the RF front end and in the IF section of the coherent dual band receiver the entire E5 band is processed and down-converted to the desired intermediate

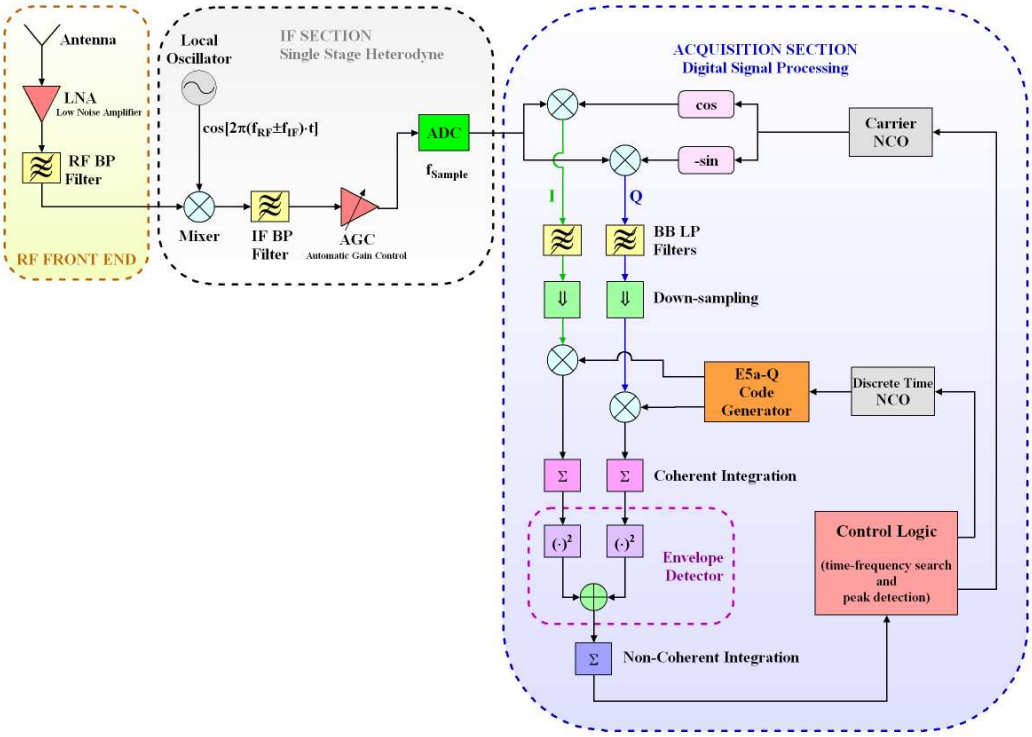

Figure 5.16: Block diagram of the coherent dual band receiver architecture, with the SSB (*E5a* sideband) acquisition section

frequency (f_{IF}). As shown in Figure 5.17, the output of the IF section in this case is a wideband signal (with both *E5a* and *E5b* side-lobes) centered to f_{IF}, while in previous arrangement only the desired side-band was down-converted (compare with Figure 5.14).

The frequency for the carrier NCO in the acquisition section must be modified with respect to previous arrangement, so as the center of the *E5a* sideband would be correctly shifted to the baseband. In fact, it must be noted that in this case f_{IF} does not correspond to the center of the *E5a* sideband in the signal at the output of the IF section: f_{IF} corresponds to the center of the two side-lobes, as depicted in Figure 5.17. Then, since the center of each side-band of the AltBOC spectrum is shifted with respect of the central carrier by the amount of the subcarrier frequency ($f_{sub} = R_{S,E5} = 15.345\,\text{MHz}$), as previously demonstrated in Section 2.2.4, the frequency value that must be used for the carrier NCO is equal to $(f_{IF} - f_{sub} + f_{Doppler})$, where $f_{Doppler}$ is the searched Doppler shift. In this way the *E5a* sideband is correctly down-converted to the baseband ($f = 0$) and the low pass filters in the acquisition section could select just this sideband, as shown in Figure 5.17.

On the contrary, if it is necessary to acquire the other sideband (*E5b*), analogous operations can be done: the only difference is the frequency chosen for the carrier NCO, that in this case must be equal to $(f_{IF} + f_{sub} + f_{Doppler})$.

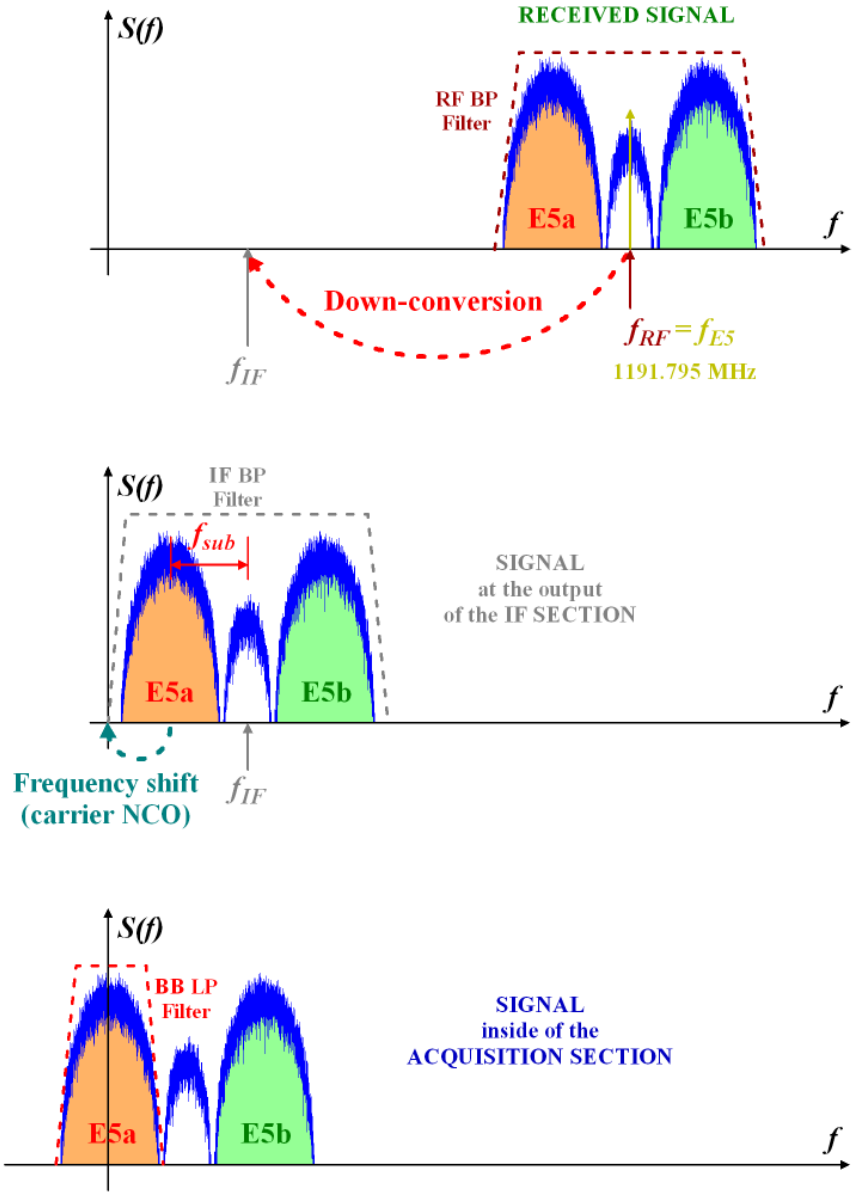

Figure 5.17: Signal bandwidth selection for the SSB (*E5a* sideband) acquisition with the coherent dual band receiver

Besides, it must be noted that a **down-sampling** is necessary for the acquisition with the coherent dual band receiver architecture: the sampling frequency required for the tracking operations (e.g. $f_{Sample} \cong 120\,\text{MHz}$, with about 12 samples/chip, as stated in Section 5.2.1) is not suitable for the acquisition, because it implies an excessive computational burden. Then, a down-sampling is performed inside the acquisition section, decimating the I and Q samples after the baseband filters (see Figure 5.16).

In this way, the acquisition in the coherent dual band receiver could be performed in a short time with a initial rough acquisition, performed on a down-sampled signal (e.g. the signal could be decimated from 12 samples/chip to 2 samples/chip), followed by a refinement (thee **progressive acquisition** technique, as discussed in Section 5.1.4) during the transition phase to the tracking.

It should be noted that during the SSB acquisition it is not necessary to locally generate the four-valued **subcarrier** waveforms used in the AltBOC modulation (see Section 2.1.1). In fact, the frequency shift needed for the down-conversion of the considered side-lobe is performed taking advantage of the local sinusoidal signals generated by the carrier NCO.

At the end of the acquisition operations and after the transition phase, the code delay and the Doppler shift are estimated with a sufficient resolution, then the frequency of the carrier NCO is shifted in order to track the entire AltBOC wideband signal. Finally, the coherent dual band tracking operations (previously discussed in Section 4.3) can start: the signal tracking is performed taking advantage of the AltBOC complex correlation, that is evaluated correlating the received signal with local complex signals, obtained generating the two pilot codes (*E5a-Q* and *E5b-Q*) and the four-valued subcarriers waveforms.

As a final remak, the Single Side-Band (SSB) acquisition technique, just illustrated in this Section for the coherent dual band receiver, is suitable also for the **receiver with the correlator-discriminator** and the other architectures derived from the coherent dual band receiver (see Section 4.4), without further modifications.

5.4 Simulation of the acquisition process

The previously discussed acquisition schemes for the AltBOC signal have been implemented in a digital simulator in order to develop and validate the acquisition process, including the energy search and transition to tracking (using the *progressive acquisition* technique, previously discussed in Section 5.1.4).

The simulations carried out for this Section have been performed by means of programs written in the thesis framework, using the *C* programming language. A program able to simulate the operations performed by all previously discussed acquisition schemes for the AltBOC receivers has been implemented. In detail, only the operations performed in the *acquisition section* of previous block diagrams are simulated, carrying out the following tasks:

- the **signal generation**, with the aim to simulate the digital signal at the output of the ADC in the *IF section* of the receiver;
- the **acquisition operations** performed in the *acquisition section* of the receiver.

5.4.1 Signal generator

The **signal generator** has been implemented in a program written in *C* language, taking advantage of the *Look-Up Table* (LUT) approach (previously discussed in Section 2.2.4), that allows an efficient modulation of the AltBOC signal.

The modulated signal is sampled with the chosen sampling frequency (f_{Sample}) and it is also possibile to use an *incommensurable* (prime) value with respect to the ranging code rate (as discussed in Section 5.2.1).

After that, an arbitrary code delay (Θ) and Doppler shift ($f_{Doppler}$) are inserted. In detail, the frequency shift performed on the signal is equal to ($f_{IF} + f_{Doppler}$), simulating also the intermediate frequency used in the receiver.

At last, an *Additive White Gaussian Noise* (AWGN) channel is simulated, adding to the signal samples a gaussian noise with zero-mean and a variance defined by the chosen *Signal-to-Noise Ratio* (SNR) or the corresponding *Carrier-to-Noise-Density Ratio* (C/N_0) at the input of the acquisition section.

It must be noted that the outputs of the signal generator are IF samples with *float* precision. The effect of the finite number of bits in the analog-to-digital conversion performed in the ADC of a real receiver is neglected (infinite number of bits approximation). The generated samples are finally saved in a binary file and subsequently processed by the acquisition section.

5.4.2 Acquisition algorithm

The **acquisition algorithm** used in the simulations is flexible and allows to simulate both the *Single Side-Band* (SSB) acquisition, performed on the *E5a-Q* pilot code, and the *Double Side-Band* (DSB) acquisition, using both the pilot codes *E5a-Q* and *E5b-Q*, with the operations previously described: down-conversion to the baseband, down-sampling, Doppler and code delay search and *progressive acquisition* technique.

In detail, the simulator performs the acquisition taking advantage of the parallel FFT acquisition technique in time delay domain (previously outlined in Section 5.1.3) to speed up the simulation time. This parallel technique has been implemented using the FFTW (this acronym means the *Fastest Fourier Transform in the West*) library: FFTW is presented in References [33] and [34] and is a widely used free-software library that computes the *Discrete Fourier Transform* (DFT) and its various special cases.

It must be noted that two Butterworth filters have also been implemented and inserted both in the signal generator and in the acquisition section: the parameters of these filters (order and coefficients) can be modified, allowing to simulate different signal bandwidths. But for the simulations performed in

the following Section the filters have not been used: an ideal acquisition system was simulated, without signal filtering and then with infinite bandwidth signals, as generally done in the articles where the acquisition performances are discussed and simulated (see Section 5.2.6).

5.4.3 Simulation results

A first simulation was performed, considering the Single Side-Band (SSB) acquisition scheme for a coherent dual band receiver architecture in ideal conditions (with infinite bandwidth and without noise). The obtained results are presented in Figure 5.18, where the obtained search spaces for the initial rough acquisition (with the down-sampled signal) and after the *progressive acquisition* technique are shown.

In this example the signal for the acquisition section has been generated without noise (SNR $= \infty$, $C/N_0 = \infty$) and without any signal filtering, considering a sampling frequency $f_{Sample} = 122.76$ MHz (12 samples/chip). In the simulator the four channels of the AltBOC modulated signal of two satellites (identified with two *Satellite Vehicle Numbers*: 1 and 2), using an arbitrary assignment[2] for the codes of two satellites, could be generated: it has been chosen to generate the signal of the second satellite (SVN = 2), that must be acquired. A code delay equal to $\Theta = 4.75$ chips (that corresponds to 57 samples at f_{Sample}) has been used and the signal has been shifted with a Doppler frequency $f_{Doppler} = -2100$ Hz. A further frequency shift has been performed, to simulate also the chosen intermediate frequency ($f_{IF} =$ 10 kHz).

Then, the Single Side-Band (SSB) acquisition has been performed in the acquisition section, using only the *E5a-Q* pilot code. The codes of two satellites are searched (SVN 1 and 2), assuming a *cold start* operative condition (see Section 5.1): this means that for each satellite the whole two-dimensional search space must be explored. An **initial rough acquisition** is performed, applying a down-sampling (with ratio 6) to the received signal, to reduce the computational burden: in this way the signal that must be correlated is sampled at $f_{Acq} = 20.46$ MHz (2 samples/chip). After that, the acquisition search could be performed, using a resolution of $\Delta f = 500$ Hz (*Doppler bin*) to sequentially scan the Doppler uncertainty domain, that ranges between -5 kHz and $+5$ kHz. On the other hand, the entire code uncertainty domain (between 0 and 10230 chips) is scanned with a resolution of $\Delta\Theta = 0.5$ chip, taking advantage of the FFTW library. Accordingly, 21 Doppler bins

[2]For the simulation of the two satellites, the codes have been assigned choosing between the 50 primary codes that are defined in SIS-ICD [4] for each E5 channel. In detail the first code of each channel has been chosen for the first satellite, while the second code of each channel has been used for the second satellite. With another arbitrary choice the results are similar, with negligible differences. In fact it must be noted that the code assignment for each satellite must still to be defined.

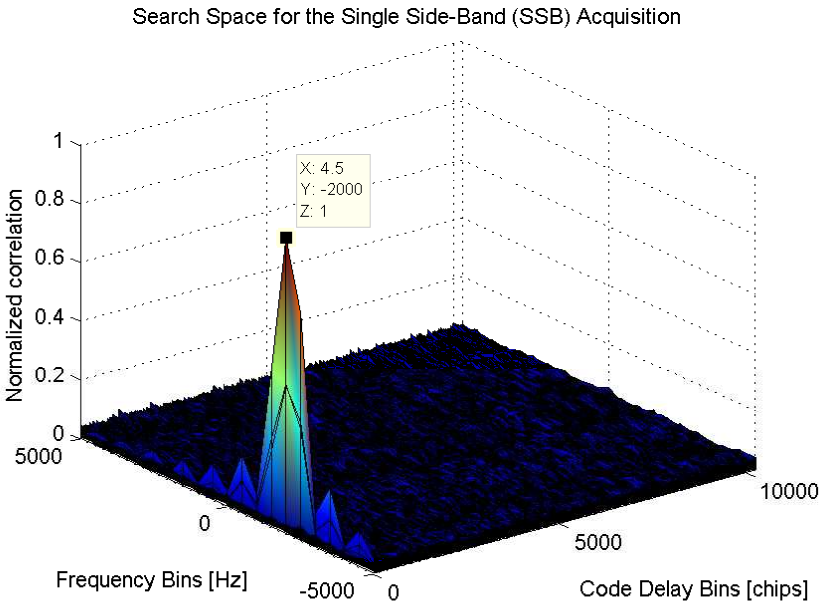

(a)

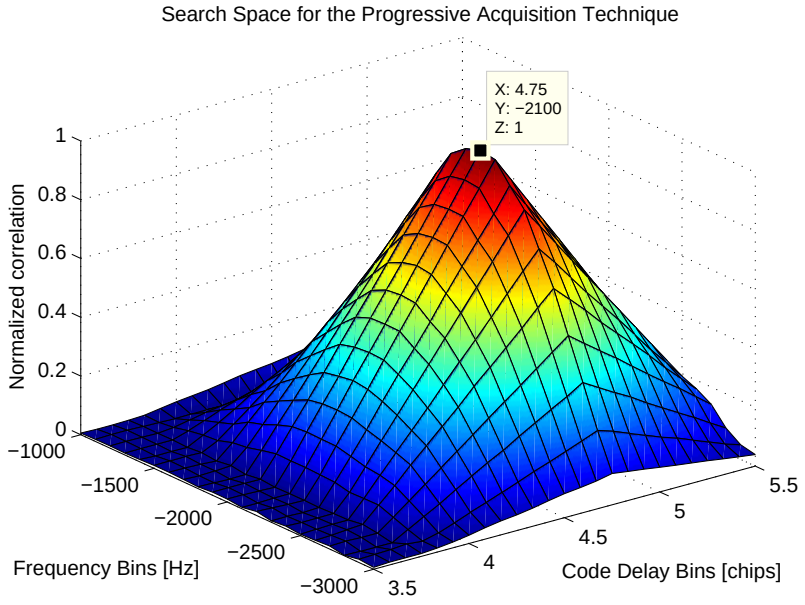

(b)

Figure 5.18: Example of SSB acquisition performed with the *E5a-Q* pilot code, simulated with a coherent dual band receiver in ideal conditions (with infinite bandwidth and without noise): resulting search spaces for the initial rough acquisition (a) and with the progressive acquisition technique (b)

and 20460 code bins must be searched for each satellite, resulting in a search space with 429660 cells (21 × 20460). In this case, each cell is evaluated with a coherent integration time of 1 ms (corresponding to 1 primary code period) and with a single non-coherent integration. The result is shown in Figure 5.18(a), where the correlation values are normalized with respect of the correlation peak. It must be noticed that the correct satellite (SVN = 2) has been correctly acquired, with an estimated code delay $\widetilde{\Theta} = 4.5$ chips and with an estimated Doppler shift $\widetilde{f}_{Doppler} = -2000$ Hz. Obviously these values are an approximation of the exact values ($\Theta = 4.75$ chips and $f_{Doppler} = -2100$ Hz), accordingly to the chosen resolution for the search space.

After this initial rough acquisition, a refinement of the estimated code delay and Doppler shift is performed, taking advantage of the **progressive acquisition** technique. This is done considering the received IF samples without down-sampling ($f_{Sample} = 122.76$ MHz, that corresponds to 12 samples/chip) and carrying out a new search with improved resolution: this search is done only in the portion of the search space around previously estimated values ($\widetilde{\Theta}$ and $\widetilde{f}_{Doppler}$). In this example, a resolution of $\Delta f = 100$ Hz has been used to search a Doppler range of 1 kHz around the estimated Doppler shift (between −1 kHz and −3 kHz) and the code delay search has been performed with a resolution of $\Delta\Theta = 1/12$ chip in the range of 1 chip around the estimated delay (between 3.5 chips and 5.5 chips), as shown in Figure 5.18(b). The correlation result for each cell has been separately evaluated, with a coherent integration time of 1 ms and with a single non-coherent integration. In fact the parallel FFT approach could not be used for scan only a portion of the search space, then the *linear search* approach must be used. However, only few cells must be evaluated (21 Doppler bins and 25 delay bins, that corresponds to 525 cells), then the computational burden is not excessive, if compared with the initial rough acquisition (where 429660 cells are searched).

After the refinement of the estimated values, the output of the algorithm is a code delay $\widetilde{\Theta} = 4.75$ chips and a Doppler shift $\widetilde{f}_{Doppler} = -2100$ Hz, then the signal is correctly acquired. Accordingly, the previously discussed acquisition schemes are validated by this simulation: they are suitable for the acquisition of the AltBOC signal, since they allow to correctly estimate the code delay and the Doppler shift.

Two further simulations have been carried out, to validate the acquisition algorithm also in presence of noise. The same parameters as in previous case, for the initial rough acquisition, has been used, except for the *Signal-to-Noise Ratio* at the input of the acquisition section that is chosen SNR = −10 dB (and corresponds to a $C/N_0 = 60$ dB-Hz). As previously stated in Section 5.2.5, a suitable way to improve the acquisition performance in presence of noise is to increase the number of **non-coherent accumulations**. Then, a first simulation has been performed, considering a single non-coherent integration (see Figure 5.19(a)), and has been compared with the result obtained with 10 non-coherent accumulations (see Figure 5.19(b)), with the same noise.

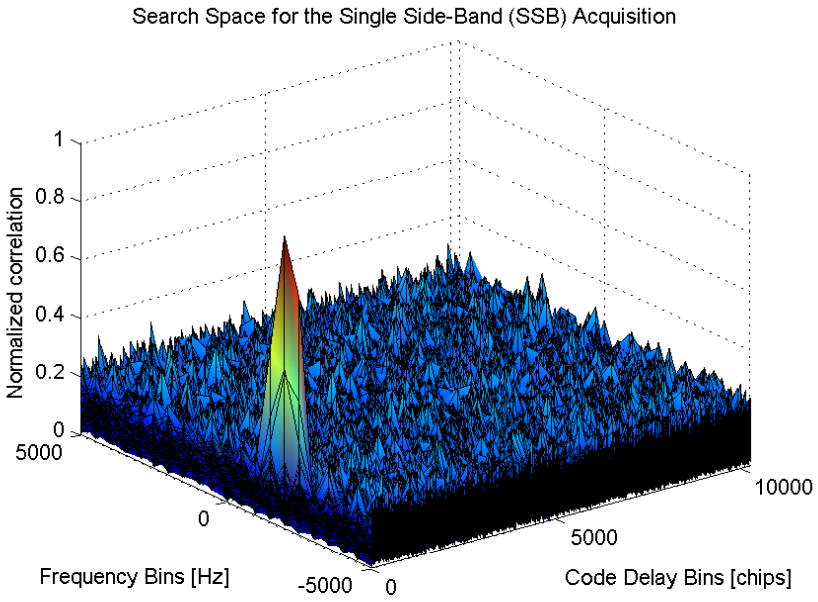

(a)

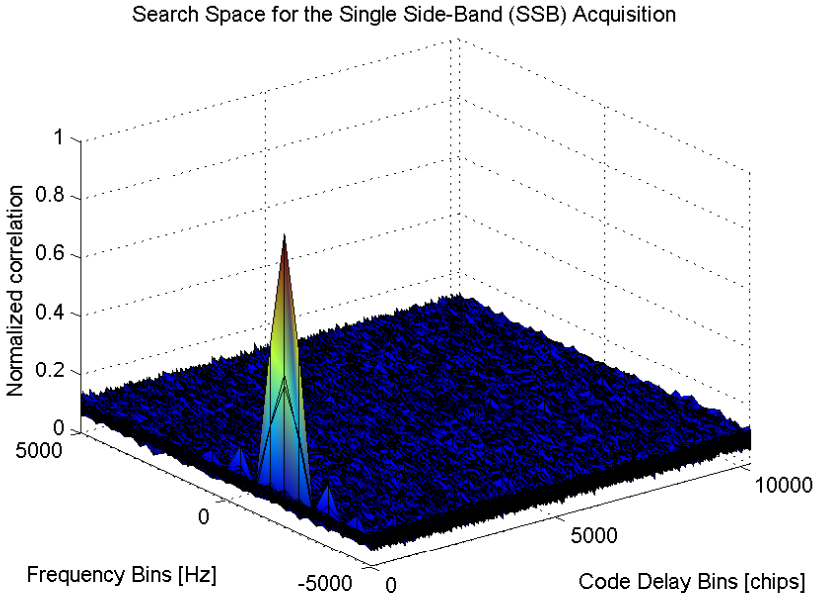

(b)

Figure 5.19: Example of SSB acquisition performed with the *E5a-Q* pilot code, simulated with a coherent dual band receiver, with infinite bandwidth and in presence of noise (SNR = -10 dB, C/N_0 = 60 dB-Hz at the input of the acquisition section): resulting search spaces with 1 single non-coherent accumulation (a) and with 10 non-coherent accumulations (b)

In Figure 5.19 it is shown that with 10 non-coherent accumulations the correlation peak[3] is more evident with respect of the noise floor, therefore the values of the code delay and the Doppler shift could be estimated in a more reliable way (with reduced *false alarm probability* and improved *detection probability*).

Accordingly, an increase of the number of non-coherent accumulations is a suitable way to improve the acquisition performance in presence of noise, but it implies also a heavier computational burden and a longer acquisition time. In conclusion, the number of non-coherent accumulation is a critical parameter for the acquisition section and it must be chosen as a compromise between acquisition speed and performances in presence of noise.

5.5 Conclusions

A complete study of acquisition strategies for the AltBOC signal, that at the moment is not present in literature, has been done in this Chapter for the first time. The receiver architectures previously presented in Chapter 4 have been considered and suitable acquisition techniques have been discussed for each architecture.

At the end of this Chapter, some simulations have been carried out, validating the previously discussed acquisition schemes. It must be remarked that a complete simulator, that performs the AltBOC signal generation and the acquisition processing, has been developed and could also be used for further works about the acquisition of the AltBOC signal (e.g. validation of innovative acquisition strategies, analysis of the *false alarm probability* and the *detection probability*, performance assessment with *Receiver Operative Characteristic* curves, introduction of *statistical improvement algorithms*, etc.), that are not concerned in this thesis.

[3]It must be noted that both the correlation peaks are normalized to 1. If this normalization is not done, the correlation peak in Figure 5.19(b) is about ten times higher than the peak in Figure 5.19(a).

Chapter 6

Code multipath mitigation

The future Galileo receivers will support a wide variety of services and applications. Some of these will require high accuracy in real time, and therefore the major error sources which affect the receiver have to be reduced. One of the most important error contribution is the **multipath**, which can be seen as the superimposition of the same signal reaching the receiver at different times, due to reflections from any surface around the receiver antenna.

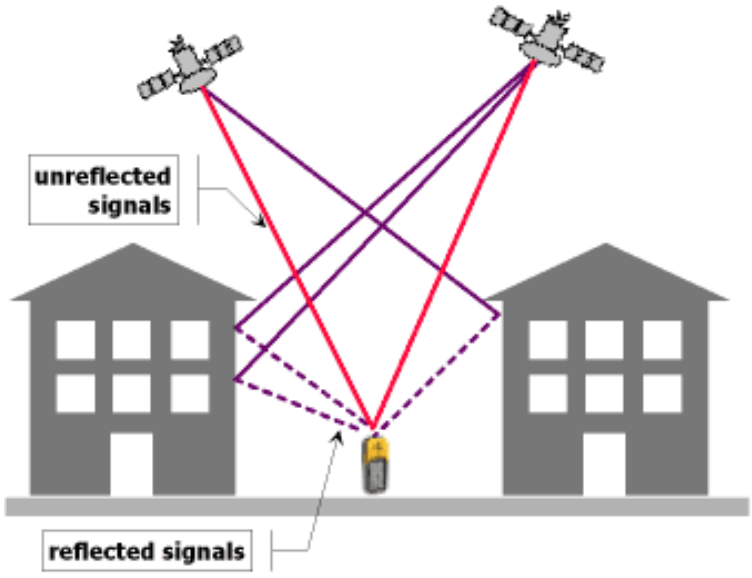

Figure 6.1: Scheme of the multipath effect on a Galileo receiver [35]

The presence of multipath signals generally results in ranging and carrier phase errors, because the reflected signals leads to bias error on the lock point of the code tracking loop (DLL) and on the carrier tracking loop (PLL) of the receiver.

The effect of the multipath on the code tracking (the so-called **code multipath**) typically is mitigated using an appropriate setup of the DLL. In detail

for the common GPS receivers there are several techniques based on different types of discriminators that could achieve good multipath mitigation performances. These techniques could be adapted and employed also with a Galileo receiver architecture.

The multipath affects also the carrier phase measurements (**carrier multipath**), but the impact of this error on the receiver performances is smaller than the code multipath. However for high precision applications, as worldwide geodetic networks, kinematic survey and aircraft precision landing, also the carrier multipath must be mitigated, to obtain a precise carrier phase positioning. It must be highlighted that the carrier multipath mitigation is generally treated separately from the code multipath mitigation, because it does not depend on the type of discriminator used for the DLL: only the prompt correlation channel is used by the PLL for the carrier phase tracking. As well as for the code multipath, also for the carrier multipath there are common mitigation techniques, that could be successfully adapted for the Galileo signals.

The code and the carrier multipath could also be mitigated using an appropriate antenna system. For geodetic GPS receivers it is possible to use an antenna with particular shape (for example choke ring), with a radiation pattern that is shaped to reduce signals arriving at low elevation angles; these features decrease the errors caused by multipath. Another solution is to use an antenna array. Multiple closely-spaced antennas are used with the concept of digital beamforming: with specific algorithms it is possible to create an adaptive multibeam antenna pattern, in order to track satellites and place null in the direction of the reflected signals. These techniques are not used in common mass-market receivers, because there are expensive and imply a bulky antenna system and a more complex signal processing.

In spite of fact that in literature there are several articles that discuss the code multipath mitigation with the GPS signals and the Galileo BOC signals (see for example [15], [32], [35], [36], [37], [38], [39], [40], [41], [42], [43], [44], [45], [46], [47], [48]), the multipath performances of the AltBOC modulation are outlined only in few papers (see [9], [11], [14], [49], [50]): an exhaustive comparison between the different mitigation techniques for the AltBOC signal is not present at the moment and is done for the first time in this thesis.

In this Chapter the code multipath mitigation problem is discussed for the Galileo E5 AltBOC signal, trying to adapt the well-known discriminator-based techniques used in common GPS receivers to the architectures proposed and described in Chapter 4. After a brief introduction about the code multipath errors and the receiver parameters involved in multipath mitigation, the multipath performances of the current mitigation approaches will be assessed and compared in Section 6.4, using two typical methods: the **multipath error envelopes** and the **running average of multipath error envelopes**. In addition, two emerging mitigation techniques (the *S-curve shaping* and

the *gating technique*) are also presented and assessed in Section 6.5. In Section 6.6 the performances of an innovative receiver architecture (the *receiver with the correlator-discriminator*, proposed in Section 4.4.3) will be also evaluated and compared with the previous arrangements. At last (see Section 6.7) the possibility to adapt some multipath mitigation approaches with the innovative receiver will be studied, comparing the results with those obtained with previous receiver architectures and mitigation techniques.

6.1 Code multipath errors

The multipath effect refers to the presence of signals arriving at the receiver antenna by means of multiple reflected paths. Due to the extra path length they travel, multipath signals arrive at the antenna with a phase delay relative to the direct one (the so-called LOS, the *Line Of Sight* signal); thus, multipath signals combine with the direct component and distort the received code phase. This distortion can cause a ranging error, because the receiver wrong estimate the correct *Time Of Arrival* (TOA) of the received signal.

Multipath propagation can be classified in three categories, based on the physical phenomenons that produce it:

- **specular reflection**: coming from a reflection on a smooth surface, being the resulting wavefront a delayed copy of the direct signal, differing from this one only in phase and amplitude; the resulting error typically lies in the range of a few meters and behaves as a constant bias for a motionless receiver;
- **diffraction**: due to reflection from the edge or corners of the reflecting objects; reflections from abrupt edges tend to be diffuse, thus producing rapidly varying errors with magnitude limited to several millimeters;
- **diffuse multipath**: due to reflection in rough surfaces, similar to various specular reflections; as for diffraction, reflections from rough surfaces produce rapidly varying errors with limited magnitude.

Some important characteristics of multipath are as follows:

1. the multipath signal will always arrive after the direct path signal because it must travel a longer propagation path;
2. the multipath signal will normally be weaker than the direct path signal since some signal power will be lost from the reflection. It can be stronger if the direct path signal is hindered in some way;

3. if the delay of multipath is less than a certain number N of PRN code chip lengths (depending on the specific modulation), the internally generated receiver signal will partially correlate with it, and the receiver could wrong estimate the pseudorange between the transmitting satellite and the user position; otherwise if the delay is greater than N chips, the PRN codes are designed so that the correlation power will be negligible, and the pseudorange is correctly estimated.

In detail, for GPS receivers the value of N is of 2 chips, as noticed in Reference [45]. This statement is also true for all the navigation systems based on BPSK signals, with an autocorrelation function of the PRN codes that has a triangular shape between -1 and +1 chip and is zero for larger delays. In fact, as shown in Figure 6.2, varying the delay of the reflected signal between 0 and 2 chips the correlation function results as a composition of two triangular peaks and appears distorted: this could lead to an error in the position estimation. On the contrary, if the multipath delay is equal or larger than 2 chips, the received signal shows two distinct peaks and the main peak is not distorted. Assuming that the receiver is able to distinguish and track the correct code correlation peak, that is higher that the peak caused by the multipath, the pseudorange is then correctly estimated if the multipath delay is equal or greater than 2 chips.

Similar considerations can be done for the AltBOC signal. Observing Figure 6.3, it is evident that the AltBOC combined complex correlation function (previously discussed in Section 3.4) has the same support of the previous triangular correlation: this function has an oscillating shape between -1 and +1 chip and is zero for larger delays. Then only the reflected signals with delay of less than 2 chips could lead to ranging errors.

However some additional remarks must be done about the value of N for the AltBOC. It must be noted that only the main peak of the correlation function of the AltBOC signal is usually tracked by the receiver, whereas the other lower peaks are not used. This implies that only the multipath signals that affect the shape of the main correlation peak can cause multipath errors. Since the first zero-crossings around the main peak occurs at $\pm 1/6$ chip (± 0.1667 chip), the maximum delay of the multipath component that could distort the main peak of the direct signal is equal to 7/6 chip (1.1667 chip), as illustrated in Figure 6.4. Accordingly, the value of $N = 7/6$ chip could be assumed for the AltBOC.

In general, if the difference between the direct path and the reflected path is less than a chip, but is large enough, the detrimental effect of the reflected signal can be reduced with several **multipath mitigation techniques** (some of these signal processing techniques are presented in following Sections). Unfortunately, the strongest reflected signals in terms of received power usually have a short excess of path length, because near reflected signals are more probably received than far ones (see Reference [40]). In this common case, the

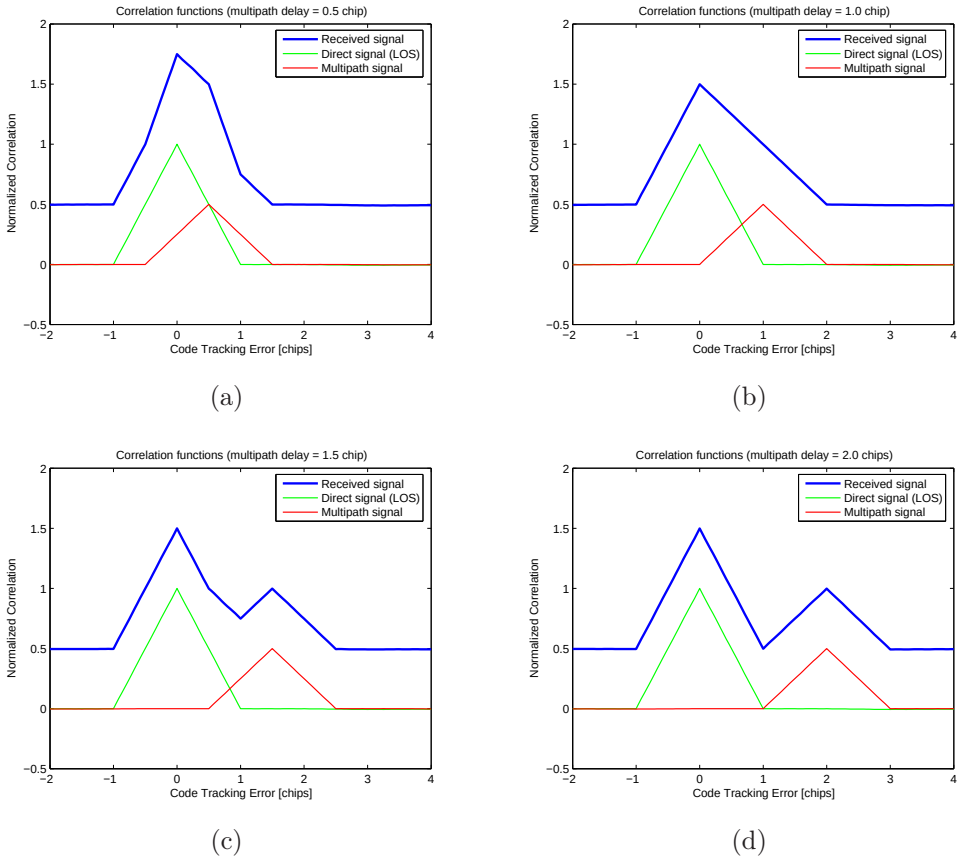

Figure 6.2: Multipath effect on the triangular correlation peak of a BPSK signal, considering a direct signal (LOS, depicted with a green line) and a multipath signal (red line) with half of the amplitude of the direct signal ($\alpha = 0.5$), in phase with it and varying the delay between the two components. The four figures are obtained considering respectively a delay of 0.5 chip (a), 1 chip (b), 1.5 chip (c) and 2 chips (d). The compound correlation function of the received signal (blue line) is plotted with an offset, for the sake of clarity

mitigation techniques do not work well, then the receiver is not able to distinguish the reflected from the direct signal and thus additional pseudorange errors are experienced.

It is important to remark that the problem of multipath is present in both conventional and differential GNSS systems, since it is mainly dependent on the environment in which the receiver is operating. Reflected signals, present in different locations, even though slightly distant, are strongly uncorrelated, therefore, it cannot be elided employing differential corrections (like for example EGNOS data). The errors induced by the multipath typically are not zero-mean, thus measurements collected over a long time are ineffective in multipath error reduction (as demonstrated in Reference [36]). In this sense,

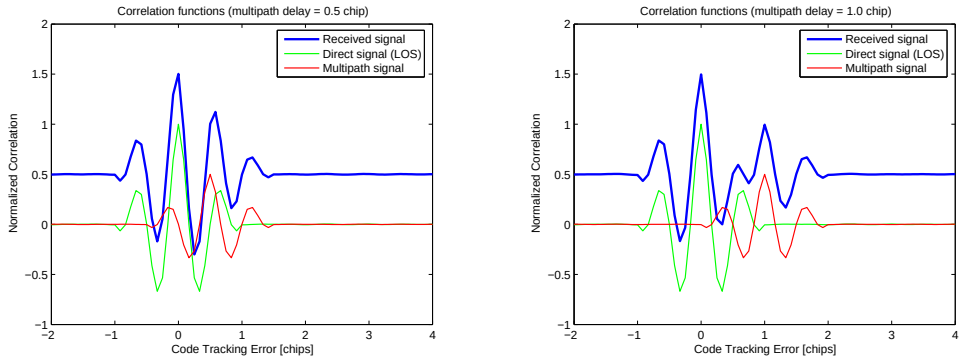

(a)

(b)

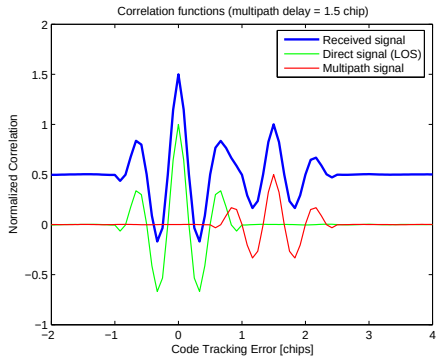

(c)

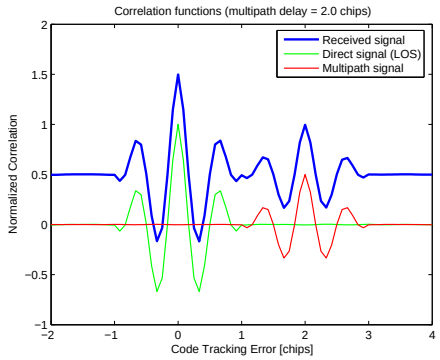

(d)

Figure 6.3: Multipath effect on the correlation function of the AltBOC signal, considering a direct signal (LOS, depicted with a green line) and a multipath signal (red line) with half of the amplitude of the direct signal ($\alpha = 0.5$), in phase with it and varying the delay between the two components. The four figures are obtained considering respectively a delay of 0.5 chip (a), 1 chip (b), 1.5 chip (c) and 2 chips (d). The compound correlation function of the received signal (blue line) is plotted with an offset, for the sake of clarity

since the *Selective Availability* (S/A) was turned off, multipath represents the dominant error source in GNSS receivers of present (GPS) and future generation (Galileo), becoming a critical issue for high-accuracy applications.

Considering the fact that a professional Galileo receiver needs to reach the best performances of *Position, Velocity and Time* (PVT) computation, the code multipath rejection has to be considered as one of the core technologies to be developed.

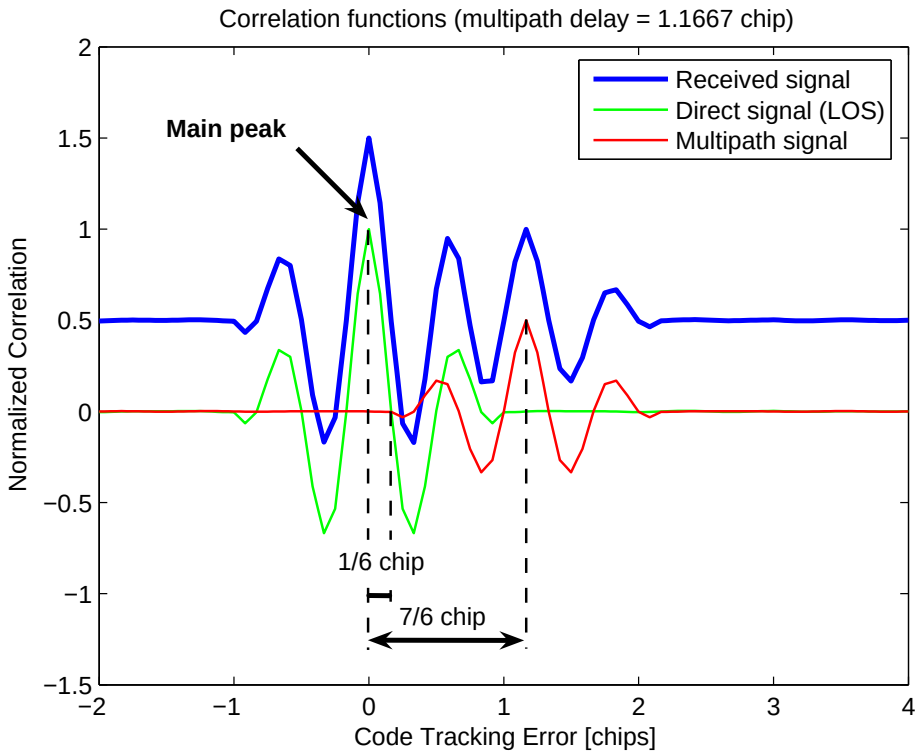

Figure 6.4: Multipath effect on the correlation function of the AltBOC signal: illustration of the maximum delay of the multipath component (red line) that could distort the main peak of the direct signal (LOS, depicted with a green line). The multipath signal has half of the amplitude of the direct signal ($\alpha = 0.5$) and is in phase with it. The compound correlation function of the received signal (blue line) is plotted with an offset, for the sake of clarity

6.2 Multipath performance assessment

There are several methods for assessing the multipath performances of a dedicated signal/receiver/environment combination and to compute realistic multipath errors for a GNSS error budget.

As illustrated in [40], the most complex ones are the **statistical channel models**. They allow the computation of reliable multipath errors, simulating the multipath environment under realistic conditions, but they are very complex and require time consuming and laborious data processing. Another drawback of these models is the fact that the resulting estimated errors are related with the simulated multipath environment: it is then difficult to evaluate the general performances of a receiver, because they depend on the parameters chosen for the model.

Much simpler models are the computation of the **multipath error envelopes** and the **running average of multipath error envelopes**. They

are presented in the following, and will be used to assess the discriminator-based multipath mitigation techniques presented in Section 6.4.

6.2.1 Multipath error envelopes

The computation of the **multipath error envelope** is the common approach used to assess the effect of the specular multipath, since it permits to compare multipath performances of different signals and receiver setups, with a very low computational burden. The obtained ranging errors can be considered as general results: they are independent from the multipath environment, because they are calculated with substantial simplifications and under idealized conditions.

With the multipath error envelopes, the resulting ranging errors are plotted as a function of the geometric path delay (i.e. the geometric path length difference between the direct and the delayed signal component). An example of a multipath error envelope is shown in Figure 6.5(a), where a GPS receiver with a wide correlator ($d = 1$ chip) and infinite bandwidth is considered.

The computation of multipath error envelopes is based on the following assumptions:

- the direct signal component is always available (no shadowing effects);
- only one reflected signal is present;
- the multipath signal undergoes an attenuation, that usually is $\alpha = 0.5$: this means that the reflected component has half of the amplitude of the direct signal (this corresponds to a *Signal-to-Multipath power Ratio* $SMR = 6\,\text{dB}$, as will be discussed in Section 6.3.1);
- the environment is under static conditions (no relative motions between receiver and satellite, no changes in multipath signal).

The correlation proprieties of the received signal is used by the receiver to determine the pseudorange between the receiver and the transmitting satellite. For the receiver there are several alternatives of code discriminators. They take advantage of the correlation peak using different early and late correlation values to obtain the so-called *S-Function*. Pseudorange determination is generally performed by tracking the zero-crossing of this function.

The presence of multipath signals results in a distortion of the *S-Function* and then in a shift of the tracking point. The resulting offset can be deemed to be the ranging error caused by the multipath signal. The obtained multipath error in chips can be converted to meters by simply multiplying with the code chip length (c/R_C): this corresponds to 293.25 meters for the GPS C/A code ($R_C = 1.023$ Mchip/s) and to 29.33 meters for the E5 codes that will be used

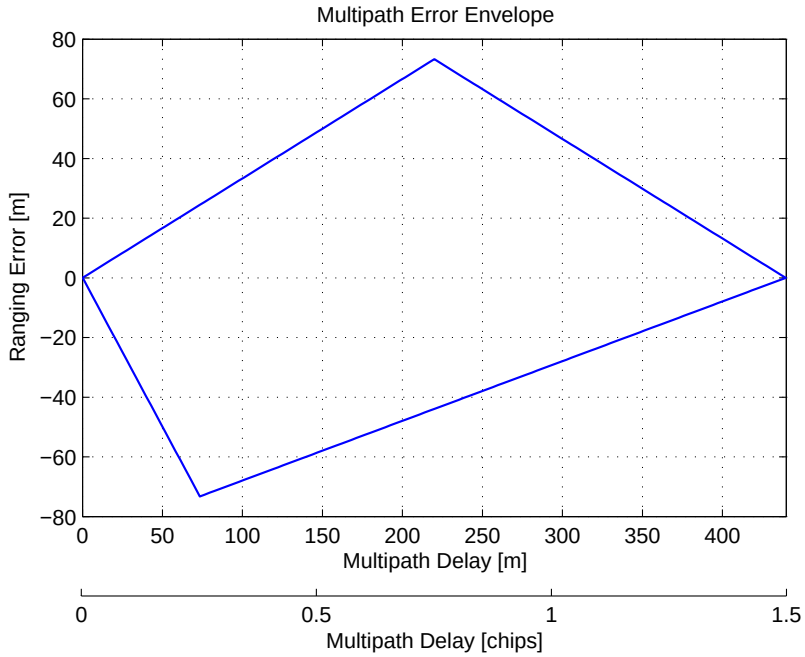

(a)

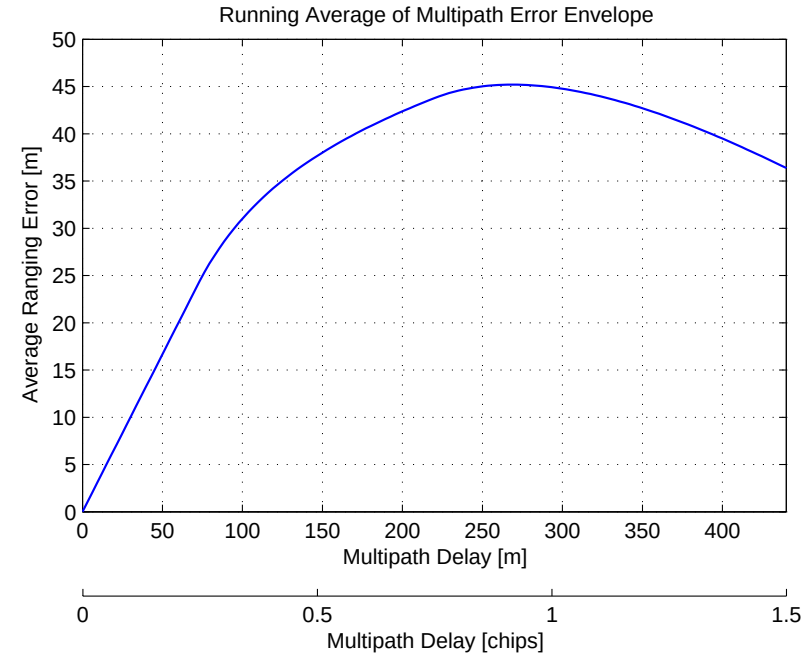

(b)

Figure 6.5: Examples of multipath error envelope (a) and running average of multipath error envelope (b), for the GPS C/A code ($R_C = 1.023$ Mchip/s), considering an ideal receiver (infinite bandwidth) with a wide correlator ($d = 1$ chip)

in the Galileo system ($R_C = 10.23$ Mchip/s). The multipath error envelopes are finally computed by constantly increasing the geometric path delay of the multipath signal (beginning with a relative path delay of 0 meters) and determining the corresponding zero-crossing offset.

Typically (as stated in Reference [39]) the error envelopes are evaluated twice, firstly for a multipath carrier phase shift of 0° with respect to the direct signal component and secondly for a shift of 180°, that corresponds to a reflected signal with opposite phase. In this way the multipath envelopes represent the worst case ranging errors that a receiver could experience with one single multipath signal, with constant relative amplitude. A single reflected signal with a carrier phase shifts between 0° and 180° could only produce errors confined in the envelope.

Another usual choice is to evaluate the envelope for multipath delays between 0 and 1.5 chips, as done in Figure 6.5(a), that corresponds to a range of 439.88 meters for the GPS C/A code and 43.99 meters for the Galileo E5 codes. On the contrary in following Sections the multipath error envelopes for the AltBOC signal will be evaluated in a wider range, between 0 and 100 meters (that corresponds to 3.41 chips), in agreement with the simulations performed in Reference [38] for the BOC(15,10) signal. This choice is also justified because with some receiver configurations the multipath envelope could be non zero for delays greater than 1.5 chips (e.g. with the shaping technique, discussed in Section 6.5.1).

To analyze the effect of different amplitudes of the reflected signal, it is sufficient to scale the multipath envelope (evaluated for a fixed multipath relative amplitude α). In this way the multipath envelope could be used for a more realistic analysis, evaluating it for the typical mean *SMR* of a defined multipath environment, obtaining the so-called **weighted multipath error envelopes** (as discussed in [40]).

In conclusion the multipath error envelopes are a useful criterion for multipath performance assessment, because these graphs clearly reflect the proprieties of the underlying signals and the receiver performances. On the other hand, analysis of error envelopes allow only general and qualitative statements about the multipath performances, because the estimated errors are only valid for a simplified scenario (one single multipath signal with constant relative amplitude), whilst for a realistic environment analysis (e.g. with multiple reflected signals) other methods are necessary. Furthermore, it is difficult to extract meaningful typical multipath errors from these envelopes, because they only represent worst case errors.

6.2.2 Running average of multipath error envelopes

To overcome the limitations of the multipath error envelopes, they can be further modified to obtain a more reliable way for multipath performance assessment, to provide better means for comparing the multipath performances of different signals or receiver setups and to be able to derive typical and meaningful multipath error contributions to the overall error budget.

To achieve these goals, one possible criteria that can be considered is the computation of the **running average of multipath error envelope** (as discussed in [40]). For this purpose, only the absolute envelope values are considered and their cumulative sum is used to compute average ranging errors. An example of a running average of multipath error envelope is shown in Figure 6.5(b), where a GPS receiver with a wide correlator ($d = 1$ chip) and infinite bandwidth is considered.

In detail, the computation of the running average is performed evaluating the mean value of the unsigned in-phase (0°) and the unsigned 180° phase shift component of the multipath error envelopes, for every point of the envelope, that is for every relative path delay τ. The obtained modified envelope is then used to compute the running average, evaluated like a moving average with an increasing number of addends to be averaged.

The resulting values can be interpreted as mean multipath errors: choosing a relative path delay τ_0 which is representative for a dedicated multipath environment (typical geometric path delay), the corresponding running average value is an average multipath error resulting from reflected signals with path delays between $\tau = 0$ and $\tau = \tau_0$. The impact of longer path delays remain unconsidered in this model; this is a reasonable simplification, as most multipath is short-delay multipath (as demonstrated in [40]).

The main benefit of computing and analyzing running average plots is that both qualitative and quantitative conclusions can be drawn. Obviously a good multipath performance is characterized by a small maximum average value and a rapid decrease toward zero, increasing the geometric path delay. In addition, since the computation of running averages bases on multipath error envelopes, no complex and extensive preparatory computations are necessary. It should be noted, however, that multipath errors derived from running average plots still base on one single reflection with dedicated relative amplitude. However, different multipath environments could be considered and analyzed knowing their fundamental characteristics (typical *SMRs* and path delays), obtaining the so-called **weighted running average of multipath error envelopes** (as discussed in [40]). This weighting technique is not applied in the following, where only the multipath error envelopes and the running average plots are used to obtain graphics that are simple and reflect mainly the signal characteristics and the receiver configuration.

6.3 Parameters involved in multipath errors

The actual code multipath, that causes ranging errors, depends on various signal and receiver parameters:

- relative power levels of multipath signals (signal attenuation α due to reflection);
- actual number of multipath signals;
- geometric path delay of multipath signal;
- signal type (e.g. BPSK, BOC or AltBOC);
- code rate;
- receiver bandwidth (pre-correlation bandwidth and filter characteristics);
- type of discriminator (e.g. early minus late wide correlator, narrow correlator, double delta correlator);
- correlators spacing.

The first three parameters give a description of the multipath environment, because they strongly depend on the receiver location. On the contrary, the other parameters are related with the transmitted signal features and the receiver architecture.

6.3.1 Multipath environment parameters

Multipath errors are related with the environment where the signal propagates and reaches the receiver. For example a urban area is characterized by strong multipath, with a large number of reflected signals, typically with high power and coming from near reflections. Otherwise in a rural environment typically there are not much multipath signals, with large delays and strongly attenuated with respect of the direct signal (for a detailed analysis of different models of multipath environments see [40]).

Generally the multipath performance are not assessed using realistic and detailed models of the environment, because these approaches are complex and time consuming, and it is difficult to evaluate the general performances of a receiver, because they depend on the choice of the parameters of the environment. It is common to study the performances of a receiver using a simplified multipath model, with only one reflected signal, and to evaluate the multipath error varying the relative power level and the geometric path

delay of the reflected component. On this idea are based the multipath errors envelopes (previously described in Section 6.2.1).

It must be remarked that the relative power level of multipath signal with respect of the direct signal is one of the most important parameters for the performance analysis. Obviously a stronger multipath signal could imply errors larger than these caused by a weak reflected signal. Usually (see for example [11]) the code multipath error envelopes are evaluated with $\alpha = 0.5$, that is the relative signal attenuation of the multipath: this means that the reflected signal has an amplitude that is half of the direct signal amplitude.

Instead of the relative attenuation α, often in literature it is used another parameter: the **Signal-to-Multipath power Ratio** (SMR). It is a power ratio between the direct signal and the reflected signal, and is defined in decibels with the expression:

$$SMR = 20 \cdot \log_{10}\left(\frac{\alpha_{sign}}{\alpha_{refl}}\right) = 20 \cdot \log_{10}\left(\frac{1}{\alpha}\right) \text{[dB]} \tag{6.1}$$

where α_{sign} is the direct signal amplitude and α_{refl} is the multipath amplitude. In this way the typical relative attenuation $\alpha = 0.5$ corresponds to the Signal-to-Multipath power Ratio $SMR = 6\,\text{dB}$.

6.3.2 Signal and receiver parameters

The code multipath error is also influenced by the features of the received signal and by the receiver setup.

The multipath performances of the AltBOC modulation are very promising for the large bandwidth of the transmitted signal and for the high code rate that will be used for the four E5 channels.

In detail the spreading codes that will be used in E5 band will have a **code rate** $R_C = 10.23\,\text{Mchip/s}$, that is ten times the chip rate of the existing GPS C/A codes. Considering this feature and also the fact that the ranging codes will be very long (thanks to the *tiered code structure*), the processing gain of the codes will be higher than the one of GPS, ensuring better performance. About the code multipath error, it must be noticed that the receiver uncertainty between the direct path and the reflected signals will be scaled with the chip length: using shorter chips with an high chip rate, the multipath could produce a lower bias in the DLL, causing smaller ranging errors.

Besides the **AltBOC modulation** will intrinsically have better multipath performances than other modulations planned for the Galileo system, as outlined in some articles and shown in Figure 6.6.

The **signal bandwidth** is another important parameter that will influence the receiver performances. The AltBOC signal will be transmitted from Galileo satellites with a large bandwidth (92.07 MHz [4]), that will include

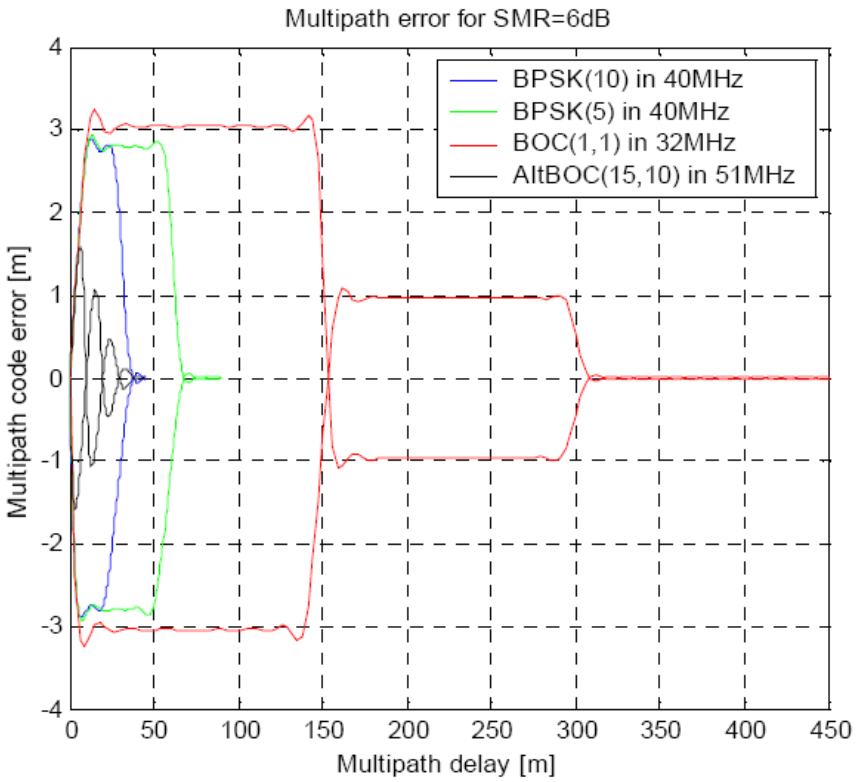

Figure 6.6: Comparison of the code multipath error envelopes for different modulations planned for Galileo, for a Signal-to-Multipath power Ratio of 6dB [11]

both the E5a and E5b sidebands. A wideband signal typically brings to better multipath performances, because it is possible to obtain a steeper discriminator function (with narrow correlation spacing), less sensitive to multipath distortions. But it must also consider that the maximum receiver bandwidth, also called **pre-correlation bandwidth**, is limited essentially by two reasons:

- **receiver complexity**: a very large bandwidth imply an expensive hardware for the receiver, because higher sampling frequency are necessary and the implementation of wideband components is more complex;
- **interfering signals**: receivers of Galileo signals transmitted in E5a or E5b bands will have to tolerate *Distance Measuring Equipment* (DME) and *Tactical Air Navigation* (TACAN) transmissions for aeronautical civil users, and also *Multifunction Information Distribution System* (MIDS) and *Joint Tactical Information Distribution System* (JTIDS) transmissions in the same frequency bands for military users. They will also have to tolerate out-of-band emissions of Radars transmitting in the L2 frequency band [50]. The effects of these pulsed interferences could be mitigated using digital pulse blanking techniques [14], but it

is also crucial to reduce the receiver filter bandwidth, in order to filter only the useful signal and to reduce the interference power.

Recalling the receiver architectures proposed in Chapter 4, it must be noted that the receiver bandwidth influence also the shape of the **correlation function**. In fact, choosing to receive only one sideband of the AltBOC signal spectrum, the correlation function has the same shape of a BPSK signal (triangular shape), whilst with a coherent dualband receiver it is possible to obtain the *combined complex correlation function*, previously described (see Section 3.4). The two correlation functions are plotted in Figure 6.7, assuming to use ideal receivers with infinite bandwidth[1].

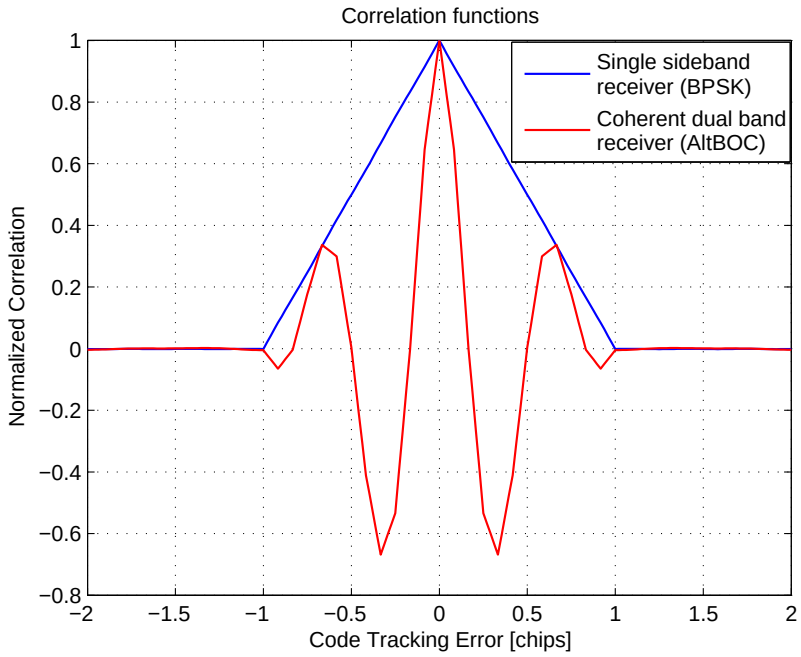

Figure 6.7: Comparison of the correlation functions for the single sideband and the dual band receivers, simulated with infinite bandwidth

It must be noticed that the triangular correlation is obtained both with the *single band receiver* (*CC-SSB tracking*) and the *separate dual band receiver* (the first two architectures presented in Chapter 4), because both process the received signal as two adjacent BPSK modulations in E5a and E5b sidebands. On the contrary, the multipeak correlation function is achieved only with the *coherent dual band receiver* (the third architecture in Chapter 4), that fully

[1]The normalized correlation functions has been obtained simulating the E5 AltBOC(15,10) signal oversampled with 48 samples per code chip, with infinite bandwidth (without any signal filtering), and correlating the signals with an integration time of 1 ms (1 primary code period). The ordinate axis of the graphs are normalized with the peak of the correlation function, so that the amplitude of the function is independent on the sampling frequency.

exploits the complex correlation function of the AltBOC using a wideband setup. This oscillating correlation function has a sharper main peak, that leads to better performances in presence multipath; however the presence of secondary peaks implies also an ambiguity issue for the acquisition and the tracking of the correlation peak, that could be resolved using ad hoc unambiguous acquisition and tracking techniques, as in BOC signals (e.g. see the bump-jumping algorithm in [32] or the technique in [42]).

The correlation function is affected by the receiver bandwidth because a narrow filter causes a loss in the correlation peak. As shown in Figure 6.8 for a single sideband receiver, a bandwidth reduction implies a correlation loss, because the peak is slightly reduced and the correlation function is distorted[2]. It is then important to use a wide bandwidth to achieve good performance.

But a large bandwidth, as previously discussed, is a real issue for the receiver complexity and cost and for the vulnerability of interfering signals, that could degrade the performance. It is then possible to find an optimal value for the receiver bandwidth, as a compromise between correlation losses and interference rejection. Obviously this value strongly depends on the receiver architecture (single or dual band, type of filters used, etc.) and on the presence of other interfering signals.

For a *single sideband receiver* it is also important to use a narrow bandwidth to reduce the code cross-correlation effects with the other Galileo channels. In fact, assuming to process only the E5a signal, if the receiver bandwidth is too large the codes of the Galileo channels in E5b could cross-correlate with the locally generated code, causing losses and distortions in the correlation function.

In Reference [8] an **optimal filtering bandwidth** of around **30 MHz** is evaluated for the single band receiver (*CC-SSB tracking*), considering the detrimental effect of the code cross-correlations. This value for the receiver bandwidth seems a good compromise between the correlation losses caused by the limited bandwidth, the interference vulnerability and the receiver complexity and cost.

The obtained optimal value of 30 MHz is greater than the typical value of 24 MHz suggested in older articles (for example in [9]), where the E5 signal was still proposed to be generated with two QPSK(10) signals, filtered in 24 MHz and transmitted separately in the two E5a and E5b sidebands. With the wideband AltBOC signal generation it is now possible to receive a single sideband with a larger bandwidth, obtaining better performance.

Otherwise, using the *coherent dual band architecture*, the recommended receiver bandwidth is **51.150 MHz**, as pointed out in the Galileo SIS-ICD [4]. This value, named **received reference bandwidth**, is the smallest possible

[2]For the correlations in Figure 6.8 and following, there was adopted the same simulation setup used for Figure 6.7, apart from the filtering effect: the signal has been filtered with a Butterworth filter with order 16.

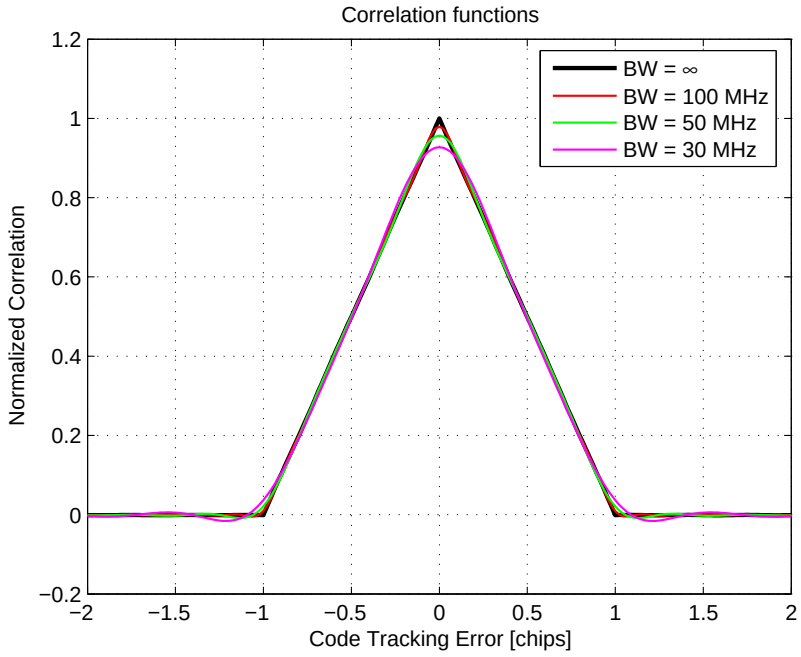

(a)

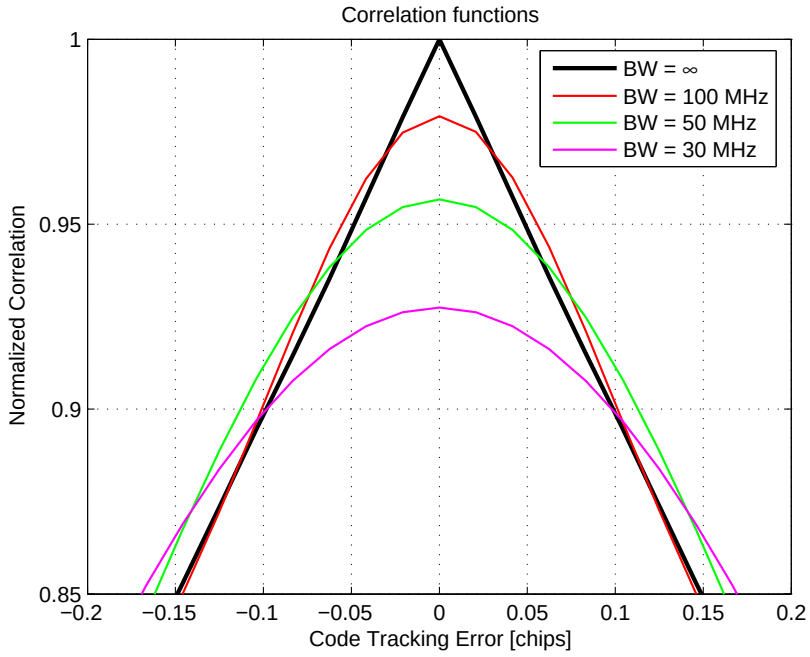

(b)

Figure 6.8: Comparison of the BPSK correlation peak, obtained processing only E5a for different signal bandwidths: shape of the correlation functions varying the bandwidth (a) and zoom around the correlation peak (b)

bandwidth that contains the two main lobes (E5a and E5b) of the AltBOC signal, and could be calculated with the following expression:

$$\begin{aligned} BW_{min}^{AltBOC} &= 2 \cdot (R_C + R_{S,E5}) \\ &= 2 \cdot (10.23\,\text{MHz} + 15.345\,\text{MHz}) = 51.150\,\text{MHz} \end{aligned} \quad (6.2)$$

In fact the two main lobes of the AltBOC spectrum have a spectral width of $2 \cdot R_C$, and the E5a and E5b center frequency are separate by $2 \cdot R_{S,E5}$, as shown in Figure 6.9.

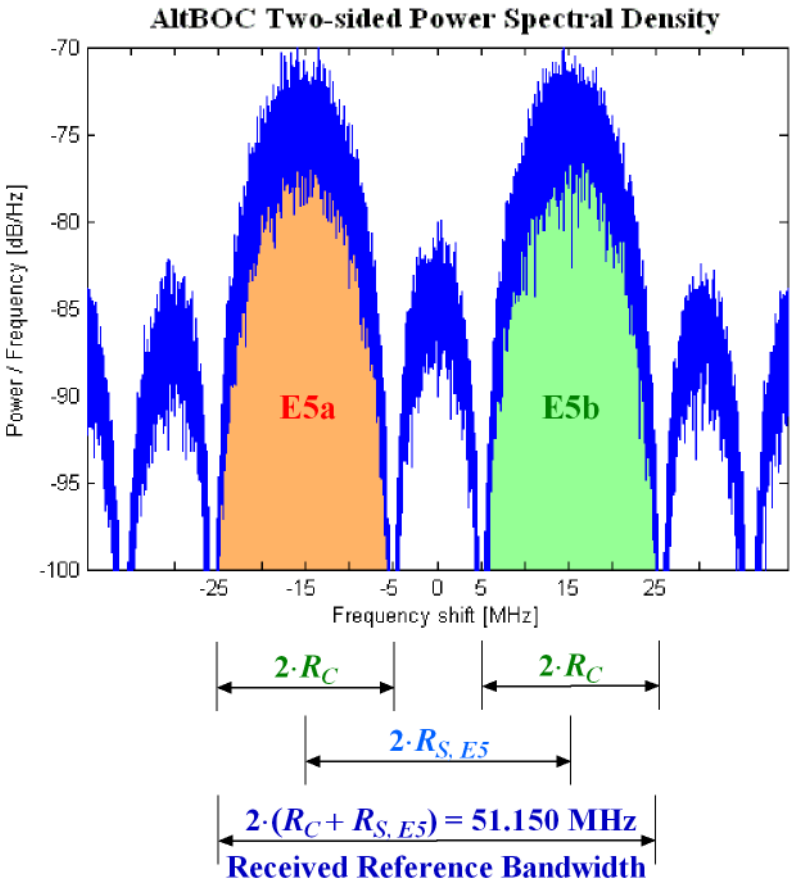

Figure 6.9: Illustration of the AltBOC received reference bandwidth

As previously noted for the BPSK correlation peak, a limited bandwidth introduces a correlation loss also for the AltBOC correlation peak, that could be seen in Figure 6.10. But in this case, a bandwidth of 51.150 MHz causes a slight reduction of the correlation peak and the shape of the correlation function is not significantly affected.

The analysis performed in [11] demonstrates that further increasing the receiver bandwidth above 50 MHz, the performance improvement is then negligible. In fact the multipath envelopes in Figure 6.11 show that the multipath error is not significantly reduced increasing the bandwidth, and this implies a major receiver complexity and interference vulnerability.

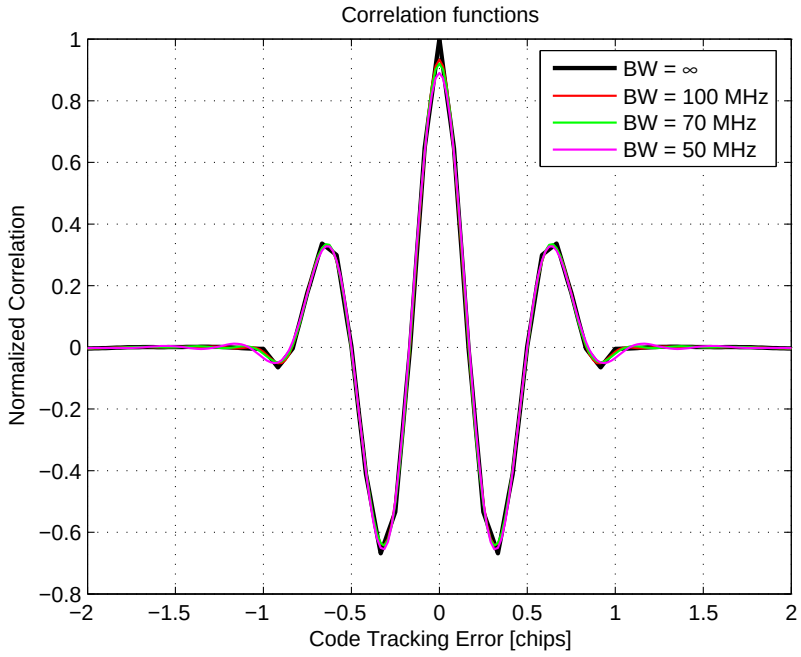

Figure 6.10: Comparison of the AltBOC complex correlation peak for different signal bandwidths

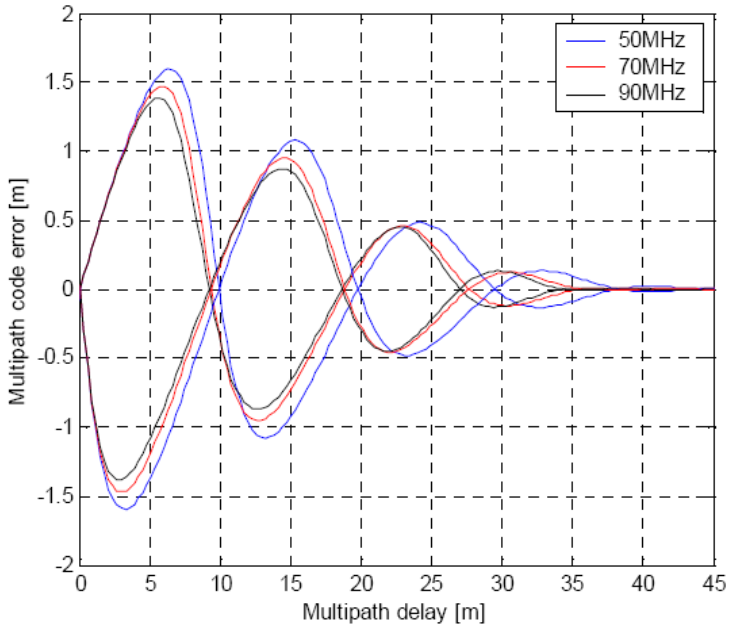

Figure 6.11: Comparison of the AltBOC code multipath error envelopes for different signal bandwidths [11]

It is possible to conclude that for the *coherent dual band architecture* the optimum bandwidth value is near 50 MHz. For example the Galileo receiver implemented in [31] uses for the AltBOC signal a bandwidth of 56 MHz. Then

the previous value of 51.150 MHz seems to be a good compromise between the correlation losses, the receiver complexity and the interference rejection, and will be used in the following as the optimal bandwidth for the AltBOC receiver (the same optimal value will be used also for the *receiver with the correlator-discriminator*, in Section 6.6).

In Figure 6.12 there are plotted the resulting correlation functions for the two receiver architectures, using the optimal filter bandwidths previously discussed.

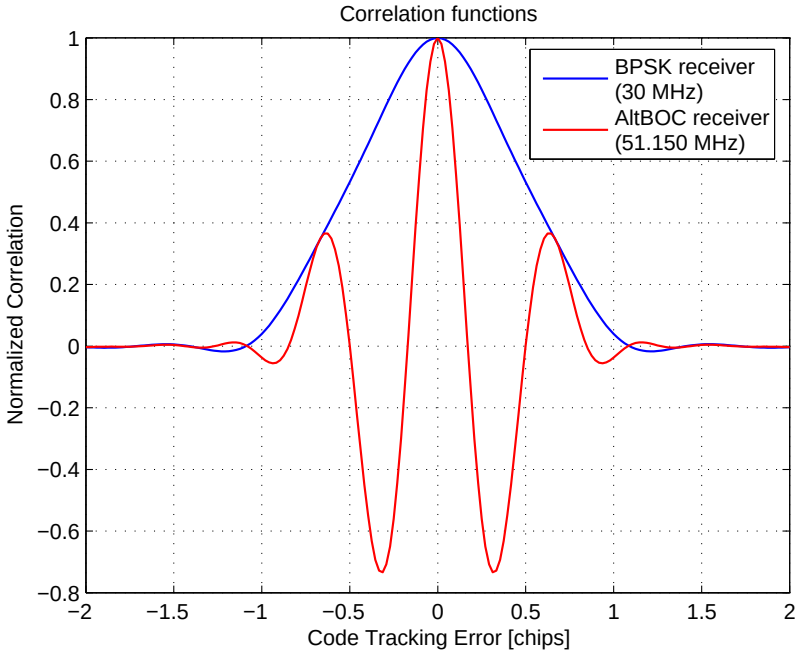

Figure 6.12: Comparison of the correlation functions for the single sideband and the dual band receivers, simulated with their optimal receiver bandwidths

Comparing Figure 6.12 with Figure 6.7 (finite vs infinite bandwidth), it is possible to see the correlation loss caused by the filter, that slightly reduces the correlation peaks and smooths the functions. However the correlation functions in Figure 6.12 will be assumed as reference for the multipath analysis performed in following Sections.

The last important receiver parameters that influence the multipath performance are the **discriminator type** and the **correlators spacing**. In fact the choice of the discriminator implies different shapes of the discriminator function, and its slope is connected with the correlator spacing; then these parameters could lead to different code multipath errors.

A detailed analysis of the impact of the discriminator setup on the multipath errors will be performed in following Sections, considering current and emerging multipath mitigation techniques, applied to the receiver architectures previously discussed in Chapter 4.

6.4 Current multipath mitigation techniques

In this Section there are examined the receiver-internal correlation techniques, that are currently used in common GPS receivers to minimize the code multipath errors. In fact it can be stated that multipath mitigation can be achieved through judicious shaping of the discriminator function used in the DLL. The purpose of this Section is to try to apply the common discriminator-based multipath mitigation techniques to the AltBOC receiver architectures presented in Chapter 4, and to assess their multipath performances.

As a first step, every correlation technique is briefly introduced with respect to its basic functionality and implementation. In a second step, the performances of these multipath mitigation concepts are assessed, using multipath error envelopes and running average of multipath error envelopes to compare the performances of different receiver architectures.

All the simulations carried out for this Section have been performed using programs written in the thesis framework, using MATLAB® language. The simulation parameters used in the following (previously discussed in Section 6.3) are summarized in Table 6.1.

Receiver parameters	**BPSK receiver**	**AltBOC receiver**
Frequency band	E5a	E5
Center frequency	1176.45 MHz	1191.795 MHz
Modulation type	BPSK(10)	AltBOC(15,10)
Tracked channels	E5aQ	E5aQ + E5bQ
Chipping rate	10.23 Mchip/s	10.23 Mchip/s
Chip length	29.31 m	29.31 m
Pre-correlation bandwidth	30 MHz (two-sided)	51.150 MHz (two-sided)
Pass-band filter	Butterworth filter with order 16	Butterworth filter with order 16
Integration time	1 ms (10230 chips)	1 ms (10230 chips)
SMR	6 dB ($\alpha = 0.5$)	6 dB ($\alpha = 0.5$)

Table 6.1: Receiver parameters used for the simulations for the multipath performance assessment

It must be noticed that the multipath performance of the *single band receiver* and the *separate dual band receiver* (presented in Chapter 4) will coincide with these of a generic BPSK(10) receiver. In fact the two arrangements are based on the same signal processing, receiving the AltBOC signal as separate BPSK modulations in adjacent sidebands. With the second arrangement both the sidebands are received, so the code correlation peak is doubled. Nevertheless the multipath impact on the codes is the same, because also

the wrong correlation peak due to the reflected signals is doubled, then the multipath performances of the two receivers are exactly the same.

The *separate dual band receiver* shows only advantages in presence of noise, whereas its multipath performance are the same of the *single band receiver*. Accordingly, the multipath performance of the two BPSK receiver architectures will be simultaneously assessed using a generic **BPSK receiver** setup (that for simplicity is the single band arrangement, tracking only the E5aQ channel), and will be compared with the performances of the *coherent dual band architecture* (called **AltBOC receiver** in Table 6.1), that exploits the wideband AltBOC signal with the complex correlation of the two pilot channels.

It must also be noted that the simulations performed in this Chapter have been carried out supposing that the received signal $s_{E5}(t)$ is composed only by the two pilot channels and switching off the other two data channels in the AltBOC modulation. This choice is necessary to avoid the bias errors in the multipath error envelopes, due to the cross-correlations between the codes: this bias error is typically neglected in GNSS receivers, because is very small and is overcome by noise and other error sources (for more details see Appendix A), but it becomes evident plotting multipath envelopes and must be avoided, switching off the not used codes.

6.4.1 Wide (standard) correlator

The **wide** (or standard) **correlator** is computed by subtracting an early and a late sample of the correlation functions (illustrated in Figure 6.12) using a chip-spacing of 1 chip, that is the spacing between the early and the late correlators. This means that the discriminator function (also called *S-function*, for its shape) is evaluated using the correlation values obtained with two replicas of the locally generated code, one delayed by 0.5 chip, and the other 0.5 chip early.

In detail the received signal is multiplied by its early and late local versions, and these signals are then passed through an integrator block, to complete the correlation process. The discriminator function $\mathcal{D}_{WIDE}(\tau)$ is then formed subtracting the outputs of the integrators, that are values of the correlation function $\mathcal{C}(\tau)$.

Finally, the normalized[3] form of the **discriminator function** $\mathcal{D}_{WIDE}(\tau)$ for the wide correlator is defined with the following expression:

$$\mathcal{D}_{WIDE}(\tau) = \mathcal{C}(\tau + 0.5) - \mathcal{C}(\tau - 0.5) \tag{6.3}$$

where τ is the DLL tracking error in chips and $\mathcal{C}(\tau)$ is the correlation function.

[3]The normalization of $\mathcal{D}_{WIDE}(\tau)$ is intended using the correlation functions $\mathcal{C}(\tau)$ with the peak normalized to one.

This discriminator expression is used with **coherent receiver** architectures, where the DLL is coherent and requires a PLL. The non-coherent DLLs (early-late power discriminator) can not be used with AltBOC receivers, because with the coherent dual band architecture it is indispensable to coherently track the carrier phase, to correctly perform the complex correlation. Thus, in the following, only coherent discrimination functions are considered.

In Figure 6.13 there are plotted the discriminator functions with the wide correlator, for the two receiver architecture previously discussed (see the parameters listed in Table 6.1).

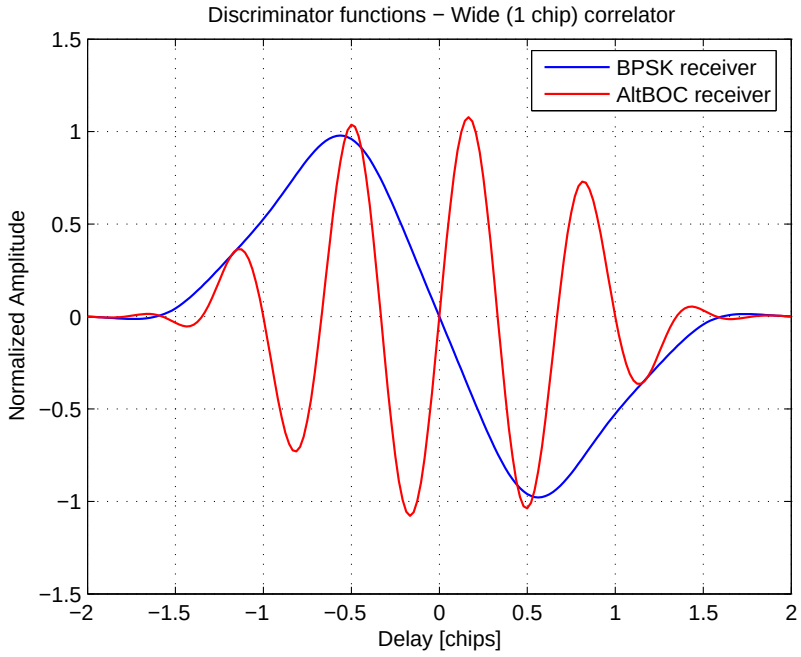

Figure 6.13: Code discriminators for the wide (standard) correlator

It must be noticed the presence of multiple zero-crossings for the discriminator function of the AltBOC receiver. This implies an ambiguity in the tracking loop, that must be resolved using ad-hoc unambiguous acquisition and tracking techniques, as in BOC receivers (e.g. see the bump-jumping algorithm in [32] or the technique in [42]). Furthermore, with the AltBOC arrangement in the correct zero-crossing the discriminator has opposite slope than with the BPSK receiver. Neglecting these ambiguity problems, the discriminator function with the AltBOC receiver is steeper than with the BPSK receiver: this peculiarity could lead to better tracking performances in presence of multipath and noise.

In presence of multipath, examining the BPSK receiver, the reflected component produces a secondary correlation peak that affects the shape of the correlation function of the direct signal, as shown in Figure 6.14(a). In this example, a single reflected signal in phase with respect of the direct path

component, with a delay of half chip and a relative amplitude of $\alpha = 0.5$ ($SMR = 6$ dB), causes an evident alteration of the shape of the correlation function, that is skewed and non-symmetric. The discriminator function in Figure 6.14(b) is then distorted, and its zero-crossing is shifted, introducing a bias in the lock point of the tracking loop. As previously mentioned, this bias causes ranging errors in the receiver.

The same considerations are valid for the AltBOC receiver. Obviously, varying the delay of the reflected signal, the discriminator function is distorted differently and in this way it is possible to evaluate the multipath error envelopes. Figure 6.15 illustrates the multipath performance of the two receiver architectures, with multipath envelopes and running averages.

Both the receiver architectures shows a good overall multipath performance, due to the high chipping rate ($R_C = 10.23\,\text{Mchip/s}$) and the very short chip length. The multipath envelopes in Figure 6.15(a) demonstrate that the two receivers are only sensitive to short-delay multipath: for path delays greater than 50 meters the multipath ranging errors are negligible. However, the AltBOC receiver outperforms the BPSK receiver with respect to its maximum ranging error, which is approximatively three times smaller than that of the BPSK receiver. Besides the error envelope with the AltBOC arrangement exhibits delays with null ranging error, for delays shorter than 50 meters: this is a typical feature of BOC modulations (see [38]).

The better performances of the AltBOC receiver with the wide correlator is also demonstrated with the running average of multipath error envelopes, in Figure 6.15(b). The AltBOC arrangement clearly shows the smallest average error.

6.4.2 Narrow correlator™

The **narrow correlation technique**, first proposed for GPS receivers in 1992 by NovAtel Inc. (see [43]), is a first approach to reduce the influences of code multipath errors.

It is possible to generalize the discriminator expression of the wide correlator in Equation (6.3), using a variable spacing d between the early and the late correlators:

$$\mathcal{D}^{d}_{NARROW}(\tau) = \mathcal{C}\left(\tau + \frac{d}{2}\right) - \mathcal{C}\left(\tau - \frac{d}{2}\right) \tag{6.4}$$

Instead of use a standard correlator with a spacing of $d = 1$ chip between early and late code, the chip spacing d of a narrow correlator is chosen less than 1 chip, as shown in Figure 6.16 (where the early correlator is denoted with E and the late correlator with L).

There are remarkable advantages in narrowing this spacing: those are primarily the reduction of tracking errors in presence of both noise and multipath. However, the narrow correlator™ implies also different disadvantages:

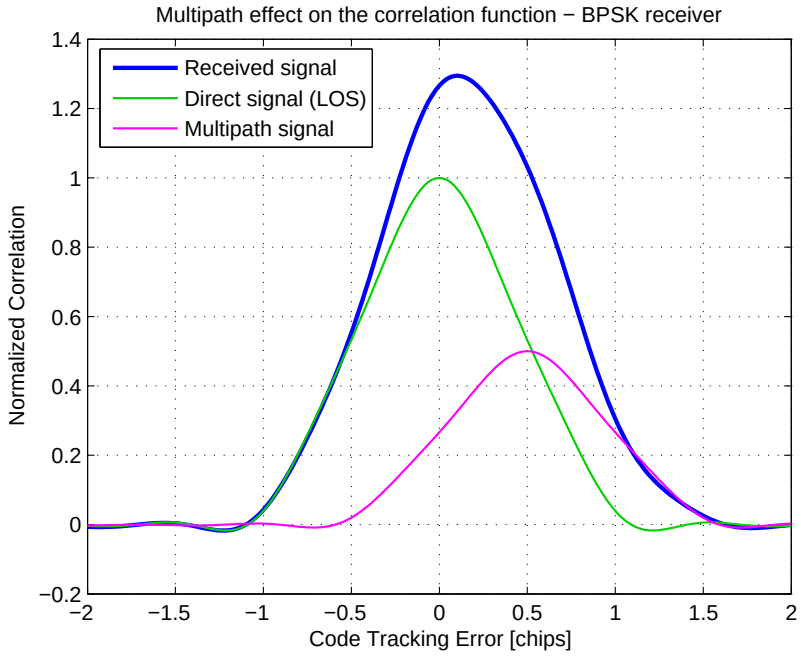

(a)

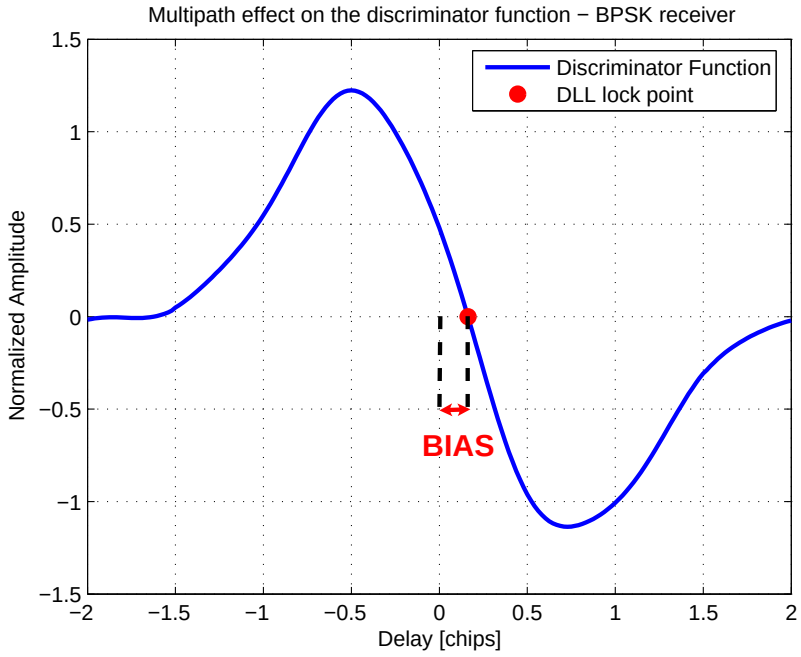

(b)

Figure 6.14: Multipath effect in BPSK receiver with wide correlator: alteration of the correlation function (a) and discriminator function distortion (b), assuming a reflected signal in phase with respect of the direct component, delayed by 0.5 chip and with $\alpha = 0.5$

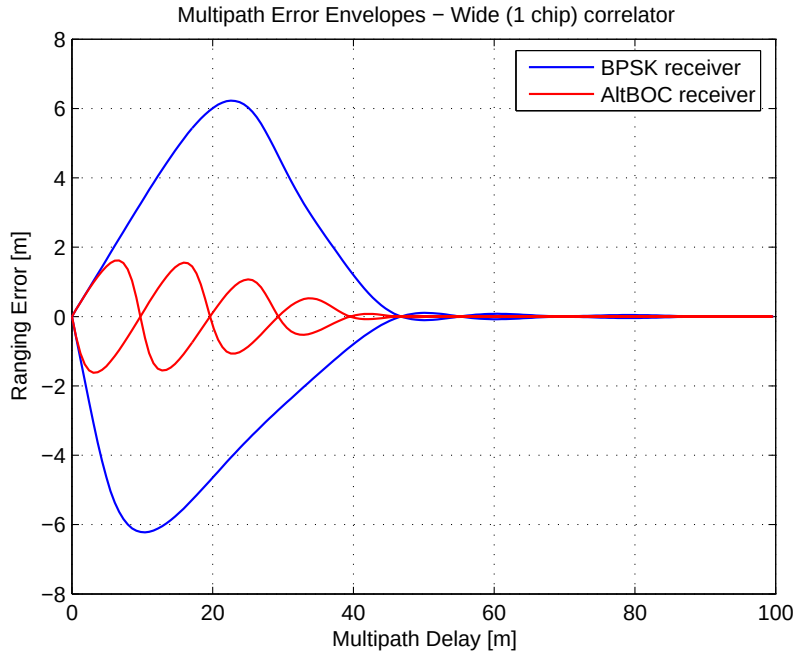

(a)

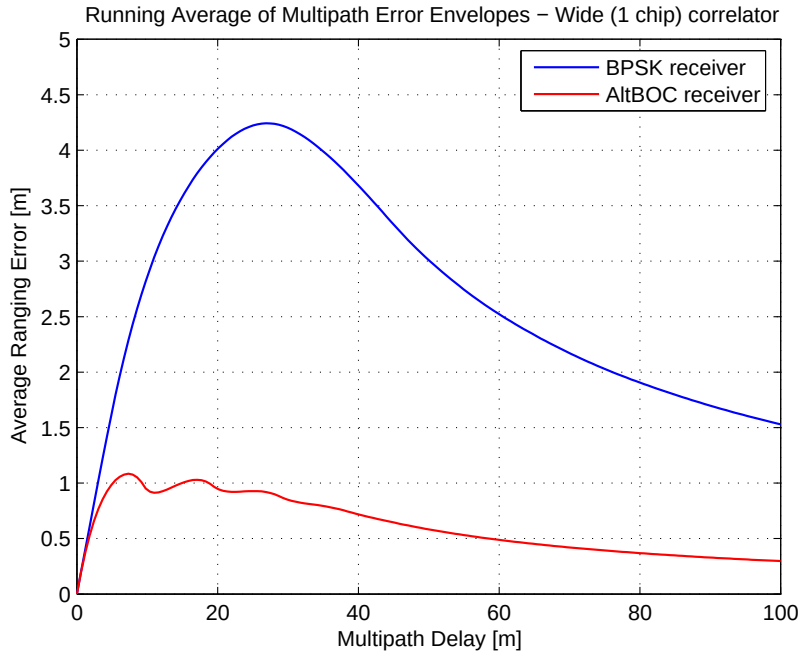

(b)

Figure 6.15: Multipath performances with the wide (standard) correlator: multipath error envelopes (a) and running average of multipath error envelopes (b), for the two receiver architectures

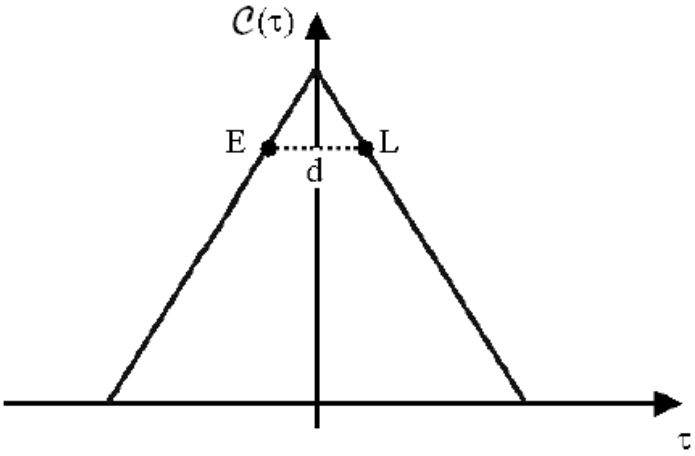

Figure 6.16: General concept of the narrow correlator™

a wider pre-correlation bandwidth is required and higher sample rate and higher processing capabilities are needed.

One key concept in receiver design is the selection of the clock epoch used to locally generate the early, punctual and late codes, to provide variable spacing between those codes, depending upon the operation mode. To achieve this goal, modern GNSS receivers use a non-integer ratio between the code rate and the clock frequency. This means that for every chip there are a non-integer number of samples and some chips results with a spare sample: the tracking loop works on these "special chips" for the code fine synchronization. This trick allows practically all correlator spacings.

As for the wide correlator, also the narrow correlator™ could be used with the AltBOC signal. In Figure 6.17 there is a comparison between the multipath envelopes of the two receiver architectures, using the narrow correlator™ and varying the correlator spacing between 1 chip (wide correlator) and 0.1 chip.

For the BPSK arrangement in Figure 6.17(a), it must be noted that the performance improves narrowing the correlator spacing. The maximum ranging error for $d = 0.1$ chip is divided by two with respect of that one of the wide correlator. Besides, the envelope decreases more quickly to zero, showing less sensitivity to multipath with long path delay.

Conversely, a narrow spacing does not significantly improve the multipath performances of the AltBOC receiver, as illustrated in Figure 6.17(b). With $d = 0.1$ chip the maximum ranging error is only slightly smaller than with the wide correlator.

It must also be noted that for $d = 0.5$ chip the maximum ranging error is slightly greater. This effect is typical with BOC modulations: the correlator spacing must be chosen carefully or the receiver performances could result

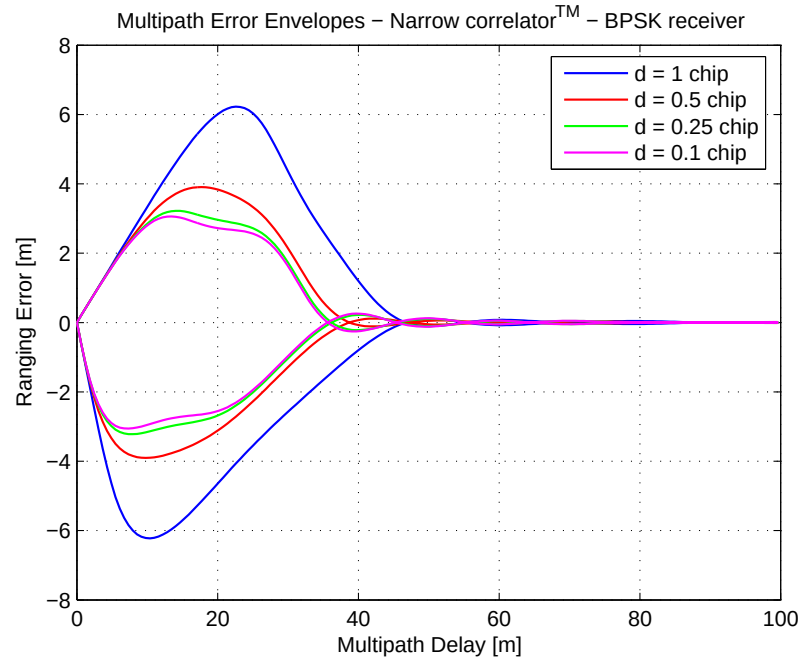

(a)

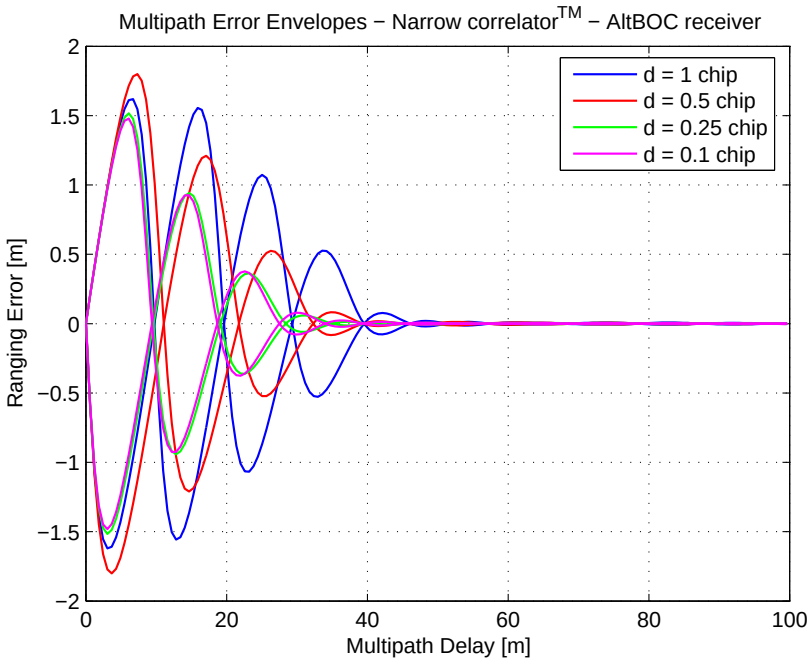

(b)

Figure 6.17: Multipath error envelopes for a narrow correlator™ using different correlator spacings, for the BPSK receiver (a) and the AltBOC receiver (b)

degraded in presence of noise and multipath, because the shape of the discriminator function strongly depends on the correlator spacing. As demonstrated in [39], some chip spacings are not appropriate because they lead to very bad code tracking accuracy, in presence of thermal noise: this occurs if the early and late tracking points are located at the positive or negative peaks of the code correlation function, or at points where the correlation function crosses the x-axes. Besides, an inattentive choice of the correlator spacing could also lead to a discriminator function with smaller slope in the zero crossing point, causing worse multipath performances.

Another important issue that must be considered choosing an optimal correlator spacing is that it is not recommended to use a too narrow spacing. In fact using $d < 0.1$ chip the receiver becomes very complex and expensive (higher sampling frequency and pre-correlation bandwidth), but its performances do not improve significantly. This is due primarily to the bandlimiting effect, that smooths the correlation peak and does not allow further performance improvements.

Besides, the use of narrow correlator spacing together with short code chip lengths (as it is the case for the E5 AltBOC signal) might not be feasible because these two parameters define the tracking threshold of the DLL. In fact, this threshold is directly proportional to the correlator spacing d and the code chip length c/R_C (as stated in [39]), then with a too narrow correlator spacing the receiver becomes more sensitive to noise, showing worse ranging accuracy.

Usually, a spacing of $d = 0.1$ chip is used in GPS receivers to build up the discriminator function (as done in [38]). Considering the AltBOC signal, this value could also be considered as a typical value for the narrow correlator ™. For the two receiver architectures introduced above, further simulations have demonstrated that a spacing of $d < 0.1$ chip does not improve significantly the multipath performances. Accordingly, the resulting multipath error envelopes and running average have been computed using a spacing of $d = 0.1$ and are illustrated in the diagrams in Figure 6.18.

As it is the case for the wide correlator, the AltBOC receiver outperforms the BPSK receiver with respect to its maximum ranging error, which is much smaller than the other one. Considering the AltBOC receiver, there are only slight differences between the multipath performance obtained with the wide correlator (see Section 6.4.1) and the multipath performance obtained with the narrow correlation technique: in both cases, the maximum ranging errors for the AltBOC are nearly identical. On the other hand, the maximum ranging error of the BPSK receiver is significantly smaller when processed with the 0.1-chip narrow correlator ™ instead of the wide correlator. Both receivers continue to be only sensitive for short-delay multipath and show a very good overall multipath performance, but it is possible to conclude that only the BPSK receiver takes advantage narrowing the correlator spacing, whilst the performances of the AltBOC receiver do not improve appreciably.

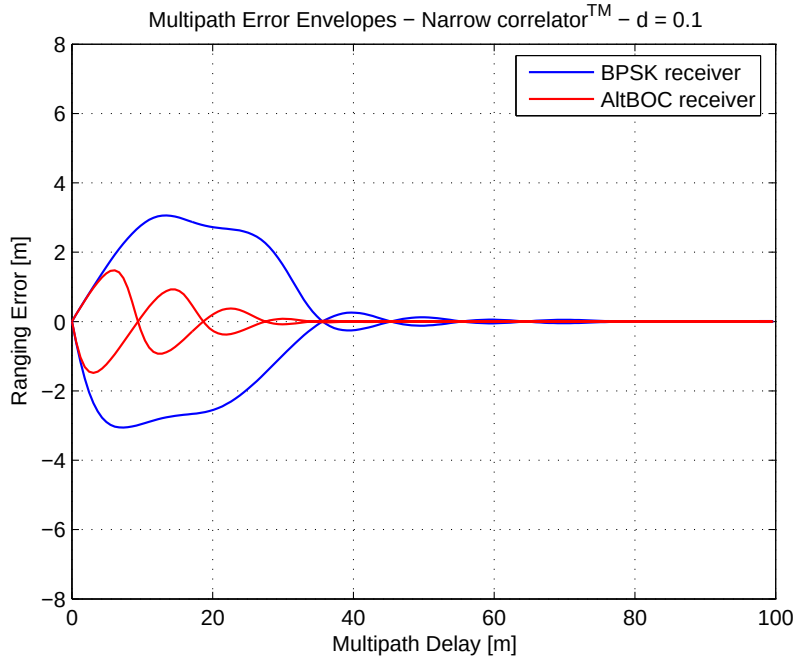

(a)

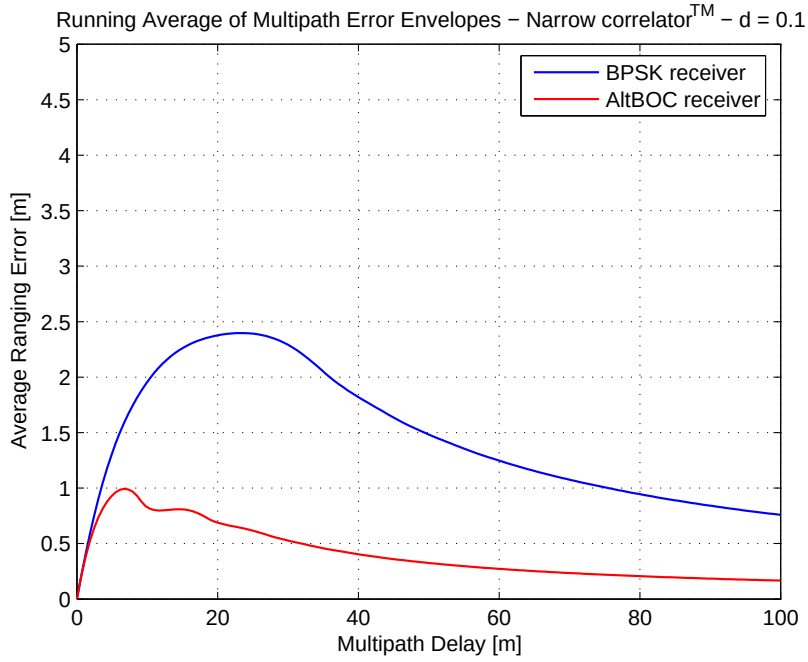

(b)

Figure 6.18: Multipath performances with the narrow correlator™, using a spacing of $d = 0.1$ chip: multipath error envelopes (a) and running average of multipath error envelopes (b), for the two receiver architectures

6.4.3 Double Delta correlator

The term "Double Delta ($\Delta\Delta$) Correlator" is a general expression for special code discriminators which are formed by two correlator pairs instead of only one.

As observed in [38], this general tracking concept is used to set up several type of discriminator functions, with similar performances. The first type is the so-called **High Resolution Correlator** (HRC, presented in detail in [44]), that will be analyzed in the following. As will be shown below, also the **Strobe Correlator**^{TM} (invented by Ashtech Inc.) is one implementation of the $\Delta\Delta$ correlation concept. Another implementation of the $\Delta\Delta$ correlator seems to be the **Pulse Aperture Correlator**^{TM} (PAC) introduced by NovAtel Inc. The multipath error envelopes obtained with the PAC technique show the same overall behavior than the error envelope obtained with the HRC or the Strobe correlator, also if they might slightly differ with respect of their actual implementation.

The $\Delta\Delta$ code discriminator can be set up by forming a linear combination of two early and two late correlators. The basic concept is illustrated in Figure 6.19, where a generic triangular correlation function $\mathcal{C}(\tau)$ is used to show the position of the two early correlators (denoted as E_1 and E_2) and the two late correlators (L_1 and L_2). The spacing between E_1 and L_1 is denoted as d and the spacing between E_2 and L_2 is assumed to be $2d$.

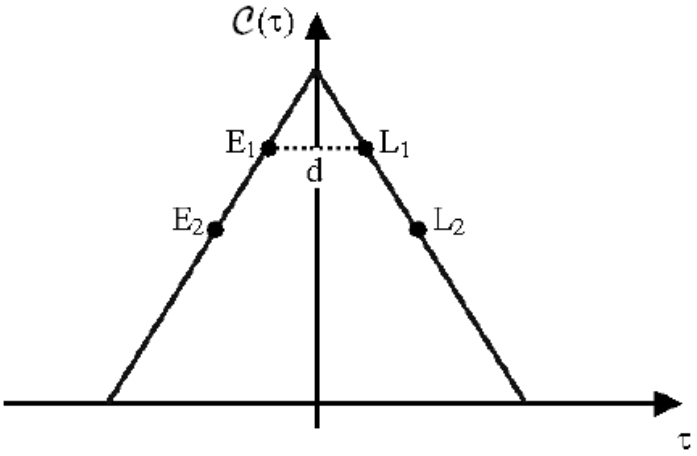

Figure 6.19: General concept of the $\Delta\Delta$ correlator [38]

In principal, several code discriminators may be set up by forming different linear combinations out of these four correlators. For the **High Resolution Correlator**, the following linear combination is used to build up the code discriminator $\mathcal{D}_{HRC}$:

$$\mathcal{D}_{HRC}(\tau) = (E_1 - L_1) - \frac{1}{2} \cdot (E_2 - L_2) \tag{6.5}$$

Since the differences $(E_1 - L_1)$ and $(E_2 - L_2)$ can be interpreted as narrow correlators, previous equation can be rewritten as follows:

$$\mathcal{D}_{HRC}(\tau) = \mathcal{D}^{d}_{NARROW}(\tau) - \frac{1}{2} \cdot \mathcal{D}^{2d}_{NARROW}(\tau) \tag{6.6}$$

$$= \mathcal{C}\left(\tau + \frac{d}{2}\right) - \mathcal{C}\left(\tau - \frac{d}{2}\right) - \frac{1}{2} \cdot \left[\mathcal{C}\left(\tau + d\right) - \mathcal{C}\left(\tau - d\right)\right] \tag{6.7}$$

The discriminator function of the HRC has the same shape as that of the **Strobe Correlator**™, which has been introduced to Ashtech's GPS receivers. Considering previous equations, the Strobe Correlator™ can be expressed as follows:

$$\mathcal{D}_{STROBE}(\tau) = 2 \cdot \mathcal{D}^{d}_{NARROW}(\tau) - \mathcal{D}^{2d}_{NARROW}(\tau) \tag{6.8}$$

$$= 2 \cdot \mathcal{D}_{HRC}(\tau) \tag{6.9}$$

Since the code multipath performance only depends on the shape of the discriminator function and not on its relative amplitude, both discriminators will result in identical code multipath error envelopes. Therefore the following analysis has been carried out only for the discrimination function of the HRC, using a correlator spacing of $d = 0.1$ chip. This one corresponds to the relative positions (τ_1, τ_2, τ_3 and τ_4) for the four correlators (respectively E_2, E_1, L_1 and L_2) listed in Table 6.2.

Correlators	E_2	E_1	L_1	L_2
Positions [chips]	$\tau_1 = -0.1$	$\tau_2 = -0.05$	$\tau_3 = +0.05$	$\tau_4 = +0.1$

Table 6.2: Correlator positions used for the High Resolution Correlator

Accordingly, the resulting multipath error envelopes and running average have been computed for the two receiver architectures introduced above, using the HRC, and are illustrated in the diagrams in Figure 6.20. In Figure 6.21 there are also the corresponding discriminator functions.

Comparing the performances of the High Resolution Correlator with these ones of the 0.1 chip narrow correlator™ (in Figure 6.18), it must be noticed that only the BPSK receiver architecture take advantage of the more complex operations required for the HRC, showing slightly smaller multipath errors. On the contrary, the AltBOC receiver does not improve its performances with this arrangement, then the complexity increase due to the two needed additional correlators is not convenient.

Another issue that must be highlighted with the AltBOC receiver is the presence of **false lock points** in the discriminator function, as shown in Figure 6.21(b). This problem is due to the shape of AltBOC complex correlation, that has multiple zero-crossing points. Then the discriminator function

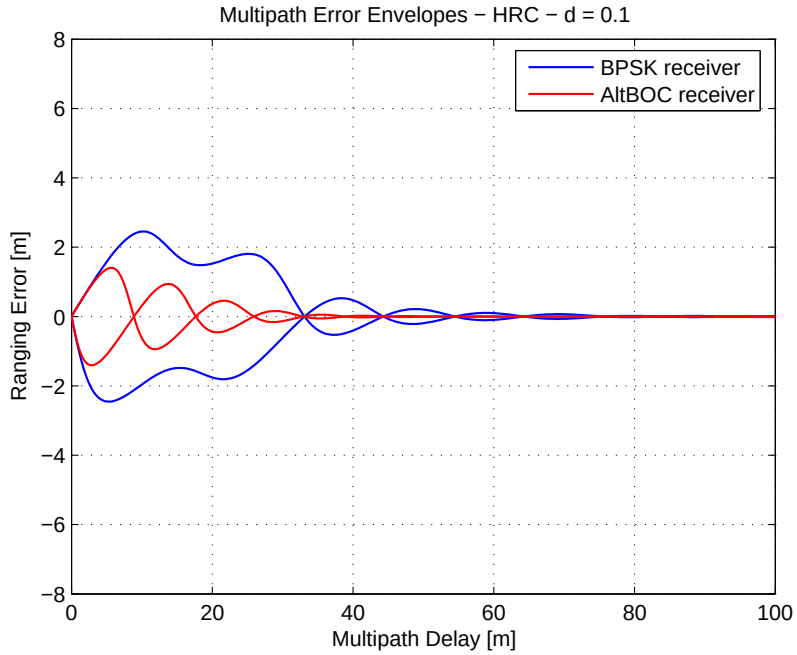

(a)

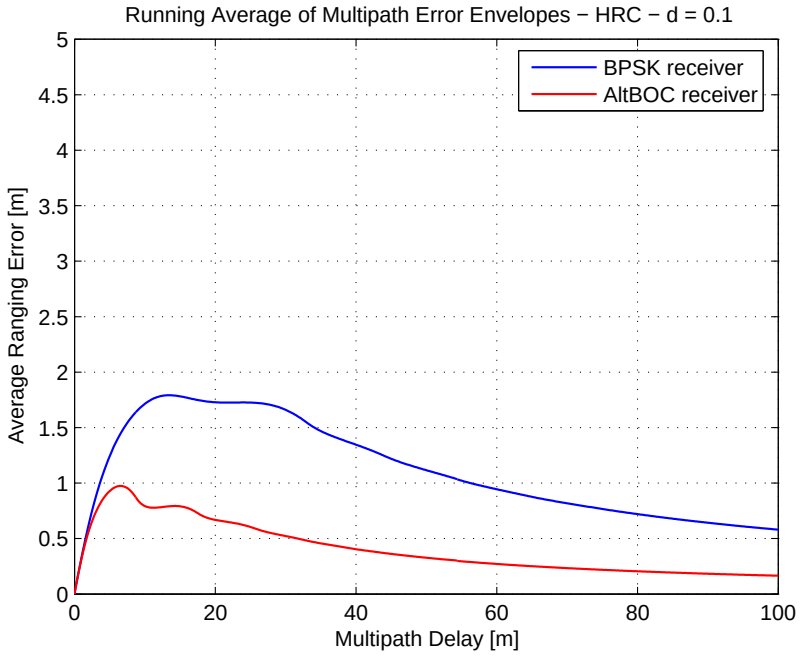

(b)

Figure 6.20: Multipath performances with the double delta correlator, using a spacing of $d = 0.1$ chip: multipath error envelopes (a) and running average of multipath error envelopes (b), for the two receiver architectures

presents multiple zero-crossings with the correct slope, where the tracking loop could lock, leading to a bias error. If the DLL is not able to select the correct lock point, also in presence of strong multipath, a major error can be experienced.

In conclusion, the double delta correlation technique is not recommended for the AltBOC receiver, whereas it could improve the multipath performances of the BPSK receiver.

6.4.4 Early/Late Slope technique

The general idea behind the **Early/Late Slope** (ELS) technique is to determine the slope at both sides of the correlation function's central peak (as illustrated in Reference [45]). Once both slopes are known, they can be used to compute a pseudorange correction that can be applied to the measured pseudorange. This multipath mitigation technique has temporarily been used in some of NovAtel's GPS receivers, where it has been called *Multipath Elimination Technology* (MET™).

The principle of forming the pseudorange corrections is illustrated in Figure 6.22. The slope on each side of the correlation function is determined by means of four correlators (K_1,...,K_4): two per side with fixed positions determined with the respective τ-coordinate (τ_1,...,τ_4). The correlators are used to determine the corresponding ordinates (y_1,...,y_4) of the correlation function. By use these ordinates, the slopes a_1 and a_2 can be determined and two first order polynomials (defined by K_1,K_2 and K_3,K_4, respectively) can be set up. The τ-coordinate of the intersection of these two straight lines can be interpreted as the desired pseudorange correction T and can be determined with the following expression:

$$T = \frac{y_1 - y_4 + s/2 \cdot (a_1 + a_2)}{a_2 - a_1} \tag{6.10}$$

where $s = \tau_4 - \tau_1$. A complete demonstration of this equation is derived in Appendix B (it must be noted that the expression presented in References [37] and [38] is not correct with the four correlators).

It should be noted that Figure 6.22 illustrates the peak of a generic triangular correlation function, which is rounded due to band-limiting effects and deformed due to the influence of multipath. As a result, the autocorrelation function's peak is not at $\tau = 0$, but is biased by an error equal to T.

The actual code multipath performance of this technique can be easily obtained by comparing the pseudorange correction T with the actual peak location. In fact, assuming to perform the simulations in a manner that the direct signal component (LOS) is present for a delay $\tau = 0$, the estimated pseudorange correction T is the multipath error (if $T \neq 0$).

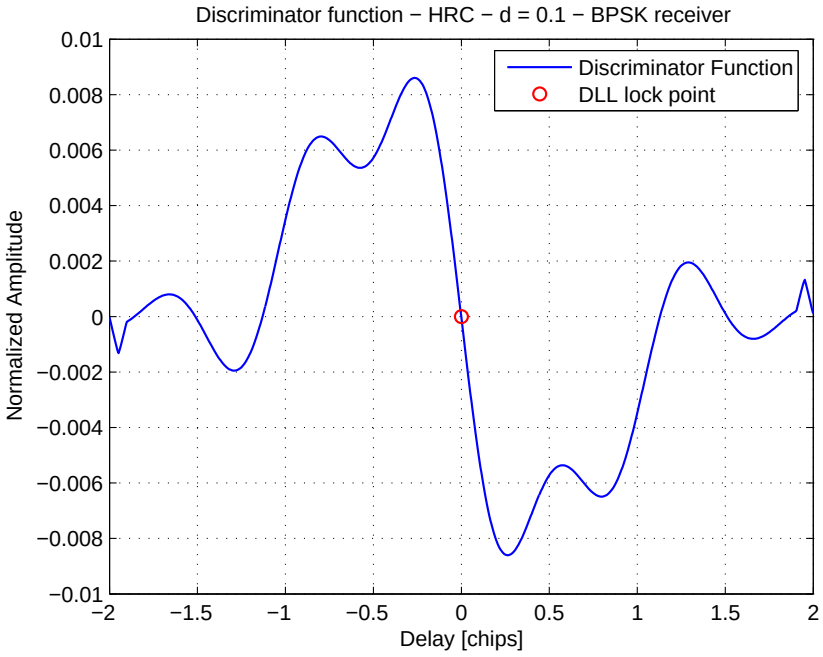

(a)

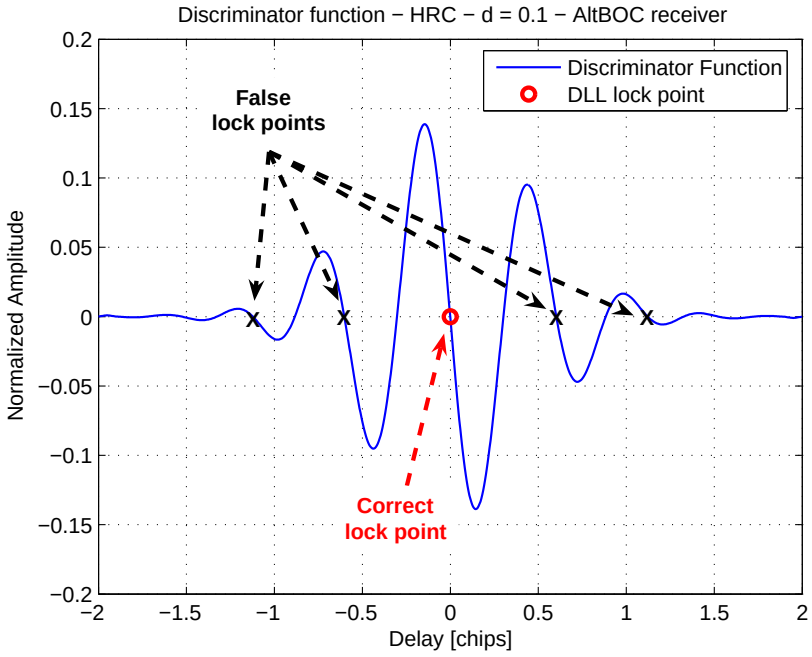

(b)

Figure 6.21: Discriminator functions with the High Resolution Correlator, using a spacing of $d = 0.1$ chip, for the two receiver architectures: with the BPSK receiver (a) and with the AltBOC receiver (b)

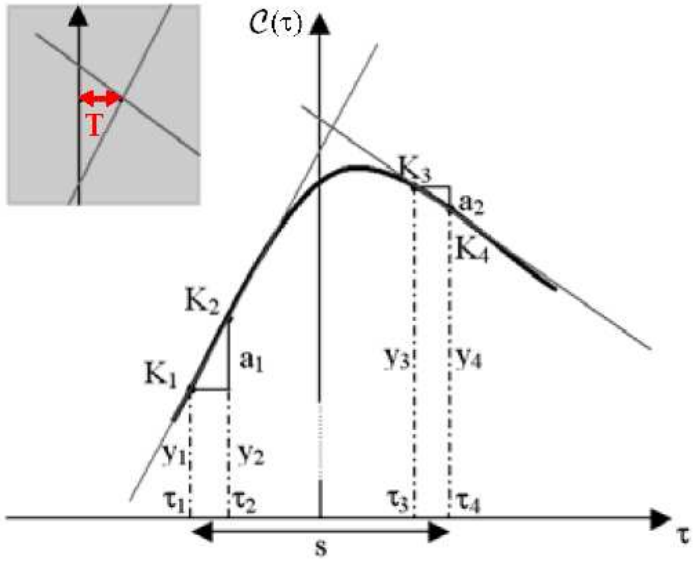

Figure 6.22: General concept of the Early/Late Slope technique: computation of a pseudorange correction T by analyzing the slopes on both sides of the correlation function

As for the previous mitigation techniques, also the ELS has been tested with the AltBOC signal. The resulting multipath error envelopes and running average errors are illustrated in Figure 6.23.

For the multipath performance assessment, the correlators used in the ELS technique have been placed following the positions listed in Table 6.3. They are the correlator spacings used in [37], that lead to better performances than the positions used in [38] for the scenario in the E5 band with the BPSK(10) signal.

Correlators	K_1	K_2	K_3	K_4
Positions [chips]	$\tau_1 = -0.1$	$\tau_2 = -0.06$	$\tau_3 = +0.06$	$\tau_4 = +0.1$

Table 6.3: Correlator positions used for the Early/Late Slope technique

Observing the multipath envelopes in Figure 6.23(a) for the two architectures, a substantial performance improvement is noticeable using the early/late slope technique, with respect to previously discussed mitigation approaches. As shown by the running average errors in Figure 6.23(b), it is evident that the BPSK receiver outperforms the AltBOC architecture, with the setup used for the simulations. It seems that the first one take advantage of the ELS better than latter, resulting in extremely small ranging errors. But it should also be noted that the code multipath performance strongly depends on the actual positions of the correlators. Slight changes will result in a fairly different appearance of the resulting multipath envelope. Besides the BPSK

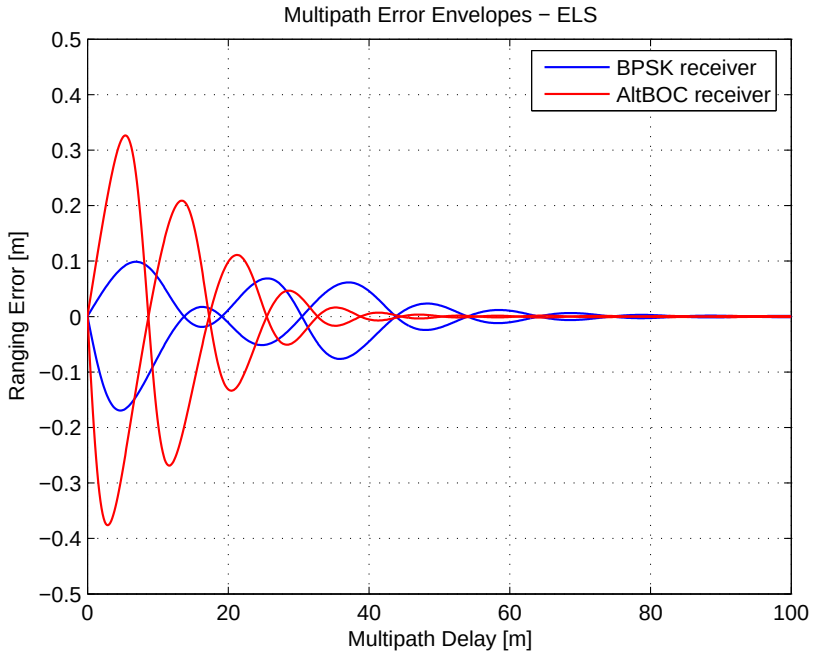

(a)

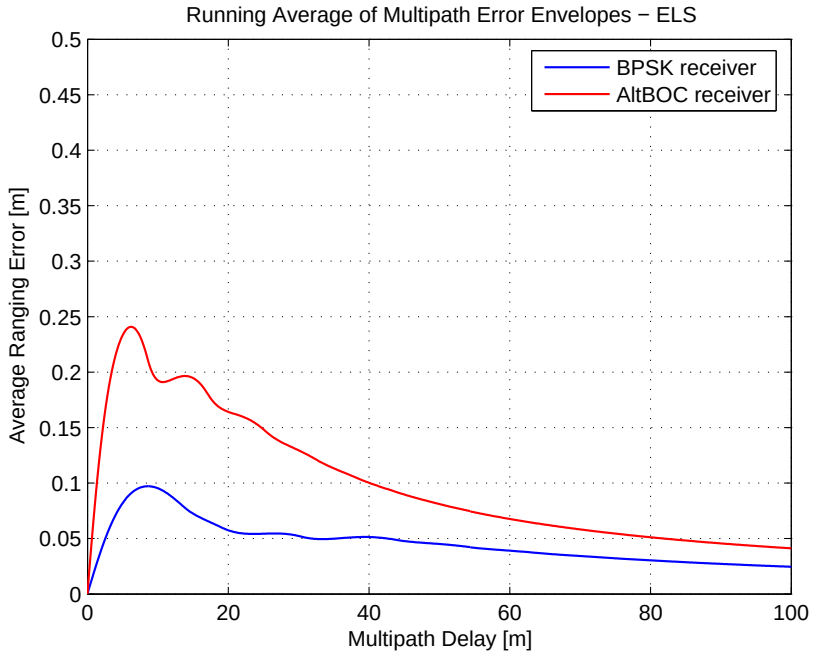

(b)

Figure 6.23: Multipath performances with the Early/Late Slope technique: multipath error envelopes (a) and running average of multipath error envelopes (b), for the two receiver architectures

receiver performs better only for multipath with short path delay, whereas in Figure 6.23(a) the multipath envelope of the AltBOC receiver decreases to zero more quickly, showing better robustness to medium path delay.

Finally, it is difficult to make a general statement which of the discussed receiver architectures shows the best multipath performances, because such a statement is only valid for a specific choice of the correlator spacing. It is therefore possible to find optimal correlator positions, but they strongly depends on the multipath environment and on the signal and the receiver parameters (e.g. pre-correlation bandwidth, filter order).

6.4.5 Early1/Early2 tracking technique

The **Early1/Early2** (E_1/E_2) **tracking** technique is based on the concept of *MultiPath Invariance* (MPI). The premise of MPI is that there exist regions and/or proprieties of the autocorrelation function that do not vary as a function of the multipath parameters. The multipath invariant regions and/or points are located at the plateaus of the autocorrelation function of a particular PRN code, and are not always located adjacent to the peak.

As described in [37], the main purpose of the E_1/E_2 correlation technique is to find a tracking point on the autocorrelation function that is not distorted by multipath. To achive this, two correlators with a chip spacing of d chips are both located on the early slope of the autocorrelation function. The basic approach for this multipath mitigation technique is illustrated in Figure 6.24, for a generic triangular autocorrelation function.

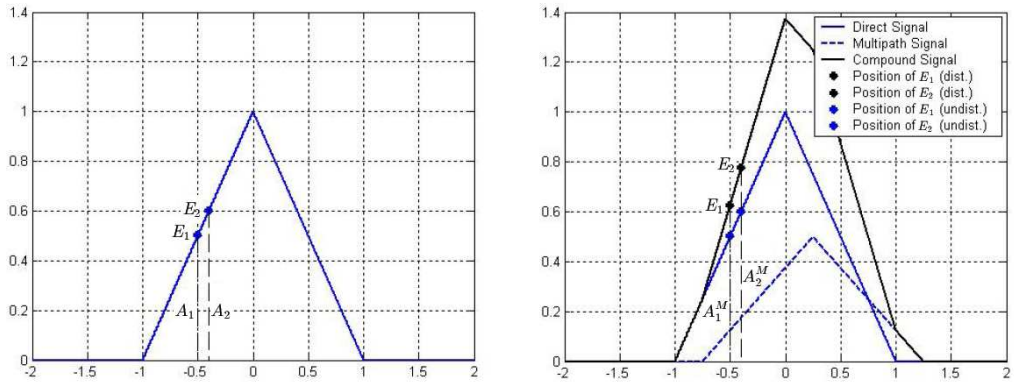

Figure 6.24: Basic E_1/E_2 tracking concept [37]

In case that the actual position of the two correlators E_1 and E_2 and the shape of the autocorrelation function is known, the amplitudes at both correlator positions can be used to set up an error function for this correlation technique.

By first having a look at the undistorted function (blue triangular function, on the left side of Figure 6.24), it is evident that the nominal amplitudes of

both correlators are given by A_1 and A_2, respectively. The ideal ration of both amplitudes can be expressed by:

$$R = \frac{A_2}{A_1} \tag{6.11}$$

In presence of multipath, the actual amplitudes A_1^M and A_2^M will be observed. The resulting ranging error can then be computed by means of the following error function:

$$\begin{aligned} \Delta R &= A_2^M - R \cdot A_1^M & (6.12) \\ &= A_2^M - \frac{A_2}{A_1} \cdot A_1^M & (6.13) \end{aligned}$$

If the resulting autocorrelation function is undistorted between E_1 and E_2, the error function becomes:

$$\Delta R = A_2 - \frac{A_2}{A_1} \cdot A_1 = 0 \tag{6.14}$$

To achieve this, the multipath signal has to be delayed by a minimum of $(1 + E_2)$ with respect to the direct signal. As a result, the resulting ranging error decreases to zero for multipath delays greater than $(1 + E_2)$. From this point of view, it is desirable to set E_1 and E_2 as early as possible. On the other hand, the noise performances suffer when E_1 and E_2 are shifted to the left slope of the correlation function, where its amplitude is lower. As a result, there is a trade-off between the increment of the thermal noise with too early correlators and the multipath mitigation capabilities [37].

The multipath performances of this mitigation technique has been assessed for the two previously discussed receiver architectures, as shown in Figure 6.25. The tracking point was set to $t = 0.5$ chip, with a spacing of 0.1 chip, so that the relative positions of two early correlators (E_1 and E_2) was the ones listed in Table 6.4. They are the same positions chosen in [37], because they seem a good compromise between noise and multipath performances.

Correlators	E_1	E_2
Positions [chips]	$\tau_1 = -0.55$	$\tau_2 = -0.45$

Table 6.4: Correlator positions used for the Early1/Early2 tracking technique

The multipath error envelopes in Figure 6.25(a) show for both the receivers a resulting ranging error that is zero for path delays greater than approximatively 20 meters. This is in agree with previous statement, that the resulting ranging error decreases to zero for multipath delays greater than $(1 + E_2)$. In fact, for $E_2 = -0.45$ chip, the corresponding maximum delay is:

$$\tau_{MAX} = 1 + E_2 = 1 - 0.45 = 0.55\,\text{chip} \tag{6.15}$$

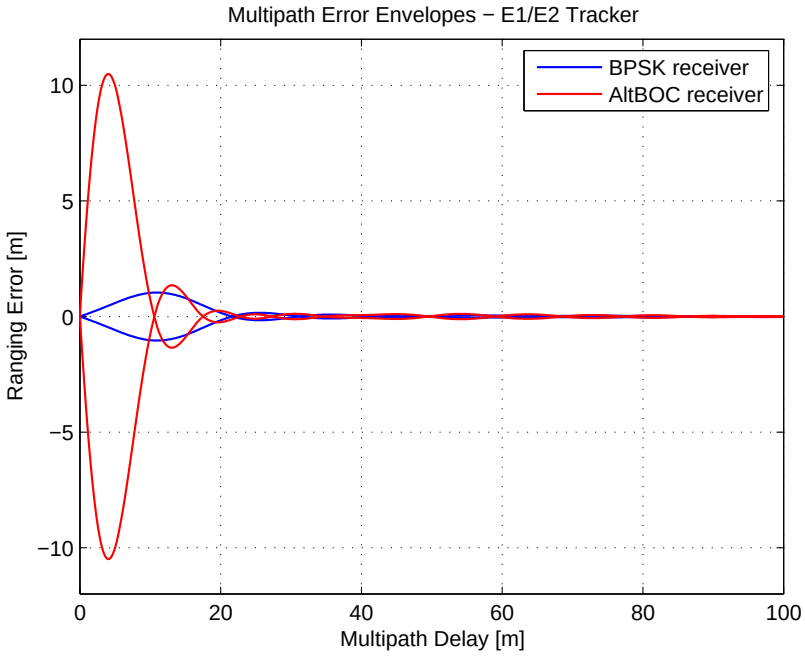

(a)

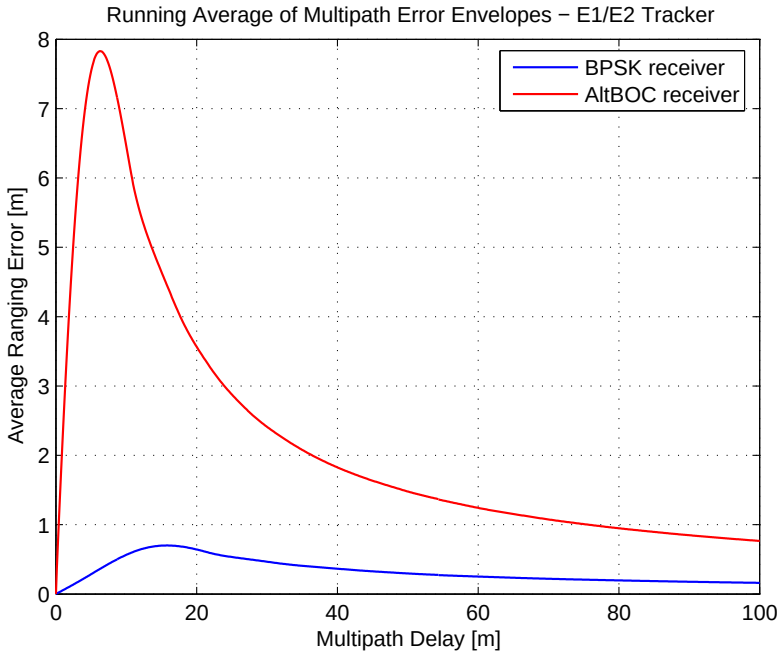

(b)

Figure 6.25: Multipath performances with the Early1/Early2 tracking technique: multipath error envelopes (a) and running average of multipath error envelopes (b), for the two receiver architectures

that corresponds to approximatively 16 meters.

It must be noted that the E_1/E_2 tracker is suitable for the BPSK receiver, because its mutipath performances improve with respect of the case with wide correlator. On the contrary, the AltBOC receiver shows worse maximum ranging error, then this arrangement is not appropriate. However is it sensitive only for short-delay multipath, with a multipath envelope that decreases very rapidly to zero increasing the delay.

The poor multipath performances of the AltBOC receiver in this case are primarily due to the positions of the correlators, that result near to a zero-crossing of the correlation function (see Figure 6.12). Furthermore, placing the two correlators in a earlier position, the multipath envelope could be improved: however this worsens the noise sensitivity.

As concluded in previous Section (for the Early/Late Slope technique), also the E_1/E_2 tracker seems more suitable for the BPSK receiver, but it is difficult to make a general statement because the performances strongly depend on the positions of the correlators.

6.4.6 Performance comparison of current techniques

The receiver-internal correlation techniques, that are currently used in common GPS receivers to minimize the code multipath errors, have been examined in previous Sections, assessing their multipath performances for the two receiver architectures chosen for the AltBOC signal.

It must be noted that the correlator spacings chosen for the simulations were the same as in Reference [38] (for the BOC(15,10) and BPSK(10) signals), except for the Early/Late Slope (see Section 6.4.4) and the Early1/Early2 tracking techniques (see Section 6.4.5), where the spacings were the same as that ones used in [37].

For the BPSK receiver architecture, the obtained multipath performances slightly differ from the results in [38] for the BPSK(10) signal, because an optimal pre-correlation bandwidth and an higher filter order was used for the simulations (see Table 6.1). Furthermore the transmitted signal was the AltBOC modulation, that with the BPSK arrangement is received as a BPSK(10) signal: obviously this leads to small differences for the multipath performances, with respect of the case where a true BPSK(10) signal is transmitted (as in [38]).

A complete analysis of the multipath performances of the innovative AltBOC receiver architecture has also been performed in previous Sections, adapting to the AltBOC signal all the current multipath mitigation techniques. It must be remarked that a similar analysis is not present at the moment in literature (e.g. in Reference [38] only the BOC(15,10) and BPSK(10) modulations are assessed) and is done for the first time in this thesis.

In Figure 6.26 there is a comparison of the multipath performances of the mitigation techniques previously illustrated, for the two receiver architectures. The running average of multipath error envelope has been chosen for the comparison, because it allows to easily compare the different performances.

As shown in Figure 6.26(a), all the current multipath mitigation techniques used in GPS are suitable for the BPSK architecture. In fact, with the setups used in simulations, all the techniques allow to improve the multipath performances, outperforming the wide (standard) correlator. The best multipath mitigation is obtained with the Early/Late Slope technique; in the other hand this one is also the most complex technique, because it needs four correlators for the tracking loop. Good multipath performances are also obtained with the Early1/Early2 tracking technique, that seems a good compromise between the multipath mitigation and the hardware complexity of the receiver (only two correlators are needed).

Otherwise, the multipath performances of the AltBOC architecture are intrinsically good, also with the wide correlator: the maximum ranging error is considerably lower than the one obtained with the BPSK receiver with the wide correlator. Besides the standard mitigation techniques seem not appropriate for the AltBOC receiver, as illustrated in Figure 6.26(b). Almost all the discussed mitigation techniques do not improve significantly the multipath performances of the AltBOC receiver: the Narrow correlator^{TM} and the Double Delta ($\Delta\Delta$) correlator have the same performances, and the Early1/Early2 tracking technique leads to a performance worsening, with the correlator spacings used for the simulations. The only exception is the Early/Late Slope technique, that significantly improves the performances of the AltBOC receiver, but it is not recommended because it significantly increases the hardware complexity and leads to performances that are outperformed by the BPSK receiver with the same mitigation technique (ELS).

As noticed before, the obtained multipath performances are only valid for the actual correlator configurations and for the chosen setup of the other receiver parameters (pre-correlation bandwidth and filter characteristics). In fact the results strongly depends on actual correlator positions: slight position changes can result in fairly different error envelopes, especially for the AltBOC receiver, because its complex correlation function is oscillating and presents multiple zero-crossing points.

The correlator positions could be adjusted for each individual receiver architecture and mitigation technique, such that optimum multipath performance is achieved, but this seems difficult for the AltBOC architecture and the performance improvement generally are not convenient, considering the increase in receiver cost and complexity.

In conclusion, it is possible to state that the current mitigation techniques could be successfully employed with the BPSK receiver, obtaining a considerable performance improvement. The best performances have been obtained

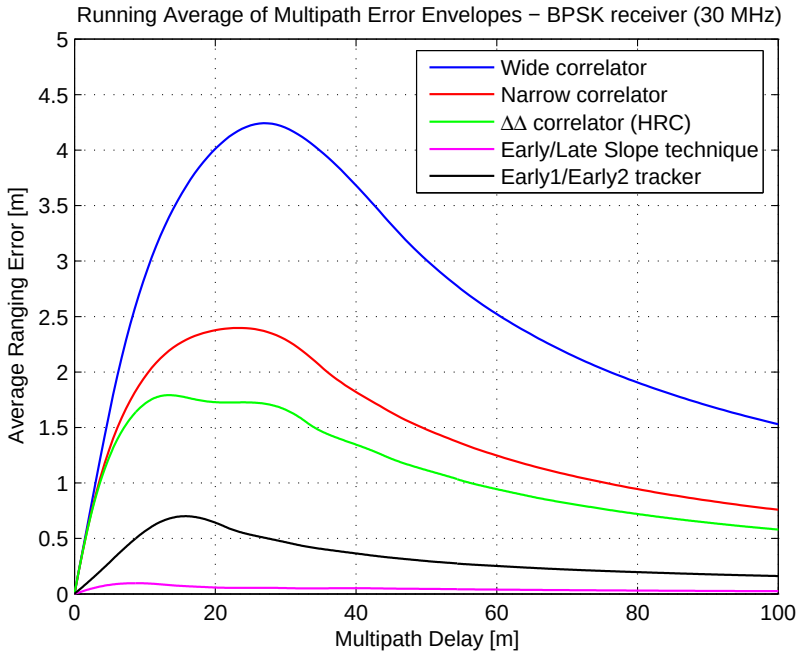

(a)

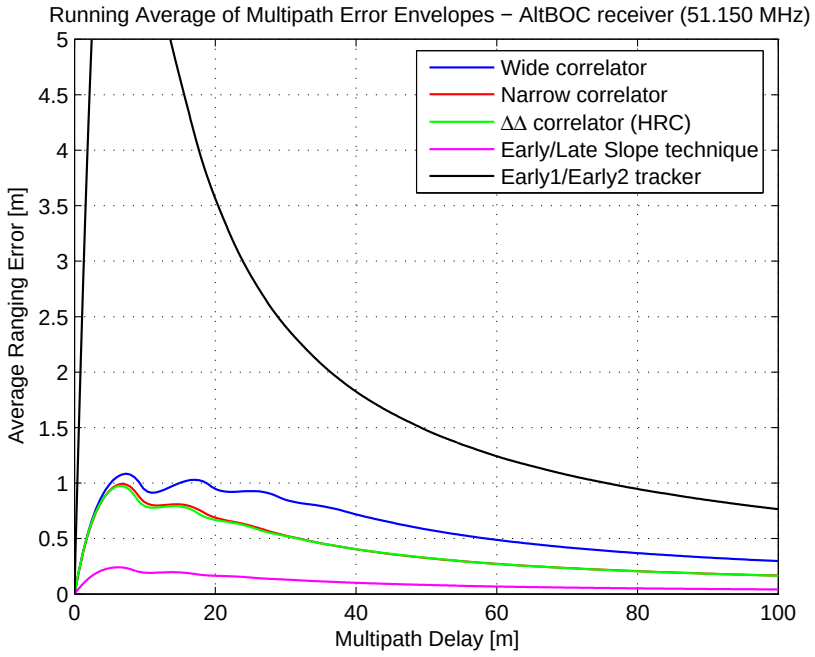

(b)

Figure 6.26: Comparison of multipath performances with the current mitigation techniques: running average of multipath error envelopes for the BPSK receiver (a) and for the AltBOC receiver (b)

with the ELS technique applied to the BPSK receiver, but this arrangement is expensive. On the contrary, the excellent performances of the AltBOC receiver (with the wide correlator) are difficult to further improve with the current techniques. For the AltBOC receiver innovative mitigation techniques are foreseeable and necessary (see next Section), because the current techniques seem not suitable because the slight performance gain not justify the increase in receiver cost. At the moment, the best compromise between the receiver complexity and the multipath performance is the BPSK architecture with the Early1/Early2 tracking technique.

6.5 Emerging multipath mitigation techniques

In previous Sections, the code multipath performances of the BPSK architecture (*single band receiver*, presented in Section 4.1) and of the AltBOC architecture (*coherent dual band receiver*, illustrated in Section 4.3) has been assessed, taking advantage of current multipath mitigation techniques.

Two emerging code multipath mitigation approaches are then presented and discussed in the following. In detail the first assessed technique is the **S-curve shaping**. This technique, assuming a multi-correlator receiver architecture, achieves a code multipath mitigation by coherent linear combination of the outputs of several correlators. The second approach is the **gating technique**, based on a reference function that operated a blanking on the signal, with the aim of reducing multipath errors.

In following Sections these techniques are then adapted to the AltBOC signal, using the two receiver architectures previously discussed and their multipath performances are assessed in different configurations.

6.5.1 S-curve shaping technique

This novel code multipath mitigation technique was recently introduced for BPSK and BOC modulations in Reference [46], assuming a multi-correlator receiver architecture.

The "*shaping correlator*" is also outlined for BOC(1,1) signals in [47], but with a different approach: the gating technique, that will be discussed in Section 6.5.2. The approach presented in [47] is not used in the following. The shaping technique is implemented using an approach similar to that described in [46], adapting the AltBOC receiver architectures previously presented to this multi-correlation technique.

The **S-curve shaping technique** is based on the optimization of the shape of the code discrimination function. This process is simply performed placing a distinct amount of correlators along the signal's correlation function and combining them with the aim of optimizing the tracking performance. In

the presence of multipath, the resulting multipath errors can be minimized by a well chosen placement and combination of the correlators. This procedure depends on the shape of the signal autocorrelation function. It also influences the code noise performance. As a consequence, careful correlator placing and combination of correlator outputs can optimize the overall tracking performance.

The first step for the shaping technique is to introduce a generic code tracking channel model, similar to the **multi-correlator architecture** schematized in Figure 6.27.

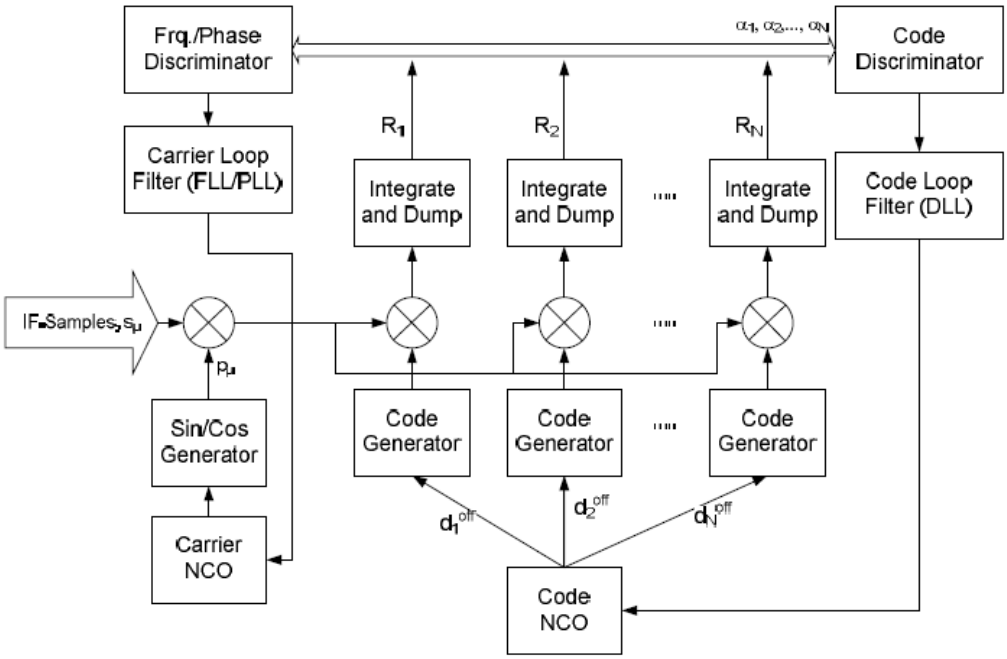

Figure 6.27: Generic multi-correlator channel architecture for the S-curve shaping technique [46]

In this scheme the received IF samples s_μ are correlated with locally generated replicas, using multiple correlators. Each local signal is shifted with respect to the punctual channel by a certain delay d_i^{off} and it is correlated with the received signal to obtain the output of the i^{th} correlator R_i. There are N correlators and their outputs are linearly combined to obtain the coherent phase discriminator $\mathcal{D}(\Delta\tau)$, as defined in following expression:

$$\mathcal{D}(\Delta\tau) = \sum_{i=1}^{N} \alpha_i \cdot R_i(\Delta\tau) \tag{6.16}$$

where $\Delta\tau$ is the code tracking error, $R_i(\Delta\tau)$ is the autocorrelation function of the received signal shifted by d_i^{off} and α_i is the weight applied to the i^{th} correlator output.

The discriminator function is then completely defined by choosing the positions d_i^{off} and the weights α_i of the individual correlators.

It is possibile to adapt the two receiver architectures previously discussed (the *BPSK receiver*, presented in Section 4.1, and the *AltBOC receiver*, illustrated in Section 4.3) to this innovative multi-correlator arrangement. This can be done simply increasing the hardware of the receivers, using a larger number of correlators. In detail, in previous block diagrams of the receivers (see Figure 4.3 and Figure 4.8) only three correlators were used (Early, Punctual and Late), for the Early-Late discriminator. Instead of three correlators, it is possibile to use an arbitrary number N of correlators with arbitrary positions d_i^{off}, obtaining multi-correlator architectures similar to the scheme in Figure 6.27. It must also be noted that the hardware increase with this arrangement is not limited to the additional correlators (that are complex correlators, for the *AltBOC receiver*), but implies also additional local code generators, to generate the local replicas with the correct time-shifts.

After the architecture requirements, for the shaping technique it is necessary to define an **ideal discriminator** $\mathcal{D}_{ideal}(\Delta\tau)$, that is the optimal shape for the S-curve required to obtain the best tracking and multipath performances. As shown in Figure 6.28, the optimum S-curve must be linear, with an unitary slope in the so-called *linear region* and with just one stable tracking point at $\Delta\tau = 0$. The linearity around the tracking point is required to realize a linear DLL, that is the common tracking approach. Non-linear tracking loop is a rather unusual approach.

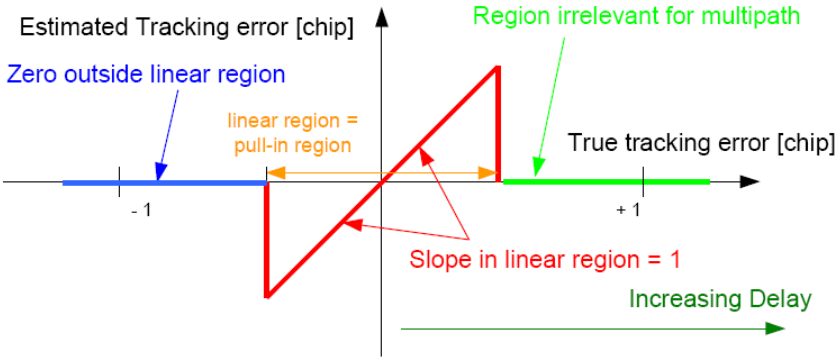

Figure 6.28: Optimum linear S-Curve for the shaping technique [46]

The *linear region* should be sufficiently large to cover the range of expected tracking errors, caused by thermal noise or transient errors, and to avoid loss of lock. But for the multipath performances it is important to keep this region as small as possibile, because only reflected signals with delays that falls in the linear region can cause code tracking errors. Outside this region the S-curve vanishes (see Figure 6.28), then for multipath delays larger than

the linear region the tracking error is negligible. As demonstrated in [46], it is necessary to impose the zero value outside the linear region only for the left side of the ideal S-curve, while the shape of the S-curve right to the linear region is irrelevant for multipath mitigation, as multipath delays are always positive. In fact a reflected signal arrives always with a positive delay with respect of the direct signal, causing a parasitic response in the discriminator that is a delayed and scaled replica of the ideal S-curve. Then if the delay of the multipath signal is larger than the extension of the linear region, the S-curve results undistorted at the tracking point and multipath-error-free.

The *pull-in region* is defined as the range of code delay values which can be captured (and tracked) by the code tracking loop. In the case of Figure 6.28 it is equivalent to the linear region, since code tracking errors outside the linear region result in a null discriminator output. In this case the code tracking loop makes no attempt to follow the received signal and, if the *pull-in region* is too small, this implies the risk of a loss of lock for the DLL.

In conclusion, it must be remarked that the amplitude of the *linear region* must be carefully chosen, as a compromise between the tracking performances in presence of noise (tracking jitter, risk of loss of lock) and the multipath mitigation capabilities.

As a side remark, in [46] it is also introduced a slightly modified version of the optimum code discriminator, that features interesting proprieties. This modified discriminator, presented in Figure 6.29, does not vanish outside the linear region, but retains a small **offset** whose sign is different on the left and right side.

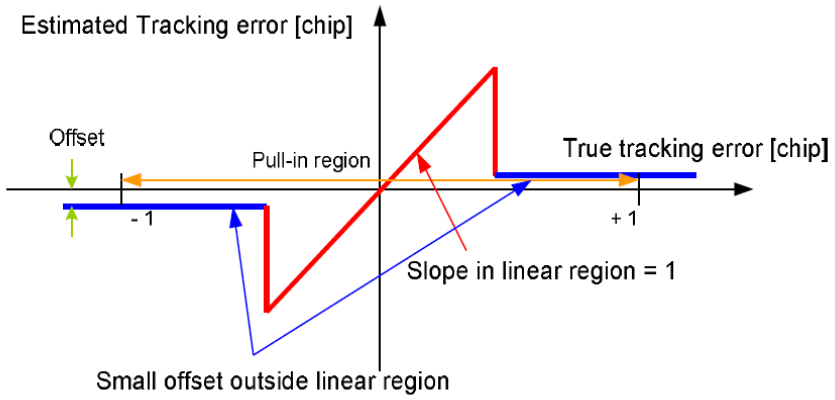

Figure 6.29: Optimum linear S-Curve plus offset to increase pull-in region, for the modified S-curve shaping technique [46]

By imposing this additional requirement, the *pull-in region* of the discriminator results increased and is larger than the linear region. The discriminator is then capable of following signals even if they have large code tracking errors. In that case the tracking loop is non-linear, until tracking errors fall within

the linear region. This modified S-curve is especially important if the linear region is kept small to limit maximum multipath errors. Besides (as it will be illustrated at pag. 189), with a bandlimited AltBOC receiver this approach allows to achieve only one stable tracking point for the code discriminator.

After defining the shape of an ideal code discriminator $\mathcal{D}_{ideal}(\Delta\tau)$, it is now possible to realize it by choosing proper positions d_i^{off} and weights α_i for the correlators. To do this, it is possible to follow a *discrete approach*, similar to that presented in [46]. A set of control points $\Delta\tau_l$ could be defined around the tracking point in the S-curve, assuming that those control points correspond to the positions d_i^{off} of the individual correlators. These control points are equally distributed within a chosen fitting range and with a given resolution, that is the distance between two adjacent correlators.

Recalling Equation (6.16) for the discriminator with multiple weighted correlators, it is possibile estimate the weights $\hat{\alpha}_i$ of the correlators with a *least square* approach, minimizing the difference between the obtained discrimination function and the ideal S-curve:

$$\hat{\alpha}_i = \min_{\{\alpha_i\}} \sum_l \left(\sum_{i=1}^{N} \alpha_i \cdot R_i(\Delta\tau_l) - \mathcal{D}_{ideal}(\Delta\tau_l) \right)^2 \tag{6.17}$$

Essentially this method try to fit the ideal S-curve by a linear combination of shifted autocorrelation functions. The estimated weights $\hat{\alpha}_i$ can be obtained by solving this equation using standard methods of least-squares adjustment.

This approach is not used in following simulations, because it could lead to problems of numeric instability[4]. A more simple method is usable, reformulating the problem of the evaluation of the weights like a solution of a *linear system of equations*.

First it is necessary to define two vectors (S_{ideal} and W) and a matrix ($\overline{M}_R$), to represent the linear system. The vector S_{ideal} is a row vector that contains the desired optimum S-curve $\mathcal{D}_{ideal}(\Delta\tau)$, sampled in agreement with the chosen positions of the N correlators (d_i^{off}):

$$S_{ideal} = \begin{bmatrix} \mathcal{D}_{ideal}(d_1^{off}) & \mathcal{D}_{ideal}(d_2^{off}) & \cdots & \mathcal{D}_{ideal}(d_N^{off}) \end{bmatrix} \tag{6.18}$$

Furthermore the vector W is composed by the estimated weights $\hat{\alpha}_i$ for the multiple correlators:

$$W = \begin{bmatrix} \hat{\alpha}_1 & \hat{\alpha}_2 & \hat{\alpha}_3 & \cdots & \hat{\alpha}_N \end{bmatrix} \tag{6.19}$$

[4]Some attempts to use this least-squares technique with an oversampled AltBOC correlation function have produced unreliable results, obtaining unstable weights with very high values and non symmetrical with respect to the tracking point. As obtained in [46] and in following sections, the weights typically must be symmetric. Otherwise the multipath performances result degraded and the multipath error envelopes show bias effects, caused by numeric instability problems.

At last, $\overline{M}_R$ is the matrix which rows contains the sampled and shifted correlation functions (a shifted replica per row):

$$\overline{M}_R = \begin{bmatrix} R_1(d_1^{off}) & R_1(d_2^{off}) & \cdots & R_1(d_N^{off}) \\ R_2(d_1^{off}) & R_2(d_2^{off}) & \cdots & R_2(d_N^{off}) \\ \vdots & \vdots & \ddots & \vdots \\ R_N(d_1^{off}) & R_N(d_2^{off}) & \cdots & R_N(d_N^{off}) \end{bmatrix} \tag{6.20}$$

In this way the first row of $\overline{M}_R$ corresponds to the correlation function provided by the first correlator, the second row corresponds to the second correlator output and so on. It must be remarked that $\overline{M}_R$ is a square matrix, with $N \times N$ elements, then it is invertible.

The shaping technique could then be applied with a *linear* approach (instead of the *least square* method proposed in [46]), solving the linear system of equations summarized with the following expression:

$$S_{ideal} = W \cdot \overline{M}_R \tag{6.21}$$

The vector W contains the unknown weights, that could be directly evaluated inverting the matrix $\overline{M}_R$:

$$W = S_{ideal} \cdot \left(\overline{M}_R\right)^{-1} \tag{6.22}$$

This approach allows to obtain the weights for the correlators with a remarkable computational simplicity. It must also be noted that this method produces always stable solutions, if the matrix $\overline{M}_R$ is square and invertible. This requirement is easily satisfied if the autocorrelation function used to build the matrix $\overline{M}_R$ and the desired discriminator function $\mathcal{D}_{ideal}(\Delta\tau)$ are sampled in N points, corresponding to the correlator positions.

Thus this discrete approach tries to fit the ideal S-curve by a finite amount of coefficients, that are equally distributed. The result of this fit (a fitted S-curve) is in general not in exact agreement with the ideal S-curve. The agreement is better when more control points are used (increasing the number of correlators) and if the shape of the autocorrelation function is suitable to reproduce the ideal S-curve.

Besides it is also possible to move the correlator positions, choosing an irregular distribution with the purpose of improve the fitting of the ideal S-curve. For example it is possible to concentrate the correlators around the tracking point, to fit with a better resolution this region. Another possible choice is to use a non-symmetric fitting region (as proposed in [46]), for a better representation of the left side of the ideal S-curve, ignoring the right side that is irrelevant for the multipath. But these choices make more complicated the evaluation of the weights, then it is usual to place the correlators equally distributed in a fitting region that is symmetrical around the tracking point, as it is done in the following.

In next Sections, the shaping technique is applied to different simulation scenarios, with the two receiver architectures previously discussed and varying the simulation parameters.

Results for infinite bandwidth receivers

The shaping technique, illustrated in previous Section, is then applied to the BPSK and AltBOC receivers, modified with a multi-correlator structure in the code tracking loop. The first two simulations have been done with infinite bandwidth receivers and the main parameters of the simulation scenarios are summarized in Table 6.5. The other parameters remain the same as in previous simulations for the multipath performance evaluation, as in Table 6.1. It must be noticed that the BPSK receiver has been simulated generating only the tracked code ($E5aQ$), and switching off all the other codes, to avoid cross-correlation problems, whereas for the AltBOC receiver only the two pilot codes ($E5aQ$ and $E5bQ$) have been generated, for the same reasons (for more details, see Appendix A).

SIMULATIONS	**Scenario 1**	**Scenario 2**
Receiver architecture	BPSK receiver	AltBOC receiver
Linear region	$\pm 1/12$ chip	$\pm 1/12$ chip
Fit range	± 2 chip	± 2 chip
Resolution	1/12 chip	1/12 chip
Number of correlators	49	49
Bandwidth	∞	∞
Offset	0	0

Table 6.5: Simulation settings for infinite bandwidth receivers with the S-curve shaping technique

The fitting parameters have been chosen considering a *resolution* of $1/12$ chip, that means 12 correlators for each chip in the x-axis of the autocorrelation function. This choice is due to the particular shape of the AltBOC autocorrelation function (recalled in Figure 6.30, together with the correlation function for the BPSK receiver).

Remembering the waveforms of the AltBOC subcarrier functions (8 transitions for each subcarrier period, see Section 2.1.1) and the fact that in a code chip time there are 1,5 subcarrier periods (see Section 3.1), it is evident that in a chip time the AltBOC signal could experience 12 transitions. These transitions cause the slope changes in the AltBOC autocorrelation function, that are evident in Figure 6.30. It is then reasonable to place the fitting points in correspondence of these 12 slope changes, that are equally distributed in a chip time. The same distribution of the correlators is used for the triangular autocorrelation obtained with the BPSK receiver architecture.

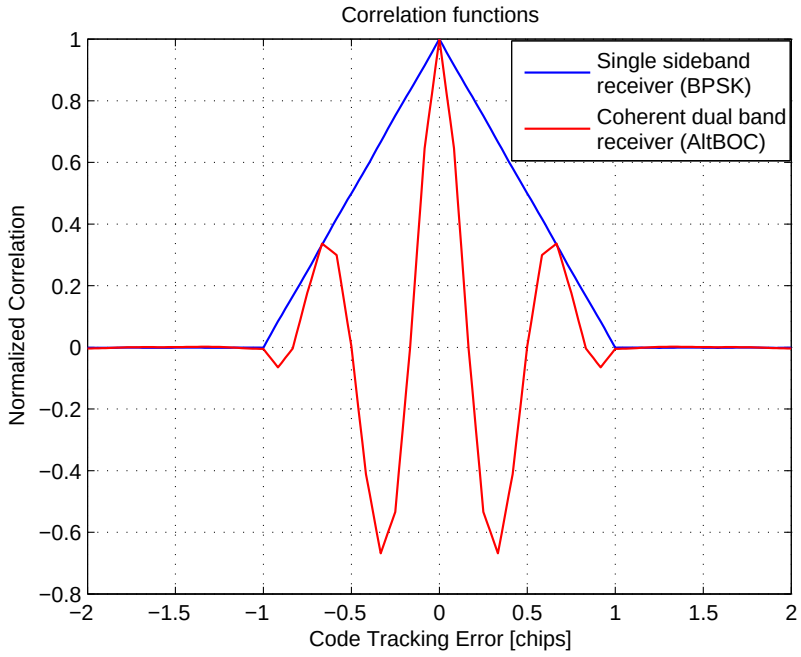

Figure 6.30: Correlation functions for the single sideband (BPSK) and the dual band (AltBOC) receivers, simulated with infinite bandwidth

The shaping technique is then applied to the two receivers, fitting the ideal S-curve between -2 chips and +2 chips (*fit range*). Considering the chosen *resolution* of 1/12 chip, this means that 49 correlators must be employed.

It must be noted that the *linear region* is chosen the smallest possible (it is wide only 2/12 chip), in accord with the resolution. The reason of this choice is to obtain the best multipath performances, neglecting for the moment the other tracking problems (jitter, pull-in region).

The *offset* in the desired S-curve is set to zero, performing a fitting on the first ideal discrimination function previously discussed (see Figure 6.28). The effect of the *offset* in the receiver performances will be discussed later (see pag. 189).

The correlators weights have been computed for the two simulation scenarios, with the linear approach previously discussed: for each correlator a weighting factor is found, in order to fit the optimum S-curve within the fitting range. The obtained weights are presented in Figure 6.31.

Observing the weights for the BPSK receiver in Figure 6.31(a), it must be noted that most of the correlators have a null weight and are thus irrelevant to compute the coherent code discriminator. One of them is the punctual correlator. It is possible to choose to remove these correlators, in order to reduce the receiver hardware. The remaining correlators are anti-symmetrical around the origin.

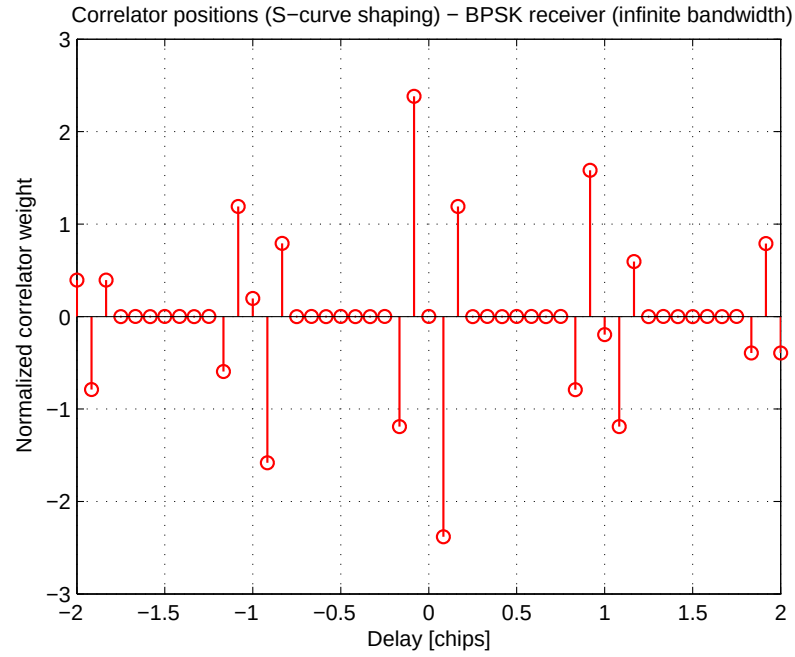

(a)

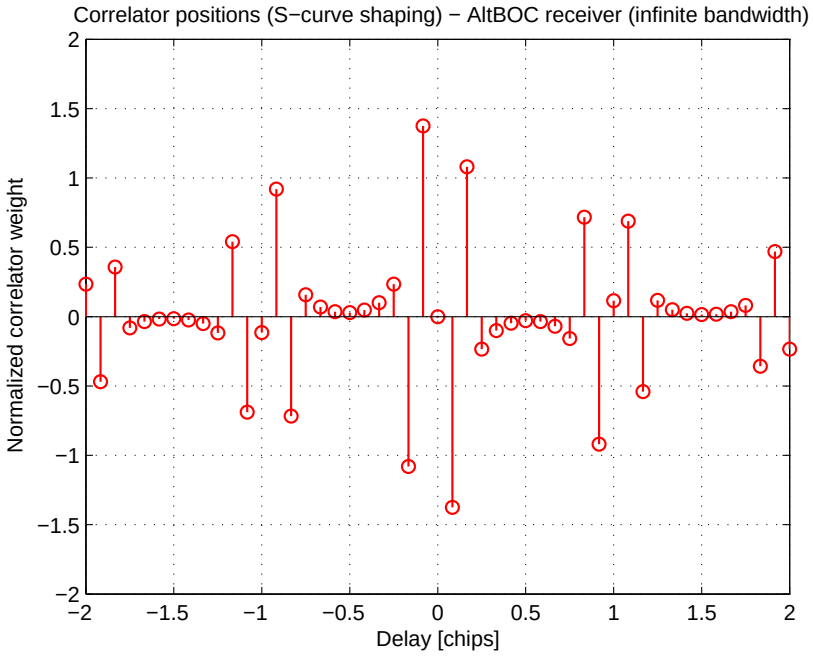

(b)

Figure 6.31: Correlator diagrams for infinite bandwidth receivers with the S-curve shaping technique: correlator positions and weights with the BPSK receiver in scenario 1 (a) and with the AltBOC receiver in scenario 2 (b)

The four correlators nearest to the origin form a structure that is similar to a $\Delta\Delta$ correlator. They are equivalent to two narrow correlators, one with a correlator spacing of 2/12 chip, the other one with a correlator spacing of 4/12 chip. The more inner correlator pair has twice the amplitude as the outer correlator pair. Furthermore it is possible to observe two $\Delta\Delta$-like correlator structures around ± 1 chip, with slight differences (the weights of central correlators are not null). They ensure that the resulting S-curve vanishes within the fitting region, as shown in Figure 6.32(a). This is not the case for the standard $\Delta\Delta$-correlator, where non-vanishing S-curve values are located around ± 1 chip.

Similar considerations could be done with the AltBOC receiver. The weights in Figure 6.31(b) are disposed with only small differences with respect of these obtained with the BPSK receiver. The absolute values are different and seem re-scaled. Furthermore, with the AltBOC receiver no one weight is null, whereas with the BPSK receiver the correlators between the $\Delta\Delta$-like structures have a null weight. These differences are due to the different shapes of the autocorrelation functions (see Figure 6.30).

It must be noticed that in the infinite bandwidth case the shaping technique produces a S-curve that is a very good approximation of the ideal S-curve, for both the receivers. One can see in Figure 6.32 that the two receiver architectures allow to obtain the same good replica of the ideal S-curve, independently from the initial shape of the autocorrelation functions.

At last, it is possible to evaluate the multipath performances of the two obtained discriminators with the multipath error envelopes and the corresponding running averages. As depicted in Figure 6.33, the performances of the BPSK receiver and the AltBOC receiver are almost identical. The curves are nearly completely superimposed in a range that corresponds to the limit of fitting region (2 chips, that in this case are equal to 58.65 meters). In this range the multipath envelopes shows ideal performances, in accord with the ideal S-curve: only small errors are present for short multipath delays, in correspondence of the linear region of the S-curve. The running average plots are then characterized by a small maximum error and a rapid decrease.

However, for delay values outside the fitting region (greater than 2 chips) the multipath error envelopes are different and can be non-zero. In fact, outside the fitting range the S-curve is unconstrained, then the multipath errors are not controlled. If this demonstrates to be problematic for a certain application, the fitting region needs to be further increased, using also a larger number of correlators. But this problem could be neglected, because typically only the region of the discrimination function between -1 and +1 chip is significative for the DLL, whereas outside this region the tracking loop loses the lock and could not produce further errors.

Obviously the obtained performances refer to the infinite bandwidth case, then can only be considered theoretical performances. In following paragraphs more realistic simulations are presented, using finite bandwidth receivers.

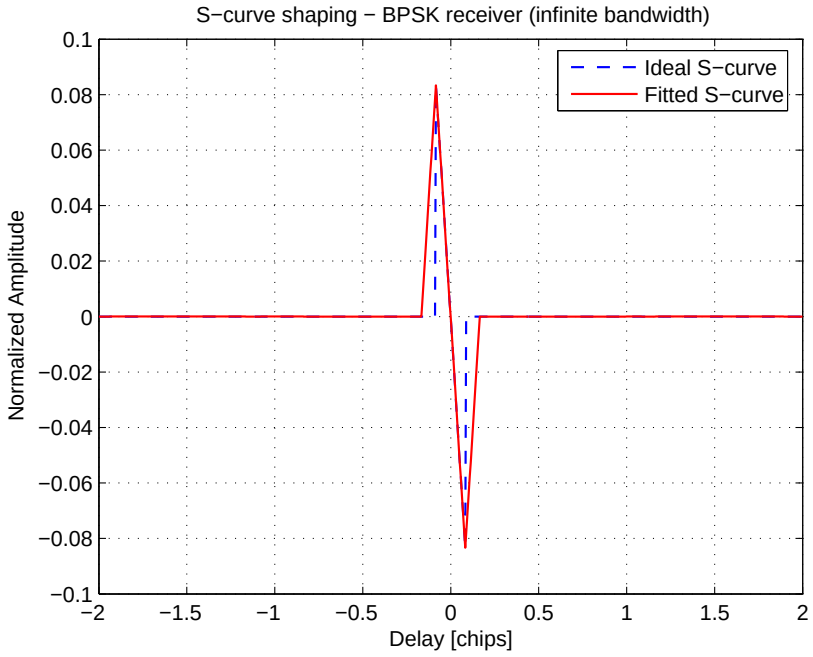

(a)

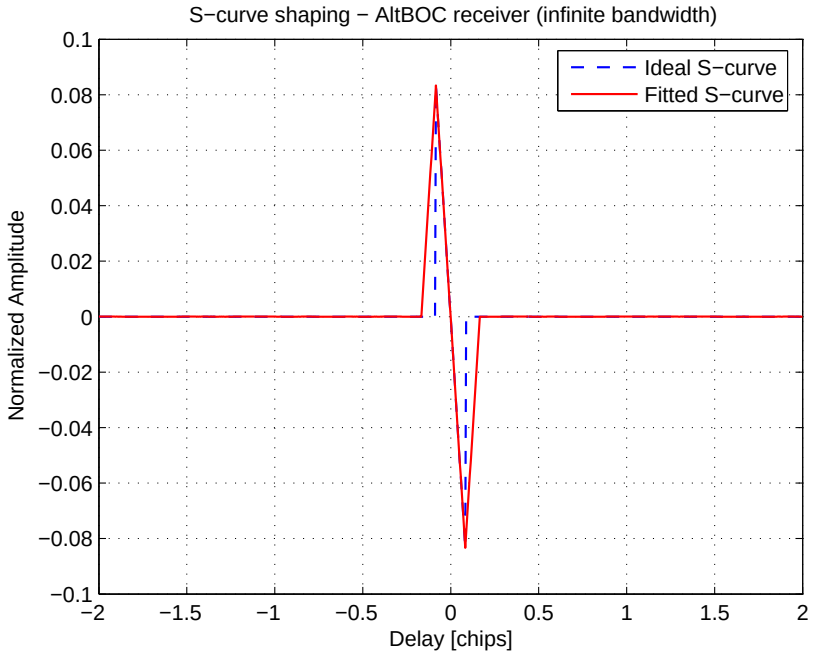

(b)

Figure 6.32: Ideal and fitted S-curves with the shaping technique, for infinite bandwidth receivers: obtained S-curves with the BPSK receiver in scenario 1 (a) and with the AltBOC receiver in scenario 2 (b)

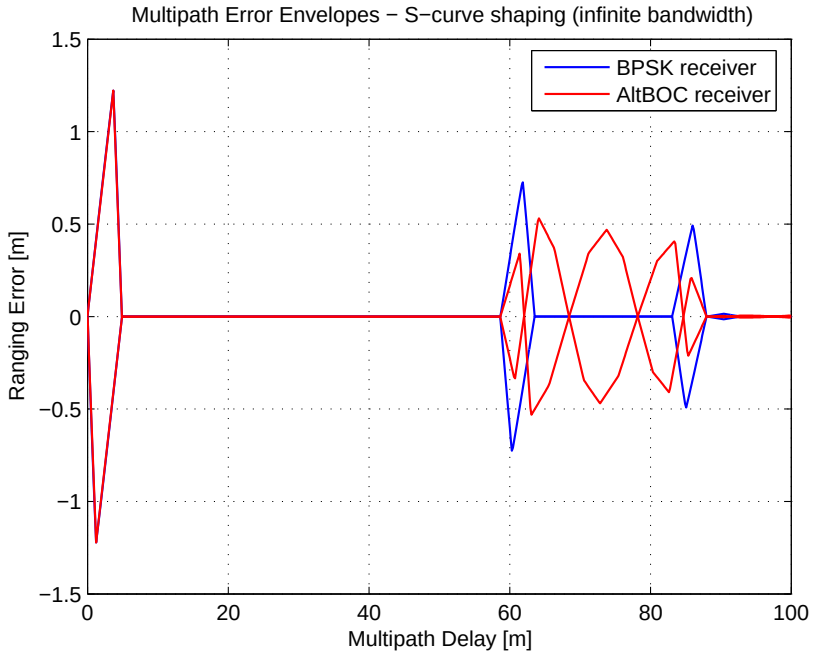

(a)

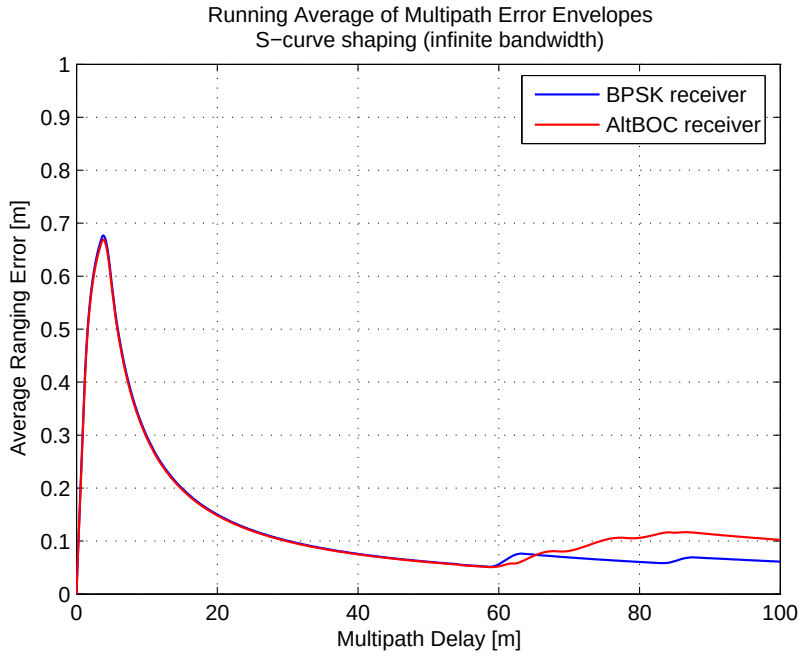

(b)

Figure 6.33: Multipath performances with the S-curve shaping technique, for infinite bandwidth receivers: multipath error envelopes (a) and running average of multipath error envelopes (b) for the BPSK receiver (scenario 1) and the AltBOC receiver (scenario 2)

Results for finite bandwidth receivers

In this Section the multipath performances of the BPSK receiver and the AltBOC receiver are assessed, considering finite bandwidth signals. In detail four scenarios are simulated, considering the two receivers in a wide-band configuration (100 MHz) and with the optimal bandwidths (30 MHz for the BPSK receiver and 51.150 MHz for the AltBOC receiver) previously discussed in Section 6.3.2.

The simulation parameters used for the BPSK receiver and for the AltBOC receiver are summarized respectively in Table 6.6 and in Table 6.7. A Butterworth filter with order 16 has been used to limit the signal bandwidth, in agreement with previous simulations.

It must be noticed that the fitting parameters are the same as in previous two simulation scenarios (see Table 6.5). In this way the weights evaluated in previous Section can be reused also in these four scenarios, without the need of recalculate the solution of the linear system of equations[5]. Then the correlators diagrams for the two receivers remain the same as in Figure 6.31.

SIMULATIONS	**Scenario 3**	**Scenario 4**
Receiver architecture	BPSK receiver	BPSK receiver
Linear region	±1/12 chip	±1/12 chip
Fit range	±2 chip	±2 chip
Resolution	1/12 chip	1/12 chip
Number of correlators	49	49
Bandwidth (two-sided)	100 MHz	30 MHz
Offset	0	0

Table 6.6: Simulation settings for the BPSK receiver with finite bandwidth, with the S-curve shaping technique

For the BPSK receiver, the results obtained in scenario 3 and in scenario 4 are illustrated in Figure 6.34 and in Figure 6.35.

It must be observed that the obtained S-curves in Figure 6.34 are degraded with respect of the infinite bandwidth case and the shape of the discrimination function worsens narrowing the bandwidth. In fact with a bandwidth of 100 MHz the S-curve slightly diverges from the ideal S-curve, but the difference is acceptable, whereas with a bandwidth of 30 MHz the result is strongly distorted.

[5]Some attempts to evaluate the weights with filtered autocorrelations, for the finite bandwidth receivers, have pointed out that this method leads to degraded multipath performances and could produce numerical instability problems, obtaining unstable weights with very high values and non symmetrical with respect to the tracking point. Accordingly, it is recommended to evaluate the weights for the fitting in a infinite bandwidth situation, and then to use these weights with finite bandwidth.

SIMULATIONS	Scenario 5	Scenario 6
Receiver architecture	AltBOC receiver	AltBOC receiver
Linear region	±1/12 chip	±1/12 chip
Fit range	±2 chip	±2 chip
Resolution	1/12 chip	1/12 chip
Number of correlators	49	49
Bandwidth (two-sided)	100 MHz	51.150 MHz
Offset	0	0

Table 6.7: Simulation settings for the AltBOC receiver with finite bandwidth, with the S-curve shaping technique

Observing also the multipath performances in these two scenarios, that are illustrated in Figure 6.35, it is evident that the performances of the shaping technique strongly depend on the available bandwidth. A wide bandwidth is a fundamental requirements to achieve good multipath performances with the shaping technique, independently form the initial shape of the correlation function (BPSK or AltBOC). Then the bandwidth of 30 MHz for the BPSK receiver seems inadeguate and leads to poor performances. But this bandwidth has been previously determined (in Section 6.3.2) as a compromise between the correlation losses, the interference vulnerability and the receiver complexity, then it is recommended to not vary the previously discussed optimal bandwidth for the BPSK receiver.

Similar remarks can be done observing the results obtained with the AltBOC receiver, that are presented in Figure 6.36 and in Figure 6.37. The optimal bandwidth value of 51.150 MHz leads to a performance degradation with respect of wide-band case.

The wide-bandwidth configuration of the AltBOC receiver (scenario 5) performs similarly than the BPSK receiver with the same bandwidth (scenario 3). Some differences are evident only comparing the receivers with their respective optimal bandwidth (scenario 4 and scenario 6): the AltBOC receiver performs better than the BPSK one, as shown in Figure 6.38, but it must be noted that the former uses a wider bandwidth than the latter.

It must also be noted that the obtained S-curves with these bandlimited configurations shows multiple zero-crossing (see Figure 6.34 and Figure 6.36). This leads to false lock problems, that are typical of the BOC-like modulations and affect also the the previous multipath mitigation techniques. A solution for this issue could be to use a bump-jump approach for the tracking loop (see [32]), as done in BOC receivers. Another solution is to insert an offset in the S-curve, to obtain only one stable tracking point for the code discriminator; this solution will be discussed later (see pag. 189).

The results obtained with the AltBOC receiver with a bandwidth of 51.150 MHz (scenario 6) will be used in the following Sections as a reference, to

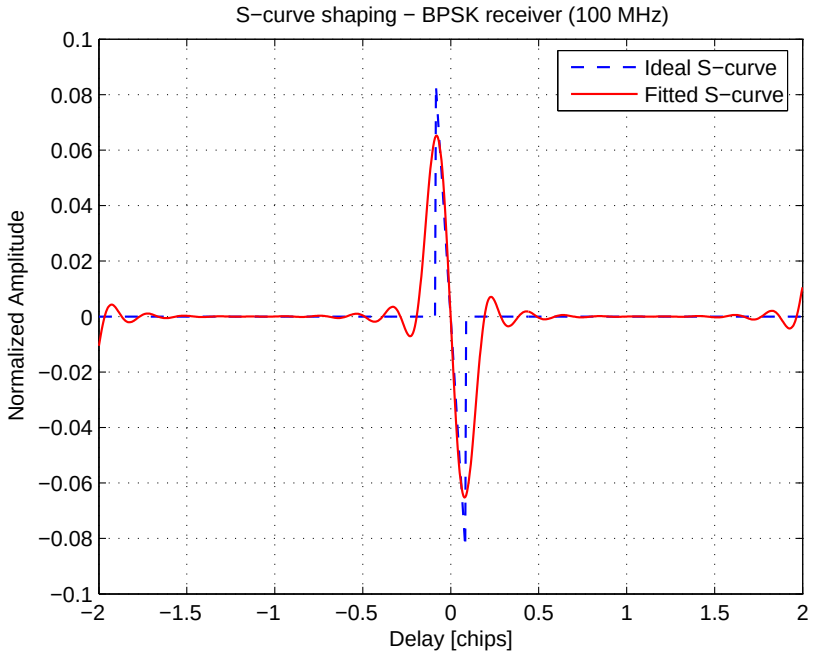

(a)

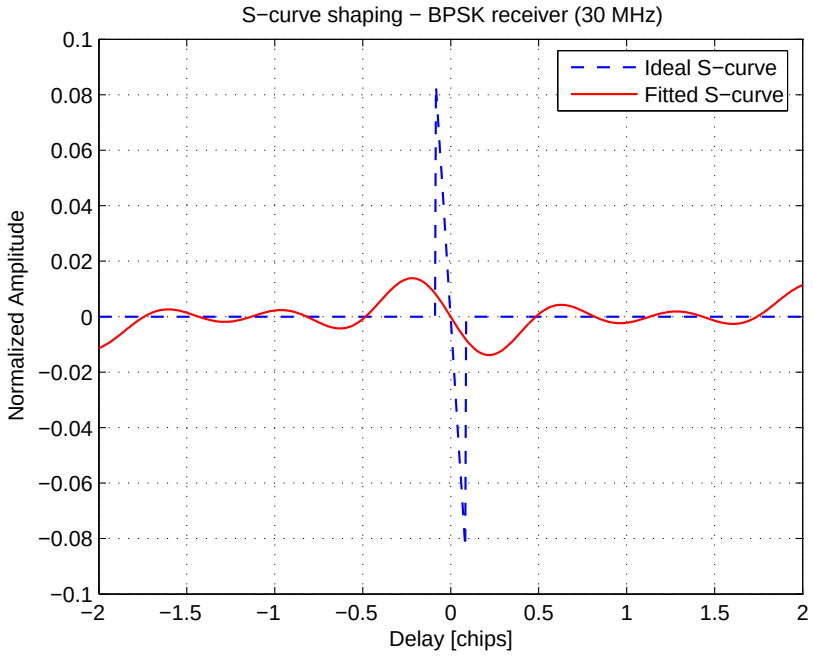

(b)

Figure 6.34: Ideal and fitted S-curves with the shaping technique, for the BPSK receiver with finite bandwidth signals: obtained S-curves in scenario 3 (a) and in scenario 4 (b)

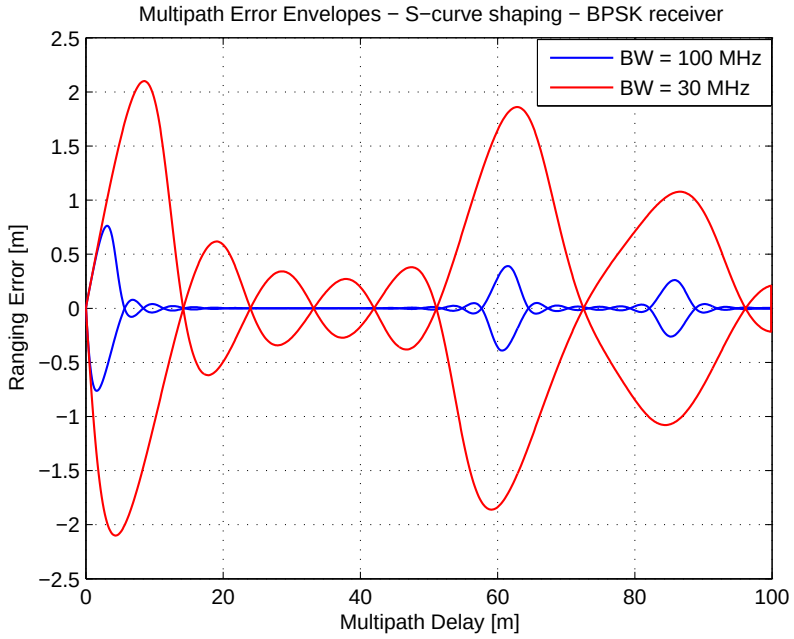

(a)

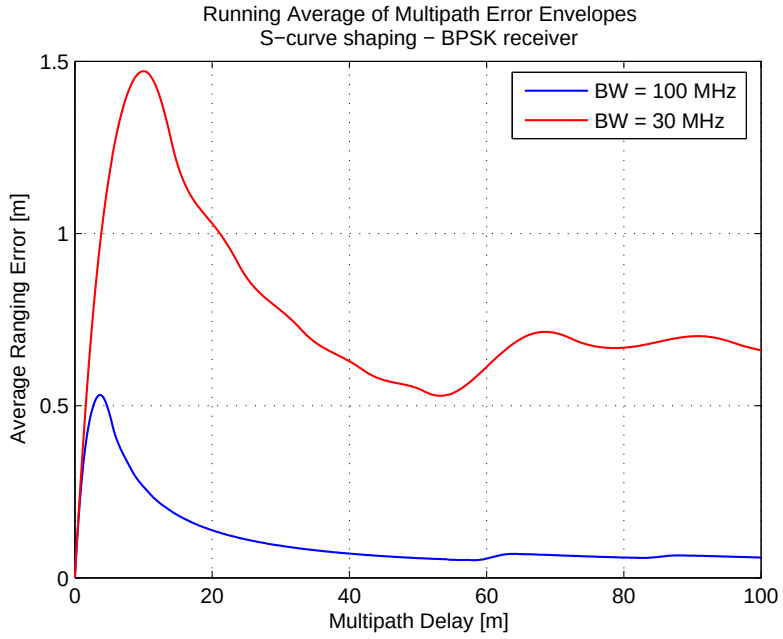

(b)

Figure 6.35: Multipath performances with the S-curve shaping technique, for the BPSK receiver with finite bandwidth signals: multipath error envelopes (a) and running average of multipath error envelopes (b), for a bandwidth of 100 MHz (scenario 3) and 30 MHz (scenario 4)

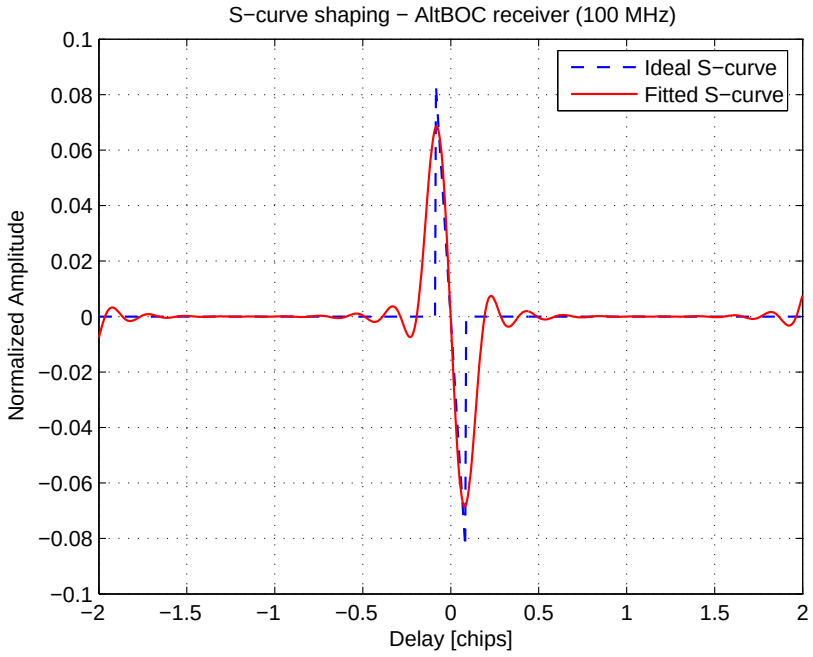

(a)

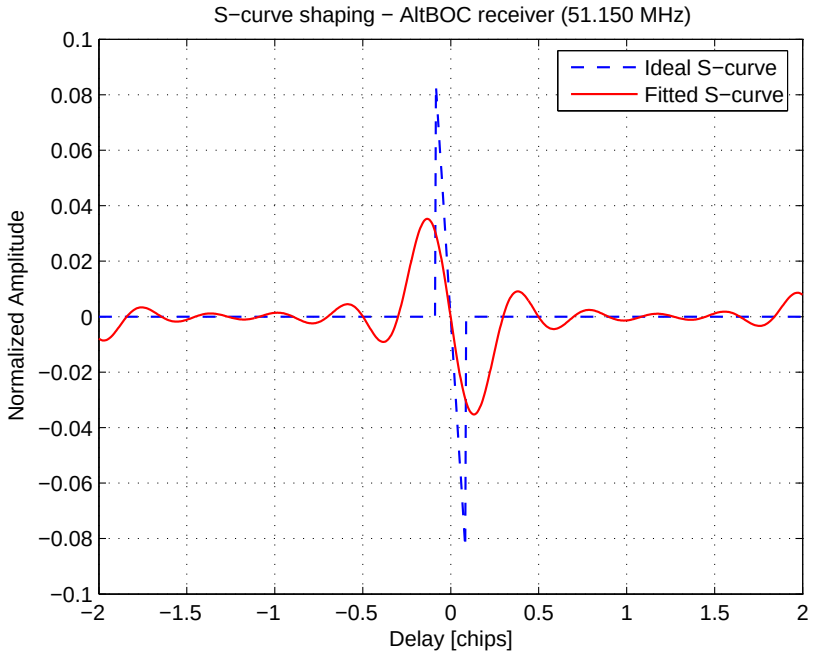

(b)

Figure 6.36: Ideal and fitted S-curves with the shaping technique, for the AltBOC receiver with finite bandwidth signals: obtained S-curves in scenario 5 (a) and in scenario 6 (b)

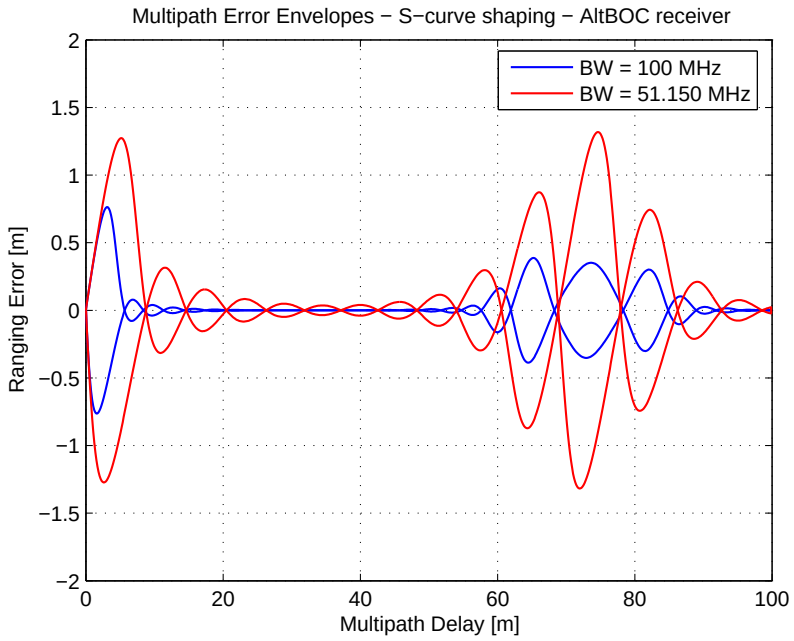

(a)

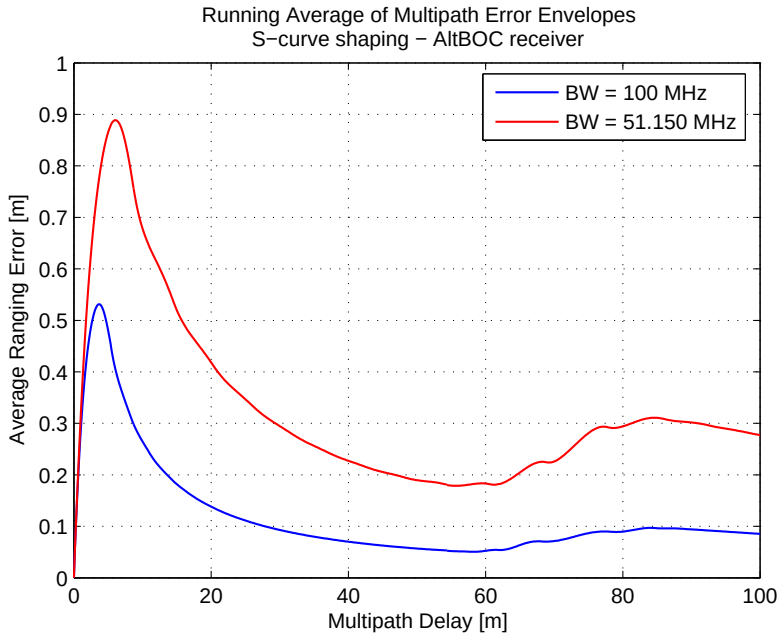

(b)

Figure 6.37: Multipath performances with the S-curve shaping technique, for the AltBOC receiver with finite bandwidth signals: multipath error envelopes (a) and running average of multipath error envelopes (b), for a bandwidth of 100 MHz (scenario 5) and 51.150 MHz (scenario 6)

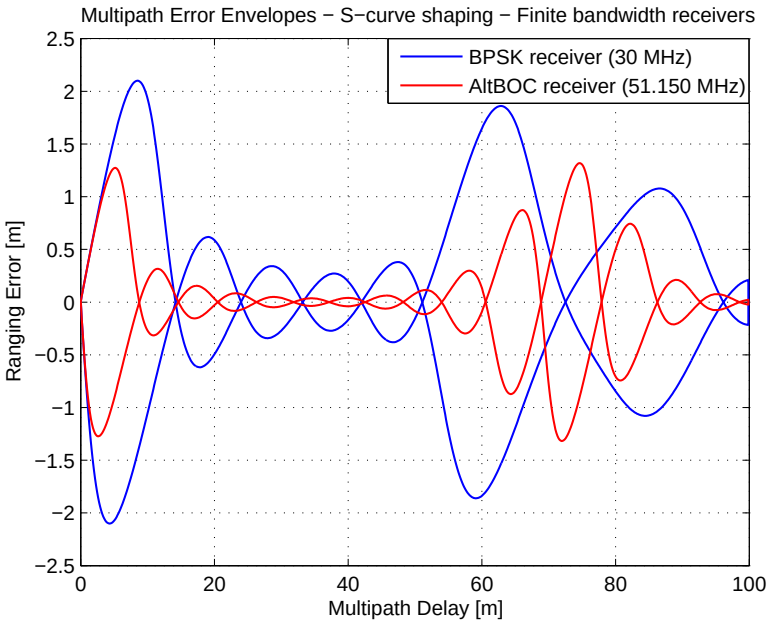

(a)

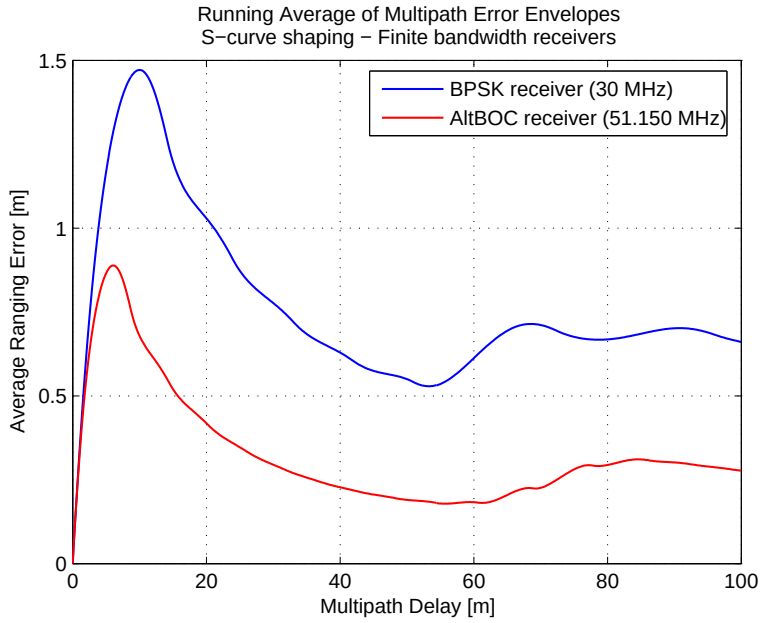

(b)

Figure 6.38: Comparison of multipath performances with the S-curve shaping technique, for the two receiver architectures using their respective optimal bandwidth (30 MHz and 51.150 MHz): multipath error envelopes (a) and running average of multipath error envelopes (b) with the BPSK receiver (scenario 4) and the AltBOC receiver (scenario 6)

examine the influence of some changes on the parameters of the shaping technique.

Results for S-curve with extended linear region

As mentioned above (see pag. 170), the amplitude of the *linear region* of the desired S-curve must be carefully chosen, because influences the noise performances and the multipath mitigation capabilities of the receiver.

This is particularly evident using receivers with limited bandwidth. In fact in this case a larger linear region allows to better fit the ideal S-curve, whereas imposing a narrow linear region the obtained S-curve is distorted and the performances of the receiver are degraded with respect to the infinite bandwidth case.

To illustrate these concepts, a further simulation has been done and the used parameters are presented in Table 6.8. The fitting parameters are the same as in scenario 6 (AltBOC receiver with a bandwidth of 51.150 MHz), with the only difference that the linear region is larger (doubled with respect of scenario 6).

SIMULATION	**Scenario 7**
Receiver architecture	AltBOC receiver
Linear region	±2/12 chip
Fit range	±2 chip
Resolution	1/12 chip
Number of correlators	49
Bandwidth (two-sided)	51.150 MHz
Offset (normalized value)	0

Table 6.8: Simulation settings for the S-curve shaping technique with extended linear region

To simulate this new scenario the weights have been recalculated, assuming an infinite bandwidth (as in previous simulations) and imposing the extended linear region for the fitting. The obtained weights are presented in Figure 6.39(a). They slightly differ from the weights calculated in previous Sections and no interpretation can be given any more about the correlators ($\Delta\Delta$ structures are not present in this case).

The obtained weights have been used with the bandwidth of 51.150 MHz and the result of the fitting is plotted in Figure 6.39(b). It must be noted that in this case the obtained S-curve is a good approximation of the ideal S-curve, thanks to the larger linear region, and the result is better than the fitting obtained in previous scenario (compare with Figure 6.36(b)).

(a)

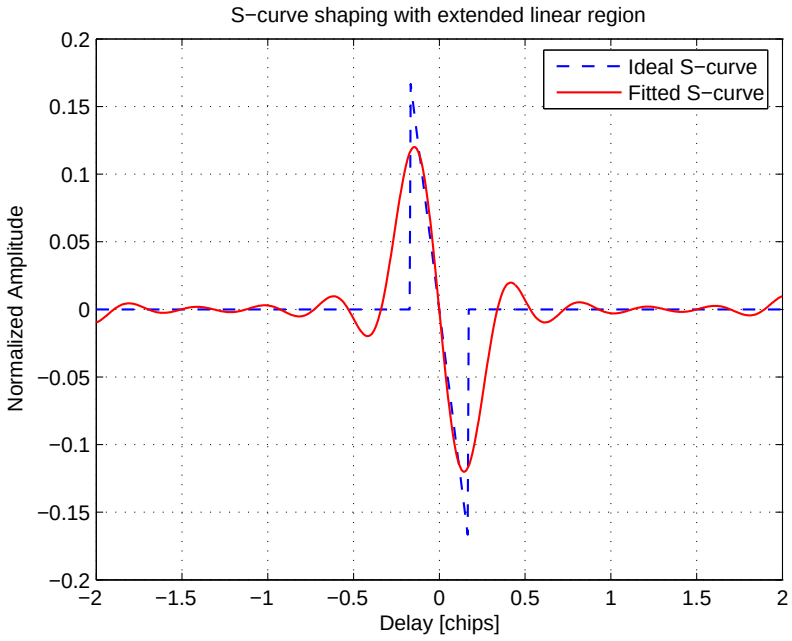

(b)

Figure 6.39: Correlator diagram and obtained S-curve for the shaping technique with extended linear region (scenario 7): correlator positions and weights (a) and obtained S-curves (b) with the AltBOC receiver, using a bandwidth of 51.150 MHz and a linear region of ±2/12 chip

Finally, the multipath performances of the receiver with the extended linear region are presented in Figure 6.40.

A comparison of these graphs with these obtained with the narrow linear region (scenario 6) is presented in Figure 6.41.

Varying the linear region from ±1/12 chip to ±2/12 chip, the multipath performances shows some differences. With the extended linear region the maximum ranging error (obtained with short delay multipath) is slightly bigger, because it is increased the amplitude of the region of the ideal S-curve that is vulnerable to multipath errors. But in this case the running average plot decreases more rapidly and lower errors are experienced for long delays. This effect is due to the fact that the S-curve obtained with the larger linear region is a better approximation of the ideal S-curve than the curve obtained in the other case.

In conclusion, the amplitude of the linear region must be chosen with attention, with particular consideration of the available bandwidth: with a narrow-band receiver could be difficult to fit an ideal S-curve with a narrow linear region, then in some cases an extended linear region could lead to better performances.

Results for modified S-curve with offset

The ideal S-curve used for the fitting could be modified with the insertion of an *offset*, as previously suggested (see pag. 171). This choice is useful to extend the *pull-in region* of the discriminator, reducing the risk of loss of lock for the code tracking loop, that in this way is then capable of following signals even in presence of large errors due to noise or multipath.

Besides, by imposing this offset it is also possible to achieve for bandlimited signals that the code discriminator has only one stable tracking point. In this way the false lock problem, that is typical of the BOC-like modulations and affect also the previous multipath mitigation techniques, is avoided.

The ideal S-curve has been modified inserting an offset of 0.01 (this value is normalized with respect of the peak of the autocorrelation function), that is sufficient to ensure that the discriminator has only one stable tracking point. The parameters of the simulation scenario are illustrated in Table 6.9.

The fitting parameters are the same of these previously used for the scenario 6 (AltBOC receiver, with a bandwidth of 51.150 MHz), except for the offset, that in this case is not null. In this way it is possible to compare the receiver performances in the same configuration, varying only the offset in the S-curve (without offset in scenario 6 and with an offset of 0.01 in this case, that is the scenario 8).

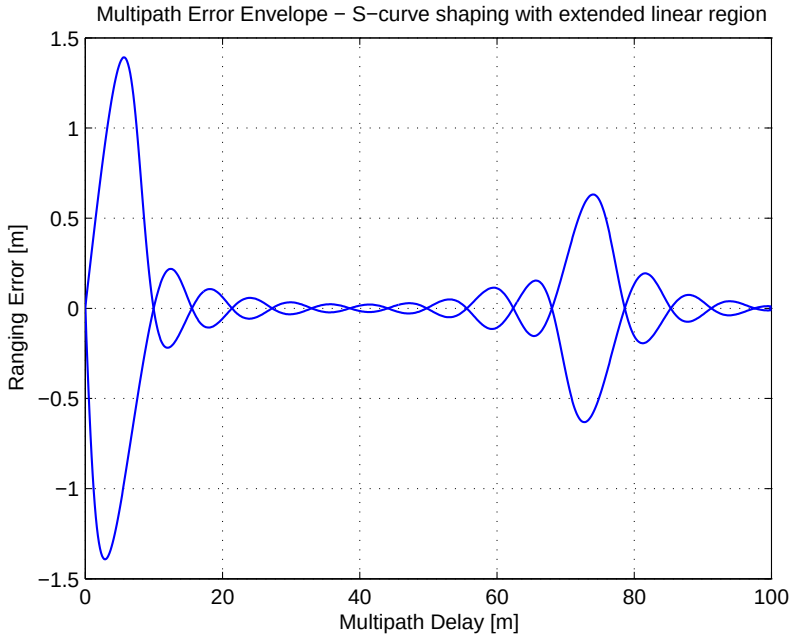

(a)

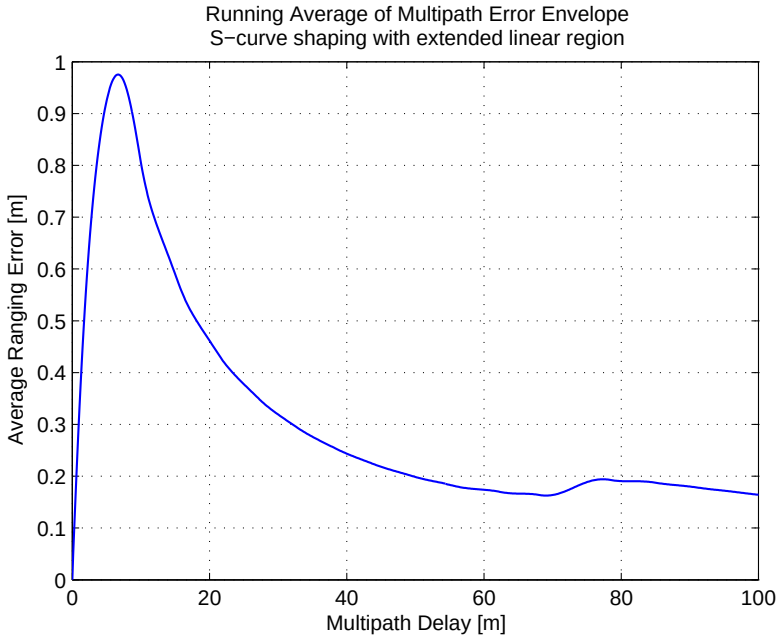

(b)

Figure 6.40: Multipath performances with the S-curve shaping technique with extended linear region (scenario 7): multipath error envelope (a) and running average of multipath error envelope (b) with the AltBOC receiver, using a bandwidth of 51.150 MHz and a linear region of $\pm 2/12$ chip

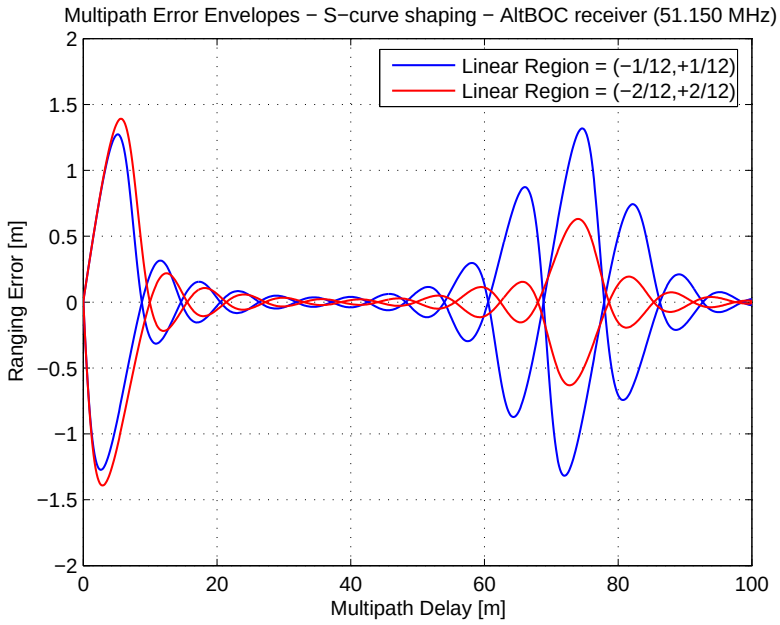

(a)

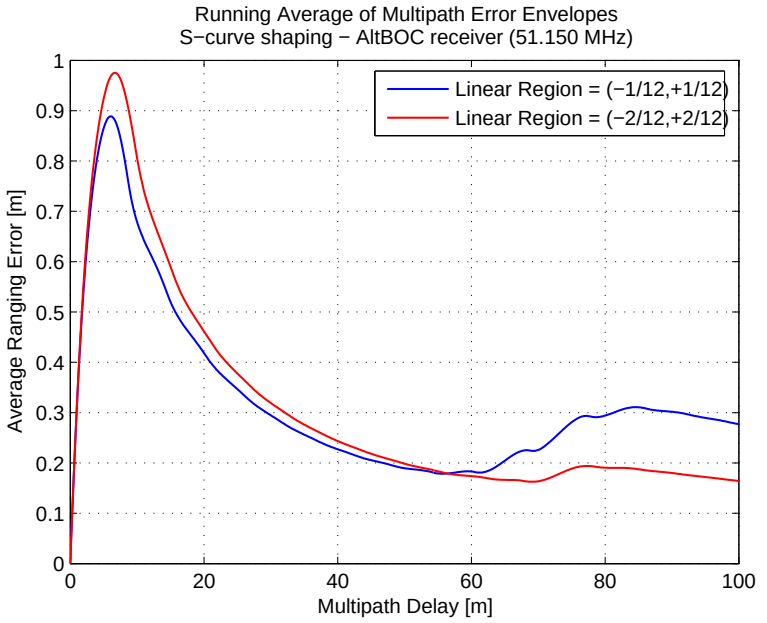

(b)

Figure 6.41: Comparison of multipath performances with the S-curve shaping technique, varying the linear region: multipath error envelopes (a) and running average of multipath error envelopes (b) with the AltBOC receiver with a bandwidth of 51.150 MHz, using a linear region of $\pm 1/12$ chip (scenario 6) and a linear region of $\pm 2/12$ chip (scenario 7)

SIMULATION	Scenario 8
Receiver architecture	AltBOC receiver
Linear region	±1/12 chip
Fit range	±2 chip
Resolution	1/12 chip
Number of correlators	49
Bandwidth (two-sided)	51.150 MHz
Offset (normalized value)	0.01

Table 6.9: Simulation settings for the S-curve shaping technique with offset

The weights for the shaping have been calculated imposing an infinite bandwidth (as in previous Sections) and then they are used with the limited bandwidth. In Figure 6.42 there are plotted the obtained weights and the corresponding S-curve. One can clearly see the offset in the S-curve, that extend the pull-in region and avoid spurious zero-crossing.

The multipath performances obtained with this receiver configuration are presented in Figure 6.43. The multipath error envelope points out that the performances of the receiver are degraded with respect of previous simulation scenarios. The imposed offset on the S-curve produces a non null ranging error outside the linear region, thus the multipath envelope worsens for medium and long delay multipaths.

In Figure 6.44 a comparison between the multipath performances in the case without offset (scenario 6) and with offset (scenario 8) is shown. It is evident that the offset strongly affects the receiver performances in presence of multipath.

Unless this performance degradation, the introduction of an offset on the S-curve could be considered as an alternative of the unambiguous tracking techniques typically used with BOC-like signals (e.g. see the bump-jumping algorithm in [32] or the technique in [42]). This technique then avoids the risk of false lock in the tracking loop, without increase the complexity of the receiver, but with a worsening in the multipath performances.

Remarks about the S-curve shaping technique

In previous Sections the shaping technique has been adapted to the two receiver architectures for the AltBOC signal and the multipath performances in 8 different simulation scenarios has been assessed.

A first remark about this technique, as conjectured in [46], is that the best possible multipath mitigation performance with a coherent multi-correlator architecture is a feature of the signal bandwidth and the size of linear region

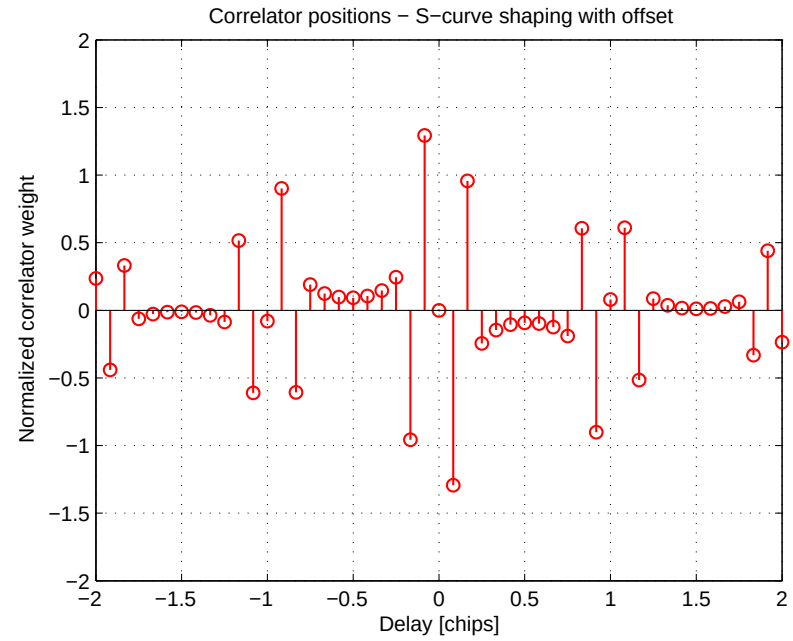

(a)

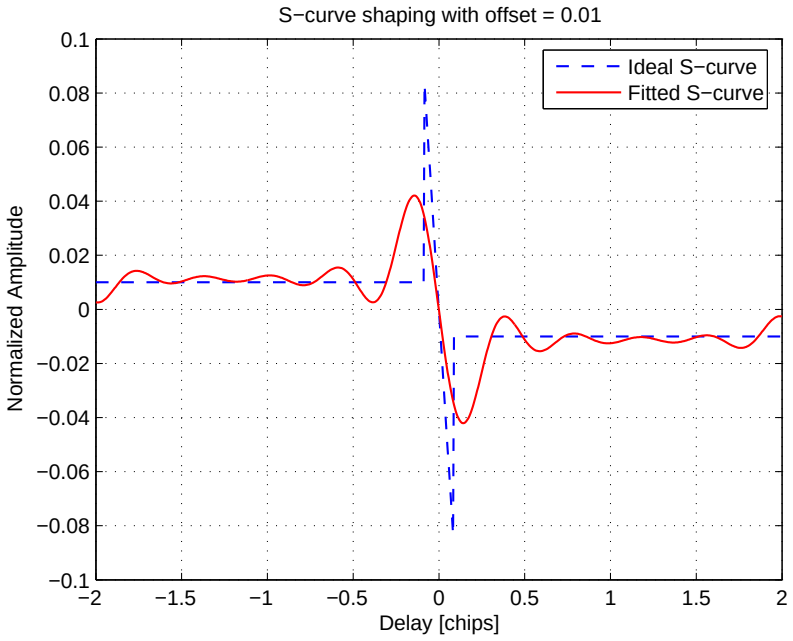

(b)

Figure 6.42: Correlator diagram and obtained S-curve for the shaping technique with offset (scenario 8): correlator positions and weights (a) and obtained S-curves (b) with the AltBOC receiver, using a bandwidth of 51.150 MHz and an offset of 0.01 (normalized value)

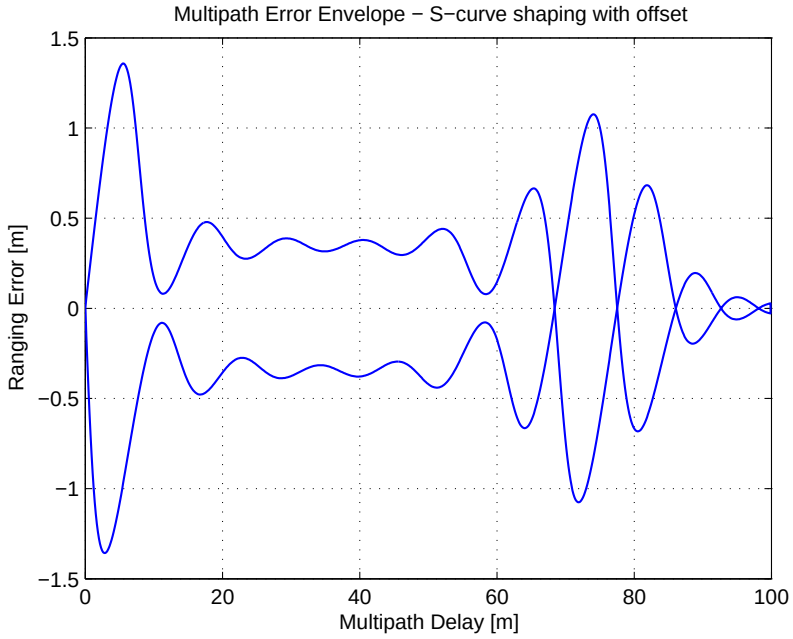

(a)

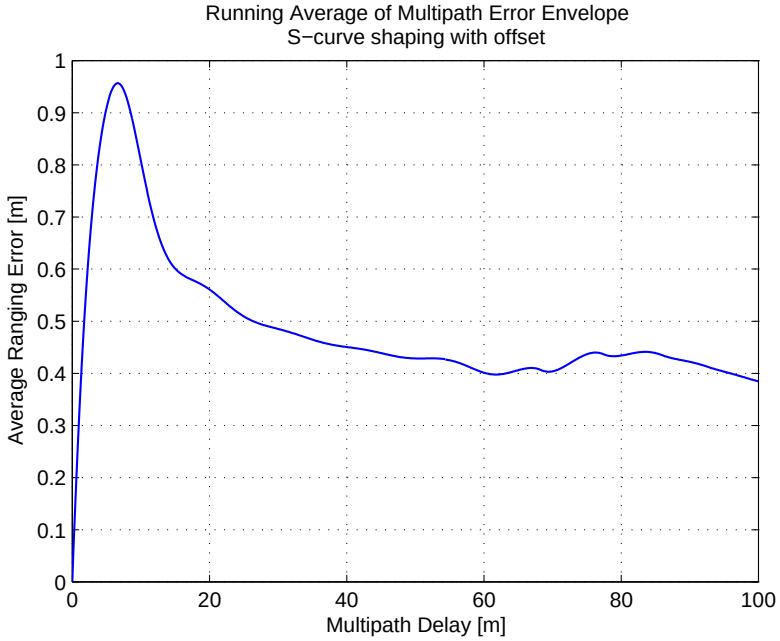

(b)

Figure 6.43: Multipath performances with the S-curve shaping technique with offset (scenario 8): multipath error envelope (a) and running average of multipath error envelope (b) with the AltBOC receiver, using a bandwidth of 51.150 MHz and an offset of 0.01 (normalized value)

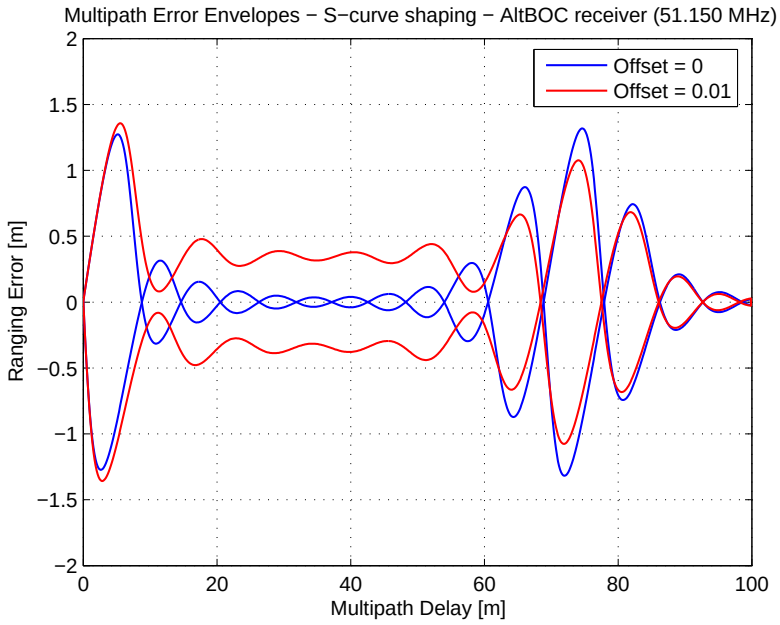

(a)

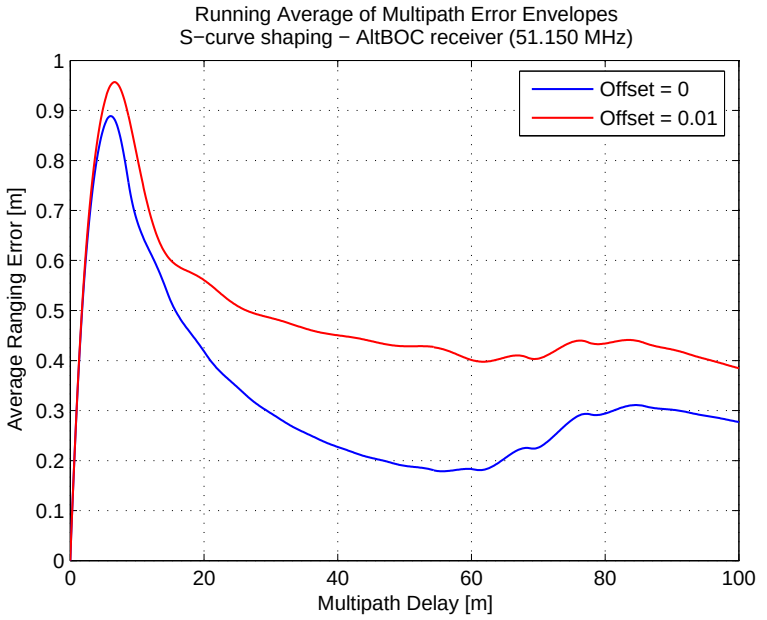

(b)

Figure 6.44: Comparison of multipath performances with the S-curve shaping technique, applied without offset or with offset: multipath error envelopes (a) and running average of multipath error envelopes (b) with the AltBOC receiver, using a bandwidth of 51.150 MHz and applying the S-curve shaping without offset (scenario 6) or with an offset of 0.01 (scenario 8)

of the corresponding code discriminator and does not depend on which modulation scheme is used. In fact, with a large bandwidth the BPSK receiver and the AltBOC receiver show the same performances. In previous Sections a difference in performances was found only using the optimal finite bandwidths previously discussed, that are different for the two architectures.

A further simulation scenario is presented in Table 6.10, where the shaping technique is applied to the BPSK receiver, with the same bandwidth previously used for the AltBOC receiver (scenario 6). The obtained weights and the fitted S-curve are plotted in Figure 6.45.

SIMULATION	**Scenario 9**
Receiver architecture	BPSK receiver
Linear region	±1/12 chip
Fit range	±2 chip
Resolution	1/12 chip
Number of correlators	49
Bandwidth (two-sided)	51.150 MHz
Offset (normalized value)	0

Table 6.10: Simulation settings for the BPSK receiver, with the same bandwidth previously used for the AltBOC receiver (scenario 6), using the S-curve shaping technique

In Figure 6.46 a comparison of the multipath performances obtained in this simulation scenario for the BPSK receiver with those ones of the AltBOC receiver with the same bandwidth (51.150 MHz) is presented.

One can clearly see that the multipath envelopes and the running average plots are overlapped in the fitting region (for multipath delays less than 58.65 meters). This demonstrates that also in these conditions the BPSK receiver achieves the same performance of the AltBOC receiver, then with the shaping technique the best possible multipath mitigation performance does not depend on which modulation scheme is used. Obviously this assertion results true only if a sufficient bandwidth is used: in this case a bandwidth of 51.150 MHz was used, corresponding to 5 times the code chip rate (10.23 Mchip/s). Otherwise the performances are strongly degraded and distinct modulation schemes can lead to different performances.

Then, as shown in previous simulations, to obtain good multipath performances with the shaping technique it is indispensable to use a wide bandwidth. But this implies an increase of the complexity of the hardware. Furthermore the maximum usable bandwidth is also limited by interference issues due to signals present in adjacent bands (as previously discussed in Section 6.3.2).

Another critical parameter is the amplitude of the linear region, that must be chosen like a compromise: it must be small to obtain good multipath

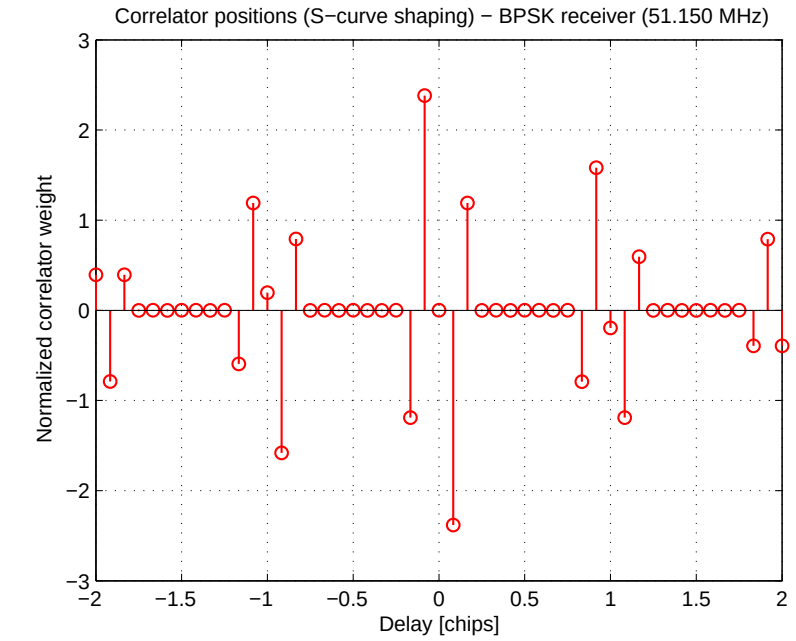

(a)

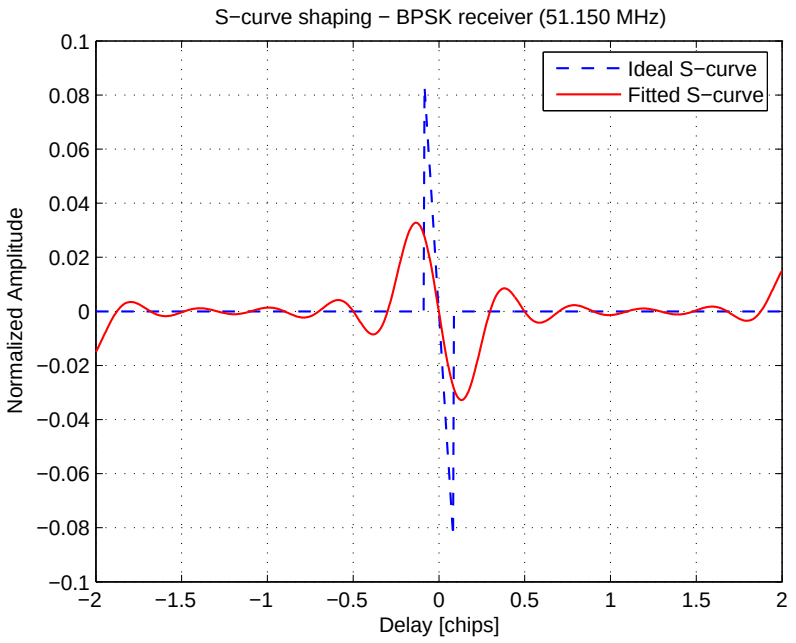

(b)

Figure 6.45: Correlator diagram and obtained S-curve with the shaping technique for the BPSK receiver, with the same bandwidth previously used for the AltBOC receiver (scenario 6): correlator positions and weights (a) and obtained S-curves (b) with the BPSK receiver, using a bandwidth of 51.150 MHz (scenario 9)

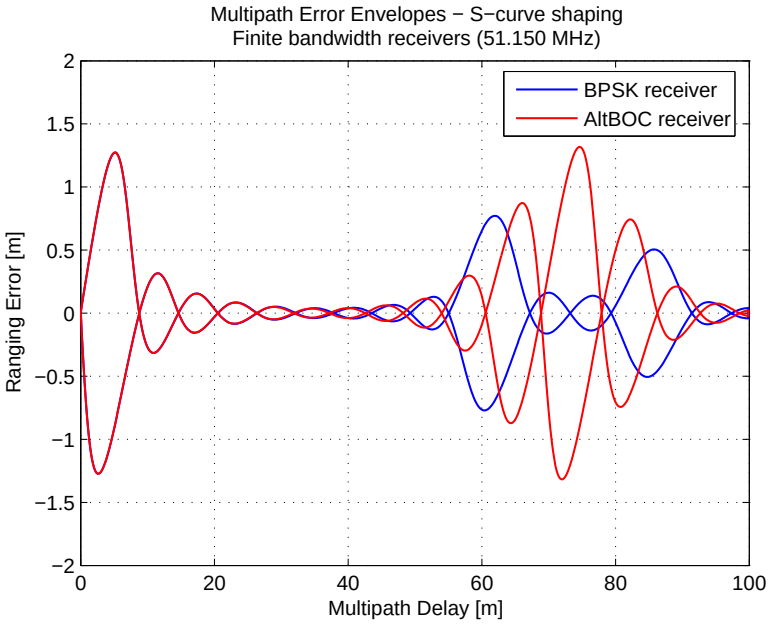

(a)

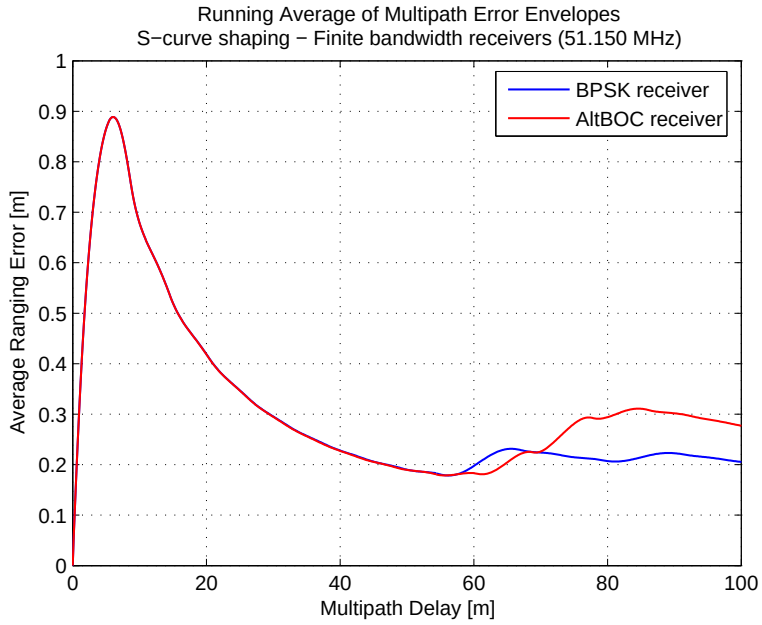

(b)

Figure 6.46: Comparison of multipath performances with the S-curve shaping technique, for the two receiver architectures using the same limited bandwidth (51.150 MHz): multipath error envelopes (a) and running average of multipath error envelopes (b) with the BPSK receiver (scenario 9) and the AltBOC receiver (scenario 6)

performances but, to avoid losses of lock in the tracking loop in presence of noise, it is necessary a large linear region.

An interesting choice is to use an offset, to enlarge the pull-in region of the discriminator without modify the linear region. In this way also the false locking points are avoided, obtaining only one zero-crossing in the S-curve. The drawback of this method is a degradation of the multipath performances.

Considering the noise performances of the coherent multi-correlator architecture needed for the shaping technique, it must also be pointed out that a linear combination of multiple correlators leads to a worsening of the tracking jitter. This is due to the fact that the contributions in term of noise of the correlators are summed. Then, increasing the number of used correlators, the receiver shows an evident worsening of the noise performances with respect of the other current multipath mitigation techniques (that uses at most 5 correlators).

Another drawback of the shaping technique is the hardware complexity implied for the receiver with respect of previous techniques. To reduce the number of correlators it is possible to remove those correlators that results with null or negligible weights.

But the multi-correlator could also be efficiently realized with less hardware taking advantage of an observation made in [46]: instead of using multiple correlators, the same result is obtained by correlating the incoming signal with a so-called *code-tracking-reference-function*. It is a linear combination of shifted replicas of the sampled PRN code and can be pre-computed and stored in memory. In this way the multi-correlator structure becomes a single coherent correlator, that uses a complicated local signal.

As final remark, it must be noticed that in previous simulations only coherent discriminators have been considered. In this way the simulations have been simplified and it is then possible to compare the obtained results with those of the previous techniques (based on coherent discriminators too). Obviously the shaping technique previously illustrated could be easily adapted for non coherent configurations (e.g. as done in [46] or in [47]).

6.5.2 Gating technique

The **gating technique** is based on the concept of the *Code Correlation Reference Waveforms* (CCRW). With this arrangement the receiver must generate a gated reference function, that is zero for almost all the time, having short spikes in presence of the received signal transitions. This gated function is used to modify the shape of the code chips of the local code. Being a large part of the received signal blanked by the correlation with the gating function, multipaths eventually present with a delay greater than the gate amplitude will be blanked too. Only short delay multipaths have effect on the locking point.

The gating technique is discussed in detail in Reference [44], using a quite complex gated function tailored to the GPS C/A signal. The gated correlator is then used to derive the *High Resolution Correlator* (HRC, previously presented in Section 6.4.3).

In Reference [47] the CCRW technique is applied to the BOC(1,1) signal, introducing a gating function called *Bipolar Reference Waveform* (BRW). Unfortunately it is not straightforward to extend this approach to the AltBOC modulation. It is difficult to define a simple gating function for the AltBOC, like the *Bipolar Reference Waveform* for the BOC(1,1), because the modulated signal has a multilevel waveform and the AltBOC autocorrelation function is more complicated than the BOC one, then this approach is not used in the following.

The gating technique is also discussed in Reference [15]. In this article, a simple gating function is introduced for the Galileo BOC(1,1) signal (see Figure 6.47): the local code is multiplied by a gating function that is non zero only near the chip boundaries.

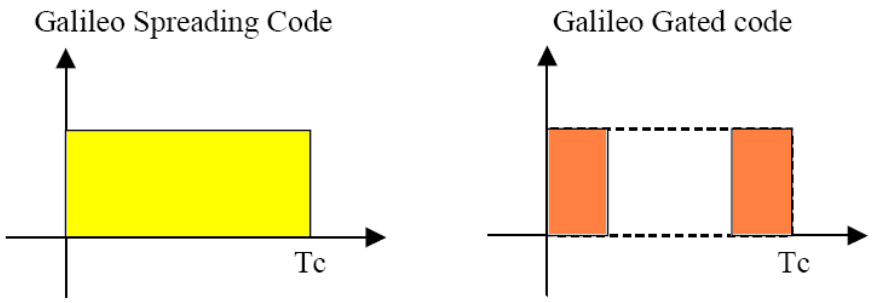

Figure 6.47: Galileo spreading code and its gated version [15]

In [15] it is demonstrated that correlating the received BOC(1,1) signal with the gated local code, the result is a S-function, that could be directly used as a discriminator function. Therefore, it is not needed to implement the early-late structure of a standard GPS architecture and then it is not needed anymore the discriminator block. In fact, the multiplication between the BOC(1,1) with the local gated code becomes equivalent to the Early-Late operation at the receiver. This innovative scheme presents then considerable advantages, because the needed hardware is reduced: only the punctual channel of the DLL remains necessary, whereas the local code generators and the correlators for the Early and Late channels and the discriminator block are no needed anymore.

This gating technique could also be applied to the previously discussed receiver architectures for the AltBOC signal, removing the structures for the Early-Late discrimination and modifying the punctual code generators with a gated reference function.

The gating function shown in Figure 6.48(a) could be used for the BPSK receiver architecture. A *blanking factor* of 11/12 ($\cong$ 92%) has been chosen: this means that the gating function is shaped in order that only 1/12 of the chip time is not blanked (1/24 at the beginning and 1/24 at the ending of the chip). This function is different from the gating function previously suggested in Figure 6.47, because in this case the processed signal is not BOC modulated as in [15], but is BPSK modulated. Then it is necessary to reverse the sign on the right side of the gating function, to obtain again a discriminator function. Accordingly, the result of the correlation between the received signal and the local gated code is the discriminator function shown in Figure 6.49(a).

Otherwise, with the AltBOC receiver the gating reference function must be further modified, because the previous ones do not work with the AltBOC signal: this is due to the fact that every code chip in the AltBOC is modulated with the subcarrier waveform, then the modulated signal could be zero at the chip boundaries.

A gating function that could work with the AltBOC signal is shown in Figure 6.48(b). This function corresponds to centrally gate the code chip around its center. As for the BPSK case, the sign of the right side of the function is reversed and the same *blanking factor* (11/12) has been used: the obtained discriminator function is shown in Figure 6.49(b).

The multipath performances of the two receivers (respectively the BPSK receiver with a bandwidth of 30 MHz and the AltBOC receiver with a bandwidth of 51.150 MHz), modified with the gating technique, are presented in Figure 6.50. Obviously, the AltBOC receiver shows better performance than the BPSK receiver.

It must be noted that the obtained performances are quite similar to those previously obtained with the narrow correlator^{TM}, as demonstrated in Figure 6.51. In fact, as previously noticed, the gating operation is equivalent to an Early-Late operation.

The gating technique could then be considered as a different way to implement an E-L discriminator structure, with considerable advantages in term of hardware (saving two correlators, two local signal generators and the discriminator block). The only cost is that the local code generated in the receiver must be modified with a gated reference function. The obtained multipath performance is very similar to those of the narrow correlator^{TM}, for both the receiver architectures.

But considering also the tracking performance in presence of noise, it must be noted that a large part of the received signal is blanked by the correlation with the gating function: this leads to conjecture a poor noise performance for the gating technique. Further analysis are necessary to prove this statement, but are not concerned in this thesis, where only the multipath mitigation is discussed.

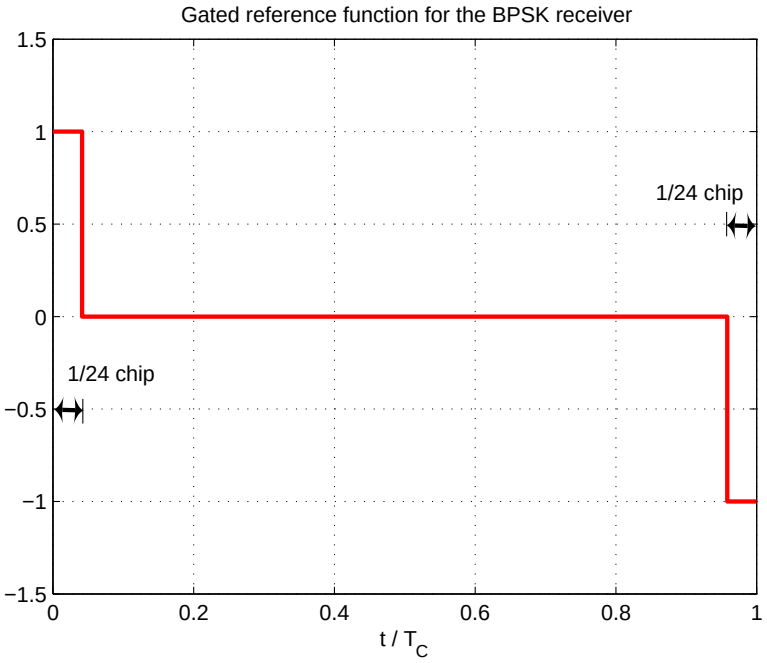

(a)

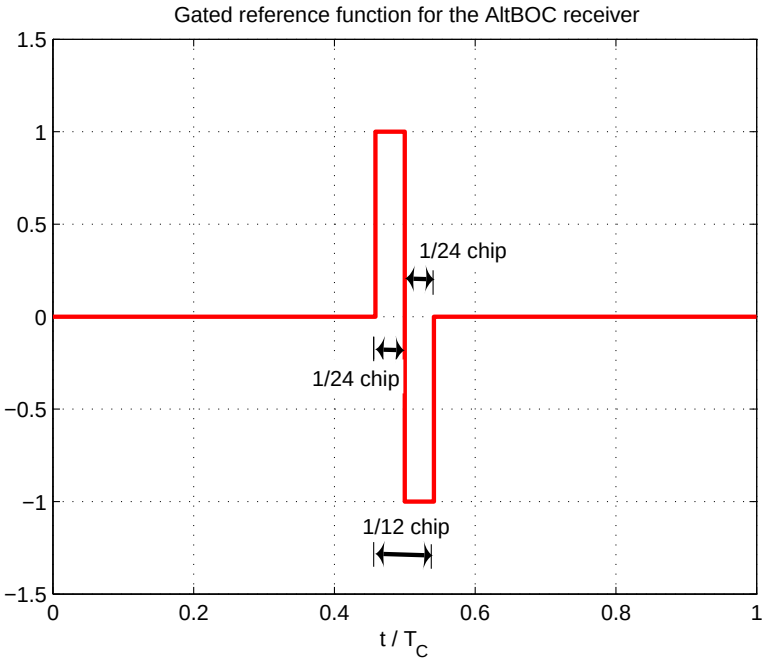

(b)

Figure 6.48: Gated reference functions for the gating technique, applied to the two receiver architectures: function for the BPSK receiver (a) and function for the AltBOC receiver (b)

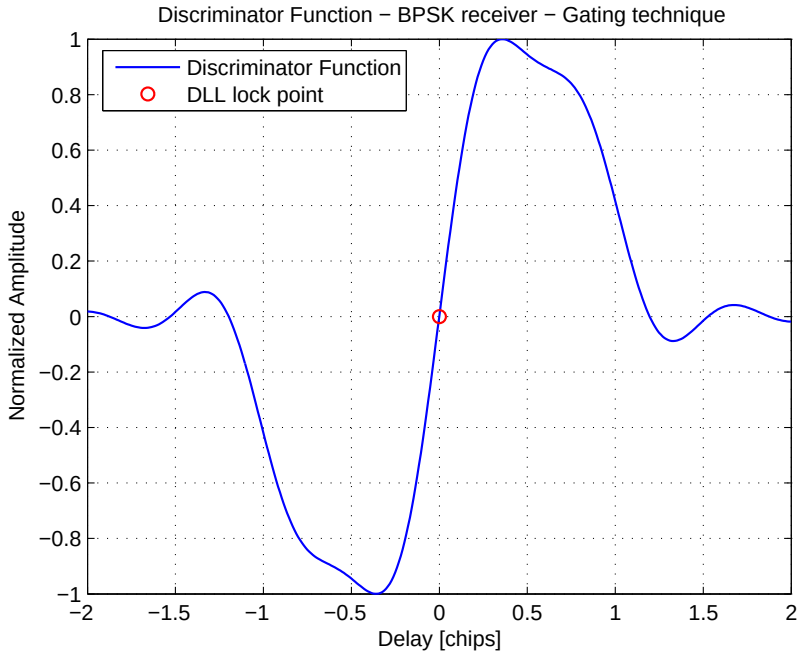

(a)

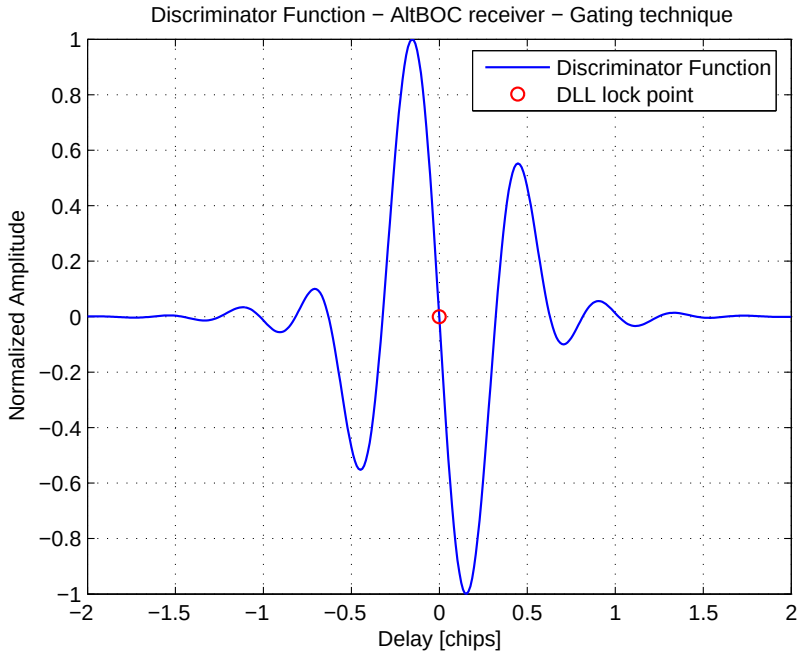

(b)

Figure 6.49: Discriminator functions obtained with the gating technique, for the two receiver architectures: discriminator function for the BPSK receiver (30 MHz) (a) and for the AltBOC receiver (51.150 MHz) (b)

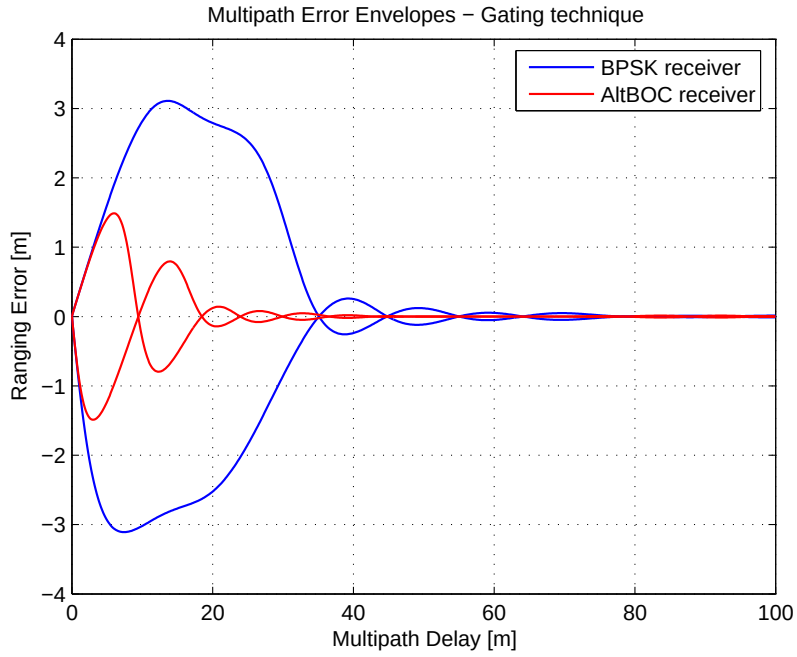

(a)

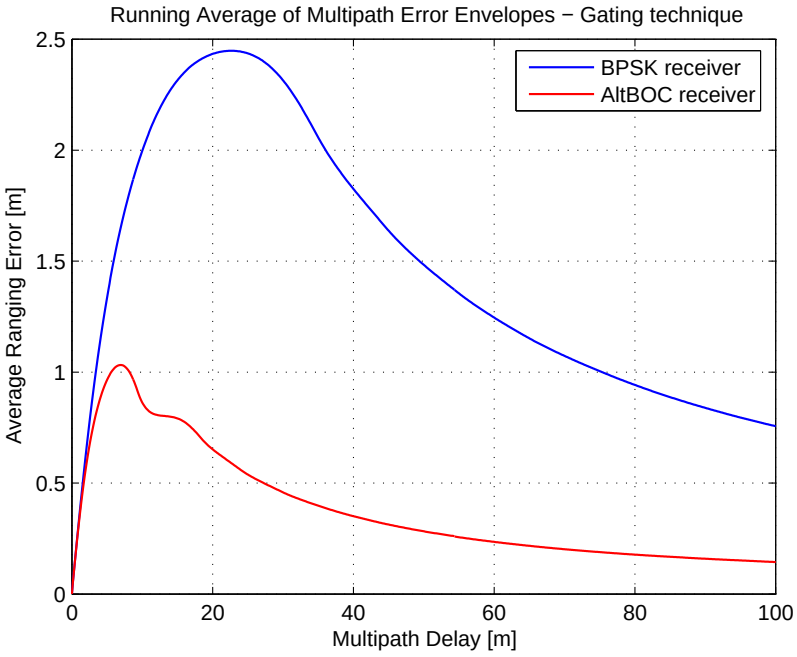

(b)

Figure 6.50: Multipath performances with the gating technique: multipath error envelopes (a) and running average of multipath error envelopes (b), for the two receiver architectures (BPSK receiver with 30 MHz and AltBOC receiver with 51.150 MHz)

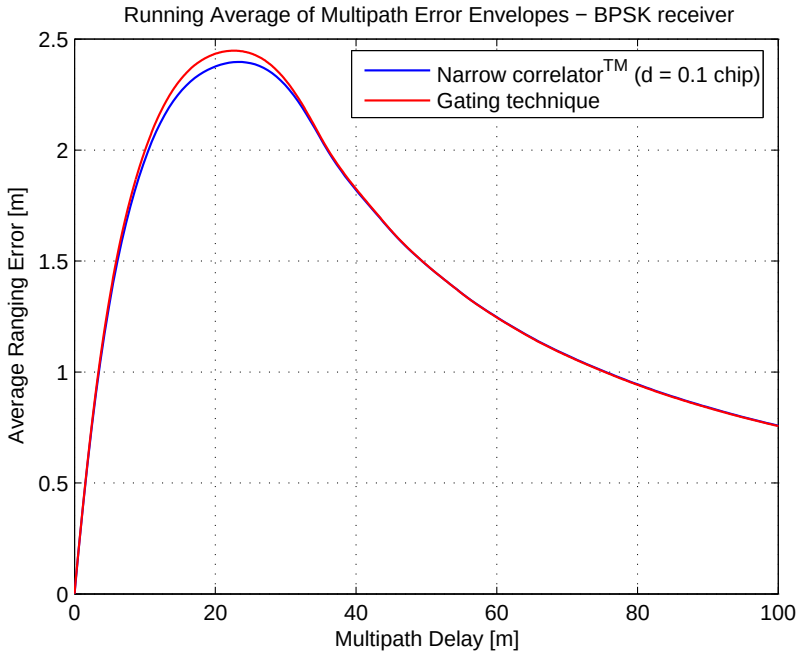

(a)

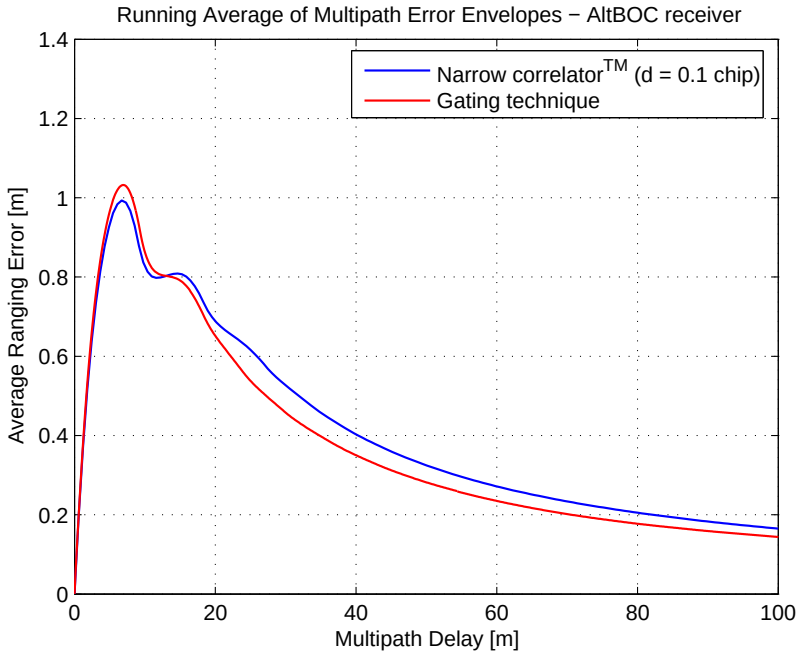

(b)

Figure 6.51: Comparison of multipath performances between the the narrow correlator™ (with d = 0.1 chip) and the gating technique, applied to the two receiver architectures: the BPSK receiver (a) and the AltBOC receiver (b)

6.5.3 Performance comparison with previous multipath mitigation techniques

The multipath performances obtained with the S-curve shaping and the gating technique must be compared with these of the mitigation techniques currently used in GPS receivers, previously presented and adapted to the two receiver architectures for the AltBOC signal (see Section 6.4).

To easily compare the performances with the different techniques, the running average of multipath error envelopes has been used (as previously done in Section 6.4.6).

For the S-curve shaping, the results obtained using the optimal bandwidths of the two receivers (respectively 30 MHz and 51.150 MHz) have been considered, to compare this technique in the same conditions of previous techniques. In detail, the results previously obtained in simulation scenario 4 (for the BPSK receiver) and in scenario 6 (for the AltBOC receiver) has been considered (see Section 6.5.1).

In Figure 6.52 the running average plots obtained with the emerging multipath mitigation techniques are compared with previous results. The performances achieved with the shaping technique are pointed out with dashed blue lines, while the results for the gating technique are plotted with dashed red lines.

One can see that in these conditions the shaping technique leads to performances that are overcome by some more simple techniques. For the BPSK receiver architecture the E1/E2 tracker and the ELS technique perform better than the shaping technique. The ELS technique outperforms the shaping technique also with the AltBOC receiver.

Besides, one can see that outside the fitting region (for multipath delays greater than 58.65 meters) the shaping technique leads to worse multipath errors than other techniques: in fact in this region the running average plots increase only for the shaping technique. To avoid this issue it is necessary to use a larger linear region.

It must be noted that the performances obtainable with the shaping technique are strongly related with the receiver bandwidth: better performances could be obtained with a larger bandwith. But this statement is also true for the other multipath mitigation techniques. Furthermore, a bandwidth increase could be problematic, for the interference vulnerability of the receiver and for its hardware complexity and cost.

Considering the gating technique, as stated in previous Section, the obtained multipath performances are similar to these of the narrow correlator ^{TM}. The other mitigation techniques could lead to better performances, then the gating technique is not recommended. The only advantage using this approach is in term of hardware, because the gated receiver results more simple.

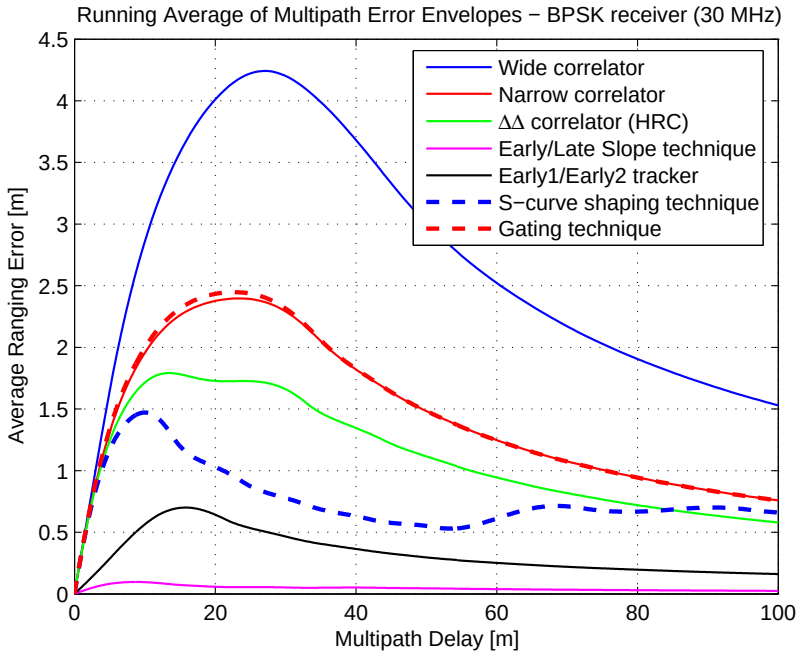

(a)

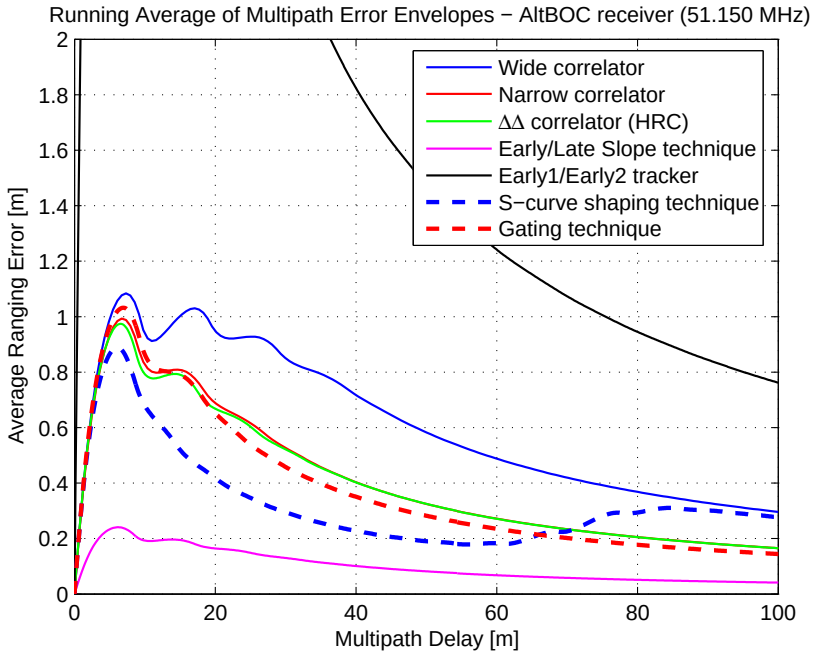

(b)

Figure 6.52: Comparison of multipath performances with current mitigation techniques and with emerging techniques: running average of multipath error envelopes for the BPSK receiver (a) and for the AltBOC receiver (b)

In conclusion, none of the two discussed emerging multipath mitigation techniques is recommended, because better performances could be obtained with some current techniques, previously discussed in Section 6.4.

6.6 Performances of the receiver with the correlator-discriminator

In Chapter 4 there was proposed an interesting and innovative receiver architecture, the **receiver with the correlator-discriminator**. It is a variant of the coherent dual band receiver, with a modified correlator that does not evaluate the complex correlation function, but directly computes a discriminator function (for more details, see Section 4.4.3). In Figure 6.53 there is plotted this function: its shape presents multiple zero-crossing points, involving a false lock issue (as previously discussed, in Section 6.4.3), and its slope in the tracking point is remarkable, allowing to foresee a good multipath performance.

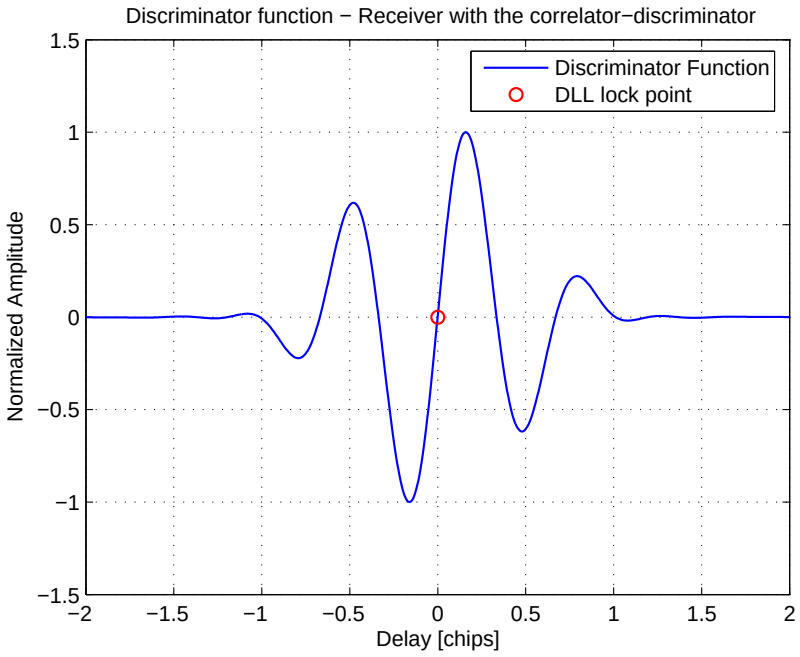

Figure 6.53: Discriminator function obtained using the receiver architecture with the correlator-discriminator, with a pre-correlation bandwidth of 51.150 MHz

It is then interesting to assess the multipath performances of this architecture, comparing the results with those ones obtained with previous arrangements. The simulations performed for this purpose have been carried out using the same parameters used for the AltBOC receiver, as shown in Table 6.11.

Receiver parameters	Receiver with the correlator-discriminator
Frequency band	E5
Center frequency	1191.795 MHz
Modulation type	AltBOC(15,10)
Tracked channels	E5aQ + E5bQ
Chipping rate	10.23 Mchip/s
Chip length	29.31 m
Pre-correlation bandwidth	51.150 MHz (two-sided)
Pass-band filter	Butterworth filter with order 16
Integration time	1 ms (10230 chips)
SMR	6 dB ($\alpha = 0.5$)

Table 6.11: Receiver parameters used for the simulations for the receiver with the correlator-discriminator

Accordingly, the multipath envelope and the corresponding running average of the receiver with the correlator-discriminator are presented in Figure 6.54.

It is also important to remark that, since the discriminator is no longer necessary, the multipath performance of the receiver with the correlator-discriminator does not depend on the correlator spacing. In fact with this arrangement the shape of the discriminator function is fixed (see Figure 6.53) and defined by the signal processing technique, and it is slightly influenced only by the receiver bandwidth.

Comparing the resulting running average in Figure 6.54(b) with the previous ones in Figure 6.52, it must be noticed that this architecture shows good multipath performances, even though some of previous arrangements can outperform this receiver.

In detail, considering the two previous receiver architectures without multipath mitigation techniques (the BPSK receiver and the AltBOC receiver, both with the wide correlator), the receiver with the correlator-discriminator obtain better performances, as illustrated in Figure 6.55.

Obviously, as previously demonstrated, the performances of the BPSK and the AltBOC receiver architectures could be successfully improved with some mitigation techniques and could overcome the actual performance of the receiver with the correlator-discriminator.

In spite of this, the receiver with the correlator-discriminator features a lower hardware complexity than the coherent dual band architecture of the AltBOC receiver, since:

- the discriminator block after the correlators is no longer necessary;

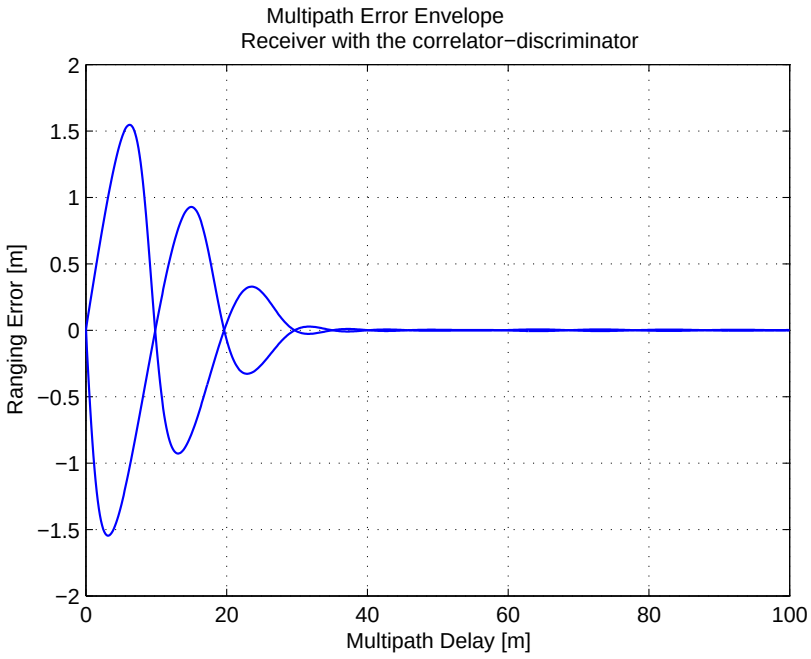

(a)

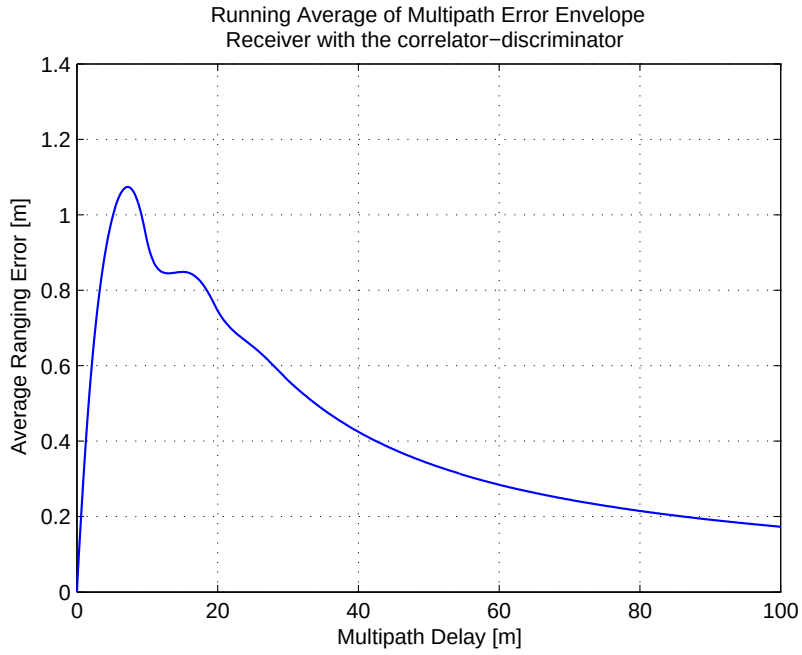

(b)

Figure 6.54: Multipath performances of the receiver with the correlator-discriminator: multipath error envelopes (a) and running average of multipath error envelopes (b)

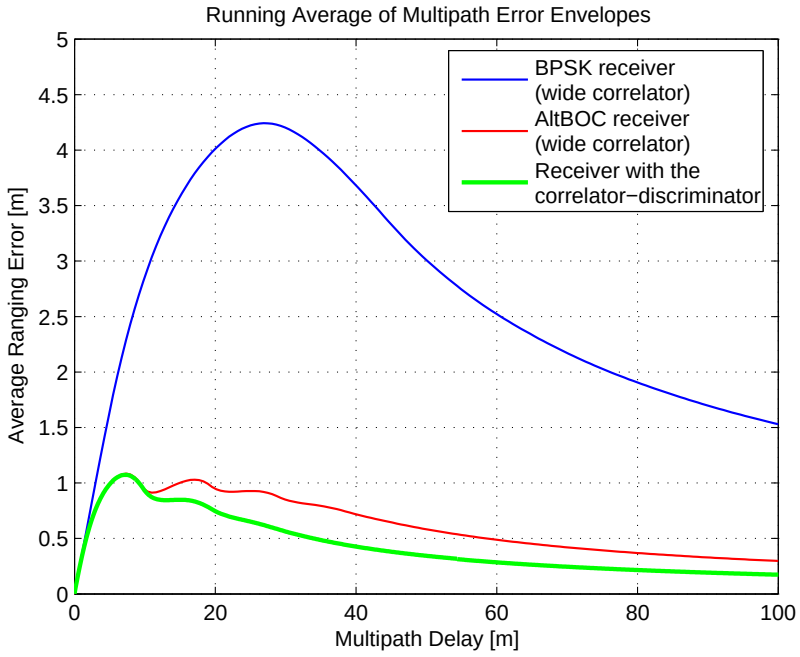

Figure 6.55: Comparison of multipath performances obtained with the three receiver architectures, without multipath mitigation techniques: running average of multipath error envelopes for the BPSK receiver (30 MHz), the AltBOC receiver (51.150 MHz) and the receiver with the correlator-discriminator (51.150 MHz)

- the tracking loop needs only one modified correlator (instead of two or more complex correlators, used in previous arrangements);
- the local signal generation section is simplified, because only the punctual channel must be generated (early and late local signal are now unnecessary).

Besides, the BPSK receiver requires the use of sophisticated mitigation techniques to obtain similar performances than the receiver with the correlator-discriminator, resulting in an increased complexity of the receiver.

In conclusion, the receiver with the correlator-discriminator seems a good compromise between the multipath performances and the receiver complexity and cost for the AltBOC signal, because shows intrinsic good multipath performances without multipath mitigation techniques. Previous architectures can reach better performances than the receiver with the correlator-discriminator, but only using a more complex hardware for mitigation techniques.

Some of these techniques could also be adapted to the receiver with the correlator-discriminator and the results will be presented and discussed in following Sections.

6.7 Multipath mitigation with the innovative architecture

The current multipath mitigation techniques (previously discussed in Section 6.4) are not suitable to the receiver with the correlator-discriminator. In fact this innovative architecture use only one modified correlator and does not include the discriminator block, that is modified with the standard mitigation techniques, using multiple correlators, to improve the multipath performance.

Only the emerging mitigation techniques (introduced in Section 6.5 for the two previous architectures) can be adapted to this innovative architecture, with some feasible adjustments. Then the **S-curve shaping** and the **gating technique** are discussed in the following, evaluating the obtainable performance improvement for the receiver with the correlator-discriminator.

6.7.1 S-curve shaping technique

The S-curve shaping technique, previously presented in Section 6.5.1, could be easily adapted to the innovative architecture simply changing the input function for the fit of the ideal S-curve. Instead of use a correlation function (as done for the BPSK and the AltBOC receivers), in this case the starting point for the fit is the discriminator function obtained with the correlator-discriminator (previously shown in Figure 6.53).

The shaping technique is then applied in a similar manner than in previous simulations (see Section 6.5.1): the weights W for the fit are estimated inverting the matrix $\overline{M}_R$, that in this case contains the shifted replicas of the discrimination function, with the following equation:

$$W = S_{ideal} \cdot \left(\overline{M}_R\right)^{-1} \tag{6.23}$$

where S_{ideal} is the vector with the samples of the ideal S-curve.

Then the performance of the innovative receiver has been assessed in two simulation scenarios, with the parameters summarized in Table 6.12. The first scenario features an infinite bandwidth, and is used to correctly evaluate the weights W (as previously done in Section 6.5.1). These weights are used in the second scenario (with a finite bandwidth of 51.150 MHz) to assess the true receiver performance.

The obtained weights are presented in Figure 6.56(a).

In this case the correlator diagram shows that the estimated weights are symmetrical around the origin, whereas in previous arrangements the weights were anti-symmetrical (see Section 6.5.1). This fact agrees with the shape of the initial function used for the fit: in previous situations the initial function was symmetrical (triangular BPSK correlation function or AltBOC correlation

SIMULATIONS	Scenario 1	Scenario 2
Receiver architecture	Receiver with the correlator-discriminator	Receiver with the correlator-discriminator
Linear region	±1/12 chip	±1/12 chip
Fit range	±2 chip	±2 chip
Resolution	1/12 chip	1/12 chip
Number of correlators	49	49
Bandwidth (two-sided)	∞	51.150 MHz
Offset	0	0

Table 6.12: Simulation settings for the AltBOC receiver with the correlator-discriminator, with the S-curve shaping technique

function) and the desired ideal S-curve was anti-symmetrical, while in this case the initial discrimination function is already anti-symmetrical, and the obtained fitted S-curve is shown in Figure 6.56(b).

The resulting multipath performances obtained with S-curve shaping technique are then presented in Figure 6.57.

It is possibile to see that with this mitigation technique the receiver achieves a good performance only in the fitting region (2 chips, that in this case are equal to 58.65 meters), as noted for previous receiver architectures. For a multipath delay greater than 2 chips the performances are strongly degraded, but this problem could be neglected because typically only the region of the discrimination function between -1 and +1 chip is significative for the DLL, whereas outside this region the tracking loop loses the lock and could not produce further errors.

Referring to the implementation complexity, the shaping technique could be efficiently implemented with a single modified correlator instead of multiple correlators (49 correlators, in previous simulations), as previously discussed at pag. 199. It is necessary to correlate the incoming signal with a reference function, evaluated like a linear combination of shifted replicas of the local signals (subcarrier and PRN codes) previously used at the input of the correlator-discriminator. In this way the hardware of the receiver is not substantially increased: only the local signal generation section is sightly more complex.

6.7.2 Gating technique

Also the gating technique (previously proposed in Section 6.5.2) could be easily adapted to the receiver with the correlator-discriminator. With this

(a)

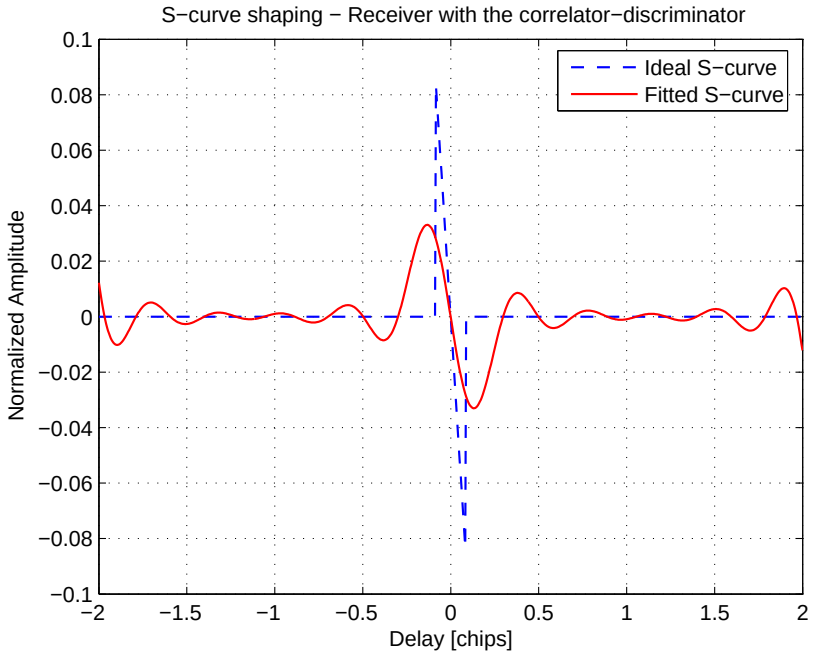

(b)

Figure 6.56: Correlator diagram and obtained S-curve with the shaping technique for the receiver with the correlator-discriminator: correlator positions and weights (a) and obtained S-curves (b)

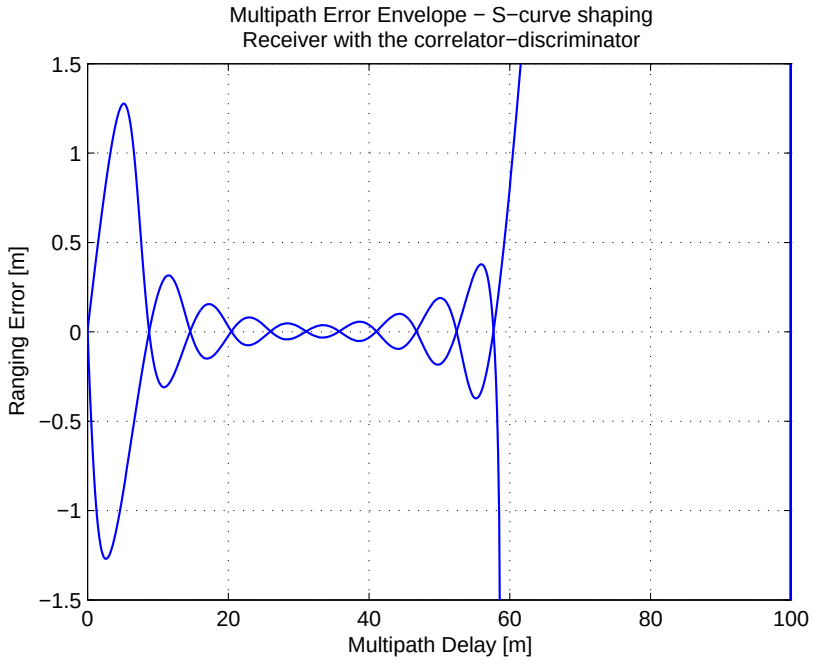

(a)

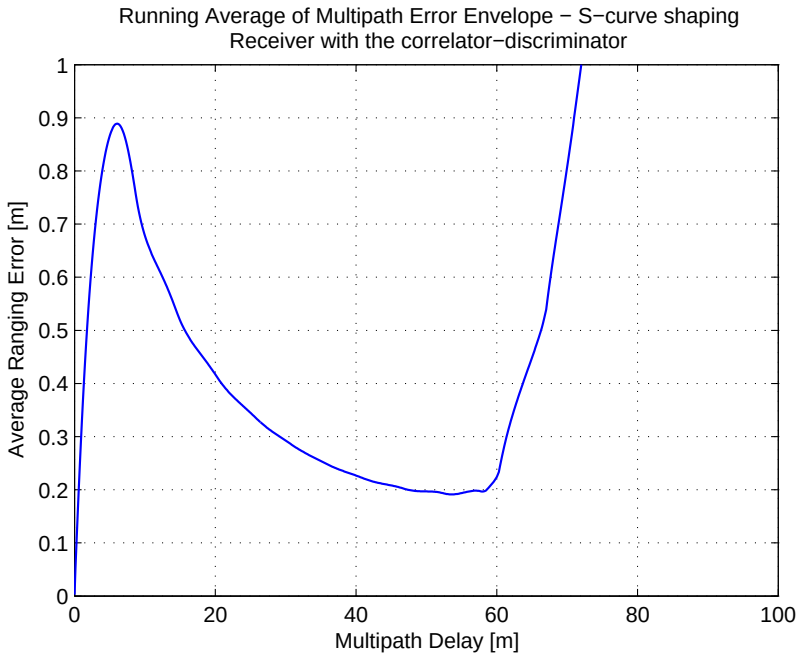

(b)

Figure 6.57: Multipath performances with the S-curve shaping technique: multipath error envelope (a) and running average of multipath error envelope (b), for the receiver with the correlator-discriminator

arrangement, it is necessary to gate the local signals (subcarrier and PRN codes) previously used at the input of the correlator-discriminator. Then the innovative receiver with the correlator-discriminator must be modified inserting a gated reference function in the local signal generation section.

Similarly to the AltBOC receiver, a gating function that could work with this architecture is shown in Figure 6.58(a) and corresponds to centrally gate the code chips around their centers. As previously done, a *blanking factor* of 11/12 has been used: this means that only 1/12 of the chip time is not blanked.

The only difference with respect of the technique previously used for the AltBOC receiver (compare with Figure 6.48(b), at pag. 202) is that in this case the gated reference function is symmetrical around its center, because the output of the correlator-discriminator already is a S-curve. On the contrary the gated reference function for the AltBOC receiver was anti-symmetrical, in order to transform the output of the punctual complex correlator in a S-curve (see Section 6.5.2).

The gated discrimination function is then plotted in Figure 6.58(b), where the S-curve obtained with the gating technique is compared with the original S-curve of the receiver with the correlator-discriminator. It is evident that the shape of the curve is near the same in the central region of the discriminator (around the tracking point) and false lock points are present too. But the side lobes of the S-curve are slightly reduced by the gating function, allowing to conjecture a better multipath performance, with a minor influence of long delay multipath.

The multipath performance of this innovative receiver with the gating technique have been simulated and the results are shown in Figure 6.59.

The gating technique leads to a performance improvement, that will be compared with the performances obtained with previous arrangements in next Section.

It must be remarked that the gating technique, in this case, does not imply considerable advantages in term of hardware (as with previous receiver architectures). In fact the innovative architecture directly evaluates the discrimination function, without the need of two of more correlators and one discriminator block, but using only one modified correlator. For the gating technique it is then necessary to modify the local signals with the gated reference function.

Besides, the improved multipath performance of the receiver with this technique must be carefully considered, taking in account also the tracking performance in presence of noise, that are degraded because a large part of the received signal is blanked by the correlation with the gating function.

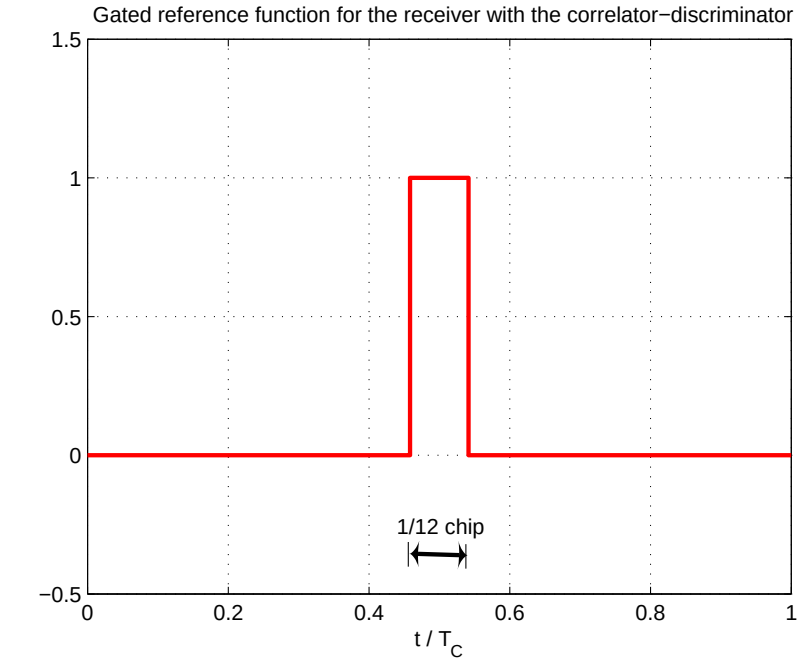

(a)

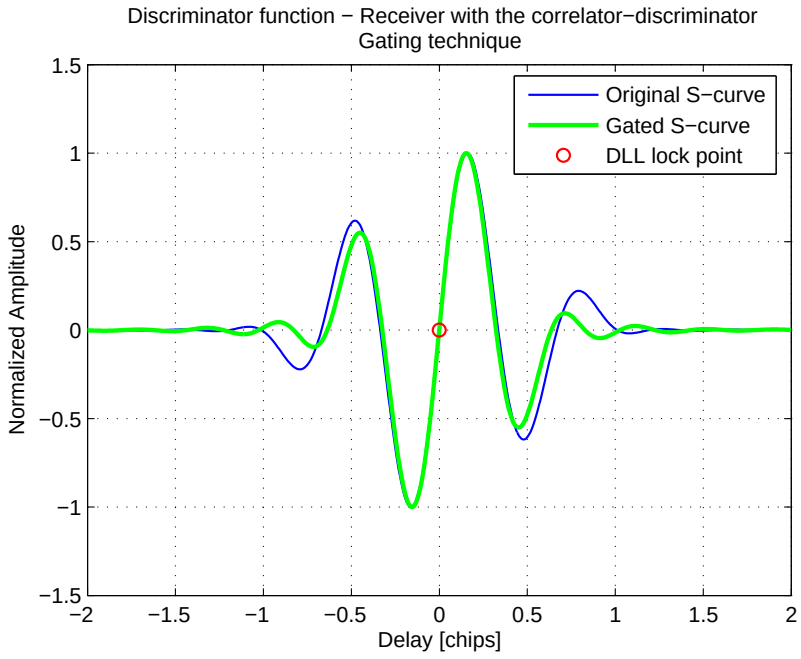

(b)

Figure 6.58: Gated reference function (a) for the gating technique, applied to the receiver with the correlator-discriminator, and obtained discrimination function (b)

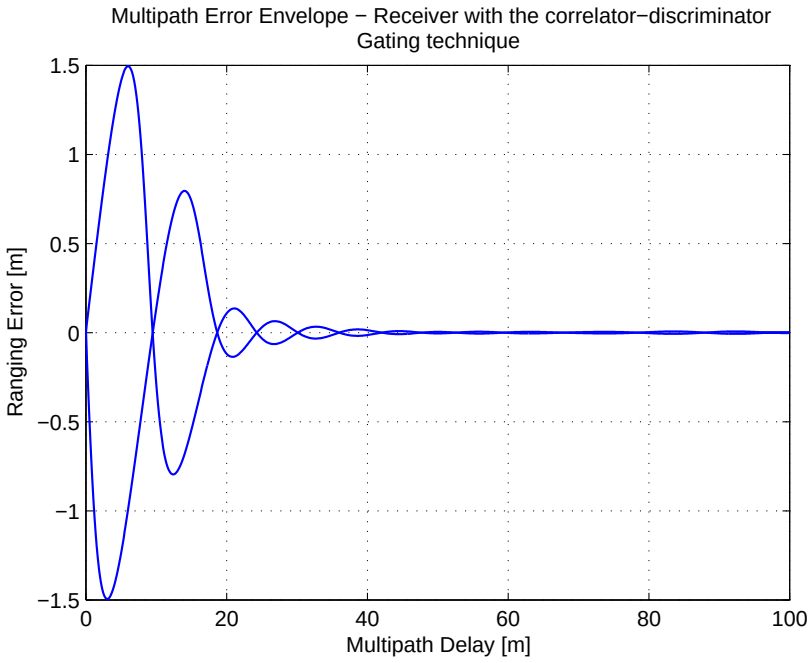

(a)

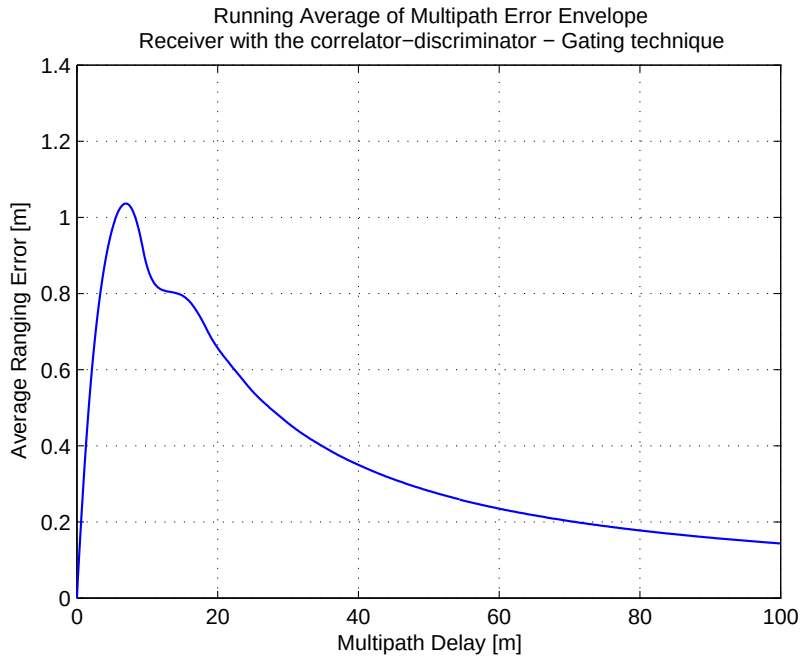

(b)

Figure 6.59: Multipath performances with the gating technique: multipath error envelopes (a) and running average of multipath error envelopes (b), for the receiver with the correlator-discriminator

6.7.3 Performance comparison

Previous Sections, about the multipath mitigation techniques applied to the innovative receiver with the correlator-discriminator, could be concluded with a final comparison between the obtained performances.

In Figure 6.60 the intrinsic multipath performance of the innovative receiver without multipath mitigation is compared with the performances obtained using the S-curve shaping and the gating technique.

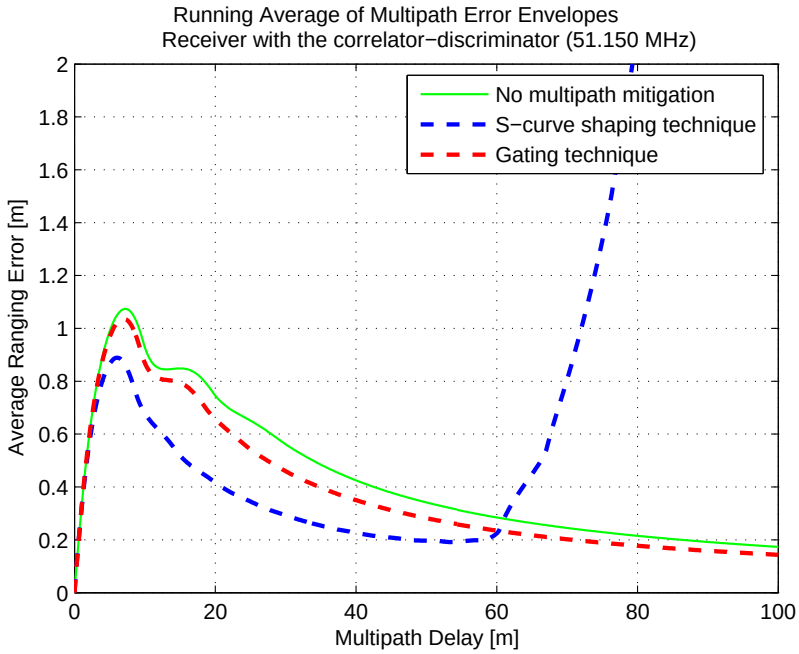

Figure 6.60: Comparison of multipath performances obtained with the receiver with the correlator-discriminator, applying the multipath mitigation techniques

Some performance improvements have been obtained: the running average plot with the gating technique is slightly lower than the curve without mitigation techniques. A further slight improvement is obtained with the S-curve shaping that achieves the best performance, but only for multipath delays contained in the fitting region (58.65 meters), whereas for greater delays the curve diverges.

Then the gating technique is not recommended for this receiver architecture, because could lead only to a negligible multipath mitigation, worsening the tracking performance of the receiver in presence of noise (as previously mentioned).

Also the S-curve shaping technique does not achieve remarkable multipath mitigation and implies a more complex implementation of the receiver, that seems not convenient if compared with the small performance improvement.

Besides, this technique is based on a multi-correlator approach that allows to conjecture a worsening of the tracking jitter of the receiver (a linear combination of multiple correlators implies a sum of the noise contributions, degrading the receiver performance). Further analysis are necessary to prove this statement, but are not concerned in this thesis, where only the multipath mitigation is discussed.

In conclusion, the obtained results demonstrate that the multipath mitigation techniques considered in previous Sections are not convenient for the innovative receiver architecture, because its intrinsic good performance in presence of multipath could be only slightly improved with these techniques.

6.8 Conclusions about the multipath performances

In this Chapter the code multipath mitigation problem has been studied in deep for the Galileo E5 AltBOC signal, adapting the well-known discriminator-based approaches used in common GPS receivers and two emerging mitigation techniques (the *S-curve shaping* and the *gating technique*) to the architectures proposed and described in Chapter 4 (the BPSK receiver, the AltBOC receiver and the receiver with the correlator-discriminator).

Considering the intrinsic receiver performances, without the mitigation techniques, it has been demonstrated that the best performance in presence of multipath is achieved with the innovative receiver with the correlator-discriminator. In fact, the BPSK receiver and the AltBOC receiver show worse performances, as shown in Figure 6.61(a).

In detail, the performance of the BPSK receiver is limited by its finite bandwidth (30 MHz) and because it is based on the reception of one or both the E5 sidebands (*single band receiver* or *separate dual band receiver*), that are processed like BPSK signals, similarly to that done in a classical GPS receiver: this choice does not take advantage of the AltBOC signal features.

On the contrary, the AltBOC receiver (*coherent dual band architecture*) exploits the complex correlation of the wideband AltBOC signal, but achieves a multipath performance that is overcome by the receiver with the correlator-discriminator, for multipath delays greater than approximatively 10 meters (see Figure 6.61(a)). Furthermore, this last innovative receiver features a lower complex architecture than the other two receivers (only one modified correlator is used instead of two or more correlators and a discriminator block) and seems a good compromise between multipath performances and receiver complexity and cost.

Nevertheless, if the implementation complexity of the receiver is not constrained and it is required to achieve the best possible multipath performances, the previous architectures presented in Chapter 4 could be modified

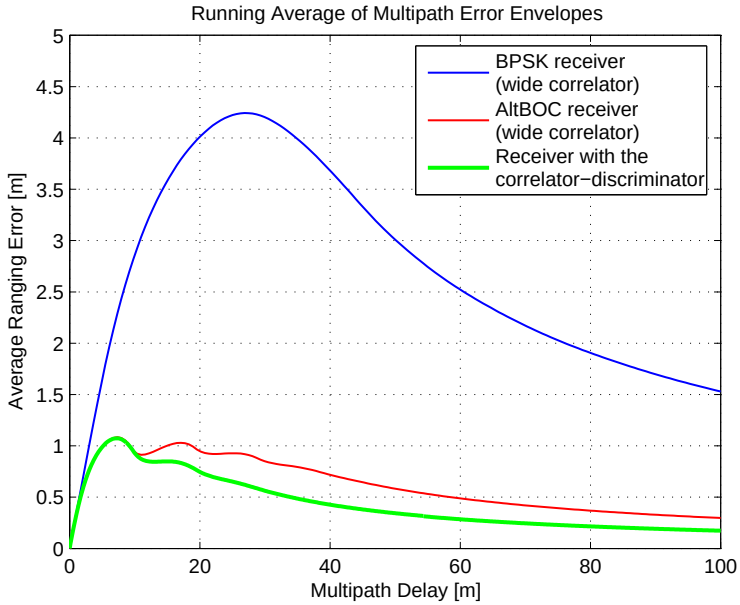

(a)

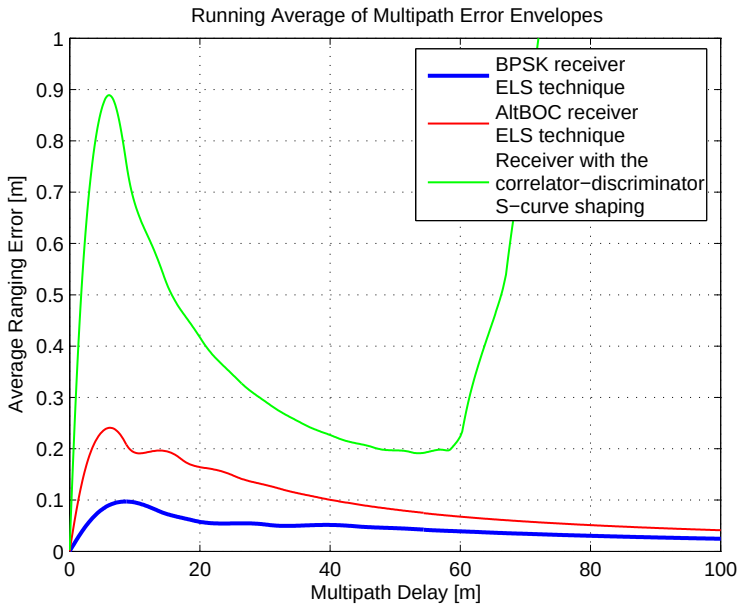

(b)

Figure 6.61: Comparison of multipath performances obtained with the three receiver architectures: the BPSK receiver (30 MHz), the AltBOC receiver (51.150 MHz) and the receiver with the correlator-discriminator (51.150 MHz). Comparison of running average of multipath error envelopes for the three receivers without multipath mitigation (a), and multipath performances obtained with the best multipath mitigation technique for each receiver (b)

using multipath mitigation techniques. The simulations done in previous Sections demonstrate that the best performances with the BPSK and the AltBOC receivers are obtained with the *Early/Late Slope* (ELS) technique, whereas for the innovative receiver the *S-curve shaping* approach must be used. The results with these configurations are compared in Figure 6.61(b).

Considering the best possible mitigation approach for each receiver architecture, the situation appears reversed with respect of the considerations done above, for the receivers without multipath mitigation. In fact in this case the best performance is obtained with the BPSK receiver with the ELS technique. The AltBOC receiver with the same mitigation approach achieves a worse performance, because this technique is suitable for the BPSK receiver, that uses a signal processing similar to that in a GPS receiver. On the contrary it seems difficult to adapt the ELS technique and the other current mitigation approaches to the complex signal processing used in the AltBOC receiver. In detail, it is difficult to choose optimum correlator spacings with the AltBOC complex correlation function, since these optimum spacings strongly depend on the multipath environment and on the signal and receiver parameters.

The current discriminator-based approaches can not be adapted to the receiver with the correlator-discriminator and this innovative architecture does not take a remarkable advantage from the only two mitigation approaches (the *S-curve shaping* and the *gating technique*) that could be used (as explained in Section 6.7.3).

In conclusion, the existing multipath mitigation approaches seems suitable only for the BPSK receiver, leading to excellent performances if the ELS technique is used. Ad-hoc multipath mitigation techniques, that are not known at the moment, are foreseeable and will be probably discovered in the future for the AltBOC receiver and for the receiver with the correlator-discriminator, leading to significative performance improvements.

At the moment, the best possible multipath performance could be achieved only with the BPSK receiver, with an expensive hardware (five correlators and five local signal generators, for the ELS technique). The innovative receiver with the correlator-discriminator could not reach similar performances until now, but it is an interesting and promising receiver with less hardware than other architectures and seems a good compromise between multipath performances and receiver cost.

Chapter 7

Conclusions and future activities

A complete and exhaustive study of the AltBOC modulation has been performed for the first time in this thesis. In fact, it must be remarked that this modulation is only outlined in few articles in literature, that often result generic and difficult to understand.

The features of the AltBOC modulated signal, that will be used for the E5 band of the Galileo system, have been analyzed in this thesis, considering also the possible receiver architectures, the acquisition strategies and the multipath mitigation techniques that are suitable for this signal.

The analysis needed for this thesis have been performed from the analytical point of view and by means of simulations, that have been carried out using several programs written in *C* and MATLAB® languages in the thesis framework. These simulation programs allow to generate the samples of the AltBOC modulated signal and have been used to simulate the acquisition operations for the different AltBOC receivers and to assess the performances of the multipath mitigation techniques that are suitable for the AltBOC signal.

During this thesis some innovative concepts have been proposed and analyzed for the AltBOC receivers: the *sideband translator* (that is presented in Section 4.3.3 and is patent pending) for the *coherent dual band receiver*, the innovative architecture of the *receiver with the correlator-discriminator* (see Section 4.4.3) and the *progressive acquisition* technique (see Section 5.1.4).

Some open problems still remain and can be the subject of future works about the AltBOC modulation. In detail, the simulation programs implemented for this thesis can be used for further performance analysis of the discussed acquisition techniques (e.g. analysis of the *false alarm probability* and the *detection probability*, performance assessment with *Receiver Operative Characteristic* curves, introduction of *statistical improvement algorithms*, etc.) or for the validation of innovative acquisition strategies. Besides, it is possible to assess the performances of new multipath mitigation techniques,

that probably will be proposed in future, comparing them with the techniques discussed in this thesis.

Another interesting field of activities will be the analysis of the noise performances (the so-called *tracking jitter*) of the receiver architectures and the multipath mitigation techniques discussed in this thesis.

Finally, the proposed techniques and architectures can be tested and validated also using the signals transmitted from the experimental GIOVE-A satellite and the future GIOVE-B satellite of the Galileo system.

Appendixes and Bibliography

Appendix A

Cross-correlation analysis for the E5 PRN codes

As previously outlined in Section 2.1.2, the PRN codes that will be used in Galileo E5 band are quasi-orthogonal codes. This implies a non null cross-correlation between the transmitted channels, that could produce a small **bias** in the tracking loop of the receiver, affecting the estimated position.

Typically this problem is neglected in common GPS receivers, because the induced offset is very small and is overcome by noise and other error sources. Besides, this effect is time varying because depends on the number of satellites that are in view and on their relative positions. In the following, it is demonstrated that the bias effect of the cross-correlations is negligible also for the codes that will be used in Galileo E5 band.

To assess the bias effect introduced by the non null cross-correlation, the eight codes presented in Table A.1 have been generated, using an arbitrary assignment[1] for the codes of two satellites (SVN 1 and 2). The four channels in E5 band (two data channels and two pilot channels) of both satellites have been simulated.

To analyze the correlation proprieties of the eight codes, it is possible to evaluate the correlation for all the possible combinations of two codes. Considering the maximum correlation value for each code pair, the results presented in Table A.2 and in Figure A.1 has been obtained. The correlation values have been evaluated using an integration time of 1 ms (1 primary code period) and normalizing the correlation functions with the amplitude of the auto-correlation peak (that in this way is equal to 1).

[1]For the simulation of the two satellites, the codes have been assigned choosing between the 50 primary codes that are defined in SIS-ICD [4] for each E5 channel. In detail the first code of each channel has been chosen for the first satellite, while the second code of each channel has been used for the second satellite. With another arbitrary choice the results are similar, with negligible differences. In fact it must be noted that the code assignment for each satellite must still to be defined.

Code number	SVN	Channel
1	1	*E5a-I*
2	1	*E5a-Q*
3	1	*E5b-I*
4	1	*E5b-Q*
5	2	*E5a-I*
6	2	*E5a-Q*
7	2	*E5b-I*
8	2	*E5b-Q*

Table A.1: Parameters of the eight simulated codes

Normalized correlation values								
Code	**1**	**2**	**3**	**4**	**5**	**6**	**7**	**8**
1	1	0.0323	0.0323	0.0326	0.0318	0.0325	0.0324	0.0347
2	0.0323	1	0.0384	0.0295	0.0326	0.0333	0.0347	0.0334
3	0.0323	0.0384	1	0.0380	0.0321	0.0361	0.0344	0.0361
4	0.0326	0.0295	0.0380	1	0.0351	0.0354	0.0346	0.0328
5	0.0318	0.0326	0.0321	0.0351	1	0.0340	0.0351	0.0330
6	0.0325	0.0333	0.0361	0.0354	0.0340	1	0.0343	0.0387
7	0.0324	0.0347	0.0344	0.0346	0.0351	0.0343	1	0.0335
8	0.0347	0.0334	0.0361	0.0328	0.0330	0.0387	0.0335	1

Table A.2: Matrix of maximum values for the normalized correlation of eight spreading codes

The values on the diagonal corresponds to the normalized auto-correlation peaks of the eight codes, and are all ones. The others are worst-case normalized cross-correlation values, obtained considering for each pair of codes the delay that maximize the cross-correlation. In the table the maximum cross-correlation value is 0.0387, which is small compared to the auto-correlation peak, but it could slightly affect the receiver performances, introducing a bias in the tracking point.

It must be noticed that the results have been obtained evaluating the correlation of code sequences of 10230 chips, which corresponds to one entire period of the primary code. But it is necessary to recall that the spreading codes contain also the secondary codes (see Section 2.1.2). They extend the code length with the *tiered code structure* from 1 ms (10230 chips) up to 100 ms (for pilot channels). The receiver can take advantage of this, generating a local replica of the entire tiered code period, an correlating it with the received signal. Indeed this idea imply an increase of computational complexity for the correlators, and can be used only for the tracking of the pilot channels. With the data channels there are data transitions that limit the correlation

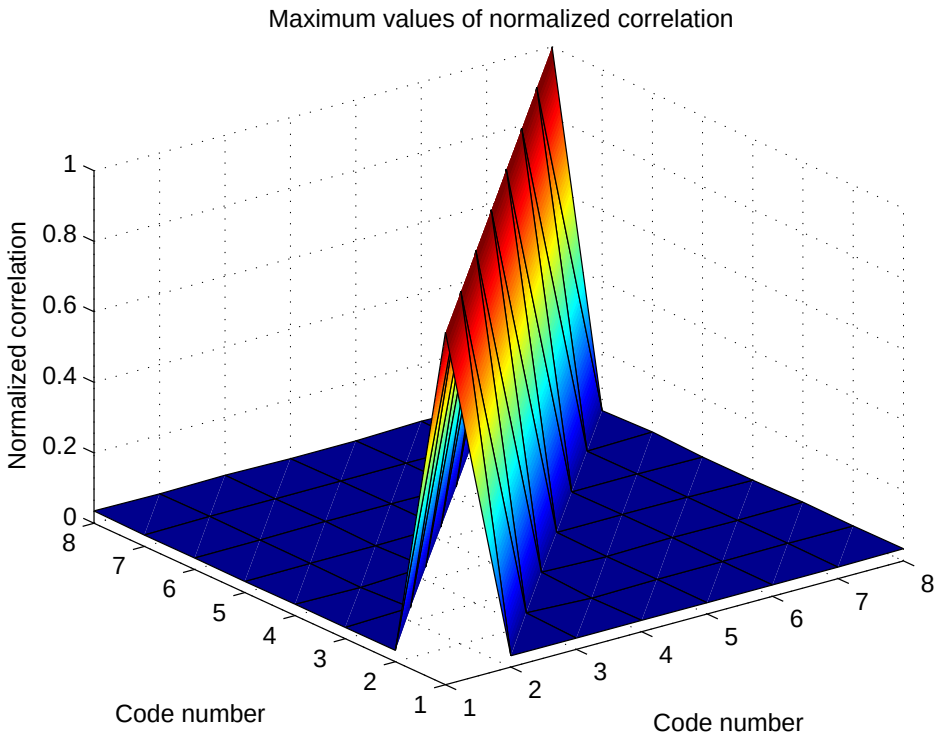

Figure A.1: Maximum values for the normalized correlation of eight codes

length, and during the acquisition process it is preferable to use only one primary code period, to reduce computational complexity and speed up the acquisition.

Additional simulations (not presented here for shortness) have demonstrated that the cross-correlation of the entire tiered codes bring to only slight reduction of the cross-correlation values, but with an huge computational complexity. This justify the choice of correlate only one primary code period (10230 chips).

Obviously the cross-correlation values can also vary considering different codes and different satellites, and in a real receiver only the satellites in view can cause cross-correlation problems. Moreover the relative delays of the four channels transmitted from each satellites are equals, but the signals coming from distinct satellites have different delays, that can vary in time. Accordingly, in a realistic receiver the errors caused by different satellites can also compensate each other. In fact, considering the results presented in Table A.3 and in Figure A.2 (obtained taking the normalized correlation values in the zeroth lag for each code pair) it is possible to see that the cross-correlation can take also negative values.

The cross-correlation values in this case range between the minimum value of -0.0147 and the maximum of 0.0266.

Normalized correlation values								
Code	**1**	**2**	**3**	**4**	**5**	**6**	**7**	**8**
1	1	-0.0084	0.0082	-0.0070	-0.0053	0.0033	-0.0111	0.0121
2	-0.0084	1	-0.0031	0.0266	-0.0053	-0.0037	-0.0147	0.0098
3	0.0082	-0.0031	1	0.0217	-0.0125	0.0086	-0.0043	0.0041
4	-0.0070	0.0266	0.0217	1	0.0027	0.0141	0.0086	-0.0127
5	-0.0053	-0.0053	-0.0125	0.0027	1	-0.0037	0.0022	0.0203
6	0.0033	-0.0037	0.0086	0.0141	-0.0037	1	0.0096	-0.0012
7	-0.0111	-0.0147	-0.0043	0.0086	0.0022	0.0096	1	0.0012
8	0.0121	0.0098	0.0041	-0.0127	0.0203	-0.0012	0.0012	1

Table A.3: Matrix of normalized correlation values of eight spreading codes in the zeroth lag

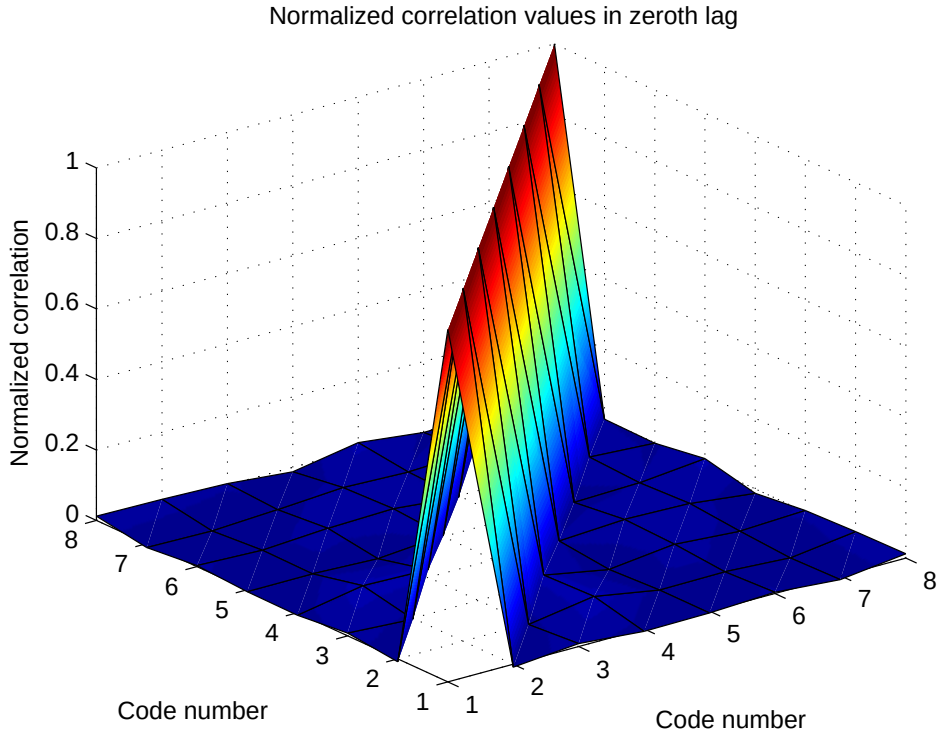

Figure A.2: Normalized correlation values of eight codes in the zeroth lag

It must be remarked that the code assignment for each satellite is currently in the process of being defined. Optimizing the code assignment, the bias introduced by the cross-correlation could be reduced.

It is also possible to try to correct the bias, writing a look-up table with bias correction for each code, but this is feasible only considering the four codes of a single satellite. In fact only the relative delays between the codes of a

satellite are fixed, whereas the codes from different satellites come with time varying delays.

About the tracking errors, it is interesting to analyze to effect on the AltBOC correlation function of the non null cross-correlation between the Galileo codes. The *combined complex correlation function* is obtained considering only the two pilot channels in the E5a and E5b transmission bands of one satellite (for more details, see Section 3.4). It is a symmetrical function, assuming that the received signal is composed by only the desired pilot codes and neglecting the cross-correlation with the other received codes. However, if also the other channels are considered, in a more realistic simulation, the correlation function results **non symmetrical**.

An example of this problem is presented in Figure A.3, where all the four channels transmitted in E5 band by a single Galileo satellite have been simulated and correlated with the two local pilot codes.

It can be seen that the error is very small and it is observable only for the secondary lobes of the correlation function (slight differences between the left and the right side). The main peak, that is utilized for the code tracking, seems not affected by this error and the distortions on the discriminator function will be very small.

Accordingly to the previous results, it is possible to conclude that the effect of the code cross-correlation could be neglected in Galileo receivers, as well as in common GPS receiver.

To avoid the cross-correlation bias errors, the simulations performed in Chapter 6 have been carried out supposing that the received signal $s_{E5}(t)$ is composed only by the pilot channels $e_{E5a\text{-}Q}(t)$ and $e_{E5b\text{-}Q}(t)$ and switching off the other two channels $e_{E5a\text{-}I}(t)$ and $e_{E5b\text{-}I}(t)$.

Otherwise, if the complete E5 AltBOC signal is simulated, some unavoidable bias errors could be seen in the multipath error envelopes.

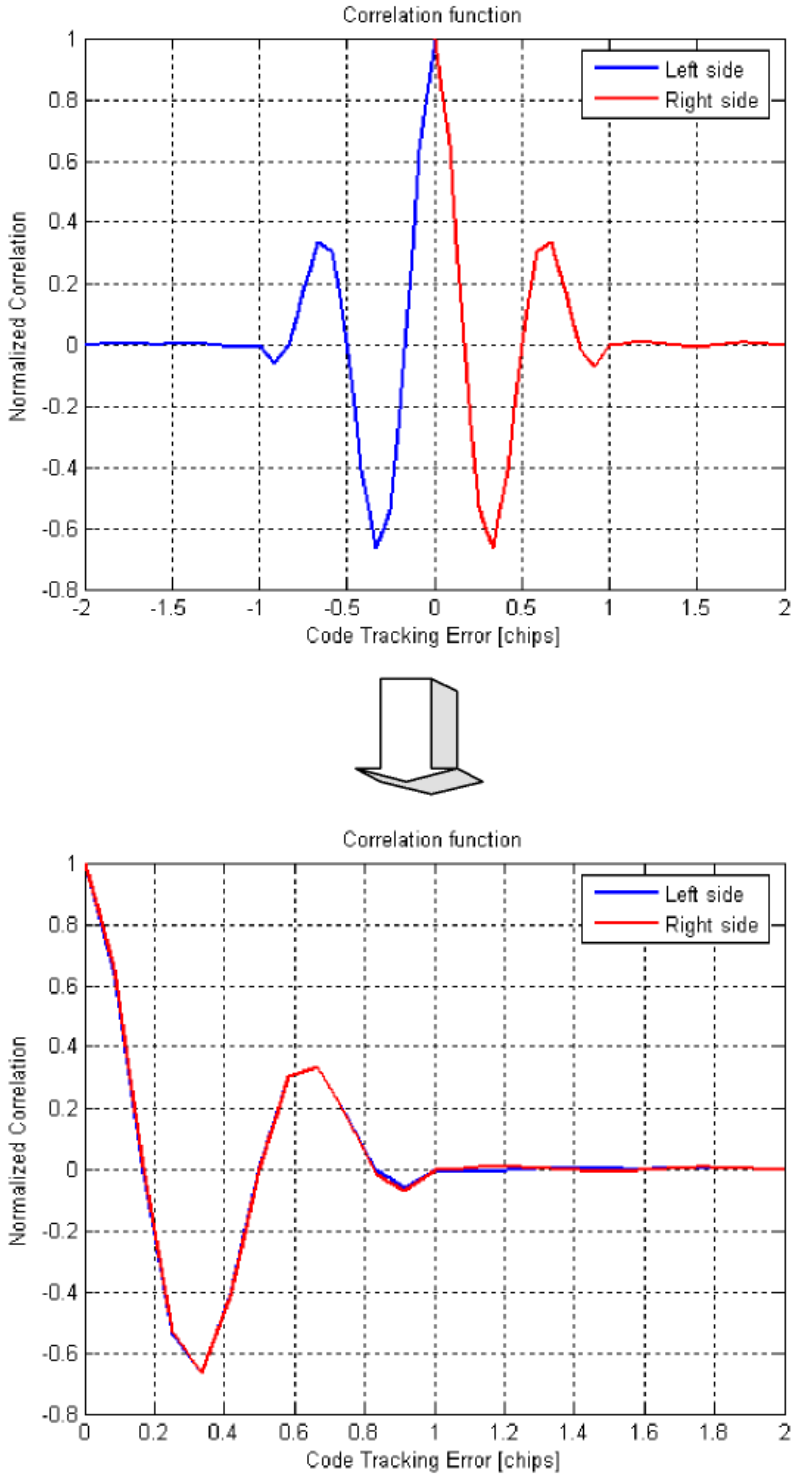

Figure A.3: Illustration of the non symmetrical correlation function, simulating all the Galileo codes in E5 band transmitted by a single satellite

Appendix B

Demonstration for the Early/Late Slope technique

The **Early/Late Slope** (ELS) technique is illustrated in Section 6.4.4 considering four correlators. This technique is derived from Reference [45], adapting the expression in this article to the notation used for the four correlators.

A demonstration of Equation (6.10), that evaluates the pseudorange correction T, is then presented in the following. It must be noted that the expression presented in References [37] and [38] is different from Equation (6.10) and is not correct, considering the notation used in these articles for the four correlators.

In Figure B.1 it is shown a generic triangular correlation function and the positions of the four correlators. The peak of the correlation function is rounded due to band-limiting effects and deformed due to the influence of multipath. As a result, the autocorrelation function's peak is not at $\tau = 0$, but is biased by an error, that is equal to the pseudorange correction T that must be evaluated with the ELS technique.

First of all, the slope on each side of the correlation function must be determined by means of the four correlators (K_1,...,K_4). They are placed two per side of the correlation peak, with fixed positions determined with the respective τ-coordinate (τ_1,...,τ_4). The outputs of the four correlators correspond to the ordinates (y_1,...,y_4) of the correlation function. By use these ordinates, the slopes a_1 and a_2 can be determined with the following expressions:

$$a_1 = \frac{y_2 - y_1}{\tau_2 - \tau_1} \tag{B.1}$$

$$a_2 = \frac{y_4 - y_3}{\tau_4 - \tau_3} \tag{B.2}$$

Then two first order polynomials can be set up, to define two straight lines corresponding to the two sides of the correlation function. The first polynomial, related to the left side, define a straight line between the two correlators

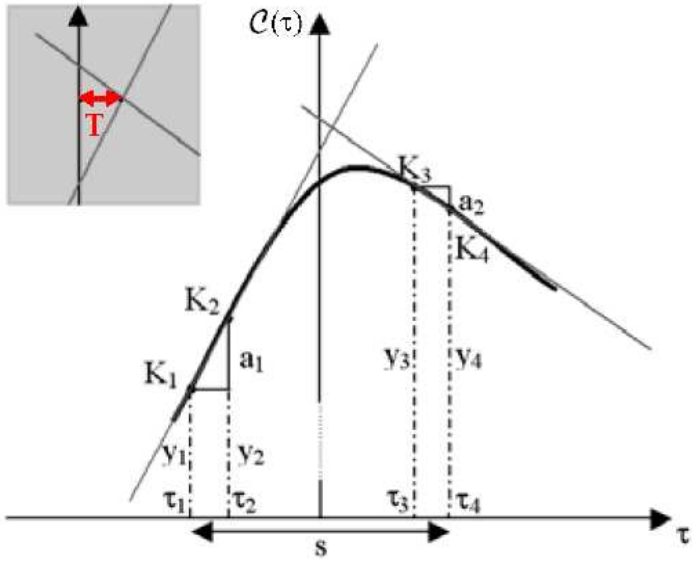

Figure B.1: General concept of the Early/Late Slope technique: computation of a pseudorange correction T by analyzing the slopes on both sides of the correlation function

K_1 and K_2:

$$y = a_1 \cdot \tau + b_1 \tag{B.3}$$

where the b_1 term is a unknown constant. It is necessary to impose that this line passes through the position of the K_1 correlator (τ_1, y_1), obtaining the following expression:

$$y_1 = a_1 \cdot \tau_1 + b_1 \tag{B.4}$$

Thus the b_1 constant could be evaluated as follows:

$$b_1 = y_1 - a_1 \cdot \tau_1 \tag{B.5}$$

In a similar manner the second polynomial, related to the right side of the correlation function, is defined by a straight line between the two correlators K_3 and K_4:

$$y = a_2 \cdot \tau + b_2 \tag{B.6}$$

Imposing that this line passes through the point (τ_4, y_4), that is the position of the K_4 correlator, the following expression is obtained:

$$y_4 = a_2 \cdot \tau_4 + b_2 \tag{B.7}$$

Thus the b_2 constant could be evaluated as follows:

$$b_2 = y_4 - a_2 \cdot \tau_4 \tag{B.8}$$

The τ-coordinate of the intersection of the two straight lines can then be interpreted as the desired pseudorange correction T and can be determined

combining Equations (B.3) and (B.6) in the following linear system of equations:

$$\begin{cases} y &= a_1 \cdot \tau + b_1 \\ y &= a_2 \cdot \tau + b_2 \end{cases} \tag{B.9}$$

The intersection of the two straight lines could then be determined resolving this system, imposing that $\tau = T$. In this way the value of T could be determined, with the following computations:

$$a_1 \cdot T + b_1 = a_2 \cdot T + b_2 \tag{B.10}$$

$$T \cdot (a_1 - a_2) = b_2 - b_1 \tag{B.11}$$

$$T = \frac{b_2 - b_1}{a_1 - a_2} \tag{B.12}$$

The two constants b_1 and b_2 can be substituted with the expressions in Equations (B.5) and (B.8):

$$T = \frac{y_4 - a_2 \cdot \tau_4 - y_1 + a_1 \cdot \tau_1}{a_1 - a_2} \tag{B.13}$$

Inverting the signs of the numerator and the denominator and reordering the terms of the numerator, it results:

$$T = \frac{y_1 - y_4 - a_1 \cdot \tau_1 + a_2 \cdot \tau_4}{a_2 - a_1} \tag{B.14}$$

Since the spacing between the first and the forth correlator is $s = \tau_4 - \tau_1$ and the correlators are placed in symmetrical positions ($\tau_1 = -\tau_4$, as shown in Figure B.1), the following expression is valid:

$$\tau_4 = -\tau_1 = \frac{s}{2} \tag{B.15}$$

Substituting τ_1 and τ_4 in Equation (B.14), the final expression of the pseudo-range correction T is obtained:

$$T = \frac{y_1 - y_4 + s/2 \cdot (a_1 + a_2)}{a_2 - a_1} \tag{B.16}$$

where $s = \tau_4 - \tau_1$.

Bibliography

[1] European Space Agency (ESA) website, *First Galileo Lauch*, http://www.esa.int/SPECIALS/Galileo_Launch/index.html.

[2] European Commission (EC) website, Directorate-General Energy and Transport, *GALILEO - European Satellite Navigation System*, http://ec.europa.eu/dgs/energy_transport/galileo/intro/index_en.htm.

[3] European Commission Press Release, *GALILEO - Involving Europe in a New Generation of Satellite Navigation Services*, Resolution No. 9004/99, 2191 st Transport Council Meeting, Luxembourg, June 17, 1999.

[4] Galileo Joint Undertaking, *Galileo Open Service Signal In Space Interface Control Document (OS SIS ICD)*, GAL OS SIS ICD/D.0, Draft 0, ©, 2006, European Space Agency / Galileo Joint Undertaking, May 23, 2006.

[5] G. W. Hein and T. Pany, "Architecture and Signal Design of the European Satellite Navigation System Galileo - Status Dec. 2002", in *Journal of Global Positioning Systems*, Vol. 1, No. 2, pp. 73-84, 2002.

[6] G. W. Hein, J. Godet, J.-L. Issler, J.-C. Martin, R. Lucas-Rodriguez, and T. Pratt, "The GALILEO Frequency Structure and Signal Design", in *Proceedings of ION GPS 2001*, pp. 1273-1282, Salt Lake City, Utah, September 11-14, 2001.

[7] G. W. Hein, J. Godet, J.-L. Issler, J.-C. Martin, P. Erhard, R. Lucas-Rodriguez, and T. Pratt, "Status of Galileo Frequency and Signal Design", in *Proceedings of ION GPS 2002*, pp. 266-277, Portland, OR, 24-27 September 2002.

[8] M. Soellner and Ph. Erhard, "Comparison of AWGN Code Tracking Accuracy for Alternative-BOC, Complex-LOC and Complex-BOC Modulation Options in Galileo E5-Band", in *Proceedings of ION ENC GNSS 2003*, Graz, Austria, April 2003.

[9] L. Ries et al, "A Software Simulation Tool for GNSS2 BOC Signals Analysis", in *Proceedings of ION GPS 2002*, Portland, Oregon, September 24-27, 2002.

[10] L. Ries et al, "New Investigations on Wideband GNSS2 Signals", in *Proceedings of the ION ENC GNSS 2003*, Graz, Austria, April 2003.

[11] J. M. Sleewaegen, W. De Wilde, and M. Hollreiser, "Galileo AltBOC

Receiver", in *Proceedings of ION GNSS 2004*, Rotterdam, Holland, May 16-19, 2004.

[12] P. Erhard and E.Armengou-Miret, *Status and Description of Galileo Signals Structure and Frequency Plan*, technical note, European Space Agency (ESA), April 2004.

[13] N. Gerein, *Hardware architecture for processing Galileo alternate binary offset carrier (AltBOC) signals*, European Space Agency (ESA, Paris, FR), United States Patent No. US006922167B2, July 26, 2005.

[14] N. Gerein, A. Manz, M. Clayton, and M. Olynik, "Galileo Sensor Station Ground Reference Receiver Performance Characteristics", in *Proceedings of ION GPS/GNSS 2003*, Portland, OR, September 9-12, 2003.

[15] F. Dovis, L. Lo Presti, and P. Mulassano, "An Innovative Scheme for Tracking BOC[n,n] Signals", in *Proceedings of ION ENC GNSS 2005*, Munich, Germany, July 19-22, 2005.

[16] P. Ward, "Satellite Signal Acquisition and Tracking", in *Understanding GPS: Principle and Applications*, Norhood, MA, E. D. Kaplan, Artech House, 1996.

[17] D. J. R. Van Nee and A. J. R. M. Coenen, "New Fast GPS Code-Acquisition technique using FFT", in *Electronics Letters*, Vol. 27, No. 2, pp. 158-160, January 17, 1991.

[18] F. Johansson, R. Mollaei, J. Thor, and J. Uusitalo, *GPS Satellite Signal Acquisition and Tracking*, Undergraduate projects 1998, Luleå University of Technology, Sweden, August 21, 1998, http://www.sm.luth.se/csee/courses/sms/019/1998/navstar/navstar.pdf.

[19] C. Yang, "FFT Acquisition of Periodic, Aperiodic, Puncture, and Overlaid Code Sequences in GPS", in *Proceedings of ION GPS 2001*, Salt Lake City, UT, September 11-14, 2001.

[20] J. Takala V. Eerola and T. Ritoniemi, "Rapid Zero-Knowledge GPS Signal Acquisition", in *Proceedings of EUPSICO 2000: European Signal Processing Conference*, No. 10, pp. 2253-2256, Tampere , Finlande, September 4-8, 2000.

[21] J. W. Betz, J. D. Fite, and P. T. Capozza, "Getting to M - Direct Acquisition of the New Military Signal", in *GPS World*, pp. 40-46, April 1, 2005.

[22] N. Martin, V. Leblond, G. Guillotel, and V. Heiries, "BOC(x,y) signal acquisition techniques and performances", in *Proceedings of ION GPS/GNSS 2003*, Portland, OR, September 9-12, 2003.

[23] J. A. Avila-Rodriguez et al, "Enabling Location Based Services with a Combined Galileo/GPS Receiver Architecture", in *Proceedings of ION GNSS ITM 2004*, Long Beach, California, September 21-24, 2004.

[24] V. Heiries, J. A. Avila-Rodriguez, M. Irsigler, G. W. Hein, E. Rebeyrol, and D. Roviras, "Acquisition Performance Analysis of Composite Signals for the L1 OS Optimized Signal", in *Proceedings of ION GNSS ITM 2005*, Long Beach, CA, September 13-16, 2005.

[25] S. Macagno, *Acquisition systems for GPS and Galileo signals*, Master's thesis, Politecnico di Torino, September 2003.

[26] M. Fantino, *Study of Architectures and Algorithms for Software Galileo Receivers*, Ph.D. dissertation, Politecnico di Torino, February 2006.

[27] F. Bastide, O. Julien, C. Macabiau, and B. Roturier, "Analysis of L5/E5 Acquisition, Tracking and Data Demodulation Thresholds", in *Proceedings of ION GPS 2002*, Portland, OR, September 24-27, 2002.

[28] F. Bastide, "Galileo E5a/E5b and GPS L5 Acquisition Time Statistical Characterization and Application to Civil Aviation", in *Proceedings of ION GNSS ITM 2004*, Long Beach, CA, September 21-24, 2004.

[29] F. M. G. Sousa, F. D. Nunes, and J. M. N. Leitao, "Partial Correlation Technique for the Acquisition of Weak GPS/Galileo Signals", in *Proceedings of ION 61st Annual Meeting 2005*, The MITRE Corporation & Draper Laboratory, Cambridge, MA, June 27-29, 2005.

[30] W. De Wilde, J.-M. Sleewaegen, A. Simsky, C. Vandewiele, E. Peeters, J. Grauwen, and F. Boon, "New Fast Signal Acquisition Unit for GPS/Galileo Receivers", in *Proceedings of ION ENC GNSS 2006*, Manchester, May 7-10, 2006.

[31] W. De Wilde, J. M. Sleewaegen, K. Van Wassenhove, and F. Wilms, "A First-of-a-Kind Galileo Receiver Breadboard to Demonstrate Galileo Tracking Algorithms and Performances", in *Proceedings of ION GPS 2004*, Long Beach, California, USA, September 21-24, 2004.

[32] P. Fine and W. Wilson, "Tracking Algorithm for GPS Offset Carrier Signals", in *Proceedings of ION NTM 1999*, pp. 671-676, San Diego, January 25-27, 1999.

[33] M. Frigo and S. G. Johnson, "FFTW: An adaptive software architecture for the FFT", in *Proceedings of ICASSP 1998*, No. 3, pp. 1381-1384, 1998.

[34] M. Frigo and S. G. Johnson, "The Design and Implementation of FFTW3", in *Proceedings of IEEE*, vol. 93, No. 2, pp. 216-231, 2005.

[35] A. Köhne and M. Wößner, *GPS explained - Sources of Errors in GPS*, http://www.kowoma.de/en/gps/errors.htm.

[36] R. D. J. Van Nee, "Multipath Effects on GPS Code Phase Measurements", in *Navigation: Journal of the Institute of Navigation*, vol. 39, No. 2, pp. 177-190, USA, Summer 1992.

[37] M. Irsigler and B. Eissfeller, "Comparison of Multipath Mitigation Techniques with Consideration of Future Signal Structures", in *Proceedings of ION GPS/GNSS NTM 2003*, Portland, Oregon, September 9-12, 2003.

[38] M. Irsigler, G. W. Hein, and B. Eissfeller, "Multipath Performance Analysis for Future GNSS Signals", in *Proceedings of ION NTM 2004*, San Diego, California, January 26-28, 2004.

[39] T. Pany, M. Irsigler, and B. Eissfeller, "Code and Carrier Phase Tracking Performance of a Future Galileo RTK Receiver", in *Proceedings of ION ENC GNSS 2002*, Copenhagen, May 2002.

[40] M. Irsigler, J. A. Avila-Rodriguez, and G.W. Hein, "Criteria for GNSS

Multipath Performance Assessment", in *Proceedings of ION GNSS ITM 2005*, Long Beach, California, September 13-16, 2005.

[41] I. Ilie, R. Jr. Landry, and A. Constantinescu, "Simulation of GPS and Galileo Architectures for Anti-Jamming and Multipath Analysis", in *Canadian Aeronautics and Space Journal*, Vol. 51, No. 1, pp. 13-22, March 2005.

[42] O. Julien, M. E. Cannon, G. Lachapelle, C. Mongrédien, and C. Macabiau, "A New Unambiguous BOC(n,n) Signal Tracking Technique", in *Proceedings of ION ENC GNSS 2004*, Rotterdam, May 17-19, 2004.

[43] A. J. Van Dierendonck, P. Fenton, and T. Ford, "Theory and Performance of Narrow Correlator Spacing in a GPS Receiver", in *Navigation: Journal of the Institute of Navigation*, Vol. 39, No. 3, pp. 265-283, USA, Fall 1992.

[44] G. A. McGraw and M. S. Braasch, "GNSS Multipath Mitigation Using Gated and High Resolution Correlator Concepts", in *Proceedings of ION NTM 1999*, pp. 333-342, San Diego, January 25-27, 1999.

[45] B. R. Townsend and P. C. Fenton, "A Practical Approach to the Reduction of Pseudorange Multipath Errors in a L1 GPS Receiver", in *Proceedings of ION GPS ITM 1994*, pp. 143-148, Salt Lake City, Utah, September 20-23, 1994.

[46] T. Pany, M. Irsigler, and B. Eissfeller, "Optimum Coherent Discriminator Based Code Multipath Mitigation by S-Curve Shaping for BOC(n,n) and BPSK Signals", in *Proceedings of ION ENC GNSS 2005*, September 2005.

[47] L. J. Garin, "The Shaping Correlator, Novel Multipath Mitigation Technique Applicable to GALILEO BOC(1,1) Modulation Waveforms in High Volume Markets", in *Proceedings of ION ENC GNSS 2005*, September 2005.

[48] G. W. Hein and J. A. Avila-Rodriguez, "Performance of a Galileo PRS/GPS M-Code Combined Service", in *Proceedings of ION NTM 2005*, San Diego, California, January 24-26, 2005.

[49] A. Simsky, J. M. Sleewaegen, W. De Wilde, and F. Wilms, "Galileo Receiver Development at Septentrio", in *Proceedings of ION ENC GNSS 2005*, Munich, Germany, July 19-22, 2005.

[50] M. Hollreiser, "Galileo Receivers - Challenges and Performance", in *Proceedings of the 12$^{\text{th}}$ GAAS® Symposium*, Amsterdam, 2004.